UNIVERSITÀ DEGLI STUDI DI TRIESTE

XXXI CICLO DEL DOTTORATO DI RICERCA IN NANOTECNOLOGIE

CHARACTERIZATION, FUNCTIONALIZATION AND BIOLOGICAL EVALUATION OF CARBON NANOSTRUCTURES

Settore scientifico-disciplinare: CHIM/08

Dottorando
Akcan ISTIF

Coordinatore
Prof. Lucia PASQUATO

Supervisore di Tesi
Prof. Tatiana DA ROS

Correlatore di Tesi
Prof. Caroline A. AHAD HADAD

ANNO ACCADEMICO 2017/2018

UNIVERSITÀ DEGLI STUDI DI TRIESTE

XXXI CICLO DEL DOTTORATO DI RICERCA IN NANOTECNOLOGIE

CHARACTERIZATION, FUNCTIONALIZATION AND BIOLOGICAL EVALUATION OF CARBON NANOSTRUCTURES

Settore scientifico-disciplinare: CHIM/08

DOTTORANDO
AKCAN ISTIF

COORDINATORE
PROF. LUCIA PASQUATO

SUPERVISORE DI TESI
PROF. TATIANA DA ROS

CORRELATORE DI TESI
PROF. CAROLINE A. AHAD HADAD

ANNO ACCADEMICO 2017/2018

Acknowledgements

This PhD was a life-changing experience for me and I would like to thank to people who had unconditionally supported me.

Firstly, I would like to express my deepest gratitude to my PhD supervisor Prof. Tatiana Da Ros for her support of my PhD research, for her patience, and for sharing her immense knowledge and experience. You have inspired and motivated me in any condition.

I would like to thank especially Prof. Caroline A. Ahad Hadad for sharing her knowledge and experience, for having a big impact on my research activity, and for hosting me with Prof. Albert Nguyen Van Nhien in laboratories of Université de Picardie Jules Verne. I have been very lucky to meet you and work with you.

Thanks to the partners of Infusion Project, Ynvisible S.A, Prof. Jorge Parola and Prof. Cesar Laia for hosting me in their laboratories in Lisbon and sharing their precious knowledge.

Many thanks to labmates who supported, shared their experience and made this research more fun: Arturo, Agnieszka, Valentina, Cristina, Alice, Martina, Matteo, Federico, Alexa and all members of carbon nanotechnology group. You were more than a friend to me.

Merci and *Obrigado* to the labmates in France and Portugal for the fun lunchtime conversations and making my visit entertaining: Gaël, Pacho, Josip, Nely, Ranime, Maša, Maja, Jennifer, Tiago, Jack, Artur, Amir, Mattia. It is a small world.

I am so grateful for the precious support of my dear Chiara and your beautiful family Arturo, Leo, Francesca, Pino and Daniela. You accepted me to your family and became my second family. *Grazie!*

Of course... My dear family Ezgi, Yakup and Hilal. From my decision to do PhD to these moments, it couldn't be possible without your precious support. It is hard to describe how grateful I am to you. Thank you for believing in me. *Teşekkürler*.

List of Abbreviations

AFM	Atomic Force Microscopy
ATR	Attenuated Total Reflectance
Boc	t-butyloxycarbonyl
Boc_2O	Di-t-butyl dicarbonate
CD	Carbon Dot
CNT	Carbon Nanotube
CVD	Chemical Vapor Deposition
DCM	Dichloromethane
DIPEA	Diisopropylethiylamine
DLS	Dynamic Light Scattering
DMF	Dimethylformamide
DMAP	4-Dimethylaminopyridine
DND	Detonation Nanodiamond
Dox	Doxorubicin
DRIFTS	Diffuse reflectance infrared Fourier transform spectroscopy
ECD	Electrochromic Device
EDC	1-ethyl-3-(3-dimethylaminopropyl) carbodiimide
EFM	Electrostatic Force Microscopy
EOMA	Murine hemangioendothelioma
EtO_2	Diethyl ether
EtOH	Ethanol
FITC	Fluorescein isothiocyanate
GO	Graphene Oxide
Gpa	Gigapascal
GQD	Graphene Quantum Dot
HBTU	Hexafluorophosphate Benzotriazole Tetramethyl Uronium

HOBt	Hydroxybenzotriazole
IL	Ionic Liquid
IR	Infrared Spectroscopy
LDH	Lactate dehydrogenase
MeOH	Methanol
MTT	3-(4,5-Dimethylthiazol-2-yl)-2,5-diphenyltetrazolium bromidefor
MWCNT	Multi-Wall Carbon Nanotube
ND	Nanodiamond
NHS	N-hydroxysuccinimide
NMR	Nuclear Magnetic Resonance
PAGE	Polyacrylamide Gel Electrophoresis
PBMC	Peripheral Blood Mononuclear Cell
PEG	Polyethyleneglycol
Pht	Phthalimide group
PPEI-EI	Poly-(propionylethylenimine-co-ethylenimine)
QY	Quantum Yield
RBM	Radial breathing mode
RDX	1,3,5-trinitroperhydro-1,3,5-triazine
SWCNT	Single Wall Carbon Nanotube
TBTU	N,N,N′,N′-Tetramethyl-O-(benzotriazol-1-yl)uronium tetrafluoroborate
TEA	Triethylamine
TEM	Transmission Electronic Microscopy
TFA	Trifluoroacetic Acid
TGA	Thermogravimetric Analysis
THF	Tetrahydrofuran
TLC	Thin Layer Chromatography
TNT	2-methyl-1,3,5-trinitrobenzene
UV-Vis	Ultra Violet – Visible

Table of Drawings

I. Organic Compounds

P1

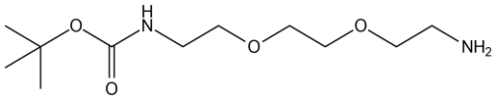

P2

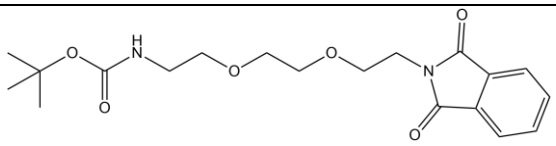

P3

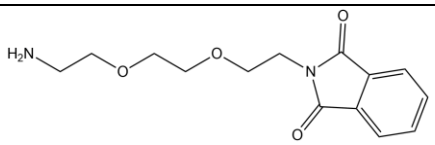

P4

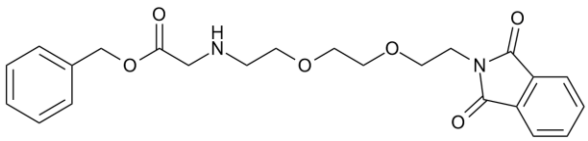

P5

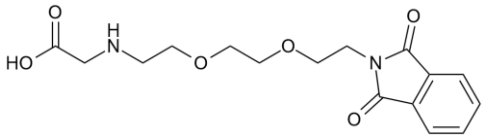

P6

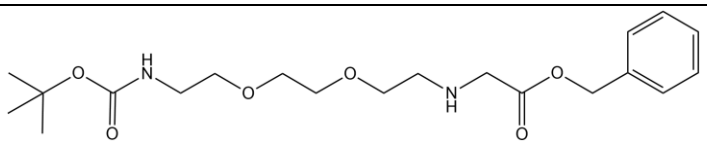

P7

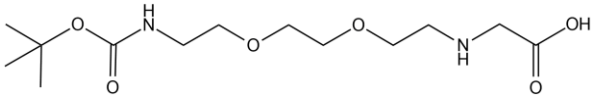

P8

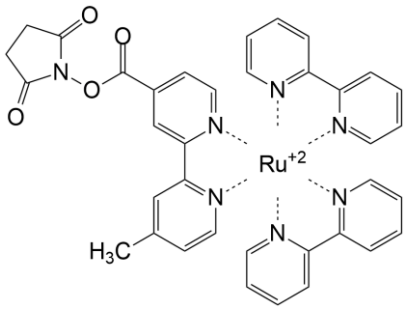

P9

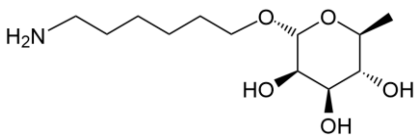

P10

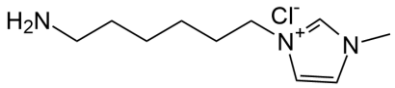

P11

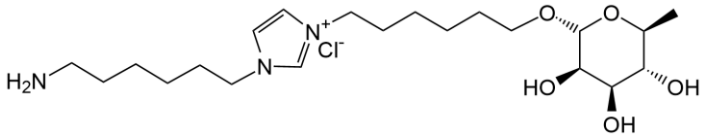

P12

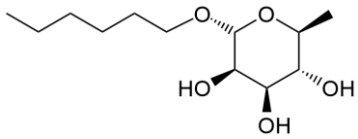

P13

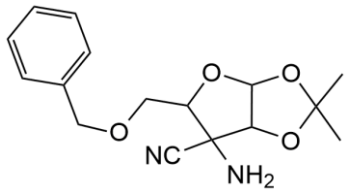

II. Carbon Nanostructures

The following cartoons are the schematic representation of the compounds and not their real reproduction. The functional groups and their distribution on the surface are reported for sake of clarity without claiming to be a perfect representation of the reality.

a. Nanodiamonds

Pristine NDs

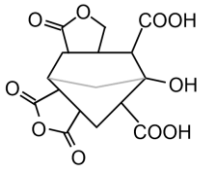

ND1

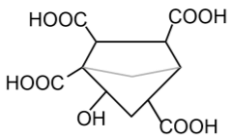

ND1.1

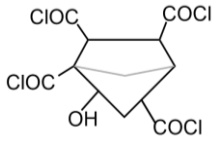

ND1.2

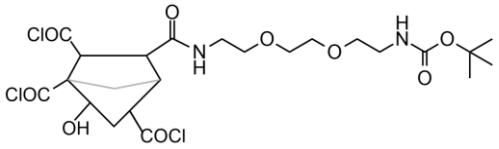

ND1.3

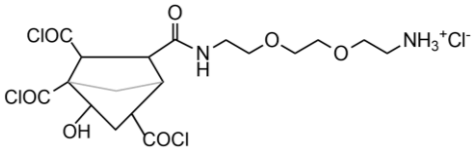

ND1.4

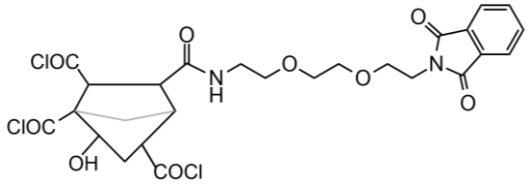

ND1.5

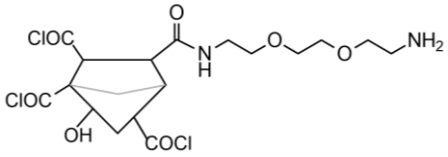

ND1.5.1

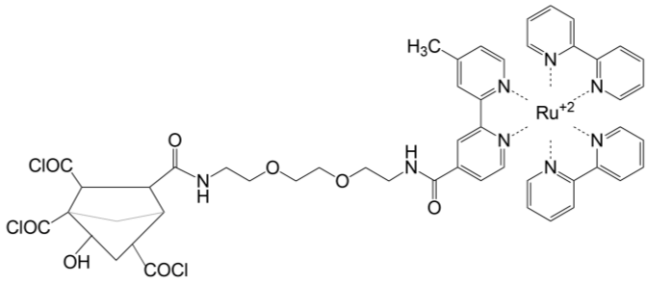

ND1.5.2

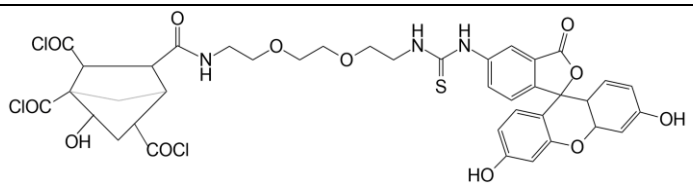

ND1.5.3

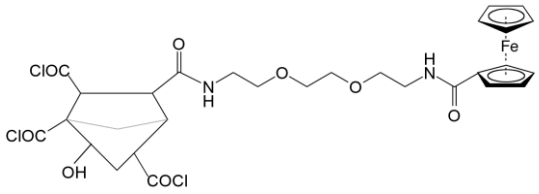

ND1.6

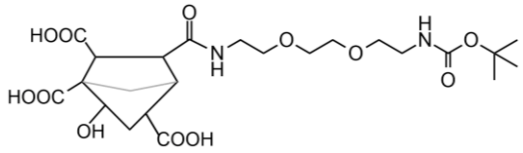

ND1.7

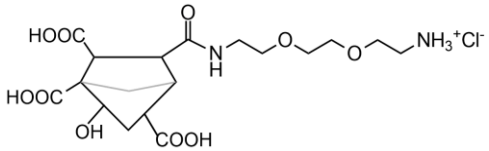

ND2

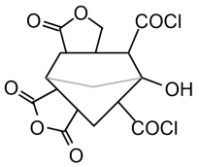

ND2.1

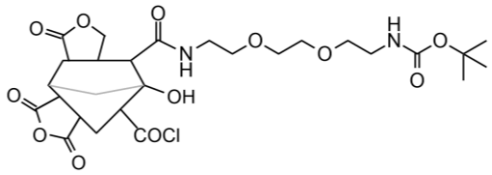

ND2.2

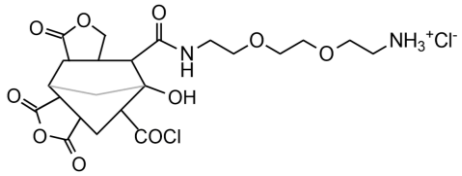

ND3.1a-b

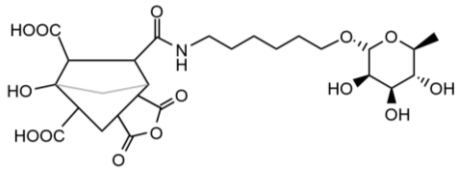

ND3.2a-b

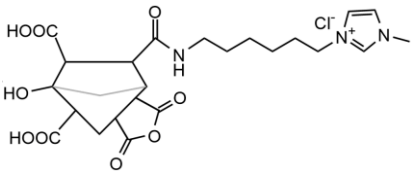

ND3.3a-b

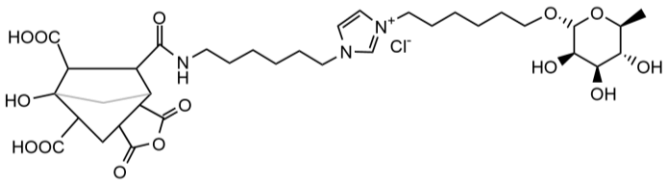

ND3.4

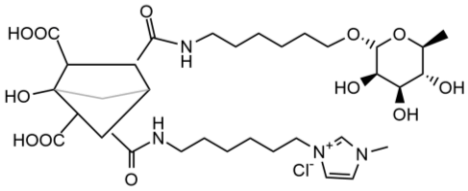

ND3.5

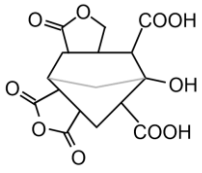

ND3.6a-b

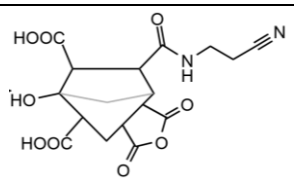

ND3.7

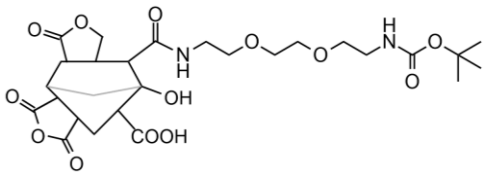

ND3.8

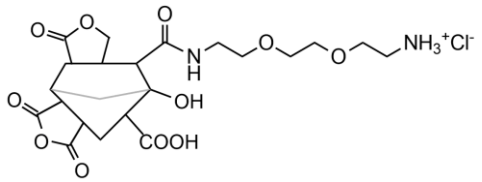

ND4.1a-e

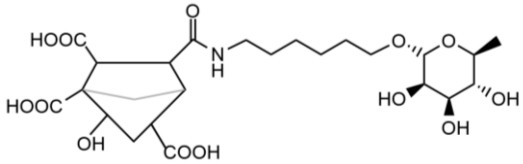

ND4.2a-b

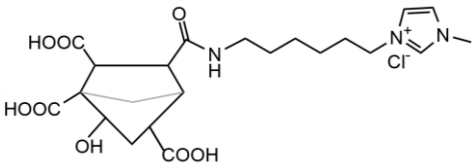

ND4.3a-b

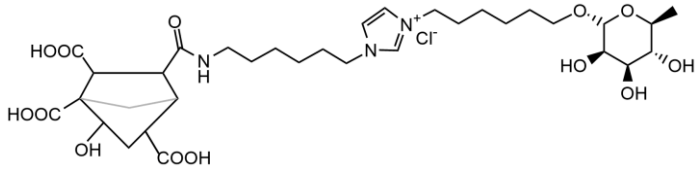

ND4.4

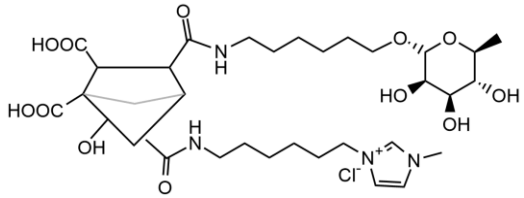

ND4.5

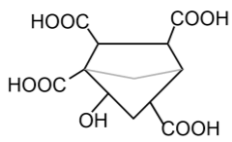

ND4.6a-b

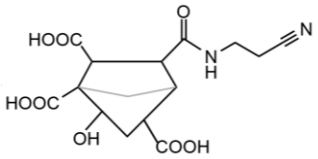

ND4.7

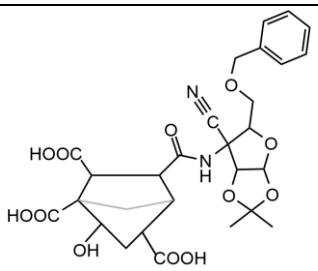

b. Graphene Quantum Dots

GO1-2

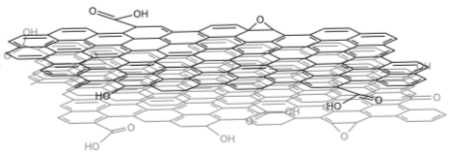

GQD1-3, GQD2.3b, GQD2.4b, GQD2.5b

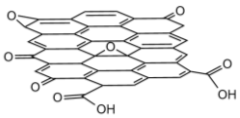

GQD2.1

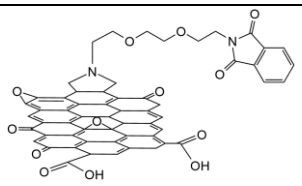

GQD2.2

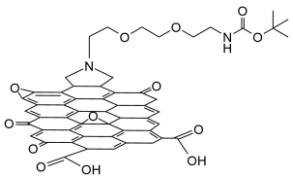

GQD2.3

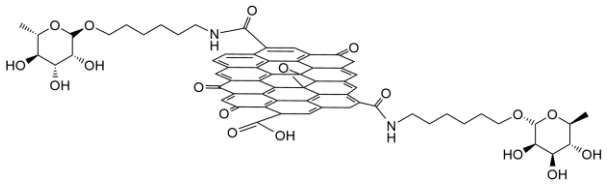

GQD2.4

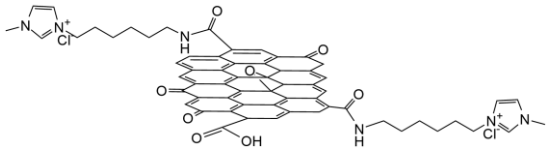

GQD2.5

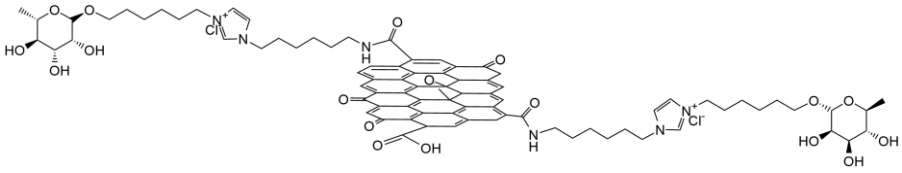

c. Carbon Dots

CD1-4

CD1.1, CD1.1b

CD4.1, CD4.1b

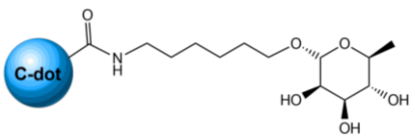

d. Multi-Walled Carbon Nanotubes (MWCNTs)

Pristine MWCNTs

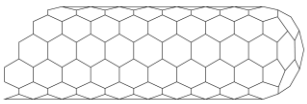

CNT1

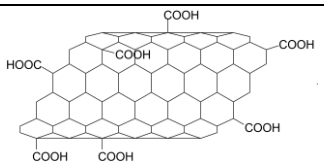

CNT1.1

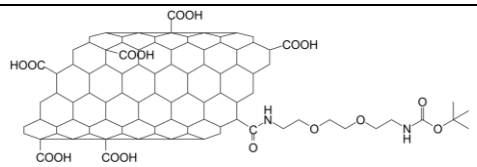

CNT1.1.1

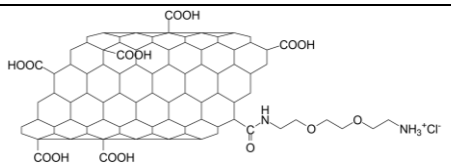

CNT1.1.2

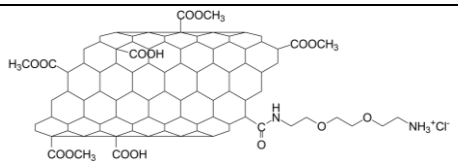

CNT2.a-b

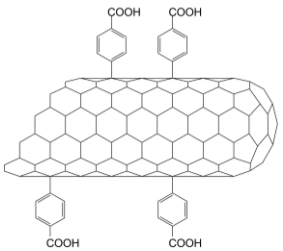

CNT2a.1

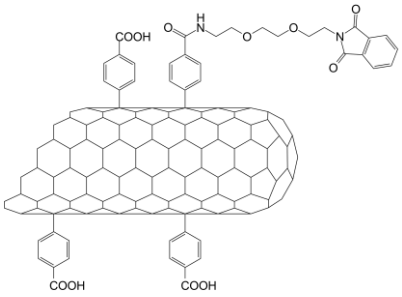

CNT2a.1.1

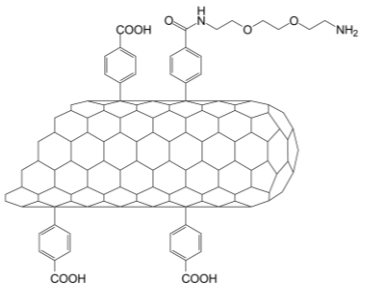

CNT2a.2, CNT2b.1

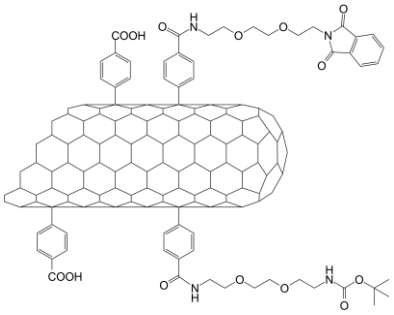

CNT2a.2.1

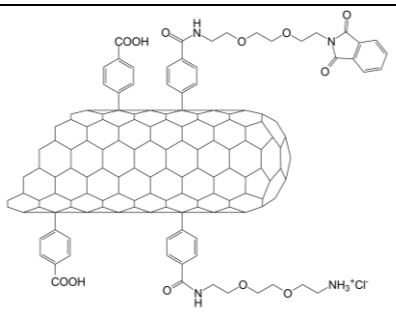

CNT2a.2.2

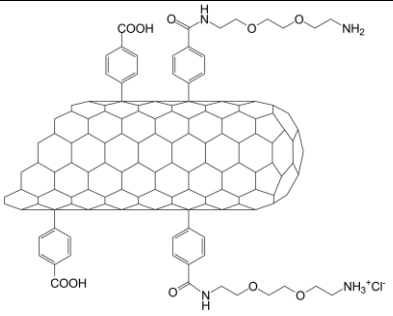

CNT3

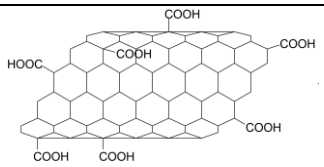

CNT3.1a-b

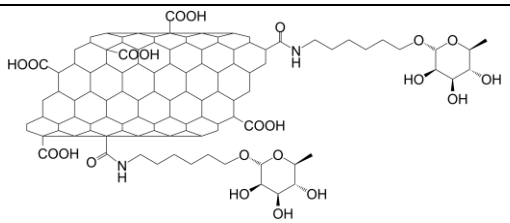

CNT3.2

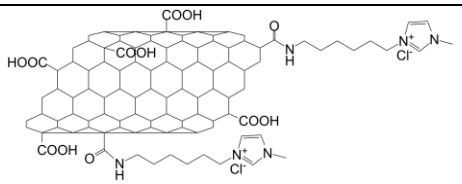

CNT3.3

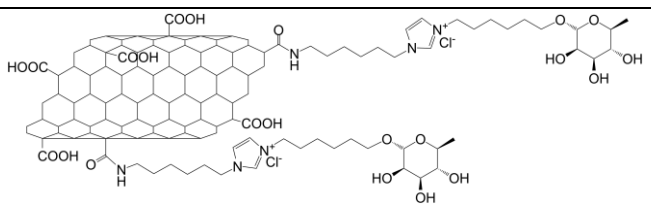

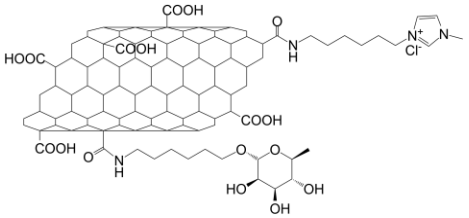

CNT3.4

Abstract

Carbon nanostructures are gaining attention due to their promising properties for a wide range of applications from electrochromic devices to drug nanocarriers. Among the members of carbon nanostructure family, nanodiamonds (NDs), graphene quantum dots (GQDs), carbon dots (CDs) and multi-walled carbon nanotubes (MWCNTs) were used in this research project. Different functionalization reactions were performed on carbon nanostructures and the obtained products were characterized and evaluated. Rhamnose, imidazolium containing ionic liquids, 2-(2-(2-(2-aminoethoxy)ethoxy)ethyl)isoindoline-1,3-dione and tert-butyl (2-(2-(2-aminoethoxy)ethoxy)ethyl)carbamate were some organic molecules used for functionalizations in order to improve the solubility of carbon nanostructures and add different physical, electronic and biological properties.

Despite promising properties, nanodiamonds tend to create big aggregates in aqueous media and this is the main obstacle for biological applications. It was shown that NDs with proper functionalizations can be dispersed in water and create stable dispersions. Thanks to fluorescent labeling with fluorescein isothiocyanate, NDs have been demonstrated to be promising nanocarrier for the delivery of functionalized molecules on their surface. The functionalization reactions of NDs were performed with different methodologies. NDs were demonstrated to be a performance tuning additive in electrochromic devices.

Graphene Quantum Dots were produced with a methodology developed by the research group. Different modifications were performed in order to improve the production. GQDs were functionalized with different organic molecules with different methodologies such as amide bond generation and cycloaddition. It was demonstrated that GQDs have big potential to improve the performance of electrochromic devices.

Carbon dots were produced from natural chitin resources: insect exoskeleton and shell of shrimp. It is shown that CDs produced from these natural and renewable

resources are strongly fluorescent. CDs obtained from the new production methodology were characterized.

Two different types of MWCNTs were functionalized and characterized for the comparison with other carbon nanostructures. The functionalization reactions were optimized in order to obtain high degree of functionalization.

New physical, biological and electronic properties were introduced to carbon nanostructures through various functionalization reactions. Graphene quantum dots and carbon dots were produced by using new methodologies. Characterization studies were performed with different techniques, such as TGA, AFM and Raman spectroscopy. Nanodiamonds were evaluated in human peripheral blood mononuclear cells for biomedical applications. Graphene quantum dots and nanodiamonds were evaluated in electrochromic devices for possible performance improvements.

Riassunto

Le nanostrutture di carbonio stanno ricevendo grande attenzione per le loro promettenti proprietà, grazie alle quali possono trovare una vasta gamma di applicazioni, da dispositivi elettrocromici a nanocarrier di farmaci. Tra i vari membri della famiglia di nanostrutture di carbonio, in questo progetto di ricerca sono stati utilizzati nanodiamonds (ND), graphene quantum dots (GQD), carbon dots (CD) e multi-walled carbon nanotubes (MWCNT). Diverse reazioni di funzionalizzazione sono state eseguite sulle nanostrutture di carbonio e i prodotti ottenuti sono stati caratterizzati e valutati per diverse applicazioni. Ramnosio, liquidi ionici a base di imidazolio, 2-(2-(2-(2-aminoethoxy)ethoxy)ethyl) isoindoline-1,3-dione e tert-butyl(2-(2-(2-aminoethoxy)ethoxy)ethyl)carbamate erano alcune delle molecole organiche utilizzate per le funzionalizzazioni delle nanostrutture di carbonio al fine di migliorarne la solubilità e aggiungere diverse proprietà fisiche, biologiche ed elettroniche.

Nonostante le promettenti proprietà, i nanodiamonds hanno un'alta propensione ad aggregarsi in mezzi acquosi e ciò ne ostacola le applicazioni biologiche. È stato dimostrato che i ND con opportune funzionalizzazioni possono essere dispersi in acqua e formare dispersioni stabili. Grazie all'etichettatura fluorescente con isotiocianato di fluoresceina, i ND hanno dimostrato di essere promettenti nanocarrier per il rilascio di molecole funzionalizzate sulla loro superficie. Le reazioni di funzionalizzazione dei ND sono state eseguite con diverse metodologie. I ND hanno dimostrato di essere un additivo per l'ottimizzazione delle prestazioni nei dispositivi elettrocromici.

I graphene quantum dots sono stati prodotti con una metodologia sviluppata dal gruppo di ricerca. Diverse modifiche sono state apportate per migliorarne la produzione. I GQD sono stati funzionalizzati con diverse molecole organiche, utilizzando diverse metodologie, come la generazione del legame ammidico e la cicloaddizione. È stato dimostrato che i GQD hanno un grande potenziale per migliorare le prestazioni dei dispositivi elettrocromici.

I carbon dots sono stati prodotti da fonti naturali di chitina: esoscheletro di insetti e guscio di gamberetti. È stato dimostrato che i CD prodotti da queste risorse naturali e rinnovabili sono fortemente fluorescenti. I CD ottenuti con questa nuova metodologia di produzione sono stati caratterizzati.

Due diversi tipi di MWCNT sono stati funzionalizzati e caratterizzati per il confronto con altre nanostrutture di carbonio. Le reazioni di funzionalizzazione sono state ottimizzate al fine di ottenere un alto grado di funzionalizzazione.

Nuove proprietà fisiche, biologiche ed elettroniche sono state introdotte nelle nanostrutture del carbonio attraverso varie reazioni di funzionalizzazione. Graphene quantum dots e i carbon dots sono stati prodotti utilizzando nuove metodologie. Gli studi di caratterizzazione sono stati eseguiti mediante diverse tecniche, come TGA, AFM e spettroscopia Raman. I nanodiamonds sono stati valutati in cellule mononucleate del sangue periferico umano per applicazioni biomediche. GQD e ND sono stati valutati in dispositivi elettrocromici per migliorarne le prestazioni.

Table of Content

1 Introduction

As one of the most common elements that exist on Earth, carbon, can be found in nature in its elemental form as graphite, diamond and amorphous. These materials are used by mankind from the ancient times due to their versality. The Neolithic people used charcoal for carving ornaments and later for the reduction of copper, zinc and tin ores. In 1500 BC, the medical uses of charcoal were cited as adsorbent for the bad smell of putrefying wounds and within the intestinal tract in Egyptian papyri. In 18th century, pharmaceutical chemist Carl Wilhelm Scheele studied the adsorption forces for porous carbon and measured the volume of gases adsorbed by the material, later Lowitz studied the decolorification of contaminated tartaric acid solutions, noting the adsorptive properties of charcoal.[1] In 1947, the theory of graphene was explored by theoretical physicist Philip Russell Wallace, investigating the electronic properties of graphite.[2] With the development of theories, production and characterization techniques, fullerenes, carbon nanotubes, nanodiamonds and many more new forms of carbon nanostructures were discovered. From the first technologies to the recent ones, carbon materials were used by mankind with almost all kind of applications.

Materials can be referred as “nanoscaled” when their size ranges from approximately 1 nm to 100 nm. The characteristics of the nanomaterials differ from their bulk counterpart because of their reduced dimensionality and also may differ between different nanoforms of the same chemical substance. The recent advances in nanotechnology are changing the traditional approaches to the material science and have a relevant role in the development and creation of new functional materials, more complex systems and novel devices presenting new properties at the nanoscale. Carbon nanostructures are gaining serious attention due to their promising properties for a broad range of applications from electrochromic devices to drug nanocarriers.

This research project is focused on modifications of Carbon Nanostructures for medical uses and other possible applications in electrochromic devices. For medical applications, biocompatibility is in the key role and can be increased

through the various functionalizations of the carbon nanostructure. Therewithal carbon nanostructure would gain new biological and electronic properties as a consequence of the functionalization.

1.1 Nanodiamonds

Nanodiamonds (NDs) belong to the family of Carbon nanostructures. NDs were first produced by a group of researchers from USSR in July 1963 through the detonation of an explosive called TG-40, a 40/60 blend of 2-methyl-1,3,5-trinitrobenzen (TNT) and 1,3,5-trinitroperhydro-1,3,5-triazine (RDX).[3] They remained unknown to the rest of the world until the discovery of 50 Å sized diamonds in meteorites in 1987.[4] In 1988, the detonation based production of NDs were first published in a Soviet magazine "Reports of the Academy of Science"[5] and Nature magazine[6]. Following these developments, the production of NDs was studied further in order to improve their production and purity.

NDs may seem old carbon nanomaterials as they were discovered many years ago but recently they are gaining popularity with the new developments in nanotechnology.

NDs have a sp^3 diamond core and could have a surface with a mixture of sp^2 and sp^3 hybridized atoms. The possible surface groups of pristine detonation NDs are characterized as ketone, aldehyde, carboxylic acid, ester, anhydride, cyclic ketone, lactone, amine, epoxide, etc. so various surface functionalizations could be performed in order to introduce new biological and electronic properties.[7]

According to the primary particle size, NDs can be classified in three main groups: nanocrystalline diamond particulate (10-100 nm), ultrananocrystalline diamond particulate (0-10 nm), diamondoids (~1 to ~2 nm) (Figure 1.1).[8] Among these types of NDs, ultrananocrystalline diamonds are promising nanomaterials for microelectronics, biotechnology and medical applications (such as targeting and drug delivery). Detonation Nanodiamonds (DNDs, 4-5 nm) are included in Ultrananocrystalline diamond particulates.

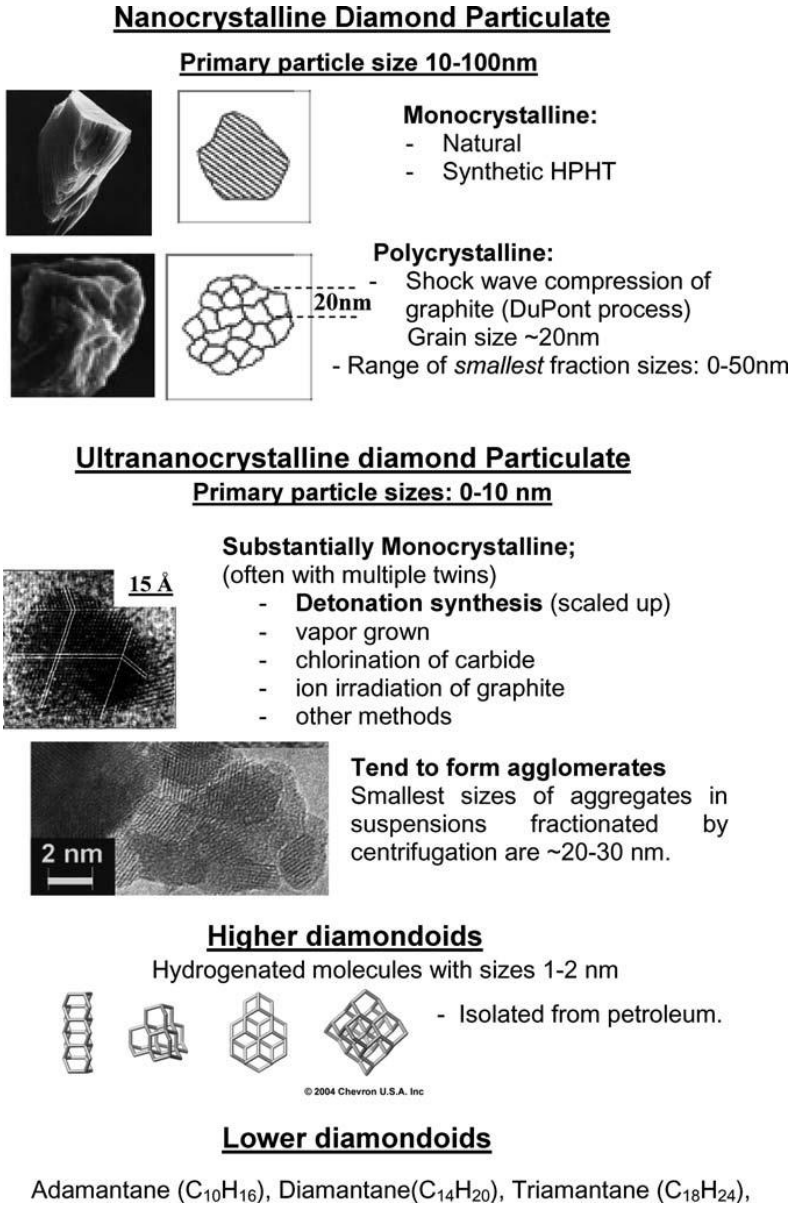

Figure 1.1: Classification of ND particles and molecular forms (diamondoids) according to the primary particle size: nanocrystalline particle, ultrananocrystalline particle, diamondoids. (HPHT: High-pressure high-temperature) Adapted from Ref. 8.

DNDs have some advantages compared to the other types of nanoparticles, such as large scale production, small primary particle size, feasible surface functionalization and, most importantly, biocompatibility.

Nanocrystalline diamonds in monocrystalline form can be found in the nature or can be produced through a process of creating high-pressure high-temperature (HPHT) by duplicating the natural process of diamond forming. Graphite is the stable crystal form of carbon, with 2 kJ mol^{-1} of an enthalpy lower than diamond

at room temperature and atmospheric pressure. Each carbon atom of graphite is bonded to three neighbors in a plane structure. Only at very high pressures carbon forms an allotrope called diamond with each atom bonding to four neighbors. The conditions to form diamond are possible with HPHT technique. The pioneering study on HPHT was done by Percy Williams Bridgman on crystal growth and was honored with the Nobel Prize in 1946.

In this research project, the most popular and promising member of Nanodiamonds family, detonation nanodiamonds were functionalized, characterized and investigated for biological applications and possible applications in electrochromic devices.

1.1.1 Properties and Structure of Nanodiamonds

Diamond is a versatile material in many respects, and nanodiamond carries most of the superior properties of bulk diamond to nanoscale. These properties are superior hardness, large specific surface area, optical properties and fluorescence (for NDs with nitrogen–vacancy centres, see later), high thermal conductivity and electrical resistivity, chemical stability, and resistance to harsh environments. Specific surface area of ND particles with 4 nm and 30 nm in diameter are 428 m^2/g and 57 m^2/g, respectively, making significant differences in adsorbing and loading capacity of the functionalization on the surface of the nanodiamonds.[9]

Nanodiamonds can be described as a crystalline diamond core with a perfect diamond lattice surrounded by a surface with a combination of sp^2/sp^3 bonds and different groups depending on the synthesis, modification or purification methodologies. ND particles have primary particle sizes ranging between approximately 2 and 20 nm, and tend to form agglomerates into larger structures. It is estimated that a single 4 nm detonation nanodiamond consists of ~10^4 carbon atoms and several hundred atoms (mostly oxygenated moieties) which are dispersed on the single detonation nanodiamond surface (Figure 1.2).[10]

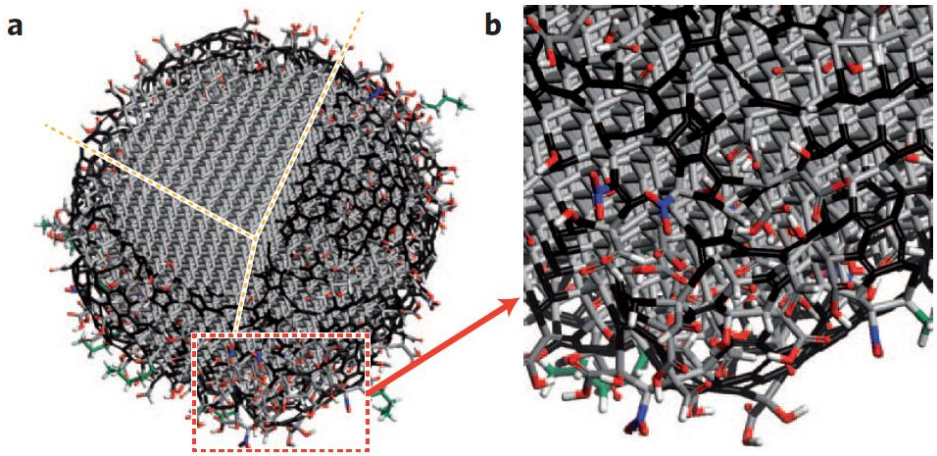

Figure 1.2: Structural simulation of single nanodiamond particle: **a)** The schematic model illustrates the structure of a detonation nanodiamond after oxidative purification. As it is shown ND has a diamond core that is covered with a layer of surface functional groups. **b)** Large number of the surface groups are terminated with oxygen-containing groups (oxygen atoms: red, nitrogen atoms: blue). Some hydrocarbon chains (green) and hydrogen terminations (hydrogen atoms: white) are also shown. Adapted from Ref. 7.

Majority of the carbon atoms are located in the bulk diamond like sp^3 hybridized carbon core.[11] Two widely accepted models for the outer shell include bucky diamond with sp^2 hybridized fullerene shell, and amorphous carbon containing both sp^2 and sp^3 hybridized carbon atoms.[12] For a particle size between 3.5 - 4.5 nm, the size of diamond core is estimated as 3 nm with the transition region consisting of 2 - 4 layers (0.8 - 1.2 nm).[9] The surface layer is covered with a large variety of functional groups. As mentioned the most commonly found functional groups are oxygen containing groups and some nitrogen containing groups.[13]

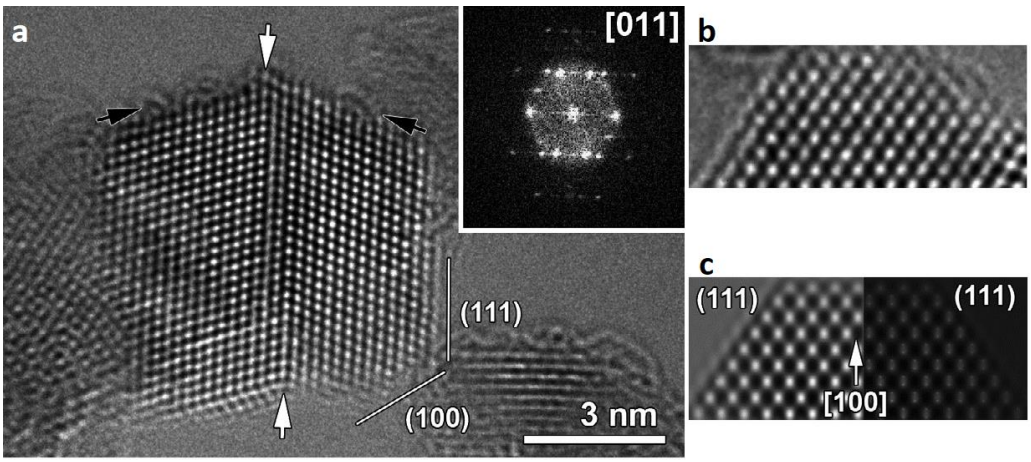

Figure 1.3: High Resolution TEM image of a detonation nanodiamond **a)** The surfaces with low amount of graphitic material **b)** Enlarged image of the (100) truncation right bottom in Image a. **c)** Image simulation performed for C_s = 15 µm, Δf = −4 nm, the right-hand side has the projected potential overlaid, demonstrating the white image contrast peaks at the atomic positions. Adapted from Ref. 11.

Nanodiamonds can show very diverse morphologies at the nanoscale. The surface structure of nanodiamonds depends on their size, shape, and surface groups. Three major low index diamond facets found on the surfaces of natural and synthetic diamonds are (100), (110), and (111), where (111) and (100) facets are the most common (Figure 1.3). The best mathematical description for the nanodiamond structure fits truncated octahedral shape which is bounded to 76% by the (111) faces, and to 24%, by the (100) surfaces.[14] The structure and stability of truncated octahedral ND particle and the effect of functionalization are studied using a quantum mechanics based multiscale method.[15] The surface atoms of a crystal are assumed a different structure than that of the bulk material and the rearrangement of the positions of the top-most atoms are necessary to yield a more energetically favorable configuration. As a result, surface reconstruction occurs and it is important for the understanding of surface chemistry for various materials, especially in the case where another material is adsorbed onto the surface. (1 × 1) means that the average lateral periodicity of the surface atoms is the same as the bulk. Pairs of surface atoms come together to form surface dimers, leaving only one dangling bond per carbon atom. This process leads to a change in the surface periodicity: the period of the surface structure is doubled in one direction and this is so-called (2 x 1) reconstruction. The (100) surface of a nanodiamond experiences (2 × 1) reconstruction to minimize the energy (Figure 1.4). In case of functionalization with carbonyl groups, it is preferred over reconstruction in the (100) surface and retains their diamond-lattice ordered state, and subsequently graphitization occurs on the (111) surface since the (111) surface atoms are delaminated from the core atoms.[9, 15]

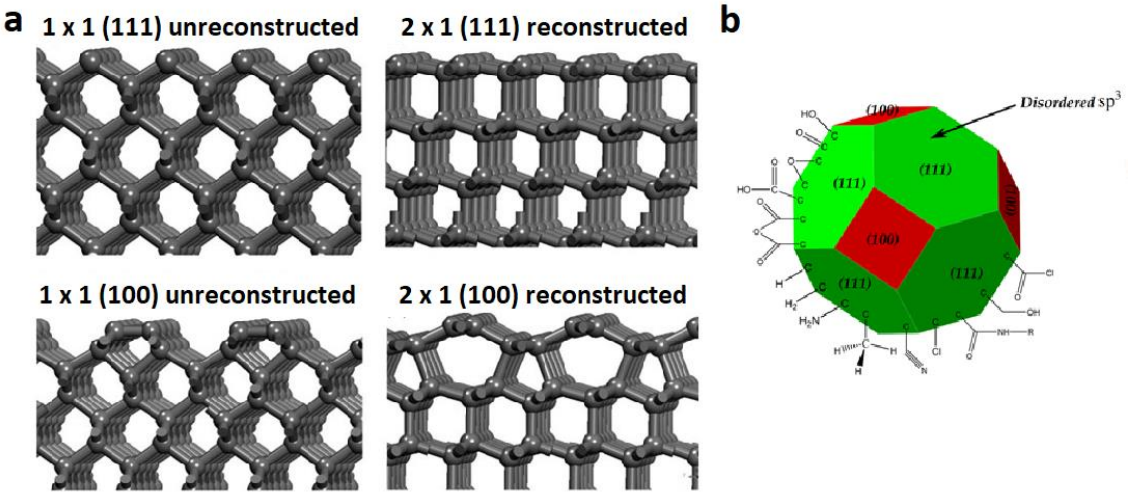

Figure 1.4: Illustration of the structure of diamond surface terminated along (111) and (100) surfaces, and surface groups **a)** The 1 x 1 (111) and (100) surfaces terminating the bulk diamond are reconstructed to structures with lower energies, the 2 x 1 surfaces with a pi-chain structure for the (111) and pi-bonded dimers for the (100) surface[16] **b)** Schematic model of detonation ND structure like a truncated octahedron. The (100) faces have reconstructed surface, and the (111) ones can be either covered by the above functional groups or feature a fullerene-like form. On the (111) faces of detonation NDs, different functional groups are attached, such as the hydroxyl, carboxyl, epoxy, anhydride, methylene and lactones.[9, 17] Scheme a is adapted from Ref. 16. Scheme b is adapted from Ref. 9, 17.

1.1.2 Synthesis of Detonation Nanodiamonds

As it was already mentioned, nanodiamonds were produced for the first time by a group of Soviet researchers in 1963. The starting materials for the synthesis of detonation nanodiamonds are generally explosives with negative oxygen balance, 40/60 blend of TNT and RDX.[18] Explosives with negative oxygen balance contain insufficient oxygen to convert all its carbon to carbon dioxide, all its hydrogen to water, and all its metal to metal oxide. The reaction is performed in a closed metallic chamber in an atmosphere of N_2, CO_2 and liquid or solid H_2O.[7] The detonator produces a shock wave, the composition mixture gets compressed and heated, and the explosion of the TNT-RDX blend occurs.[19] The resulting high pressure and temperature lead the carbon atoms of the explosives to form liquid nanodroplets around 1 - 2 nm. The diagram (b) on Figure 1.5 shows that the most stable phase of carbon is graphite at low pressures, and diamond at high pressures, with both phases melting point above 4500 K. As temperature and pressure decrease along the isentrope (red line), carbon atoms condense into nanodroplets. These droplets form larger droplets and crystallize as the

pressure and temperature decrease more (Figure 1.5).[20] When the crystallization is over, diamond-containing soot is collected from the bottom and the walls of the explosion chamber.

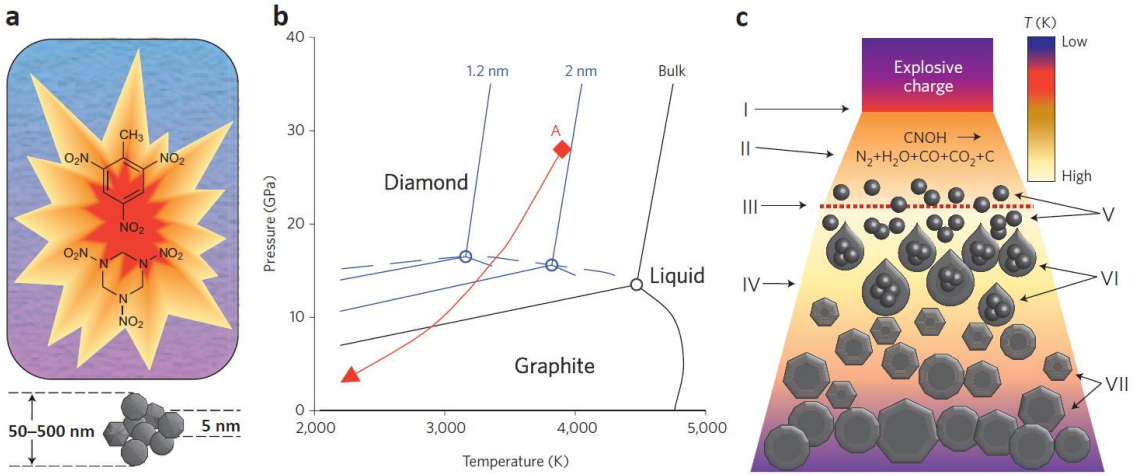

Figure 1.5: Synthesis of DNDs. a) For the synthesis of nanodiamonds, explosives with a negative oxygen balance (a mix of 60 wt.% TNT and 40 wt.% hexogen) are detonated. The collected soot after the explosion contains 50 - 500 nm agglomerates of detonation nanodiamonds with primary particle size of 4 - 5 nm. b) Phase diagram of bulk diamond and nanoscale carbon c) Illustration of the detonation wave propagation: (I) the front of the shock wave; (II) the chemical reaction zone where the explosive molecules decompose; (III) the Chapman–Jouguet plane (Point A in scheme b, when reaction and energy release are essentially complete); (IV) the expanding detonation products; (V) the formation of carbon nanoclusters; (VI) the coagulation of nanoclusters into liquid nanodroplets; and (VII) the crystallization and growth of nanodiamonds.[7, 20] Adapted from Ref. 7.

The primary particle size (4 - 5 nm) of nanodiamonds produced by the detonation technique is compatible for the medical applications but this requires high standard of purity, therefore purification process could be necessary. The collected detonation soot contains both graphite-like structures (25 - 55 wt.%) and impurities (metals and metal oxides: 1 - 8 wt.%). The detonator and the walls of the detonation chamber cause the unavoidable metal impurities. After the purification steps, detonation nanodiamonds can be considered a material containing different forms of carbon (80 - 89%), nitrogen (2 - 3%), hydrogen (0.5 - 1.5%), oxygen (up to 10%) and an incombustible residue (0.5 - 8%).[19] The carbon phase is a mixture of diamond (90–99%) and non-diamond carbon (1 - 10%).

Classical purification methodologies based upon the use of liquid oxidizers for the removal of metallic impurities are performed with sulfuric acid, sulfonitric

mixture, hydrochloric acid, potassium dichromate in sulfuric acid etc.[9] In order to oxidize and remove the sp^2 carbons, KOH/KNO_3, Na_2O_2, CrO_3/H_2SO_4, HNO_3/H_2O_2 under pressure, mixtures of concentrated sulfuric and perchloric acids are included to the purification processes.[9, 19, 21] The majority of detonation nanodiamonds vendors perform purification with strong liquid oxidizers at elevated temperatures and pressures. However, liquid phase purification is detrimental to the environment, hazardous and costly.

On the other hand, non-diamond carbon can effectively be eliminated in a more ecofriendly way by a gas phase treatment using ozone at high temperatures. The non-diamond part of the detonation synthesis reacts with ozone at the high temperature and is converted to CO_2 or CO. In this way, the surface of DNDs is depleted of non-diamond carbon by-products and enriched with oxygen-containing functional groups.[9]

1.1.3 Surface Functionalizations of Detonation Nanodiamonds

Comparing to the other nanodiamonds, DNDs have larger functionalization capacity due to their large specific surface area. Their surface contains various groups including carboxylic acids, esters, ethers, lactones, ketones, alcohol, anhydride, amine, nitro, alkene, lactone etc. (Figure 1.6),[7, 22] but these may vary depending on the purification process. However, thanks to large variety of surface groups, different functionalizations could be performed (Figure 1.6).

It is possible to perform modifications with good control over the functionalization but this requires well-purified NDs with only one kind of functional group on their surface.

Nanodiamonds with carboxylic groups (ND–COOH) are a common starting material for this purpose and they are prepared by acid or ozone purification treatment. Their surface modifications can be performed with high temperature gas treatments or room temperature wet chemistry methods. Gas treatment in H_2 reduces C=O to C–O–H and eventually at higher temperatures or with longer hydrogenation times forms C–H groups. It is possible to remove the functional

groups and convert the nanodiamond into graphitic carbon nano-onion by annealing in N_2, Ar or vacuum (Figure 1.6).[7]

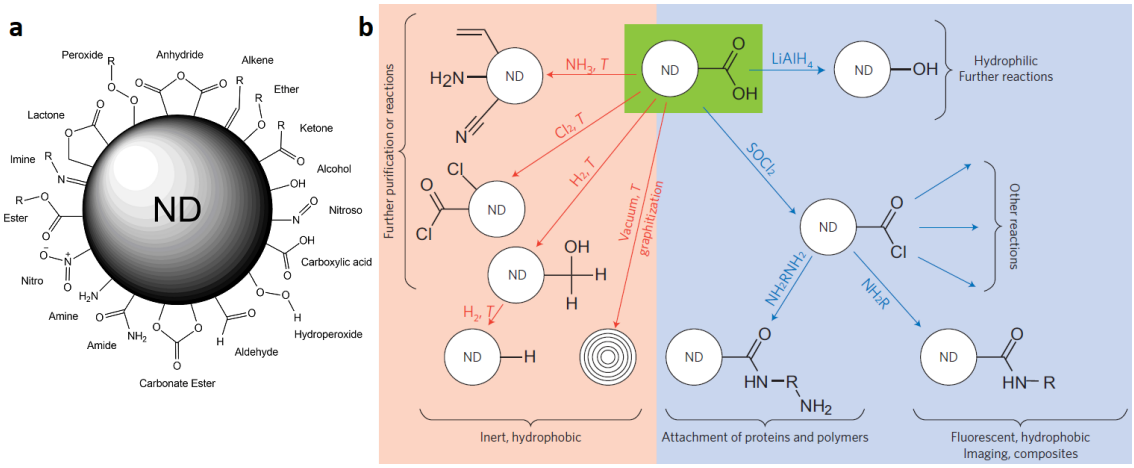

Figure 1.6: Schematics of surface groups and surface modifications of detonation nanodiamonds. **a)** Various functional groups on the surface of pristine detonation nanodiamonds **b)** Surface modifications of ND–COOH (green) with high temperature gas treatments (red) or ambient temperature wet chemistry techniques (blue). Scheme a is adapted from Ref. 9. Scheme b is adapted from Ref. 7.

Many different surface groups can be attached on nanodiamonds using wet chemistry methods and a variety of molecules with valuable properties (biological, fluorescence etc.) can be introduced by the generation of amide bond via covalent conjugation of amines on ND–COOH through the intermediate formation of active esters by means of 1-ethyl-3-(3-dimethylaminopropyl) carbodiimide (EDC) or N-hydroxysuccinimide (NHS).[23-26] These reaction conditions are suitable for covalent conjugation of delicate molecules such as DNA and proteins to NDs via amide bond.[27]

Polyethylene glycol (PEG) functionalized NDs can be obtained using amino terminated PEG. The PEG shell is biocompatible and prevents the adsorption of proteins, amino acids, and salts on the nanoparticle surface.[28-29] It is possible to perform further functionalization of ND-PEGs with various molecules in case of the functionalization of NDs with double functionalized PEG chains.[30]

1.1.4 Applications of Detonation Nanodiamonds

Nanodiamonds are chemically and physically stable nanomaterials, but their surface can be chemically modified for various purposes. They present some properties of bulk diamond (high Young's modulus and mechanical strength, high thermal conductivity), but also better characteristics: good dispersibility, high adsorption ability, solid lubricating ability and biocompatibility.[31-34]

More specifically DNDs may be used for a broad range of applications such as mechanical applications, electrochemical applications and medical purposes, either alone or mostly functionalized as they usually do not interfere with the activity of bound molecules. A potential pharmaceutical use of nanodiamonds is for detoxification as enterosorbent, due to their high biocompatibility, small size, large surface area, surface chemistry and inexpensive production.[35-36] Enterosorbent compounds bind toxins in the gastrointestinal tract and reduce the bioavailability of the toxin.

Nanodiamond based drug delivery systems have been widely explored for a broad variety of compounds ranging from small molecules to proteins and nucleic acids. Their properties attractive for drug delivery applications include a large carrier capacity and versatility, various surface functional groups, which can be modified to ensure a good drug binding with a covalent or non covalent approach, and drug accumulation at the targeted site, together with the already mentioned biocompatibility, The disadvantages of conventional antitumoral drugs are generally non-specificity, severe side effects, burst release and damaging the normal cells. To give an example, the systemic toxicity of doxorubicin can lead to significant side effects including myelosuppression, cardiotoxicity, superinfections, as well as mortality.[37-38] By the coupling of nanodiamonds with this kind of drugs, it is possible to improve bioavailability and therapeutic efficiency while providing specific targeting.

The studies with doxorubicin functionalized nanodiamond complexes demonstrated improvements against chemoresistance and enhanced chemotherapy efficacy and safety in cancer treatment.[39-41] Figure 1.7 shows how

nanodiamond mediated doxorubicin therapy inhibits tumor growth better than conventional therapy in doxorubicin resistant 4T1 tumor model.[39]

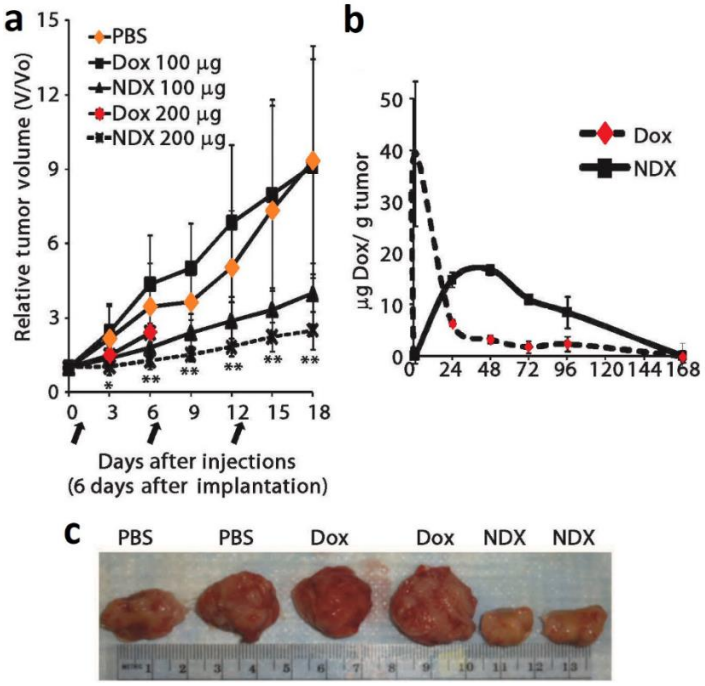

Figure 1.7: Comparison of nanodiamond mediated doxorubicin (NDX) delivery and conventional doxorubicin (Dox) delivery. 4T1 cells (5×10^6) injected mice. **a)** Treatment with phosphate-buffered saline (PBS) (n = 18), Dox (100 µg) (n = 18), Dox functionalized NDs (NDX) (100 µg of Dox equivalent) (n = 18), Dox (200 µg) (n = 10), or NDX (200 µg of Dox equivalent) (n = 10) by tail vein injection. **b)** Tumor retention analysis of treatments with Dox (200 µg) (n =4) and NDX (200 µg of Dox equivalent) (n = 4). **c)** Representative images of excised tumors from treated mice. Adapted from Ref. 39.

Lower dosage of doxorubicin (100 µg) did not affect tumor growth comparing to untreated mice. Higher doxorubicin dosage (200 µg) showed some effect on tumor growth (Figure 1.7, a) with high toxicity for the mice and none of them survived beyond day 15. Treatment with doxorubicin functionalized nanodiamond ensured longer retention in 4T1 tumors compared to unmodified doxorubicin and cleared from tumors by day 7 (Figure 1.7, b). NDX administration results in markedly reduced tumor sizes (Figure 1.7, c).[39]

Nanodiamond monolayers are also promising materials for tissue engineering and regenerative medicine. It is shown that they can be effective neuronal growth platform similar to protein-coated materials.[42]

The core of detonation nanodiamonds are electrically insulating but with the proper modifications on the surface, they can gain attractive properties for electronical, electrochemical and optoelectronic applications.[43-45] Boron-doped diamond electrodes can be used for the electrochemical detection of nucleic acids, including double stranded DNA, in aqueous solution using amperometric methodologies.[44]

Moreover NDs can be luminescent if defects induced by proton beam irradiation or by different methodologies are present in their core and this property allow new possible applications in electronics and optoelectronics. The energy treatment creates nitrogen-vacancy defect centers on nanodiamonds.[45-46]

1.2 Graphene Quantum Dots (GQDs)

Graphene is a one-atom thick two-dimensional crystal of carbon atoms. Theoretical physicist Philip Russell Wallace explained the properties of a single layer graphene, investigating the electronic properties of graphite in 1947.[2] The Nobel prize winning research on Graphene by Geim and Novoselov attracted great interest on graphene and graphene-based materials.[47] The isolation of a single layer of graphene, the studies on its excellent conductivity and optical properties boosted the research activities in this field and brought forward novel applications for graphene and its derivatives.[47-50]

In recent years, promising derivatives of graphene, Graphene Quantum Dots (GQDs), have gained significant interest due to their potential for biomedical and electrochemical applications. GQDs are zero-dimensional small fragments of graphene in the size range generally below 20 nm diameter.[51] Intrinsically, graphene is a zero-energy band-gap material but band-gap can be opened by size reduction and introduction of defects into the graphene moiety, and this leads strong photoluminescence that normally is not present in semi-conducting graphene.[52-55] The property of band-gap in GQDs arises from quantum confinement effects.[56]

1.2.1 Properties and Structure of GQDs

GQDs basically combine the structure of graphene with the quantum confinement and edge effects of CDs and possess unique properties, which are important for the applications in medicine, electronic, photoluminescence, electrochemical and electrochemiluminescence.[57-60]

GQDs mostly consist of 1 - 3 layers of graphene flakes with the diameter of less than 20 nm (Figure 1.9).[61-63] The surface groups of GQDs may vary due to the synthetic methodology, and photoluminescence peak of GQDs may shift depending on the surface functionalization.[64-66]

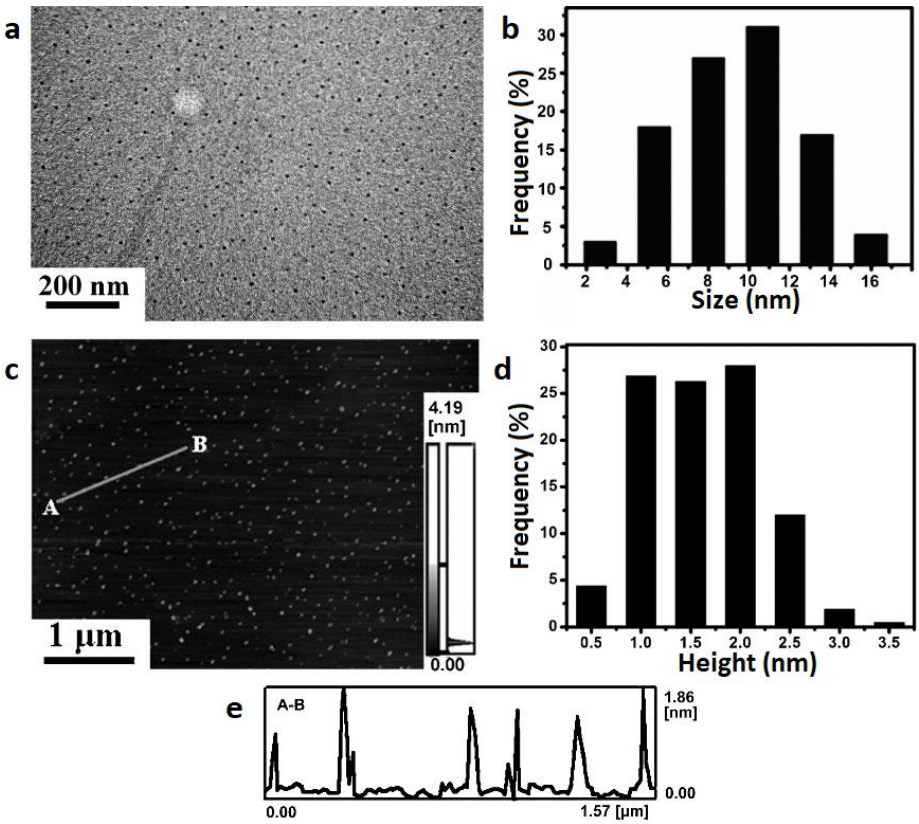

Figure 1.9: TEM and AFM images of GQDs with size and height frequency. **a)** TEM image of GQDs **b)** Diameter distribution of GQDs **c)** AFM image of GQDs **d)** Height distribution of GQDs **e)** Height profile along the line A–B in image c. Adapted from Ref. 61.

Characterization of the edge structure (zigzag and armchair edges) in graphene is important to understand the properties of GQDs (Figure 1.10).[53] It has been reported that zigzag edges introduces new electronic and magnetic properties to graphene.[67]

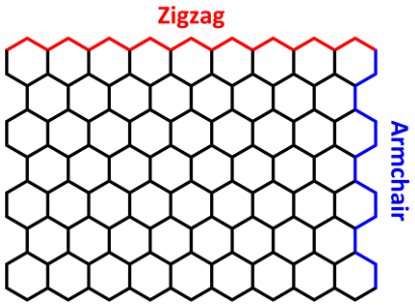

Figure 1.10: Schematic illustration of two possible edge termination of GQDs

It is shown that for GQDs with a diameter less than 100 nm, quantum confinement effect starts playing a role.[68] As a result, GQDs have a non-zero band-gap and

luminesce on excitation. This band-gap is tunable by modifying the size and surface chemistry of the GQDs.[69] The absorption spectra of GQDs show a noteworthy peak around 228 nm, which has been assigned to the π → π* excitation of the π bonds.[70] GQDs can contain functional groups which introduce different absorption features and affect their photoluminescence,[69] and their reported photoluminescence quantum yields vary significantly depending on doping, functionalization or size. The main difference between GQD and semiconductor quantum dot (QD) photoluminescence is that the bandwidth is wider in GQDs and that the photoluminescence peak shifts to longer wavelengths and decreases with increasing excitation wavelength (Figure 1.11).[61]

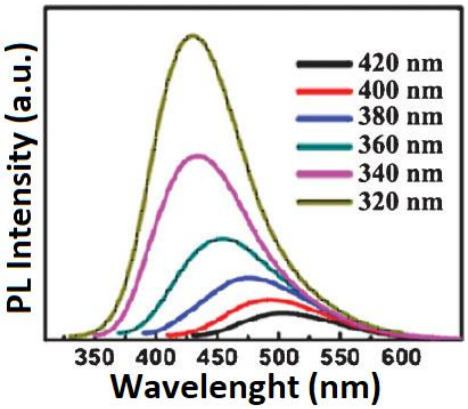

Figure 1.11: Photoluminescence spectra of the GQDs at different excitation wavelengths. Adapted from Ref. 61.

Thanks to the edge effects, the quantum confinement and the unique bulk properties of graphene and the possible functionalization,[71] GQDs have very advantageous properties for a great range of applications.

1.2.2 Synthesis of GQDs

GQD production methodologies can be classified into two broad categories, top-down and bottom-up methods. The first include the decomposition and exfoliation of bulk graphene-based materials, most commonly graphite. Top-down synthesis generally has multiple steps with concentrated acids, strong oxidizers and high temperatures. For the bottom-up methods, GQDs can be synthesized from polycyclic aromatic compounds. A larger number of publications on GQDs are

based on the top-down method however these approaches have low yield and produce GQDs with less uniform morphologies. Bottom-up approaches use more difficult chemical methodologies but it is possible to produce smaller and more uniform GQDs.[55, 72]

The first step of top-down approaches is usually the synthesis of graphite oxide or graphene oxide sheets from the starting bulk material by a modified Hummers method.[73] The second step has different methodologies to obtain graphene quantum dots from graphite oxide sheets, as hydrothermal cutting[61, 69, 74-75], electrochemical cutting[63, 76], solvothermal cutting[65], nanolithography[68], microwave-assisted cutting[70], nanotomy-based production[77], ultrasonic shearing[78], oxidation of carbon nanotubes[79], and carbon fiber[62] and others.

Hydrothermal cutting generally includes sonication with sulfonitric acid mixture at different temperatures. It is reported that GQDs produced by this methodology can have dimension of 5 – 13 nm and different photoluminescence (blue, green),[61, 69, 74, 80] but with proper surface modifications, it can shift through the red regions.[69] By the hydrothermal treatment, Graphene Sheets (GSs) are cut in GQDs with a sort of unzipping mechanism (Figure 1.12, scheme a).

With the pH change, photoluminescence intensity of GQDs varies reversibly (Figure 1.13).[80] This phenomenon can be due to the fact that the free zigzag sites of the GQDs are protonated with acidic conditions and the emissive triple carbene which is active photoluminescence state forms a reversible complex between the zigzag sites and H^+. Thus, photoluminescence disappears. Under alkaline conditions, the free zigzag sites are restored and photoluminescence activity reappears (Figure 1.12, scheme b).[61]

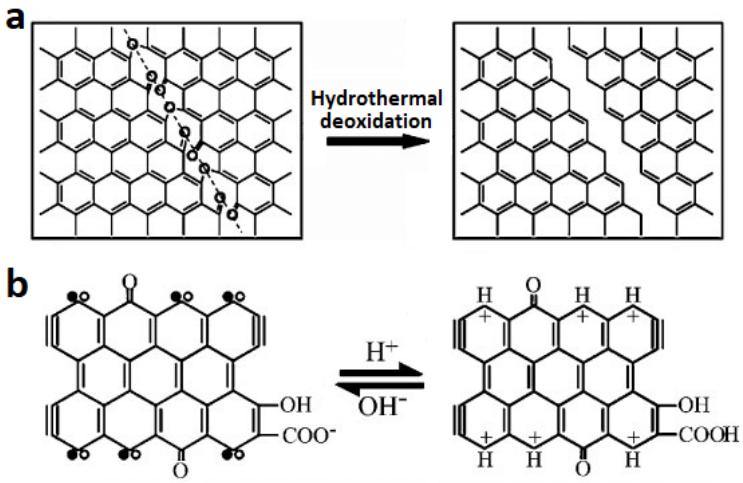

Figure 1.12: Hydrothermal cutting of oxidized Graphene sheets into GQDs **a)** Mechanism of hydrothermal cutting **b)** Illustration of the GQDs in alkali (left) and acid (right) media. Adapted from Ref. 61.

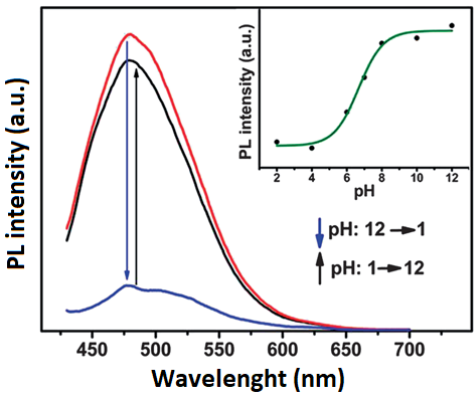

Figure 1.13: pH-dependent photoluminescence (PL) spectra when pH is switched between 12 and 1; inset: dependence of PL intensity on pH varied from 12 to 2. Adapted from Ref. 80.

Electrochemical cutting can provide water-soluble and uniform sized GQDs with strong yellow emission at room temperature in high yield.[76] The low temperature hydrazine reduction step produces hydrazide groups on the particle surface since the reducing ability of hydrazine is limited at ambient temperature. Thus, hydrazine reduces the epoxide and hydroxyl groups, and amidation may occur between hydrazine and carboxylic groups at the edge of GQD. This causes the formation of hydrazide and phthalhydrazide groups (Figure 1.14).

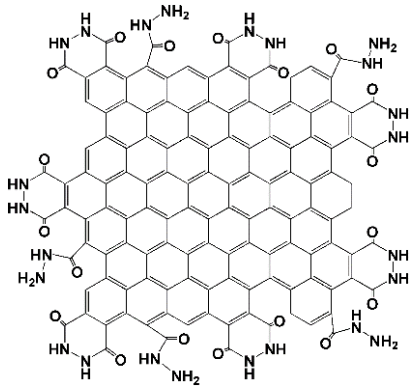

Figure 1.14: Illustration of the edge modified GQD structure determined by theoretical calculation. Adapted from Ref. 76.

Bottom-up approaches are focused on producing GQDs from small molecules and generally derive from stepwise solution chemistry, obtaining GQDs in colloidal forms. With this approach it is possible to produce graphene quantum dots with more uniform size and predefined shape comparing to the top-down methodologies.

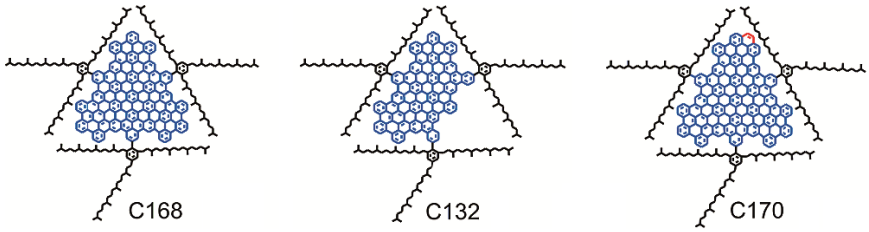

Figure 1.15: Illustration of graphene moieties containing 168, 132, and 170 conjugated carbon atoms. Adapted from Ref. 72.

Large colloidal quantum dots were produced through a step-wise organic synthesis by Yan *et al*.[72, 81] The GQDs were made up of 168, 132, and 137 conjugated carbons produced by oxidation of polyphenylene dendritic precursors (Figure 1.15) and stabilized by 2′,4′,6′-trialkyl phenyl groups. Bigger size of the quantum dot seems to cause greater inter-graphene attraction with consequent stacking, so the trialkyl phenyl groups were attached to GQDs to prevent this phenomenon.

1.2.3 Surface Functionalizations of GQDs

The synthesis of GQDs may already add different functional groups on the graphene-like surface depending on the chosen preparation. GQDs can be functionalized to adjust biocompatibility, photoluminescence, electronic properties, or optical properties. The intended modifications can be performed with the GQD production using pre-treated starting materials or proper conditions, or as post-production modifications.

The synthesis of nitrogen-doped graphene quantum dots was performed by cutting nitrogen-doped graphene with hydrothermal method.[82] The so obtained N-doped GQDs have a N/C atomic ratio of ca. 5.6% and diameter of 1 - 7 nm and show strong blue photoluminescence and upconversion photoluminescence properties. Analogously, fluorinated GQDs, with a F/C atomic ratio of ca. 23.68% and diameter of 1 - 7 nm, can be produced from fluorinated graphene as modified starting material by hydrothermally cutting method.[83] It was shown that fluorination changes the optoelectronic properties of GQDs, upconverts photoluminescence and alters electronic properties similarly to the effect of GQD nitrogen doping. The optical properties of solvothermally synthesized GQDs are tunable by the degree of surface oxidation, which brings fine solubility, high stability and upconversion photoluminescence,[65] and photoluminescence quantum yields can increase from 4.1% to 12.2% with the increase of surface oxidation.

With a simple electrochemical approach, it is possible to produce luminescent and electrocatalytically active nitrogen doped GQDs with oxygen-rich functional groups from reduced graphene oxide by using tetrabutyl ammonium perchlorate (TBAP) in acetonitrile as the electrolyte to introduce N atoms on the surface of GQDs.[64] The so produced GQDs present a N/C atomic ratio of ca. 4.3%, has blue luminescence and possess electrocatalytic activity.

After the production of GQDs, the usual functionalization is performed through the generation of amide bond via covalent conjugation of amines to the carboxyl groups of graphene quantum dots.[84] Wolk *et al.* used to activate of the carboxylic function with oxalyl chloride treatment (Figure 1.16), followed by the addition of

dodecyl amine. These modified GQDs showed excellent solubility in various organic solvents.

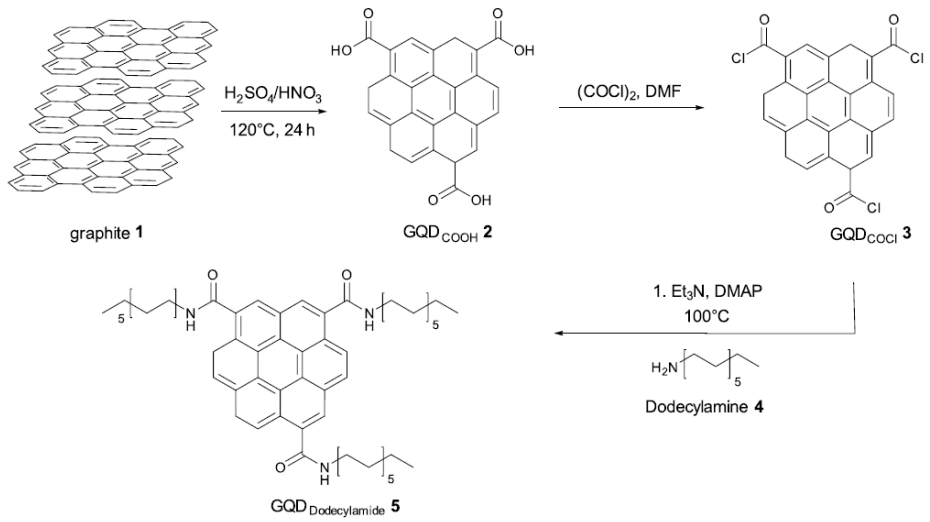

Figure 1.16: Synthesis of covalent functionalized GQDs with dodecyl amine. Adapted from Ref. 84.

Li *et al.* synthesized folic acid functionalized graphene quantum dots loaded with IR780.[85] The preparation took place by mixing folic acid, EDC, NHS and GQDs in aqueous solution saturated with $NaHCO_3$. Thus, folic acid was covalently attached to the surface of GQD. The next step was the mixture with IR780 at different concentrations and the latter was linked via strong π-π stacking interactions. The obtained complex presented improved photostability, enhanced tumor targeting ability and very high photothermal conversion efficiency (87.9%).

1.2.4 Applications of GQDs

GQDs have potential applications in biomedical, optoelectronic, and energy-related fields especially thanks to their properties such as water solubility and luminescence, which make them excellent candidates for bioimaging and drug delivery.

Kuo *et al.* synthesized GQDs with size of approximately 7.1 nm to use them in two-photon photodynamic therapy and simultaneous three-dimensional two-photon bioimaging, especially on multidrug-resistant bacteria. The GQDs

demonstrated to be photosensitizer with high two-photon absorption in the near IR region, a large absolute cross section of two-photon excitation, strong two-photon luminescence, and impressive two-photon stability. They were coated with two different antibodies Ab_{LPS} and $Ab_{protein\ A}$, in order to enhance the specificity and efficiency against Gram-negative *E. coli* and Gram-positive MRSA, respectively. To obtain maximum bactericidal activity, the relative maximum at 800 nm was chosen (Figure 1.17, a). It is shown that GQDs have highly effective photodynamic therapy against both Gram-positive and Gram-negative bacteria, thanks to the generation of reactive oxygen species with two-photon excitation with ultralow energy and in short photoexcitation time (Figure 1.17, b, c).[86]

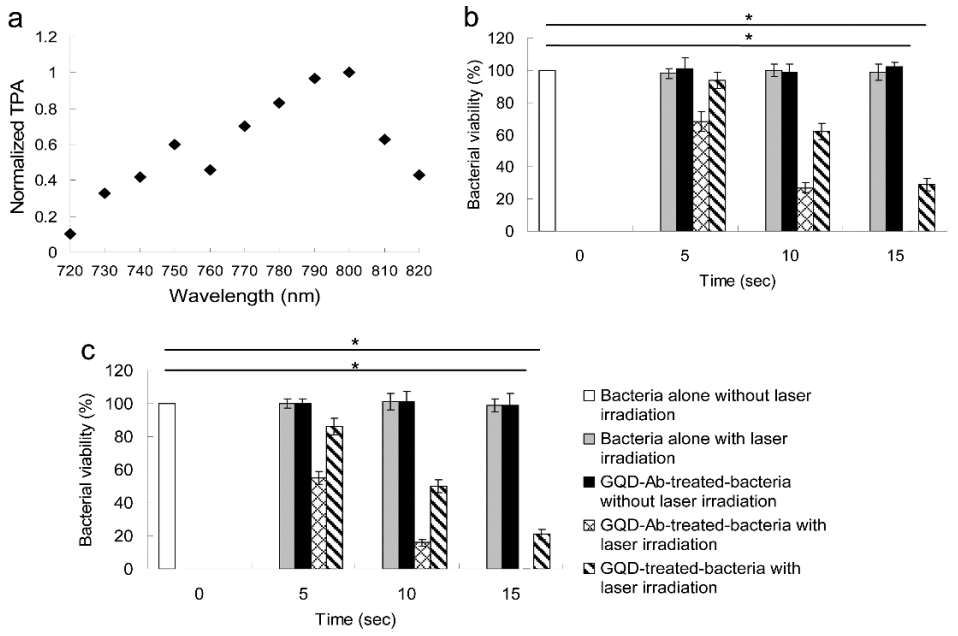

Figure 1.17: a) Relative two-photon absorption spectra of the GQDs with the two-photon excitation wavelength range of 720−820 nm. **b)** GQD-Ab_{LPS}-treated-*E. coli* and **c)** GQD-$Ab_{protein\ A}$-treated-MRSA, through CFU assay in different photoexcitation times with two-photon excitation at 800 nm. Adapted from Ref. 86.

Li *et al.* were able to synthesized GQDs with a size range of 2 - 8 nm, from the pyrolysis of maleic acid and folic acid in order to produce novel agents for cancer cell imaging and optical detection of Hg^{2+}.[87] The resulting folic acid functionalized GQDs display a strong and tunable fluorescence emission under visible light excitation. They could tune the fluorescence properties by changing the folic acid ratio in the pyrolysis process. Because of high number of folic acid groups, good

lipid-solubility and red fluorescence emission, the graphene quantum dots as turn-on fluorescent probe are suitable for cancer cell imaging. The resolution of cell imaging is improved by these GQDs since the red light has better biological tissue penetration and less back spectrum interference compared with blue light. Folic acid functionalized GQDs could be easily internalized by the HepG2 cells, human cervical epithelioid carcinoma with an over-expressing folate receptor on the cell membranes. In the same study, it is shown that the graphene quantum dots can react with Hg^{2+} and therefore a sensitive fluorescence quenching occurs, providing sensitivity and selectivity among all tested metal and nonmetallic ions.

Hwang *et al*. blended an electrochromic methyl viologen (MV^{2+}) (N, N′-dimethyl-4,4′-bipyridinium) with GQDs in order to increase the performance of Electrolyte-Free Flexible Electrochromic Device .[88]

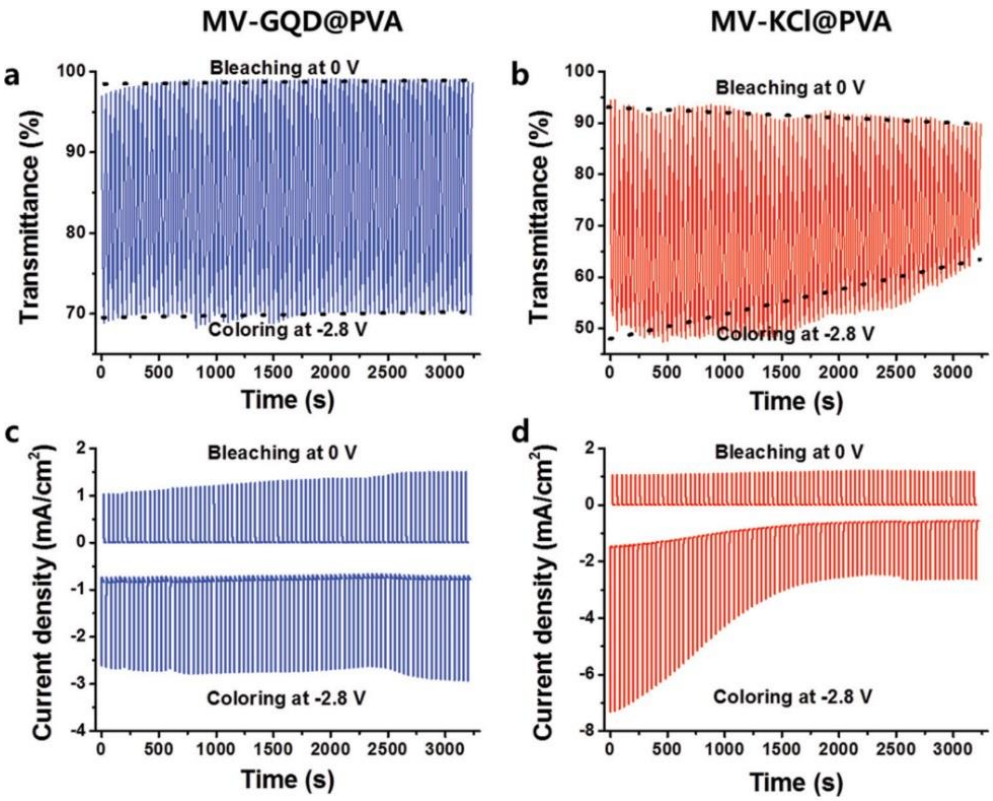

Figure 1.18: Photovoltaic studies of electrochromic devices of ITO-on-glass electrodes with 50 mM MV^{2+} with 8 mg mL^{-1} GQD in PVA (left/blue) and with 0.1 M KCl in PVA (right/red) at 550 nm. **a,b)** Voltage-controlled transmittance changes and **c,d)** corresponding chronoamperometric responses by voltage switching between 0 (bleached state) and −2.8 V (colored state). Adapted from Ref. 88.

It was demonstrated that this approach gives very stable switching performance, great cyclability with repeatable voltage switching between the colored state and the bleached state, and thermal stability to 80 °C. The voltage-controlled transmittance change of MV^{2+}-KCl electrochromic device significantly decreased from 45% to 24% over repeated cycles at 550 nm, the voltage-controlled transmittance change of the electrochromic device with MV^{2+}-GQD consistently changed by 29% over repeated cycles (Figure 1.18).[88]

1.3 Carbon Dots (CDs)

Carbon Dots (known as Carbon Nanodots, C-dots) are one of the newest members of fluorescent carbon nanomaterials. They were first reported in 2006 by Sun *et al*.[89] Since then, various applications have been shown. Their shape is described as quasi-spherical, with diameter below 10 nm and they generally have an sp^2 conjugated core and present various oxygen-containing species such as carboxyl, hydroxyl, and aldehyde groups. They possess excellent water-solubility and the possibility for functionalization with various organic, polymeric, inorganic, or biological species exploiting the presence of carboxylic functions.

The production of carbon dots is possible with large variety of simple, fast, and cheap synthetic routes. Their photoluminescence, high photostability, and low toxicity enable them potential replacements for toxic metal-based quantum dots which possess health concerns and the known environmental and biological hazards.

The applications of carbon dots have been widely demonstrated in sensing, bioimaging, nanomedicine, catalysis, optoelectronics, and energy conversion.

1.3.1 Properties and Structure of CDs

As mentioned, Carbon Dots can be amorphous or nanocrystalline with sp^2 carbon clusters (Figure 1.19) and contain various oxygen-containing species such as carboxyl, hydroxyl, and aldehyde groups.[90-91] In some rare cases, they can contain diamond-like structure with sp^3 carbons.[92] Their structural and physicochemical properties may remarkably depend on the synthetic routes, which may add various defects, heteroatoms, and functional groups to carbon dots. Their surface groups contribute their optical properties and make them water dispersible.[93]

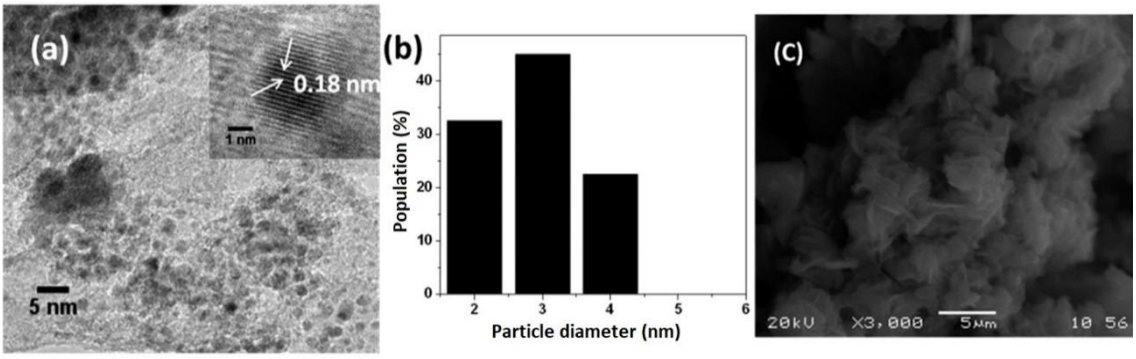

Figure 1.19: Carbon Dots from hydrothermal treatment of Orange Juice. **a)** TEM Image of Carbon Dots, **b)** Particle Size Distribution of Carbon Dots **c)** SEM Image of Carbon Dots. Adapted from Ref. 91.

Depending on production and purification methodology, the chemical composition of carbon dots may vary. It is reported that the carbon dots from purified candle soot contains 36.8% carbon, 5.9% hydrogen, 9.6% nitrogen, 44.7% oxygen and that of raw candle soot contains 91.7% carbon, 1.8% hydrogen, 1.8% nitrogen, 4.4% oxygen.[94] In the same study, the data from Solid-state ^{13}C NMR measurements shows that carbon dots do not have saturated sp^3 carbon atoms and they contain three types of carbon signals: external C=C bonds, internal C=C bonds, and C=O bonds.[94]

As GQDs, carbon nanodots also possess tunable photoluminescence properties arising from quantum confinement effects. Their photoluminescence quantum yield is usually lower than GQDs due to the emissive traps on the surface. Therefore, surface passivation layer is necessary to improve their brightness. Carbon dots are effective in photon-harvesting in short-wavelength region (260 - 320 nm) because of π - π* transition of C=C bonds.

Carbon dots are frequently studied in biological area because of their low toxicity, good biocompatibility and water solubility. These properties make them a promising bioimaging agents and drug nanocarriers.[91, 95-97] In order to evaluate *in vitro* cytotoxicity, MTT assay was performed using L929 cell lines (Figure 1.20) and no significant toxicity were reported and they resulted to be tolerable at high dose (200 $\mu g \cdot mL^{-1}$).[91]

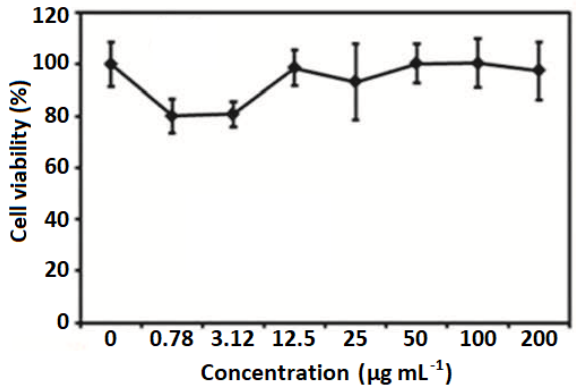

Figure 1.20: Cell viability MTT assay on L929 cell treated with Carbon Dots produced by hydrothermal treatment of orange juice. Adapted from Ref. 91.

In another study, the PEG-functionalized carbon dots were evaluated *in vitro* and *in vivo*. The results suggested that these fluorescent dots are nontoxic for MCF-7 and HT-29 (no more than that of the oligomeric PEG molecules). They do not cause any significant toxic effects on mice at dosages beyond those commonly used for *in vivo* optical imaging.[98]

1.3.2 Synthesis and Functionalization of CDs

Synthesis and functionalization of Carbon Dots cannot be separated since most of the surface decorations occur during their production depending on starting material or solvent. The synthesis of carbon dots can be generally classified into "top-down" and "bottom-up" methods (Figure 1.21). The process includes cleaving or breaking down of carbonaceous materials via chemical, electrochemical, or physical approaches. Various small organic molecules can be pyrolyzed or carbonized to obtain carbon nanodots. There are also different approaches to synthesize carbon dots such as bijective approach (Figure 1.21, c). Top-down approaches are focused on breaking off the bulk carbon material through laser ablation, arc-discharge and electrochemical soaking. In 2006, Sun *et al.* prepared CDs of around 5 nm in diameter via laser ablation of a carbon target in the presence of water vapor with argon as carrier gas.[89] The carbon target was prepared by hot-pressing a mixture of graphite powder and cement, and followed by stepwise baking, curing, and annealing in argon flow.

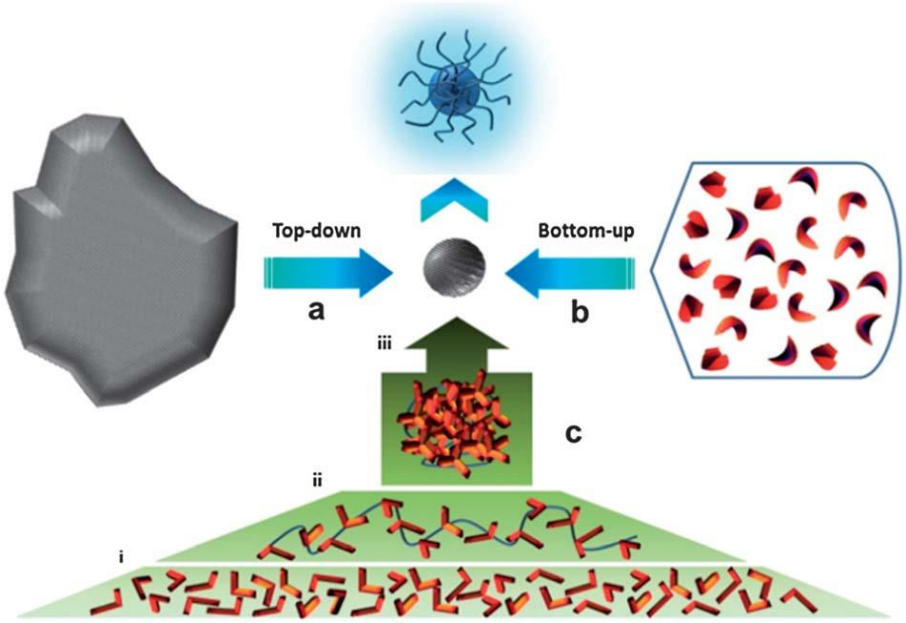

Figure 1.21: Strategies for the preparation of Carbon Dots. **a)** "Top down" approach, **b)** "Bottom-up" approach, **c)** Bijective approach which consists of a relay of three well-controlled steps: (i) living radical polymerization, (ii) Bergman cyclization mediated intramolecular chain collapse, (iii) carbonization. Adapted from Ref. 99.

As-produced carbon dots and acid-treated sample have no detectable photoluminescence. However, after surface passivation by attaching PEG_{1500N} to the acid-treated carbon structures, bright luminescence emissions were observed (Figure 1.22). Exciting at 400 nm, the photoluminescence quantum yields were ranging from 4% to 10%, probably depending on degree of surface passivation.[89]

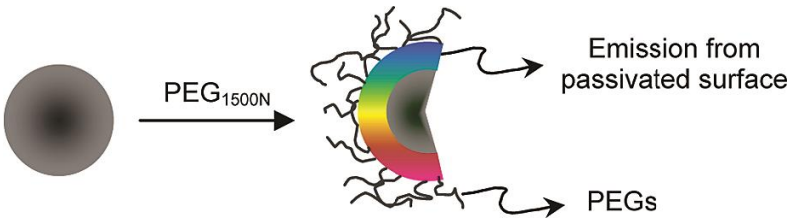

Figure 1.22: Surface passivation of acid-threated carbon dot. Adapted from Ref. 89.

Hu *et al.* synthesized carbon dots in a one-step route, by laser irradiation of a suspension of graphite powders dispersed in organic solvents and the surface modifications with PEG_{200N} occurred at the same time. The luminescence was attributed to carboxylate ligands on the surface of carbon dots and the measured quantum yields of three samples ranged from 3% to 8%. From HRTEM images

it seemed that carbon dots mostly contain defects and the lattice spacing is between 0.20 to 0.23 nm while the size distribution is of 1 - 8 nm.[92]

As mentioned in 2007, Liu *et al.* developed a new methodology to synthesize carbon dots from candle soot.[94] The same methodology was studied by Bottini *et al.*[100] The resulting products were purified using polyacrylamide gel electrophoresis (PAGE) and relatively big particles, attributed to an incomplete combustion, were removed. Oxidative acid treatment was performed to break down inherent interactions and to produce well-dispersed carbon dots, which become negatively charged and hydrophilic, thanks to the introduction of -OH and -COOH groups on their surface. Their diameter was approximately 1 nm and their quantum yields were quite low (<1%), in comparison with those produced through laser ablation.

Sahu *et al.* prepared highly photoluminescent carbon dots in one step from hydrothermal treatment of a renewable bioprecursor, orange juice *(Citrus nobilis deliciosa)*. The mechanism for the formation of carbon dots described as the hydrothermal carbonization of the main constituents of orange juice such as sucrose, glucose, fructose, citric acid and ascorbic acid, at relatively low temperature (120 °C). XPS and FTIR data indicates that the carbon dots are functionalized with hydroxyl, epoxy, carbonyl, and carboxylic acid groups and their photoluminescence quantum yield is calculated as 26%.[91]

In another study, carbon dots with an average diameter 3.4 ± 0.8 nm were synthesized by Hsu *et al.* from used green tea through grinding, calcination and centrifugation. The obtained carbon dots were highly water-soluble, biocompatible, with photoluminescentat 420 nm when excited at 345 nm (quantum yield 4.3%).[101]

Carbon Dots typically contain oxidized moieties such as carboxyl groups on their surface. Thus, they are highly water-soluble and suitable for further functionalizations with other molecules such as amidation in order to add different properties.

1.3.3 Applications of CDs

The photoluminescence and optical properties of carbon dots are interesting research topic for many aspects. The storage and transport of electrons impacted by light is another attractive research subject for carbon dots. Since the discovery of carbon dots, their potential applications in bioimaging, sensing, catalysis, optoelectronics and energy conversion have widely been studied.

Cao *et al.*[102] synthesized carbon dots following the procedure reported by Sun *et al.*[89] and passivated their surface with Poly-(propionylethylenimine-*co*-ethylenimine) (PPEI-EI, with EI fraction ~20%). The prepared carbon dots were investigated in MCF-7 cells (human breast cancer cells) as bioimaging agent with two-photon fluorescence microscopy with 800 nm excitation (Figure 1.23). It is reported that they emit strong photoluminescence both on the cell membrane and in the cytoplasm after 2 hours of incubation at 37 °C and the internalization of carbon dots was found to be temperature dependent as at 4 °C cellular uptake was not observed.

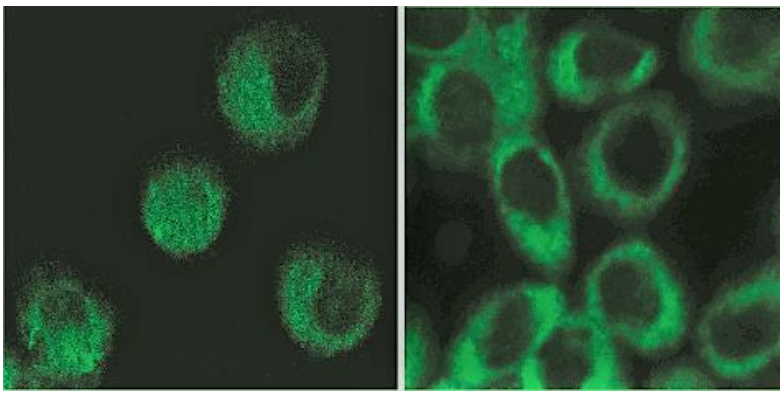

Figure 1.23: Two-photon fluorescence microscopy images (λ_{exc} = 800 nm) of human breast cancer MCF-7 cells with internalized C-Dots. Adapted from Ref. 102.

Hsu *et al.* studied the cells growth inhibition of MCF-7, MDA-MB-231, and HeLa cells, and their bioimaging with carbon dots prepared from calcination of green tea. These materials are effective cell growth inhibitors for MCF-7, MDA-MB-231, and HeLa cells, and cause low toxicity to normal cells such as MCF-10A and LLC-PK1 lines.[101]

Salinas-Castillo *et al.* developed fluorescent carbon dot nanosensor for selective and sensitive detection of Cu^{2+}. The particles, presenting an average size of 12 nm, were synthesized with a one-step method by pyrolysis of citric acid in the presence of polyethylenimine (PEI) using a microwave oven. The photoluminescence quantum yield was calculated as 30%. The selectivity of the carbon dots for Cu^{2+} was studied as variation of CD fluorescence intensities in the presence of different ionic species such as 1 mM of Cu^{2+}, Fe^{3+}, Hg^{2+}, Mn^{2+}, Zn^{2+}, Cr^{3+}, Co^{2+}, Pb^{2+}, Ni^{2+}, Al^{3+}, Cd^{2+}, K^{+}, and Na^{+}. It was shown that as produced carbon dots are highly selective for Cu^{2+} detection but Fe^{3+} ions caused quenching effect only when excited at 850 nm due to the shifting of the maximum emission (Figure 1.24). The synthesized nanosensor can be applied for intracellular sensing and imaging of Cu^{2+} in biological systems as it possesses low cytotoxicity.[103]

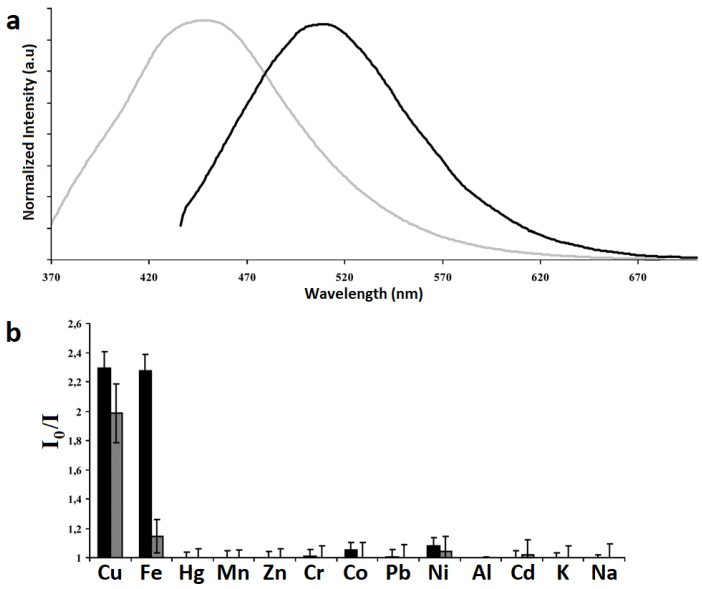

Figure 1.24: a) Fluorescent emission spectra of carbon dots, excited at 350 nm (grey line) and excited at 850 nm (black line). **b)** Selectivity of the carbon dots for Cu^{2+} over other ionic species. Adapted from Ref. 103.

Carbon dots are great candidate to replace rear earth metals and toxic elements such as cadmium and lead in electroluminescent devices due to the high quantum yield luminescence, low cost, high stability and biocompatibility. Chen *et al.* prepared white Light Emitting Diode (LED) by combining the yellow-emitting carbon dots with blue GaN-based LED chips.[104] Carbon dots with particle size in

the range of 3 - 5 nm were synthesized by a one-step pyrolysis from N-acetylcysteine. The color coordinates of (0.34, 0.35) of warm white light from the developed white LED were very close to the coordinates of balanced white light emission (0.33, 0.33).[104] Thanks to the photoluminescent properties, carbon dots are a good candidate as yellow-emitting phosphor for new generation white light emitting diodes.

1.4 Multi-Walled Carbon Nanotubes (MWCNTs)

Carbon Nanotubes (CNTs) are an important class of carbon nanostructures that have many useful properties. CNTs can be described as cylinders of one or more layers of graphene, with open or closed ends. CNTs of a single graphene layer are called Single-Walled CNTs (SWCNTs) and where there are many concentric rolled graphene layers with an interlayer spacing of about 0.34 nm, the nanotubes are named Multi-Walled CNTs (MWCNTs).

Since discovery of MWCNTs by Iijima in 1991, CNTs have attracted great interest due to their extraordinary structural, chemical, and electronic properties.[105] Many studies were performed in order to enlighten the properties of CNTs.[106-107] Thus, they have a wide range of application in nanoelectronics, electrochemistry, biotechnology and biosensors.

1.4.1 Properties and Structure of MWCNTs

MWCNTs can present an inner diameter of MWCNTs is approximately 5-10 nm and the outer 30-50 nm. There are two structure models to describe the MWCNT: Russian Doll model and Parchment model. In the first, a number of SWCNTs with increasing diameters are arranged in concentric cylinders. In the second model, a single graphene sheet is wrapped around itself a number of times as a spiral.

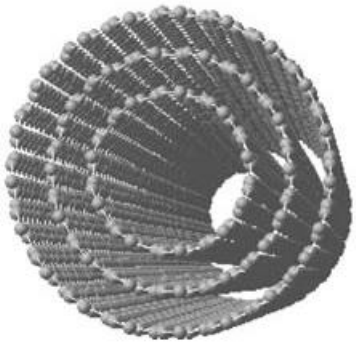

Figure 1.26: Illustration of MWCNTs. Adapted from Ref. 108.

There are three different forms of SWCNTs: rolling of a graphene sheet along lattice vectors leads the formation of armchair, zigzag, and chiral formed CNTs (Figure 1.25).

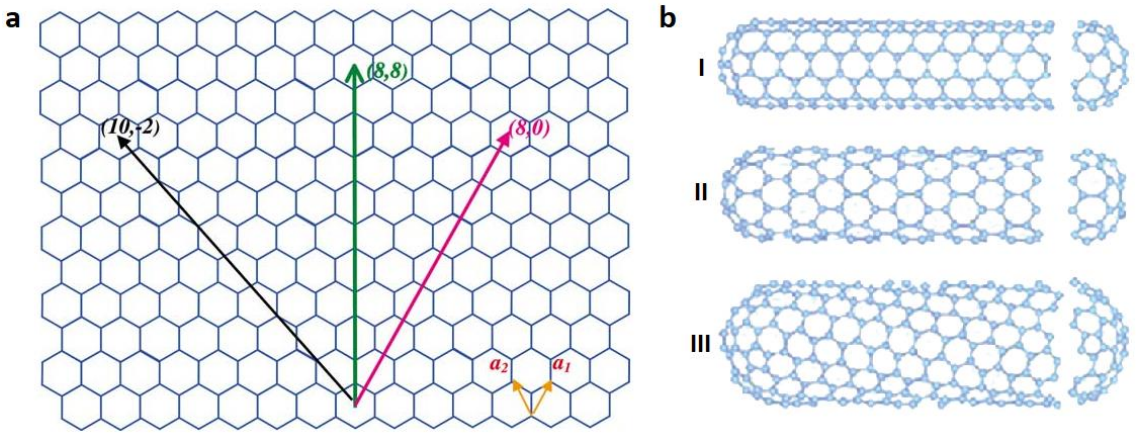

Figure 1.25: a) Illustration of honeycomb structure of a graphene sheet. Armchair (green), Zigzag (pink) and Chiral (black) formations. Adapted from Ref. 109. **b)** Schematic representation of three different types of SWCNTs (I: Armchair, II: Zigzag and III: Chiral formation)

The structures of CNTs can be characterized by two indices (n,m) that define both their diameter and chirality, which are key parameters of CNTs. Depending on the chirality angle, CNTs can be either metals or semiconductors, even though they have almost same diameters.[110] By satisfying the condition $n_1 - n_2 = 3i$ (where i is an integer), the armchair CNTs are always metallic, and zigzag CNTs are either metallic or semiconducting.[111] Due to the almost one-dimensional electronic structure, electronic transport in metallic MWCNTs occurs ballistically over the tube lengths.[112] This enables CNTs to carry high currents with no heating. It is reported that also phonons "almost ballistically" propagate along the CNTs.[113]

CNTs show the combination of superior thermal, electronic and mechanical properties, the latter due to the strength of the sp^2 carbon bonds. Despite having high tensile strength and the modulus of elasticity, their densities can be as low as 1.3 g/cm^3. CNTs Young's moduli (measure of material stiffness) are with values greater than 1000 GPa.[114] Moreover, CNTs are one of the strongest materials ever discovered by mankind. The weakest tensile strength of a CNT was measured approximately 3.4 GPa and the highest tensile strength for a CNT was 63 GPa. [114-115]

The interaction between the biological environment and CNTs is complex and in some cases unpredictable. The studies show that CNTs can have different

toxicity levels depending on their synthesis methodology, specific surface area, shape, aspect ratio, functional groups and the applied concentration.[116-119] CNTs have relatively flexible, long and needle-like shaped structure, which helps them to penetrate biological tissues.

1.4.2 Synthesis of MWCNTs

Synthesis of CNTs without structural and chemical defects in a length scale along the tube axes is desired for fundamental and technological applications. There are mainly three methods used to synthesize CNTs: arc discharge, laser ablation (laser-furnace method), and chemical vapor deposition.[120-122]

Arc discharge method was the first method to produce MWCNTs (Figure 1.26). MWCNTs are created through arc-vaporization of two graphite rods placed end to end, separated by approximately 1 mm, under inert atmosphere at low pressure, ranging between 50 and 700 mbar.[105, 123-124] The evaporated anode generates MWCNTs in the chamber with the application of DC arc voltage of 50 to 100 A between two separated graphite rods, and part of the evaporated anode is deposited on the cathode.[125]

The arc-discharge evaporation of pure graphite rods has been carried out under different gases, such as helium, argon, methane and hydrogen and their effectiveness in the synthesis of MWCNTs has been reported.[105, 122, 125] The disadvantage of arc discharge method is purification of CNTs, which is more expensive than production.

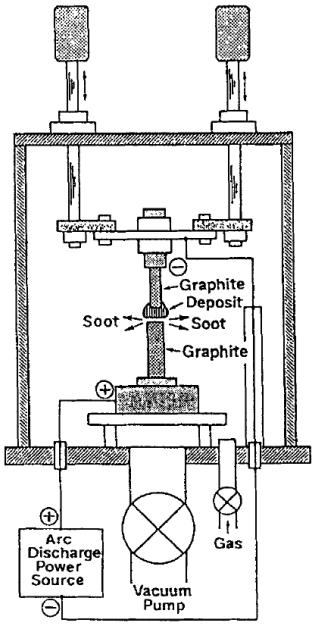

Figure 1.26: Schematic illustration of the apparatus for the arc discharge evaporation. Adapted from Ref. 125.

MWCNTs were produced through laser ablation method in 1995 by Guo et *al*.[126] In this method, intense laser pulses ablate a graphite target in a tube furnace at 1200 °C in an inert atmosphere. The laser produces carbon species and flowing inert gas moves them away from the high temperature zone to a conical water-cooled copper collector. When transition metal added to the carbon target, SWCNTs are produced. The average SWCNT diameter and size distribution can be varied by changing laser, catalyst composition, furnace temperature, type of gases, pressure.[127] As the vaporized species cool, small carbon molecules and atoms quickly condense to form larger clusters, possibly including fullerenes. The catalysts also begin to condense slowly and attach to carbon clusters. From the initial clusters, tubular shaped complexes continue growing into single-walled carbon nanotubes until the catalyst particles become too large, or until conditions cool down and carbon no longer can diffuse through or over the surface of the catalyst particles. The quality and yield of these products depend on the reaction temperature, which can be even higher than 3000 °C. High temperature is beneficial for good crystallization of the CNTs.

Chemical Vapor Deposition (CVD) method is used to produce CNTs through the decomposition of hydrocarbon vapor along with a metal catalyst at high

temperature (600 - 1200 °C), which is also nucleation site for the CNTs growth in the reactor (Figure 1.27). Produced CNTs are collected upon cooling the system to room temperature. CNTs can be produced from different precursors such as benzene,[128] ethylene,[129] acetylene,[130-131] camphor,[132] and methane.[133] When a liquid hydrocarbon such as benzene is used as a precursor, it is heated in a vessel and an inert gas is purged through it. In this way the hydrocarbon vapor is carried into the reaction zone.[128] In case of a solid hydrocarbon material, it can be directly kept in the low-temperature zone of the reaction tube. Volatile starting materials such as camphor directly sublimes, and decomposes while passing over the catalyst in the high temperature zone and CVD occurs.[132]

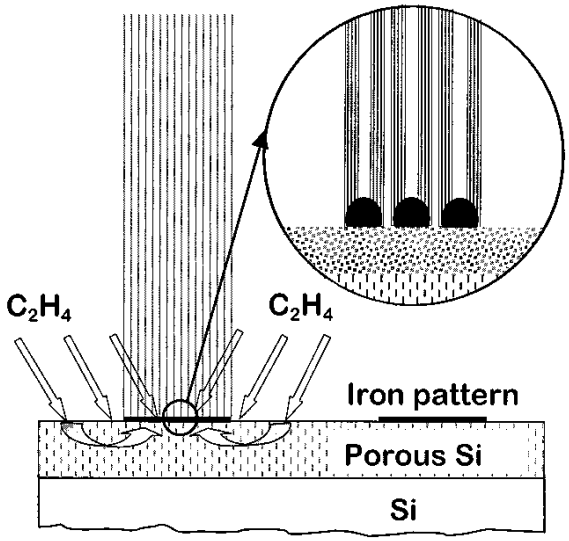

Figure 1.27: The growth of MWCNTs and their self-orientation on porous silicon substrate with the iron oxide nanoparticles during CVD growth. Adapted from Ref. 129.

Comparing to the other two methods, CVD is a preferred methodology for large-scale CNTs synthesis, allowing direct and patterned growth of CNTs on a chip. Moreover it does not require high-cost, difficult purifications and dispersion treatments as other methodologies.

However, there are still challenges about the synthesis of high quality CNTs, such as Mass production, Selective production, Organization and Mechanism. Production of MWCNTs in big amount with specific size or edge without metal impurities caused by the synthesis mechanism and organization of MWCNTs on a surface are problems needed to be solved.

1.4.3 Surface Functionalizations of MWCNTs

The chemical reactivity of CNTs presents some common characteristics with the other sp^2-hybridized carbon allotropes. The chemistry of a perfect, closed CNT differs from other carbon nanomaterials due to its unique structure without chemically unsatisfied valence (dangling bonds), comparing to graphite and graphene. The bended sp^2 carbon atoms of the nanotube induces pyramidalization and mis-alignment of the π orbitals which induce local strain on CNTs.[134] Thus, higher pyramidalization angle shows a larger reactivity. When the outer diameter of MWCNT is ranging from 20 to 50 nm the pyramidalization angle is smaller than SWCNT. Therefore, the covalent functionalization reactions of MWCNTs can require harsher conditions.

Mainly, four different approaches are developed for the functionalization of CNTs such as defect groups functionalization, sidewall functionalization, non-covalent functionalization and endohedral functionalization (Figure 1.28).[135]

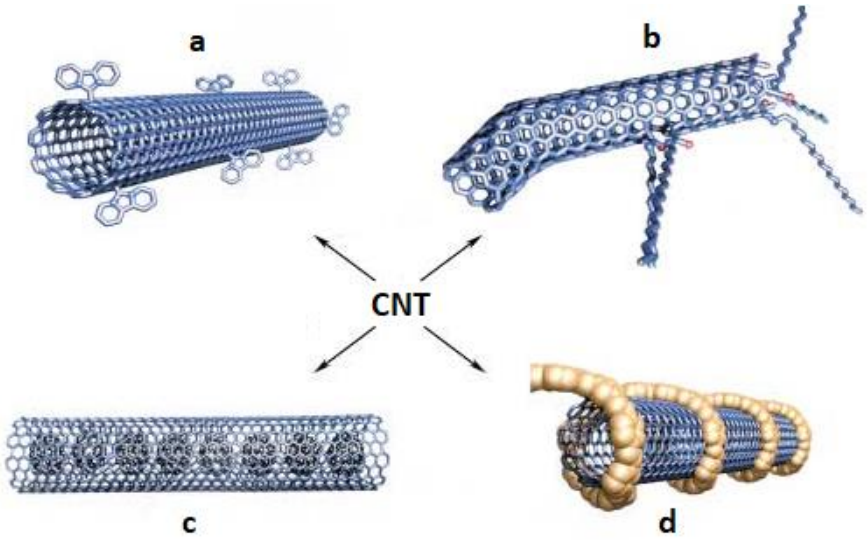

Figure 1.28: Functionalization routes for CNTs **a)** Sidewall functionalization, **b)** Defect groups functionalization, **c)** Endohedral functionalization, and **d)** Non-covalent functionalization. Adapted from Ref. 135.

The functionalizations on CNTs allow the tailoring of their properties for specific application. Pristine CNTs are almost insoluble in any aqueous solution or organic solvent, and this disadvantage limits their applications. CNTs can be briefly dispersed in solution only by sonication. The presence of oxygen-

containing functional groups eases the exfoliation of CNT bundles, and increases the solubility in polar solutions. The common oxidation methodologies for CNTs are wet chemical methods,[136-137] oxygen plasma,[138] photo-oxidation[139] or gas phase treatment,[140] in order to increase the purity and chemical reactivity of CNTs for the further functionalizations. The oxidized CNTs are shorten below 1 µm and the ends and sidewalls are enriched by oxygenated functional groups, mainly carbonyl and carboxylic groups.

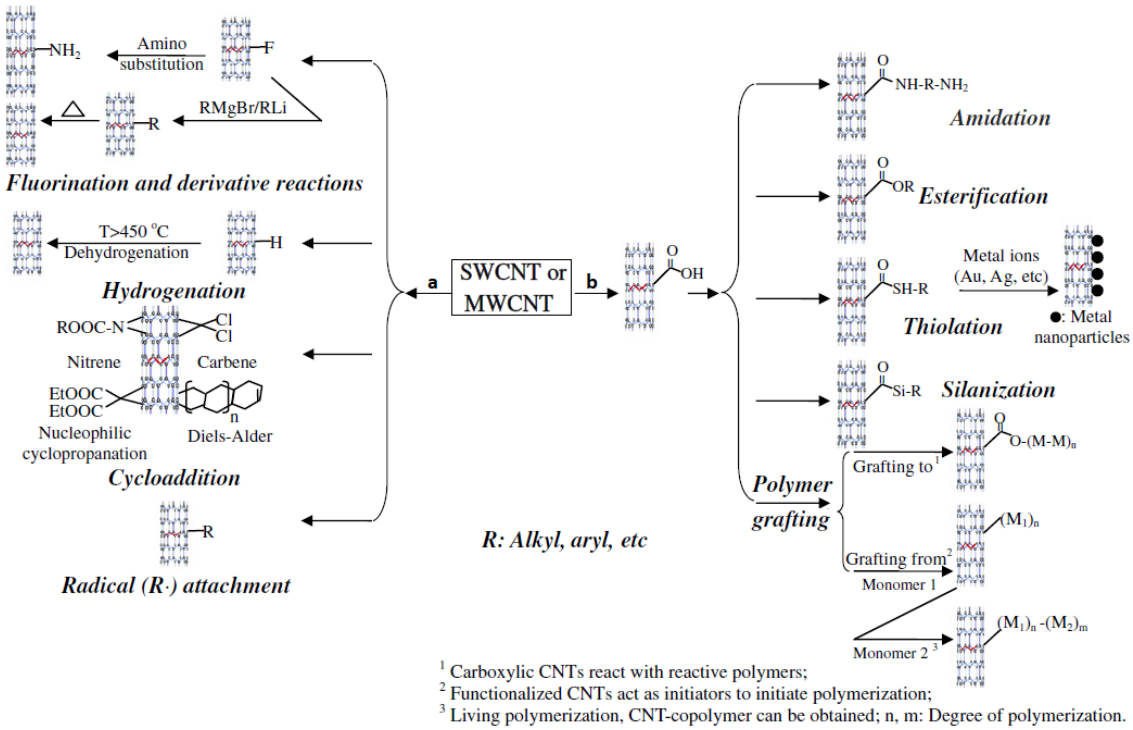

Figure 1.29: Covalent functionalization strategies for Carbon Nanotubes. **a)** Sidewall functionalization **b)** Defect group functionalization. Adapted from Ref. 141.

The defect group functionalization is based on the reactions of carboxylic groups or deformations of CNTs formed through oxidative purification or the production. The defects on the CNTs are important in their covalent chemistry because the defects can serve as anchor groups for further functionalizations. The carboxylic groups formed through oxidative reactions, are located mainly at the tips of CNTs. These carboxylic groups can be activated with different activation reagents for further reactions with amines or alcohols.[142-145]

Chen *et al.* functionalized oxidized SWCNTs with octadecylamine after treatment with thionyl chloride in 1998.[146] They could solubilize the functionalized SWCNTs in organic solvents. Since then, many research studies were performed in order to improve the properties of CNTs.

The covalent linkage of functional groups onto the sidewall of the CNTs leads the partial destruction of the conjugated sp^2 carbon lattice to give sp^3 hybridization. The sidewall modifications can be performed through reactions with molecules of a high chemical reactivity, such as fluorine, nitrenes, carbenes, and radicals.[147-151] In 1998, sidewall functionalization of CNTs was first performed through treatment with fluorine by Mickelson *et al*.[147] CNTs were treated with elemental fluorine between 150 °C and 600 °C. The obtained degree of fluorination was between 0.1% and 1%,[147] and there are many studies on replacement of fluorine atoms with amino, alkyl and hydroxyl groups.[152-153] The thermal reaction of CNTs with azidoformiates leads to N_2 extrusion and results aziridino CNTs, which dissolve in organic solvents.[149]

It is possible to functionalize the sidewalls of CNTs through the reduction of aryl diazonium salts to provide reactive radicals that can covalently attach to CNTs.[154] An electron from the CNT is transfer on to the diazonium salt, and causes the elimination of nitrogen and as a result, an aryl radical is formed. The reaction was first performed through electrochemical reduction and then a solvent-based thermally induced reaction was developed. The newer and simpler methodology generates the diazonium compounds *in situ* by reacting aniline derivatives with isopentyl nitrite.[155]

Another important covalent sidewall functionalization of CNTs is cycloaddition which was developed by Georgakilas *et al*.[156] The reaction occurs by using the 1,3-dipolar cycloaddition of azomethine ylides. CNTs were treated with an azomethine ylide generated from aldehyde and N-substituted glycine derivative resulting pyrrolidine rings on the sidewall of CNTs. It is reported that approximately one organic group per 100 carbon atoms of the nanotube is introduced and the reaction gives soluble bundles of CNTs.

It is important to modify the surface of CNTs properly depending on the attached functional groups not only to make them more soluble, but also to increase their compatibility in organic, inorganic, and biological systems. There are many approaches for CNTs functionalization, which add them different properties and make them useful for various applications in electrochemistry, biomedicine and structural material developments.

1.4.4 Applications of MWCNTs

CNTs possess unique electrical and mechanical properties which have been stimulating growing interest and curiosity in their applications as electronics, mechanics, chemistry and medicine.[157-161]

Biomedical applications of CNTs can be generally described under these titles: Drug and Gene Delivery, Bioimaging, Biosensors, Tissue Engineering and Regenerative Medicine. The lack of solubility of CNTs in aqueous conditions is a concern for biological systems. It is possible to overcome this disadvantage with the functionalizations of CNTs combining the characteristics of CNTs with those of other materials such as biologically active molecules or functional polymers. Many drug delivery systems with CNTs have been developed for treatment of a broad range of diseases. As expected, CNT-based anticancer drug approaches have attracted the greatest attention. The advantages of the treatment with CNTs are selective targeting and controlled release. Selective targeting is carried through the functionalization of CNTs with tumor addressing molecules. With the proper modification of drug-CNT complex, it is possible to stimulate the drug release only in tumor environment such as with pH lower than the physiological.[162]

Bianco *et al*. developed a multimodal drug delivery with double functionalization of MWCNTs via 1,3-dipolar cycloaddition of azomethine ylides.[163] They could introduce both fluorescein (a fluorescent probe) and methotrexate (an anticancer agent) on the sidewalls of MWCNTs in order to increase the cellular uptake of methotrexate and add simultaneous bioimaging with FITC.

The delivery of RNA, DNA, and their derivatives is also a potential application of MWCNTs. Kateb *et al.* suggested that MWCNTs could be used as a non-toxic, and biodegradable nanocarriers for targeted therapy in brain cancer.[164] The MWCNTs were functionalized with small interfering RNA (siRNA) which is a promising gene silencing compound for directed immunogenetic cancer therapy in order to stabilize siRNA and deliver it to the targeted cell more efficiently. As *in vivo* delivery of siRNAs to the target cell is limited by the scarce stability, low uptake efficiency, and pharmacokinetics of siRNA. Functionalization of MWCNTs can facilitate the release the drug or gene into the cell and thus, the loaded compound reaches the targeted tissue and escape from the lysosomal degradation.

Oxidation and shortening of MWCNTs are important processes in order to increase their biocompatibility. Jain *et al.* showed that acid treated, carboxylated MWCNTs with shorter length, hydrophilic surface, and high aqueous dispersibility are less toxic and more biocompatible than pristine MWCNTs.[165] Well-individualized MWCNTs shorter than 500 nm and high degree of oxidation were rapidly cleared out from the systematic circulation through renal excretion route without inducing any serious nephrotoxicity. Larger MWCNTs were mostly excreted via the biliary pathway in feces with minimal involvement of the kidney. The reported results show that oxidation and shortening of MWCNTs provide important benefits for their possible biomedical applications.

Another important application of MWCNTs is biosensors, where it is important to combine the biological recognition with a chemical or physical transduction to detect biomolecules. Surface functionalizations are essential for biosensor and probes. Guan *et al.* produced a glucose biosensor based on MWCNTs immobilized with glucose oxidase and screen printed carbon electrodes.[166] The results show that electrode system modified with MWCNTs efficiently performed as biosensor with higher sensitivity and wider linear response range than the typical glucose electrochemical biosensor.

Apart from the medical applications, CNTs have many more possible applications such as in electronics. Guo *et al*. studied from the theoretical point of view the

possible metal-insulator-semiconductor capacitor applications of CNTs in 2002.[167] Quantum-mechanical effects determine the electronic structure of a CNT due to the nanosize and the quantization conditions of the CNT determine whether a nanotube acts as a metal or a semiconductor. These properties are promising for new approaches for future nanoelectronics, which can be one of the most important applications of CNTs.

1.5 Characterization Techniques of Carbon Nanostructures

Under this title, the characterization techniques applied in this thesis project were described.

1.5.1 Thermogravimetric Analysis (TGA)

Thermogravimetric analysis (TGA) is a thermal analysis technique to characterize a wide variety of materials and crucial for the characterization of carbon nanostructures. TGA measures the amount of change in the mass of a sample as a function of temperature in a controlled atmosphere such as nitrogen, argon and air by its precision scale with high sensitivity. The thermal stability and composition of the sample can be analyzed with this technique.

Generally, pristine carbon nanomaterials are thermally stable at high temperatures but functionalized carbon nanomaterials contain organic moieties which are not as thermally stable as carbon nanomaterials at high temperatures. The weight loss that occurs in the range of 100 – 600 °C for the functionalized carbon nanomaterial, comparing to the starting carbon nanomaterial is considered to belong to the organic loading.

1.5.2 Transmission Electron Microscopy (TEM)

Transmission electron microscopy (TEM) is a microscopy technique where a focused monoenergetic beam of electrons is transmitted through an ultra-thin specimen. The beam of electrons interacts with the specimen and passes through. An imaging device detects the energetic changes and forms the image. Comparing to light microscopes, transmission electron microscopes can provide significantly higher resolution. Among the different microscopy techniques, the precise measurements can be performed, even the atomic structure of the material can be investigated.

TEM is used to analyze the morphology, uniformity, dispersibility and purity of carbon nanostructures. It is possible to measure the size of single particles,

create particle size frequency diagrams and study the effect of oxidation on the particle diameter and length.

1.5.3 Atomic Force Microscopy (AFM)

Atomic force microscopy (AFM) is a kind of scanning probe microscopy that provides three dimensional topographic images of the sample with high resolution. Atomic force microscope consists of a laser, a photo detector, a cantilever with a sharp tip which scans the surface of the sample and a piezoelectric tube where the sample is placed on. When the tip is enough close to the sample surface, forces between the tip and the sample lead to a deflection of the cantilever according to Hooke's law.

AFM has three different imaging modes: contact mode, non-contact mode and tapping mode.[168] For the contact mode, a constant bend of the cantilever is maintained. In non-contact mode, the cantilever oscillates above the sample surface. The tip-sample surface separation and the oscillation amplitude are 1 nm and 10 nm, respectively and tip does not touch to the sample surface. For the tapping mode, the oscillation amplitude of the tip is kept in the range of 20 nm to 200 nm and the cantilever oscillates above the sample surface but tip makes small contacts on the surface. It is possible to characterize morphology, homogeneity, dispersibility and purity of the samples with AFM techniques.

1.5.4 Infrared Spectroscopy

Infrared (IR) spectroscopy (also known as vibrational spectroscopy) presents the data about the interaction of infrared radiation with matter. The absorbed radiation by interatomic bonds in infrared region (4000 – 400 cm^{-1}) provides important information to characterize the organic structures, functional groups and adsorbed molecules. As each interatomic bond is able to vibrate in different modes such as stretching and bending, absorption may occur at more than one wavenumber region. Stretching absorptions are usually stronger than bending peaks.

Surface groups of pristine and functionalized carbon nanostructures can be characterized by IR spectroscopy. The pristine or functionalized carbon nanostructures investigated in this research project (NDs, GQDs, CDs and MWCNTs) usually present these peaks in their IR spectrum: O-H stretching (3200-3600 cm^{-1}) and bending (1600-1680 cm^{-1}), C=O stretching (1700-1800 cm^{-1}), C-H stretching (2950-2850 cm^{-1}) and overlapping absorption peaks of C-O-C stretching vibrations, epoxy C-O stretching, C-C stretching, and amide C-N stretching (1000-1500 cm^{-1}).

1.5.5 Raman Spectroscopy

Raman spectroscopy investigates the inelastic scattered light. The sample is irradiated with a monochromatic light and the photons of the radiation mostly scatter unchanged in the case of elastic scattering. In the case of inelastic scattering, frequency of photons of the radiation changes due to the interaction with the sample. The photons the light source are absorbed by the sample and then reemitted. The frequency of the reemitted photons is shifted up or down in comparison with the frequency of monochromatic light source. This effect is called the Raman effect. The Raman shift provides data about the vibrational, rotational, and other low-frequency transitions in the structure.

Raman spectrum of carbon nanostructures may contain radial breathing mode (100 – 600 cm^{-1}), a sharp Lorentz peak (at 1332 cm^{-1}) which is due to diamond crystal lattice, D band (around 1350 cm^{-1}) which is related to the disorder and defects, G mode (around 1580 cm^{-1}) which is the first-order Raman band of all sp^2 hybridized carbon materials and a relatively weaker D' band (around 1620 cm^{-1}), G' bands (2D band) (at 2450 cm^{-1} and 2705 cm^{-1}), D+G band (at 2945 cm^{-1}), 2G band (at 3176 cm^{-1}), and 2D' band (at 3244 cm^{-1}).[169-170] The technique is not destructive and requires small amount of sample.

1.5.6 Dynamic Light Scattering (DLS)

Dynamic light scattering (also known as photon correlation spectroscopy) is a technique in which a beam of monochromatic laser light is directed through the small particles in suspension/solution to determine the size-distribution profile. The laser beam passes through a beam splitter in order to detect a reference intensity at the monitor diode. In transmission it impinges on a glass cuvette immerged in a toluene bath. This bath avoids reflexes and its temperature can be controlled accurately. The beam reaches to the cuvette which is at a controlled temperature and scatters by the sample. A scattering angle is detected by a photo diode and the data is transferred as a signal to a computer.

The diameter that is measured by DLS is a value that refers to how the sample diffuses within a solvent and it is named as hydrodynamic diameter. The hydrodynamic diameter is the diameter of a sphere which has the same translational diffusion coefficient as the particle. The translational diffusion coefficient depends on the size of the particle core, any surface group, the concentration and type of ions in the medium. It is possible to characterize the particles which differ in their diffusive behavior with DLS.

Bibliography

1. A. Bhatnagar, A. Minocha; *Indian Journal of chemical technology* **2006,** *13* (5), 303-217.
2. P. R. Wallace; *Physical Review* **1947,** *71* (9), 622-634.
3. V. V. Danilenko; *Physics of the Solid State* **2004,** *46* (4), 595-599.
4. R. S. Lewis, T. Ming, J. F. Wacker, E. Anders, E. Steel; *Nature* **1987,** *326*, 160.
5. A. Liamkin, E. Petrov, A. Ershov, G. Sakovich, A. Staver, V. Titov; *DOKLADY AKADEMII NAUK SSSR* **1988,** *302* (3), 611-613.
6. N. R. Greiner, D. S. Phillips, J. D. Johnson, F. Volk; *Nature* **1988,** *333*, 440.
7. V. N. Mochalin, O. Shenderova, D. Ho, Y. Gogotsi; *Nature Nanotechnology* **2011,** *7* (1), 11-23.
8. A. M. Schrand, S. A. C. Hens, O. A. Shenderova; *Critical Reviews in Solid State and Materials Sciences* **2009,** *34* (1-2), 18-74.
9. D. Ho; *Nanodiamonds: Applications in Biology and Nanoscale Medicine*. Springer US: 2014.
10. A. E. Aleksenskiy, E. D. Eydelman, A. Y. Vul; *Nanoscience and Nanotechnology Letters* **2011,** *3* (1), 68-74.
11. O. A. Shenderova, D. M. Gruen; *Ultrananocrystalline Diamond: Synthesis, Properties, and Applications*. Elsevier Science: 2006.
12. B. I. Kharisov, O. V. Kharissova, L. Chávez-Guerrero; *Synthesis and Reactivity in Inorganic, Metal-Organic, and Nano-Metal Chemistry* **2010,** *40* (2), 84-101.
13. O. A. Shenderova, V. V. Zhirnov, D. W. Brenner; *Critical Reviews in Solid State and Materials Sciences* **2002,** *27* (3-4), 227-356.
14. A. S. Barnard, M. Sternberg; *Journal of Materials Chemistry* **2007,** *17* (45), 4811-4819.
15. D. Aditi, K. Mesut, F. Yao, C. T. Albert; *Nanotechnology* **2011,** *22* (6), 065706.
16. N. Yang; *Novel Aspects of Diamond: From Growth to Applications*. Springer International Publishing: 2014.
17. M. Angjellari, A. Peçuli; *Albanian Journal of Pharmaceutical Sciences* **2014,** *1* (1), 7.
18. O. Shenderova, A. Koscheev, N. Zaripov, I. Petrov, Y. Skryabin, P. Detkov, S. Turner, G. Van Tendeloo; *The Journal of Physical Chemistry C* **2011,** *115* (20), 9827-9837.
19. V. Y. Dolmatov; *Russian Chemical Reviews* **2001,** *70* (7), 607.
20. D. M. Gruen, O. A. Shenderova, A. Y. Vul; *Synthesis, Properties and Applications of Ultrananocrystalline Diamond: Proceedings of the NATO ARW on Synthesis, Properties and Applications of Ultrananocrystalline Diamond, St. Petersburg, Russia, from 7 to 10 June 2004*. Springer Science & Business Media: 2006; Vol. 192.
21. A. S. Chiganov; *Physics of the Solid State* **2004,** *46* (4), 620-621.
22. A. Krueger; *Journal of Materials Chemistry* **2008,** *18* (13), 1485-1492.
23. Y. Fu, N. An, S. Zheng, A. Liang, Y. Li; *Diamond and Related Materials* **2012,** *21*, 73-76.
24. H.-D. Wang, Q. Yang, C. H. Niu; *Diamond and Related Materials* **2010,** *19* (5), 441-444.
25. L. M. Manus, D. J. Mastarone, E. A. Waters, X.-Q. Zhang, E. A. Schultz-Sikma, K. W. MacRenaris, D. Ho, T. J. Meade; *Nano Letters* **2010,** *10* (2), 484-489.
26. Y. Astuti, F. D. Saputra, S. Wuning, Arnelli, G. Bhaduri; *IOP Conference Series: Materials Science and Engineering* **2017,** *172* (1), 012066.
27. P. Christiaens, V. Vermeeren, S. Wenmackers, M. Daenen, K. Haenen, M. Nesládek, M. vandeVen, M. Ameloot, L. Michiels, P. Wagner; *Biosensors and Bioelectronics* **2006,** *22* (2), 170-177.
28. K. Turcheniuk, N. M. Vadym; *Nanotechnology* **2017,** *28* (25), 252001.
29. H. M. Zareie, C. Boyer, V. Bulmus, E. Nateghi, T. P. Davis; *Acs Nano* **2008,** *2* (4), 757-765.
30. Y. Dong, R. Cao, Y. Li, Z. Wang, L. Li, L. Tian; *RSC Advances* **2015,** *5* (101), 82711-82716.

31. A. M. Schrand, H. Huang, C. Carlson, J. J. Schlager, E. Ōsawa, S. M. Hussain, L. Dai; *The Journal of Physical Chemistry B* **2007,** *111* (1), 2-7.
32. O. Shenderova, A. Vargas, S. Turner, D. M. Ivanov, M. G. Ivanov; *Tribology Transactions* **2014,** *57* (6), 1051-1057.
33. J.-I. Chao, E. Perevedentseva, P.-H. Chung, K.-K. Liu, C.-Y. Cheng, C.-C. Chang, C.-L. Cheng; *Biophysical Journal* **2007,** *93* (6), 2199-2208.
34. K. Hanada; *Surface Engineering* **2009,** *25* (7), 487-489.
35. O. A. Mogilnaya, A. P. Puzyr, A. V. Baron, V. S. Bondar; *Nanoscale Research Letters* **2010,** *5* (5), 908-912.
36. A. P. Puzyr, K. V. Purtov, O. A. Shenderova, M. Luo, D. W. Brenner, V. S. Bondar; *Doklady Biochemistry and Biophysics* **2007,** *417* (1), 299-301.
37. O. Tacar, P. Sriamornsak, C. R. Dass; *Journal of Pharmacy and Pharmacology* **2013,** *65* (2), 157-170.
38. D. L. Hershman, R. B. McBride, A. Eisenberger, W. Y. Tsai, V. R. Grann, J. S. Jacobson; *Journal of Clinical Oncology* **2008,** *26* (19), 3159-3165.
39. E. K. Chow, X.-Q. Zhang, M. Chen, R. Lam, E. Robinson, H. Huang, D. Schaffer, E. Osawa, A. Goga, D. Ho; *Science Translational Medicine* **2011,** *3* (73), 73ra21-73ra21.
40. H. B. Man, H. Kim, H.-J. Kim, E. Robinson, W. K. Liu, E. K.-H. Chow, D. Ho; *Nanomedicine : nanotechnology, biology, and medicine* **2014,** *10* (2), 359-369.
41. J. Xiao, X. Duan, Q. Yin, Z. Zhang, H. Yu, Y. Li; *Biomaterials* **2013,** *34* (37), 9648-9656.
42. A. Thalhammer, R. J. Edgington, L. A. Cingolani, R. Schoepfer, R. B. Jackman; *Biomaterials* **2010,** *31* (8), 2097-104.
43. J. M. Halpern, S. Xie, G. P. Sutton, B. T. Higashikubo, C. A. Chestek, H. Lu, H. J. Chiel, H. B. Martin; *Diamond and Related Materials* **2006,** *15* (2), 183-187.
44. C. Prado, G.-U. Flechsig, P. Gründler, J. S. Foord, F. Marken, R. G. Compton; *Analyst* **2002,** *127* (3), 329-332.
45. J. Tisler, G. Balasubramanian, B. Naydenov, R. Kolesov, B. Grotz, R. Reuter, J.-P. Boudou, P. A. Curmi, M. Sennour, A. Thorel, M. Börsch, K. Aulenbacher, R. Erdmann, P. R. Hemmer, F. Jelezko, J. Wrachtrup; *Acs Nano* **2009,** *3* (7), 1959-1965.
46. S.-J. Yu, M.-W. Kang, H.-C. Chang, K.-M. Chen, Y.-C. Yu; *Journal of the American Chemical Society* **2005,** *127* (50), 17604-17605.
47. K. S. Novoselov, A. K. Geim, S. V. Morozov, D. Jiang, Y. Zhang, S. V. Dubonos, I. V. Grigorieva, A. A. Firsov; *Science* **2004,** *306* (5696), 666-9.
48. Y. Zhang, Y.-W. Tan, H. L. Stormer, P. Kim; *Nature* **2005,** *438*, 201.
49. A. H. Castro Neto, F. Guinea, N. M. R. Peres, K. S. Novoselov, A. K. Geim; *Reviews of Modern Physics* **2009,** *81* (1), 109-162.
50. P. Avouris, F. Xia; *Materials Research Society Bulletin* **2012,** *37* (12), 1225-1234.
51. X. Sun, Z. Liu, K. Welsher, J. T. Robinson, A. Goodwin, S. Zaric, H. Dai; *Nano Research* **2008,** *1* (3), 203-212.
52. C. Zhu, S. Yang, G. Wang, R. Mo, P. He, J. Sun, Z. Di, N. Yuan, J. Ding, G. Ding, X. Xie; *Journal of Materials Chemistry C* **2015,** *3* (34), 8810-8816.
53. L. Kittiratanawasin, S. Hannongbua; *Integrated Ferroelectrics* **2016,** *175* (1), 211-219.
54. X. Yan, B. Li, X. Cui, Q. Wei, K. Tajima, L.-s. Li; *The Journal of Physical Chemistry Letters* **2011,** *2* (10), 1119-1124.
55. R. Liu, D. Wu, X. Feng, K. Müllen; *Journal of the American Chemical Society* **2011,** *133* (39), 15221-15223.
56. R. Ye, Z. Peng, A. Metzger, J. Lin, J. A. Mann, K. Huang, C. Xiang, X. Fan, E. L. G. Samuel, L. B. Alemany, A. A. Martí, J. M. Tour; *ACS Applied Materials & Interfaces* **2015,** *7* (12), 7041-7048.
57. H. Sun, L. Wu, W. Wei, X. Qu; *Materials Today* **2013,** *16* (11), 433-442.

58. S. Zhou, H. Xu, W. Gan, Q. Yuan; *RSC Advances* **2016,** *6* (112), 110775-110788.
59. J. Ge, M. Lan, B. Zhou, W. Liu, L. Guo, H. Wang, Q. Jia, G. Niu, X. Huang, H. Zhou, X. Meng, P. Wang, C.-S. Lee, W. Zhang, X. Han; *Nature Communications* **2014,** *5*, 4596.
60. J. Shen, Y. Zhu, X. Yang, C. Li; *Chemical Communications* **2012,** *48* (31), 3686-3699.
61. D. Pan, J. Zhang, Z. Li, M. Wu; *Advanced Materials* **2010,** *22* (6), 734-738.
62. J. Peng, W. Gao, B. K. Gupta, Z. Liu, R. Romero-Aburto, L. Ge, L. Song, L. B. Alemany, X. Zhan, G. Gao, S. A. Vithayathil, B. A. Kaipparettu, A. A. Marti, T. Hayashi, J. J. Zhu, P. M. Ajayan; *Nano Letters* **2012,** *12* (2), 844-9.
63. Y. Li, Y. Hu, Y. Zhao, G. Shi, L. Deng, Y. Hou, L. Qu; *Advanced Materials* **2011,** *23* (6), 776-780.
64. Y. Li, Y. Zhao, H. Cheng, Y. Hu, G. Shi, L. Dai, L. Qu; *Journal of the American Chemical Society* **2012,** *134* (1), 15-18.
65. S. Zhu, J. Zhang, X. Liu, B. Li, X. Wang, S. Tang, Q. Meng, Y. Li, C. Shi, R. Hu, B. Yang; *RSC Advances* **2012,** *2* (7), 2717-2720.
66. Y. Dong, J. Shao, C. Chen, H. Li, R. Wang, Y. Chi, X. Lin, G. Chen; *Carbon* **2012,** *50* (12), 4738-4743.
67. W. Hu, Y. Huang, L. Lin, E. Kan, X. Li, C. Yang, J. Yang; *arXiv preprint arXiv:1710.11300* **2017**.
68. L. A. Ponomarenko, F. Schedin, M. I. Katsnelson, R. Yang, E. W. Hill, K. S. Novoselov, A. K. Geim; *Science* **2008,** *320* (5874), 356-358.
69. S. H. Jin, D. H. Kim, G. H. Jun, S. H. Hong, S. Jeon; *Acs Nano* **2013,** *7* (2), 1239-1245.
70. L. Tang, R. Ji, X. Cao, J. Lin, H. Jiang, X. Li, K. S. Teng, C. M. Luk, S. Zeng, J. Hao, S. P. Lau; *Acs Nano* **2012,** *6* (6), 5102-10.
71. S. Zhu, J. Zhang, C. Qiao, S. Tang, Y. Li, W. Yuan, B. Li, L. Tian, F. Liu, R. Hu, H. Gao, H. Wei, H. Zhang, H. Sun, B. Yang; *Chemical Communications* **2011,** *47* (24), 6858-6860.
72. X. Yan, X. Cui, L.-s. Li; *Journal of the American Chemical Society* **2010,** *132* (17), 5944-5945.
73. W. S. Hummers, R. E. Offeman; *Journal of the American Chemical Society* **1958,** *80* (6), 1339-1339.
74. J. Shen, Y. Zhu, C. Chen, X. Yang, C. Li; *Chemical Communications* **2011,** *47* (9), 2580-2582.
75. F. Liu, M.-H. Jang, H. D. Ha, J.-H. Kim, Y.-H. Cho, T. S. Seo; *Advanced Materials* **2013,** *25* (27), 3657-3662.
76. M. Zhang, L. Bai, W. Shang, W. Xie, H. Ma, Y. Fu, D. Fang, H. Sun, L. Fan, M. Han, C. Liu, S. Yang; *Journal of Materials Chemistry* **2012,** *22* (15), 7461-7467.
77. N. Mohanty, D. Moore, Z. Xu, T. S. Sreeprasad, A. Nagaraja, A. A. Rodriguez, V. Berry; *Nature Communications* **2012,** *3*, 844.
78. S. Zhuo, M. Shao, S.-T. Lee; *Acs Nano* **2012,** *6* (2), 1059-1064.
79. L. Lin, S. Zhang; *Chemical Communications* **2012,** *48* (82), 10177-10179.
80. D. Pan, L. Guo, J. Zhang, C. Xi, Q. Xue, H. Huang, J. Li, Z. Zhang, W. Yu, Z. Chen, Z. Li, M. Wu; *Journal of Materials Chemistry* **2012,** *22* (8), 3314-3318.
81. X. Yan, X. Cui, B. Li, L.-s. Li; *Nano Letters* **2010,** *10* (5), 1869-1873.
82. M. Li, W. Wu, W. Ren, H.-M. Cheng, N. Tang, W. Zhong, Y. Du; *Applied Physics Letters* **2012,** *101* (10), 103107.
83. Q. Feng, Q. Cao, M. Li, F. Liu, N. Tang, Y. Du; *Applied Physics Letters* **2013,** *102* (1), 013111.
84. A. Wolk, M. Rosenthal, S. Neuhaus, K. Huber, K. Brassat, J. K. N. Lindner, R. Grothe, G. Grundmeier, W. Bremser, R. Wilhelm; *Scientific Reports* **2018,** *8* (1), 5843.
85. S. Li, S. Zhou, Y. Li, X. Li, J. Zhu, L. Fan, S. Yang; *ACS Applied Materials & Interfaces* **2017,** *9* (27), 22332-22341.
86. W.-S. Kuo, C.-Y. Chang, H.-H. Chen, C.-L. L. Hsu, J.-Y. Wang, H.-F. Kao, L. C.-S. Chou, Y.-C. Chen, S.-J. Chen, W.-T. Chang, S.-W. Tseng, P.-C. Wu, Y.-C. Pu; *ACS Applied Materials & Interfaces* **2016,** *8* (44), 30467-30474.
87. R. Li, X. Wang, Z. Li, H. Zhu, J. Liu; *New Journal of Chemistry* **2018,** *42* (6), 4352-4360.

88. E. Hwang, S. Seo, S. Bak, H. Lee, M. Min, H. Lee; *Advanced Materials* **2014,** *26* (30), 5129-5136.
89. Y.-P. Sun, B. Zhou, Y. Lin, W. Wang, K. A. S. Fernando, P. Pathak, M. J. Meziani, B. A. Harruff, X. Wang, H. Wang, P. G. Luo, H. Yang, M. E. Kose, B. Chen, L. M. Veca, S.-Y. Xie; *Journal of the American Chemical Society* **2006,** *128* (24), 7756-7757.
90. S. C. Ray, A. Saha, N. R. Jana, R. Sarkar; *The Journal of Physical Chemistry C* **2009,** *113* (43), 18546-18551.
91. S. Sahu, B. Behera, T. K. Maiti, S. Mohapatra; *Chemical Communications* **2012,** *48* (70), 8835-8837.
92. S.-L. Hu, K.-Y. Niu, J. Sun, J. Yang, N.-Q. Zhao, X.-W. Du; *Journal of Materials Chemistry* **2009,** *19* (4), 484-488.
93. L. Wang, S.-J. Zhu, H.-Y. Wang, S.-N. Qu, Y.-L. Zhang, J.-H. Zhang, Q.-D. Chen, H.-L. Xu, W. Han, B. Yang, H.-B. Sun; *Acs Nano* **2014,** *8* (3), 2541-2547.
94. H. Liu, T. Ye, C. Mao; *Angewandte Chemie International Edition* **2007,** *46* (34), 6473-6475.
95. B. Kong, A. Zhu, C. Ding, X. Zhao, B. Li, Y. Tian; *Advanced Materials* **2012,** *24* (43), 5844-5848.
96. Q. Wang, X. Huang, Y. Long, X. Wang, H. Zhang, R. Zhu, L. Liang, P. Teng, H. Zheng; *Carbon* **2013,** *59*, 192-199.
97. Q. Li, T. Y. Ohulchanskyy, R. Liu, K. Koynov, D. Wu, A. Best, R. Kumar, A. Bonoiu, P. N. Prasad; *The Journal of Physical Chemistry C* **2010,** *114* (28), 12062-12068.
98. S.-T. Yang, X. Wang, H. Wang, F. Lu, P. G. Luo, L. Cao, M. J. Meziani, J.-H. Liu, Y. Liu, M. Chen, Y. Huang, Y.-P. Sun; *The Journal of Physical Chemistry C* **2009,** *113* (42), 18110-18114.
99. B. Zhu, S. Sun, Y. Wang, S. Deng, G. Qian, M. Wang, A. Hu; *Journal of Materials Chemistry C* **2013,** *1* (3), 580-586.
100. M. Bottini, T. Mustelin; *Nature Nanotechnology* **2007,** *2*, 599.
101. P.-C. Hsu, P.-C. Chen, C.-M. Ou, H.-Y. Chang, H.-T. Chang; *Journal of Materials Chemistry B* **2013,** *1* (13), 1774-1781.
102. L. Cao, X. Wang, M. J. Meziani, F. Lu, H. Wang, P. G. Luo, Y. Lin, B. A. Harruff, L. M. Veca, D. Murray, S.-Y. Xie, Y.-P. Sun; *Journal of the American Chemical Society* **2007,** *129* (37), 11318-11319.
103. A. Salinas-Castillo, M. Ariza-Avidad, C. Pritz, M. Camprubí-Robles, B. Fernández, M. J. Ruedas-Rama, A. Megia-Fernández, A. Lapresta-Fernández, F. Santoyo-Gonzalez, A. Schrott-Fischer, L. F. Capitan-Vallvey; *Chemical Communications* **2013,** *49* (11), 1103-1105.
104. Q.-L. Chen, C.-F. Wang, S. Chen; *Journal of Materials Science* **2013,** *48* (6), 2352-2357.
105. S. Iijima; *Nature* **1991,** *354*, 56.
106. R. S. Ruoff, D. C. Lorents; *Carbon* **1995,** *33* (7), 925-930.
107. T. Natsuki, K. Tantrakarn, M. Endo; *Applied Physics A* **2004,** *79* (1), 117-124.
108. A. Merkoçi; *Microchimica Acta* **2006,** *152* (3), 157-174.
109. H. Dai; *Surface Science* **2002,** *500* (1), 218-241.
110. M. S. Dresselhaus, G. Dresselhaus, P. C. Eklund; *Science of Fullerenes and Carbon Nanotubes: Their Properties and Applications*. Elsevier Science: 1996.
111. A. Javey, J. Kong; *Carbon Nanotube Electronics*. Springer US: 2009.
112. P. J. d. Pablo, E. Graugnard, B. Walsh, R. P. Andres, S. Datta, R. Reifenberger; *Applied Physics Letters* **1999,** *74* (2), 323-325.
113. P. Kim, L. Shi, A. Majumdar, P. L. McEuen; *Physical Review Letters* **2001,** *87* (21), 215502.
114. M.-F. Yu, B. S. Files, S. Arepalli, R. S. Ruoff; *Physical Review Letters* **2000,** *84* (24), 5552-5555.

115. S. Xie, W. Li, Z. Pan, B. Chang, L. Sun; *Journal of Physics and Chemistry of Solids* **2000,** *61* (7), 1153-1158.
116. M. Foldvari, M. Bagonluri; *Nanomedicine: Nanotechnology, Biology and Medicine* **2008,** *4* (3), 183-200.
117. J. Muller, F. Huaux, N. Moreau, P. Misson, J.-F. Heilier, M. Delos, M. Arras, A. Fonseca, J. B. Nagy, D. Lison; *Toxicology and Applied Pharmacology* **2005,** *207* (3), 221-231.
118. L. Sophie, B. Jorge; *Current Molecular Medicine* **2006,** *6* (6), 651-663.
119. S. Vardharajula, S. Z. Ali, P. M. Tiwari, E. Eroğlu, K. Vig, V. A. Dennis, S. R. Singh; *International Journal of Nanomedicine* **2012,** *7*, 5361-5374.
120. T. Ebbesen, P. Ajayan; *Nature* **1992,** *358* (6383), 220.
121. A. Thess, R. Lee, P. Nikolaev, H. Dai, P. Petit, J. Robert, C. Xu, Y. H. Lee, S. G. Kim, A. G. Rinzler; *Science* **1996,** *273* (5274), 483-487.
122. J. Kong, A. M. Cassell, H. Dai; *Chemical Physics Letters* **1998,** *292* (4-6), 567-574.
123. T. W. Ebbesen, P. M. Ajayan; *Nature* **1992,** *358*, 220.
124. D. T. Colbert, J. Zhang, S. M. McClure, P. Nikolaev, Z. Chen, J. H. Hafner, D. W. Owens, P. G. Kotula, C. B. Carter, J. H. Weaver, A. G. Rinzler, R. E. Smalley; *Science* **1994,** *266* (5188), 1218-1222.
125. Y. Ando; *Fullerene Science and Technology* **1994,** *2* (2), 173-180.
126. T. Guo, P. Nikolaev, A. G. Rinzler, D. Tomanek, D. T. Colbert, R. E. Smalley; *The Journal of Physical Chemistry* **1995,** *99* (27), 10694-10697.
127. A. Thess, R. Lee, P. Nikolaev, H. Dai, P. Petit, J. Robert, C. Xu, Y. H. Lee, S. G. Kim, A. G. Rinzler, D. T. Colbert, G. E. Scuseria, D. Tománek, J. E. Fischer, R. E. Smalley; *Science* **1996,** *273* (5274), 483-487.
128. R. Sen, A. Govindaraj, C. N. R. Rao; *Chemical Physics Letters* **1997,** *267* (3), 276-280.
129. S. Fan, M. G. Chapline, N. R. Franklin, T. W. Tombler, A. M. Cassell, H. Dai; *Science* **1999,** *283* (5401), 512-514.
130. K. Hernadi, A. Fonseca, J. B. Nagy, D. Bernaerts, A. A. Lucas; *Carbon* **1996,** *34* (10), 1249-1257.
131. M. José-Yacamán, M. Miki-Yoshida, L. Rendón, J. G. Santiesteban; *Applied Physics Letters* **1993,** *62* (6), 657-659.
132. M. Kumar, X. Zhao, Y. Ando, S. Iijima, M. Sharon, K. Hirahara; *Molecular Crystals and Liquid Crystals* **2002,** *387* (1), 117-121.
133. J. Kong, A. M. Cassell, H. Dai; *Chemical Physics Letters* **1998,** *292* (4), 567-574.
134. A. Kleiner, S. Eggert; *Physical Review B* **2001,** *63* (7), 073408.
135. A. Hirsch; *Angewandte Chemie International Edition* **2002,** *41* (11), 1853-1859.
136. I. D. Rosca, F. Watari, M. Uo, T. Akasaka; *Carbon* **2005,** *43* (15), 3124-3131.
137. F. Avilés, J. V. Cauich-Rodríguez, L. Moo-Tah, A. May-Pat, R. Vargas-Coronado; *Carbon* **2009,** *47* (13), 2970-2975.
138. T. Xu, J. Yang, J. Liu, Q. Fu; *Applied Surface Science* **2007,** *253* (22), 8945-8951.
139. M. Grujicic, G. Cao, A. M. Rao, T. M. Tritt, S. Nayak; *Applied Surface Science* **2003,** *214* (1), 289-303.
140. W. Xia, C. Jin, S. Kundu, M. Muhler; *Carbon* **2009,** *47* (3), 919-922.
141. P.-C. Ma, N. A. Siddiqui, G. Marom, J.-K. Kim; *Composites Part A: Applied Science and Manufacturing* **2010,** *41* (10), 1345-1367.
142. Y. Xu, C. Gao, H. Kong, D. Yan, Y. Z. Jin, P. C. P. Watts; *Macromolecules* **2004,** *37* (24), 8846-8853.
143. J. Wang, Z. Fang, A. Gu, L. Xu, F. Liu; *Journal of Applied Polymer Science* **2006,** *100* (1), 97-104.
144. A. Abera, J.-W. Choi; *Analytical Methods* **2010,** *2* (11), 1819-1822.

145. C. V. Nguyen, L. Delzeit, A. M. Cassell, J. Li, J. Han, M. Meyyappan; *Nano Letters* **2002,** *2* (10), 1079-1081.
146. J. Chen, M. A. Hamon, H. Hu, Y. Chen, A. M. Rao, P. C. Eklund, R. C. Haddon; *Science* **1998,** *282* (5386), 95-98.
147. E. T. Mickelson, C. B. Huffman, A. G. Rinzler, R. E. Smalley, R. H. Hauge, J. L. Margrave; *Chemical Physics Letters* **1998,** *296* (1), 188-194.
148. K. F. Kelly, I. W. Chiang, E. T. Mickelson, R. H. Hauge, J. L. Margrave, X. Wang, G. E. Scuseria, C. Radloff, N. J. Halas; *Chemical Physics Letters* **1999,** *313* (3), 445-450.
149. M. Holzinger, O. Vostrowsky, A. Hirsch, F. Hennrich, M. Kappes, R. Weiss, F. Jellen; *Angewandte Chemie International Edition* **2001,** *40* (21), 4002-4005.
150. A. Hamwi, H. Alvergnat, S. Bonnamy, F. Béguin; *Carbon* **1997,** *35* (6), 723-728.
151. J.-M. Lee, S. J. Kim, J. W. Kim, P. H. Kang, Y. C. Nho, Y.-S. Lee; *Journal of Industrial and Engineering Chemistry* **2009,** *15* (1), 66-71.
152. J. L. Stevens, A. Y. Huang, H. Peng, I. W. Chiang, V. N. Khabashesku, J. L. Margrave; *Nano Letters* **2003,** *3* (3), 331-336.
153. P. J. Boul, J. Liu, E. T. Mickelson, C. B. Huffman, L. M. Ericson, I. W. Chiang, K. A. Smith, D. T. Colbert, R. H. Hauge, J. L. Margrave, R. E. Smalley; *Chemical Physics Letters* **1999,** *310* (3), 367-372.
154. J. L. Bahr, J. Yang, D. V. Kosynkin, M. J. Bronikowski, R. E. Smalley, J. M. Tour; *Journal of the American Chemical Society* **2001,** *123* (27), 6536-6542.
155. J. L. Bahr, J. M. Tour; *Chemistry of Materials* **2001,** *13* (11), 3823-3824.
156. V. Georgakilas, K. Kordatos, M. Prato, D. M. Guldi, M. Holzinger, A. Hirsch; *Journal of the American Chemical Society* **2002,** *124* (5), 760-761.
157. R. Martel, T. Schmidt, H. R. Shea, T. Hertel, P. Avouris; *Applied Physics Letters* **1998,** *73* (17), 2447-2449.
158. C. Berger, Y. Yi, Z. L. Wang, W. A. de Heer; *Applied Physics A* **2002,** *74* (3), 363-365.
159. C. L. Cheung, J. H. Hafner, C. M. Lieber; *Proceedings of the National Academy of Sciences* **2000,** *97* (8), 3809-3813.
160. E. Frackowiak, S. Gautier, H. Gaucher, S. Bonnamy, F. Beguin; *Carbon* **1999,** *37* (1), 61-69.
161. M. Das, R. P. Singh, S. R. Datir, S. Jain; *Molecular Pharmaceutics* **2013,** *10* (9), 3404-3416.
162. Y.-J. Lu, K.-C. Wei, C.-C. M. Ma, S.-Y. Yang, J.-P. Chen; *Colloids and Surfaces B: Biointerfaces* **2012,** *89*, 1-9.
163. G. Pastorin, W. Wu, S. Wieckowski, J.-P. Briand, K. Kostarelos, M. Prato, A. Bianco; *Chemical Communications* **2006,** (11), 1182-1184.
164. B. Kateb, M. Van Handel, L. Zhang, M. J. Bronikowski, H. Manohara, B. Badie; *NeuroImage* **2007,** *37*, S9-S17.
165. S. Jain, V. S. Thakare, M. Das, C. Godugu, A. K. Jain, R. Mathur, K. Chuttani, A. K. Mishra; *Chemical Research in Toxicology* **2011,** *24* (11), 2028-2039.
166. W.-J. Guan, Y. Li, Y.-Q. Chen, X.-B. Zhang, G.-Q. Hu; *Biosensors and Bioelectronics* **2005,** *21* (3), 508-512.
167. J. Guo, S. Goasguen, M. Lundstrom, S. Datta; *Applied Physics Letters* **2002,** *81* (8), 1486-1488.
168. Q. Zhong, D. Inniss, K. Kjoller, V. B. Elings; *Surface Science Letters* **1993,** *290* (1), L688-L692.
169. S. A. Solin, A. K. Ramdas; *Physical Review B* **1970,** *1* (4), 1687-1698.
170. J. Maultzsch; *AIP Conference Proceedings* **2010,** *1267* (1), 76-77.

2 Aim of the Project

Nanotechnology is a rapidly progressing multidisciplinary field, which studies the objects with typical sizes of 1-100 nm, links and covers diverse science fields such as engineering, biology, physics and chemistry. As nanotechnology is developing and searching solutions for current problems, nanotech products are inevitable to involve in our daily lives. For the development of nanotech products, we need to focus on primary nanoparticles since nanoparticles would be the building blocks of the novel systems. Therefore, carbon nanostructures were produced, functionalized, characterized and evaluated for different possible applications in this project.

Detonation nanodiamonds (4 – 5 nm primary particle size) have stable inert core and a reactive surface which lets functionalizations. Their tiny size, large specific surface area and functionalizable surface make NDs attractive for various biomedical applications. However, NDs tend to create big tight aggregates in aqueous environment and this is the biggest obstacle for especially biological applications. NDs were functionalized with a variety of molecules in order to increase water dispersibility and biocompatibility. For possible biomedical applications, bioassays were performed. Technology of electrochromic devices is still under development and there are some performance issues to be solved such as short lifetime, degradation of the materials and long response time. Preliminary tests were performed in order to improve the performance of electrochromic devices.

Graphene quantum dots are relatively new member of carbon nanostructure family. The superior properties of GQDs, such as quantum confinement, small size (~5 nm), fluorescence, water-solubility and biocompatibility make GQDs promising nanostructures for broad range of applications. GQDs were produced by a new methodology developed by the research group. Production was improved in order to provide reproducibility of the same sized GQDs.

Carbon dots are promising materials with excellent optical properties, high biocompatibility and low toxicity for biosensing, drug delivery and bioimaging. Accordingly, production of CDs have attracted great attention. In this research project, CDs were produced from chitin derived from different natural resources: insect exoskeleton and shell of shrimp. Different production parameters were used to improve the reproducibility.

Multi-walled carbon nanotubes are well-define carbon nanostructures with tubular shaped multiple graphene layers. Due to their attractive electronic, optical, mechanical and chemical properties, researchers are focused on MWCNTs for various applications, such as nanocomposites, nanoelectronics, and biomedical applications. Functionalization and improvement studies are inevitable as MWCNTs tend to form agglomerates and bundles in liquid media due to van der Waals attraction forces between the nanotubes. MWCNTs were functionalized in order to overcome the mentioned issues and develop novel nanosystems for a broad range of applications.

Functionalization reactions of carbon nanostructures were mostly performed with rhamnose (**P9**), imidazolium-based ionic liquids (**P10** and **P11**), 2-(2-(2-(2-aminoethoxy)ethoxy)ethyl)isoindoline-1,3-dione (**P3**) and tert-butyl (2-(2-(2-aminoethoxy)ethoxy)ethyl)carbamate (**P1**) in order to improve the solubility, and biocompatibility, and introduce the biological or electronic properties of organic molecule for various applications.

P9 and **P11** were used in order to increase the water solubility of carbon nanostructures as sugars are rich in hydroxyl groups. Additionally, dTDP-L-rhamnose is essential for the production of cell walls of some plants and bacteria such as *Streptococcus* and *Enterococcus*. The cell wall production in bacteria can be targeted and inhibited. increase the water solubility as sugars are rich in hydroxyl groups which form hydrogen bonds and tend to increase the solubility in water. Additionally, dTDP-L-Rhamnose is used in production of cell walls of plants and bacteria such as *Streptococcus* and *Enterococcus*. 1-position occupied rhamnose may inhibit the polymerization of rhamnose as it occurs with α-1,2-/α-1,3 linkage. *Aspergillus niger* causes black mold on fruits and vegetables

contains and contains L-rhamnose uptake receptors. **P9** or **P11** functionalized carbon nanostructures can be targeted to this fungus.

P10 is an imidazolium-based ionic liquid. Ionic liquids (ILs) can enhance the solubility of poorly soluble carbon nanostructures in aqueous solutions by changing the surface properties. ILs have potential antimicrobial, antibiofilm and antitumoral activities.

With **P1** and **P3** functionalizations, it was aimed to increase the solubility of the carbon nanostructures. Surface modifications may change the electronic properties of the nanostructure and introduce new properties which are useful for possible applications.

The research project aimed to improve the properties of carbon nanostructures with functionalizations, produce GQDs and CDs with novel methodologies and evaluate for their possible applications.

3 Results and Discussion

As it is described in the Introduction chapter, we have functionalized, characterized and evaluated four different types of carbon nanostructures for their promising applications. These carbon nanostructures were: Detonation Nanodiamonds, Graphene Quantum Dots (GQDs), Carbon Dots (CDs) and Multi-Walled Carbon Nanotubes (MWCNTs). They are made of carbon atoms but they differ in particle size and shape, solubility, conductivity, chemical structure and reactivity. Despite the pristine carbon nanostructures have fascinating properties, a chemical functionalization is generally needed in order to improve their properties.

Purpose of functionalizations with various organic units (**P1**, **P3**, **P5** and **P7**) was increasing the solubility of carbon nanostructures and allowing further reactions. When double functionalization is performed and two different, orthogonal protected groups are introduced, it is possible to attach two different molecules with different properties such as fluorescence moiety and anticancer agent.[1]

Functionalizations with rhamnose containing molecule were performed to increase the water solubility as sugars are rich in hydroxyl groups which form hydrogen bonds and tend to increase the solubility in water. Additionally, Rhamnose dTDP-L-Rhamnose is used in production of cell walls of plants and bacteria such as *Streptococcus* and *Enterococcus*.[2] Since the polymerization of Rhamnose occurs with α-1,2-/α-1,3 linkage, the cell wall production in bacteria can be inhibited as the introduced molecule was a Rhamnose which has 1-position occupied by a chain. *Aspergillus niger*, a fungus, causes black mold on fruits and vegetables contains L-rhamnose uptake receptor.[3] By exploiting the L-rhamnose uptake receptor, rhamnose functionalized nanodiamonds can be targeted to the rhamnose specific receptor containing cells.

Ionic Liquids (Imidazolium Salts) are catanionic hydrotropes with attractive properties. Both the ionic liquid cations and anions can help to enhance the solubility of poorly soluble compounds in aqueous solutions.[4] Additionally, they

have potential antitumoral, antimicrobial and antibiofilm activities,[5-6] and for example, thanks to this latter activity, they can find industrial application, considering that microbial biofilms are industrially responsible for productivity loss causing pipe blockage, corrosion and contamination.

For the explained purposes, different carbon nanostructures functionalizations were performed and the derivatives were characterized and eventually biological and electronic evaluations of our final products are in progress.

3.1 Functionalizations and Characterization of Detonation Nanodiamonds

The pristine material was characterized in order to understand their properties and then surface modifications were performed. Detonation Nanodiamonds naturally contain different functional groups on their surface.[7] It is possible to utilize these different surface groups such as epoxy and carboxyl to couple divers compounds with beneficial properties for possible applications. Thus, on NDs we have performed numerous coupling reactions with different compounds and conditions. As mentioned earlier, the main disadvantage of NDs in aqueous environments is the solubility. By these functionalizations, it was possible to increase the dispersibility of NDs in water. With the ongoing tests, it will be possible to evaluate the effects of the performed functionalizations from the biological point of view.

3.1.1 Characterization of Pristine Detonation Nanodiamonds

Pristine detonation nanodiamonds were characterized by TEM, AFM and EFM imaging, TGA, DLS measurements, Solubility test and IR and Raman spectroscopies.

Primary particle size of NDs were confirmed as 4-5 nm with a broad population of nanodiamonds by the TEM images (Figure 3.1.1).

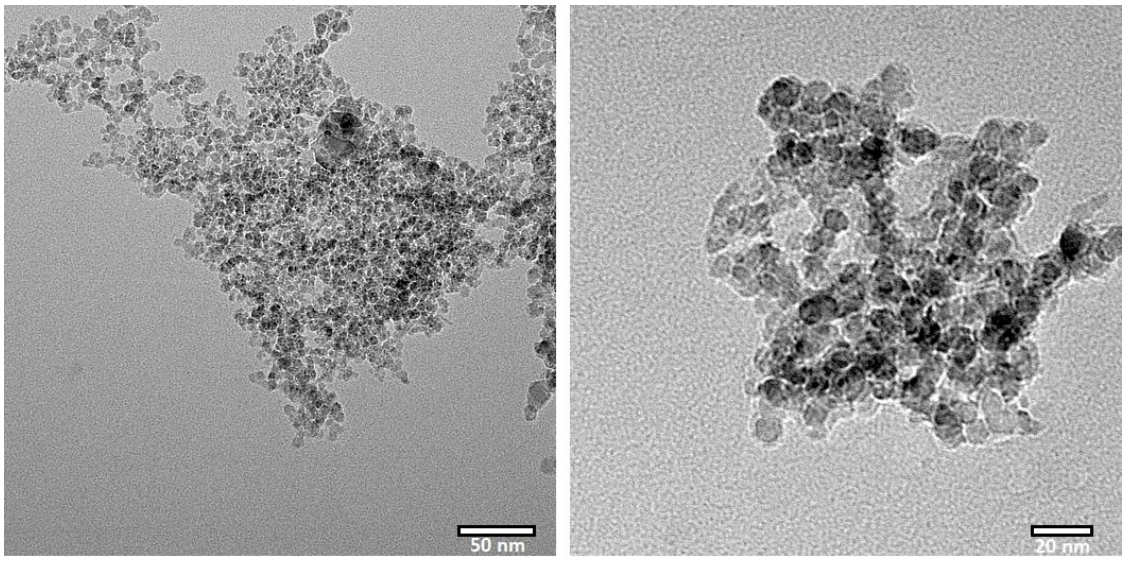

Figure 3.1.1: TEM images of pristine detonation nanodiamonds. The scale bars are 50 nm for the image on the left and 20 nm for the image on the right.

As expected, pristine NDs have shown low dispersion stability in water (1 mg/ml). The sedimentation occurs rapidly as it is shown in Figure 3.1.2 , right after the sonication for pristine NDs. Thus, on the TEM images, NDs were found as big aggregates.

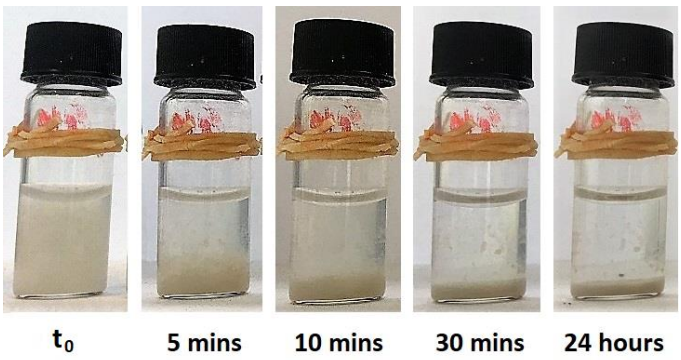

Figure 3.1.2: Solubility test of pristine detonation nanodiamonds. Time represents the time after sonication.

The agglomerate size of detonation NDs were characterized by DLS measurements, and found of around 170 nm. With time, agglomerate size population was observed to increase (Figure 3.1.3) while freshly prepared sample was containing relatively smaller NDs agglomerates.

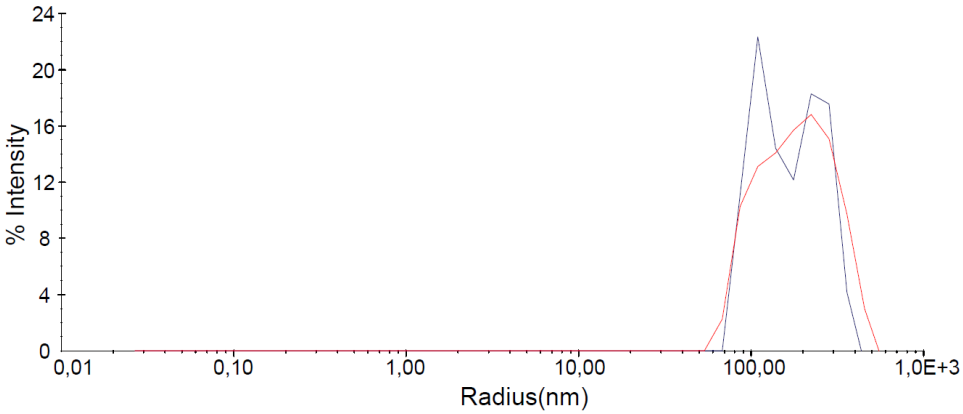

Figure 3.1.3: DLS measurements of pristine detonation nanodiamonds. Black line is freshly prepared sample. Red line represents the second measurement performed right after the first.

TGA measurements were performed in order to understand the thermal stability of pristine nanodiamonds. Above 550 °C, weight loss of pristine material increases, thus, it is possible to evaluate TGA measurements of functionalized Nanodiamonds below 550 °C (Figure 3.1.4). For the calculations, the values

under 550 °C were used to avoid any contribution related to the pristine carbon nanomaterial on the calculations of degree of functionalizations.

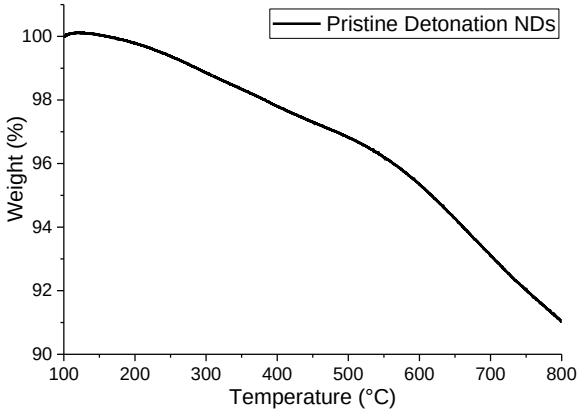

Figure 3.1.4: TGA curve of Pristine Detonation Nanodiamonds. TGA was performed under N_2 atmosphere.

The Raman spectrum of pristine detonation NDs show a sharp diamond peak at 1330 cm^{-1} with a shoulder toward lower wavenumbers, and a broader, asymmetric peak with a maximum at 1617 cm^{-1} (Figure 3.1.5, a). In the case of graphitic layers and amorphous carbon surrounded diamond core, the Raman signal of diamond cannot be observed.[8] Our results suggest that the surface of our pristine nanodiamonds is not covered with these layers since the diamond peak is clearly visible.

FT-IR spectroscopy was performed with three different methodologies: Transmission, ATR and DRIFT. Due to the technique, some peaks were observed with different intensities. The O-H stretching and O-H bending modes were detected 3200 – 3600 cm^{-1} and 1625 – 1645 cm^{-1}, respectively. C=O stretching mode was detected between 1725 – 1780 cm^{-1}. The “Fingerprint” region of NDs are between 900 – 1500 cm^{-1} and includes many overlapping contributions from the diamond core and surface groups. The main contribution from oxygen containing groups is related to C-O-C bending modes of ether groups, lactones or acid anhydrides around 1100 – 1140 cm^{-1}, besides C-O stretching modes of hydroxyl groups are detected in this region.[9-10] On FT-IR spectra, these peaks were visible between 1000 – 1200 cm^{-1} (Figure 3.1.5).

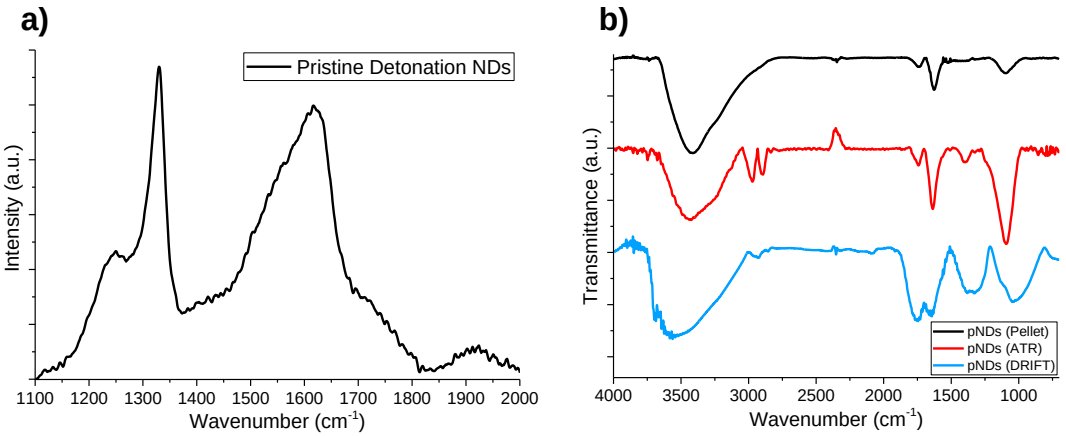

Figure 3.1.5: a) RAMAN spectrum of Pristine Detonation Nanodiamonds **b)** FT-IR spectra of Pristine Detonation Nanodiamonds measured by Transmission (black), ATR (red) and DRIFT (blue).

Additionally, AFM and EFM analyses were performed in order to study further the agglomerate size and electrical properties of NDs deposited on a perfect surface such as silicon wafer. The big agglomerates were confirmed by AFM images (Figure 3.1.6, a, c) and EFM imaging provided relatively better resolution and details, as nanodiamonds are insulator and the surface was boron doped silicon wafer (p-type) (Figure 3.1.6, b).

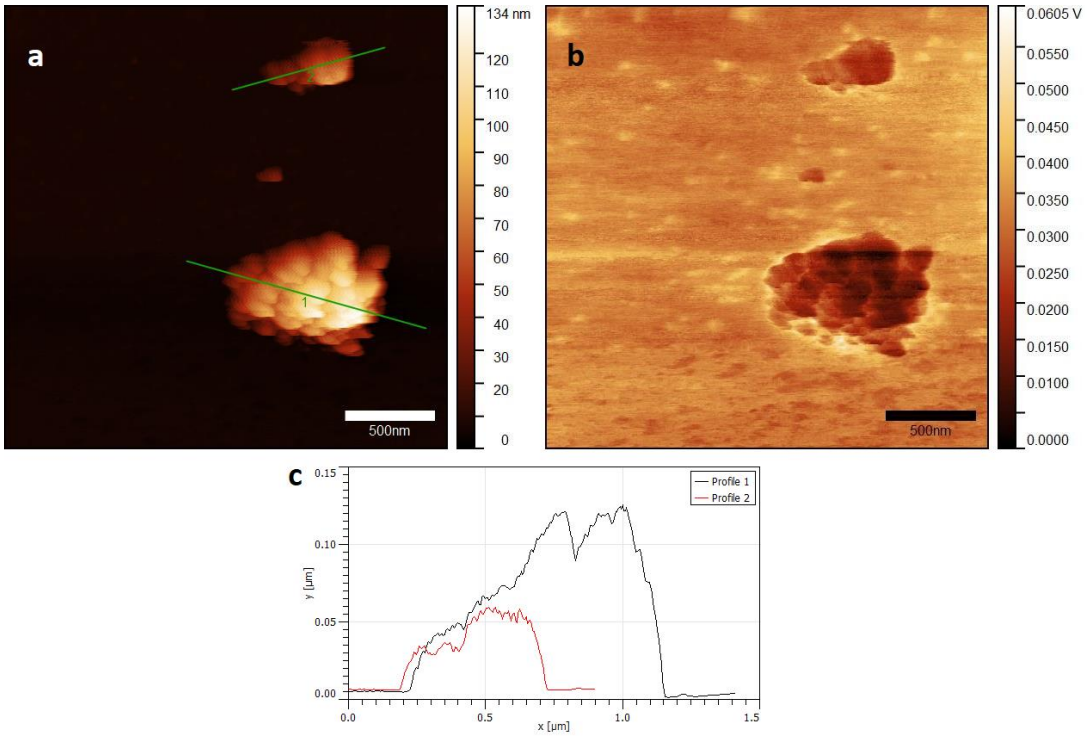

Figure 3.1.6: a) AFM image and **b)** EFM image of pristine NDs. **c)** The section analysis profile of the line on AFM image.

3.1.2 Oxidation of Detonation Nanodiamonds

As shown earlier the variety of the nanodiamond surface groups is consistent. In some cases it is important to have a homogenous surface to produce functionalized nanodiamonds with specific reactions. Acid treatment of NDs would increase the carboxylic groups on the surface of NDs and make them more prone to amidation reactions. For this purpose, we oxidized pristine NDs through acid treatment with H_2SO_4 and HNO_3 mixture (3:1) at 80 °C.

The morphology and the particle size of oxidized detonation nanodiamonds (**ND1**) were confirmed by TEM imaging and they maintained particle size distribution similar to the pristine material (Figure 3.1.7).

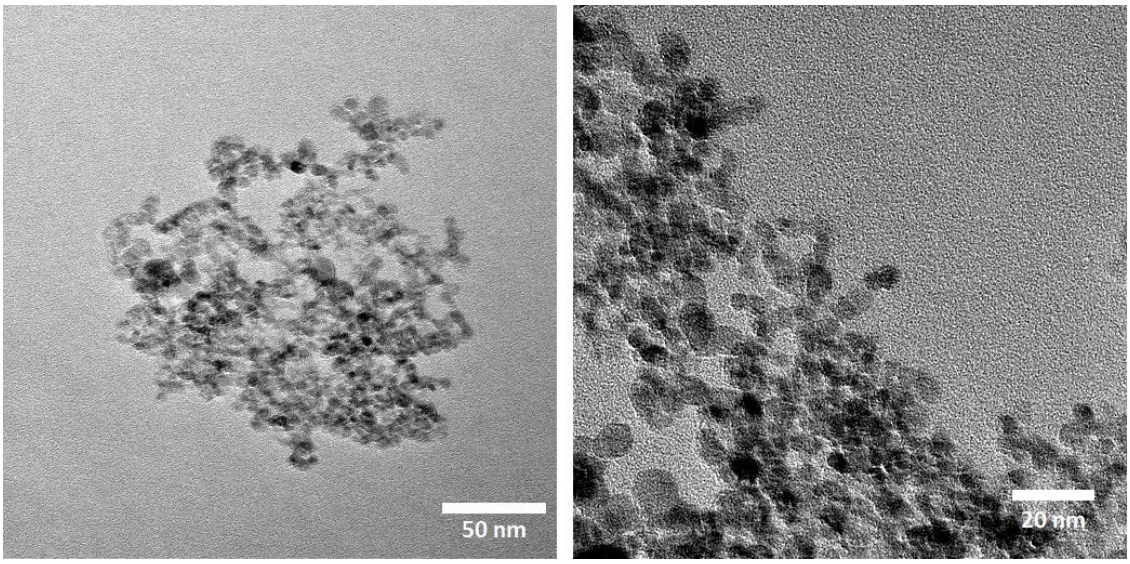

Figure 3.1.7: TEM images of **ND1**.

The water solubility of **ND1** is not different than pristine detonation nanodiamonds and their dispersion is not stable, and precipitates in less than 5 minutes as the pristine material (Figure 3.1.8).

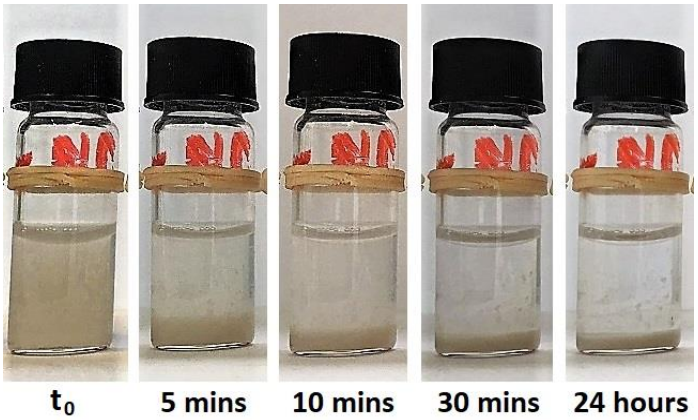

Figure 3.1.8: Solubility test of **ND1**. Time represents the time after sonication.

Also the agglomerate size of **ND1** was not significantly different from the pristine material. Two DLS measurement of the same **ND1** sample gave two similar peaks which, in this case, do not change significantly with time (Figure 3.1.9).

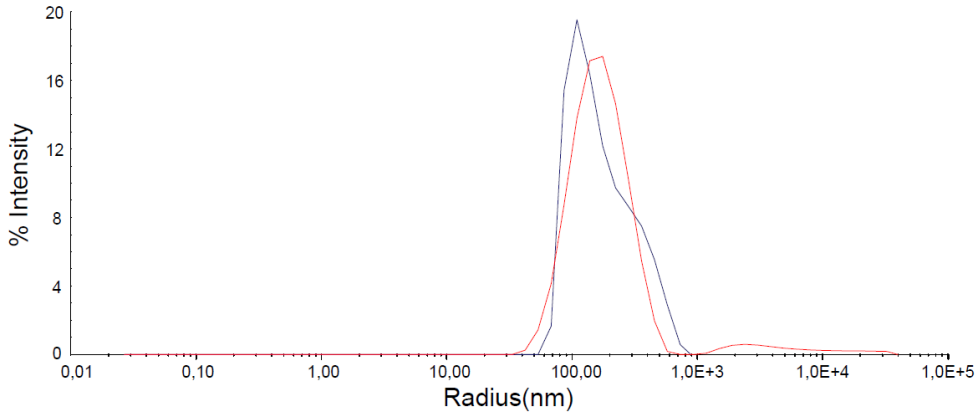

Figure 3.1.9: DLS measurements of **ND1**. Black line is freshly prepared sample. Red line represents another measurement of the same sample right after the first measurement.

TGA was performed in order to analyze the degree of functionalization obtained with the acid treatment. The weight loss at TGA at 450°C after the oxidation reaction increased of the 1.69% with respect to pristine nanomaterial, being around 5% (Figure 3.1.10).

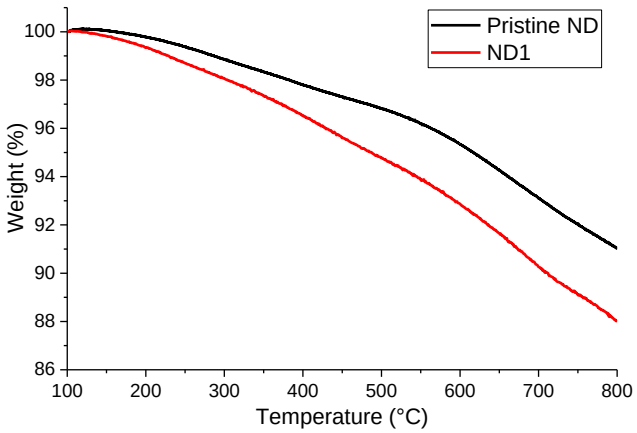

Figure 3.1.10: TGA of Pristine Detonation Nanodiamonds (black) and **ND1** (red). TGA was performed under N_2 atmosphere.

Raman spectra show that the diamond core of **ND1** is not damaged or covered with graphitic layers and amorphous carbon after acid treatment at 80 °C. In fact the diamond peak of **ND1** is shown at 1330 cm^{-1}. A shoulder at 1740 cm^{-1} is more evident, than for pristine material and it consistent with the C=O stretching, thanks to the increase of carboxyl groups on the surface of **ND1** after the oxidation (Figure 3.1.11, a).

FT-IR spectrum of **ND1** was similar to the spectrum of pristine NDs. A broad OH stretching band between 3200 – 3600 cm^{-1} was observed as for pristine NDs. Sharpening of C-O-C bending peak at around 1100 cm^{-1}, related to lactones, acid anhydrides or ether groups, was detected (Figure 3.1.11, b).

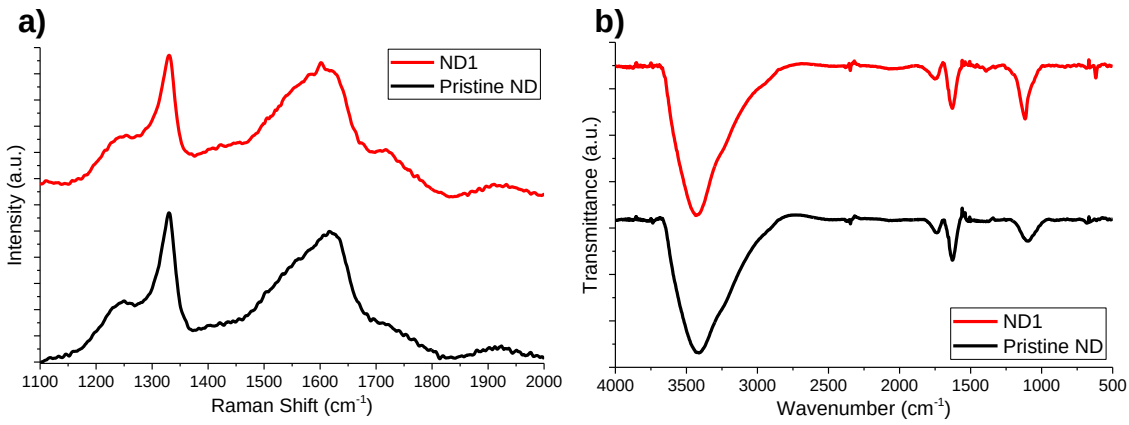

Figure 3.1.11: a) RAMAN spectra and **b)** FT-IR spectra of Pristine Detonation Nanodiamonds (black) and **ND1** (red). (Spectral acquisition mode: Transmission)

AFM images were acquired to investigate the agglomeration behavior change through the performed acid treatment. The agglomerates on the silicon surface were seen as big as pristine NDs (Figure 3.1.12).

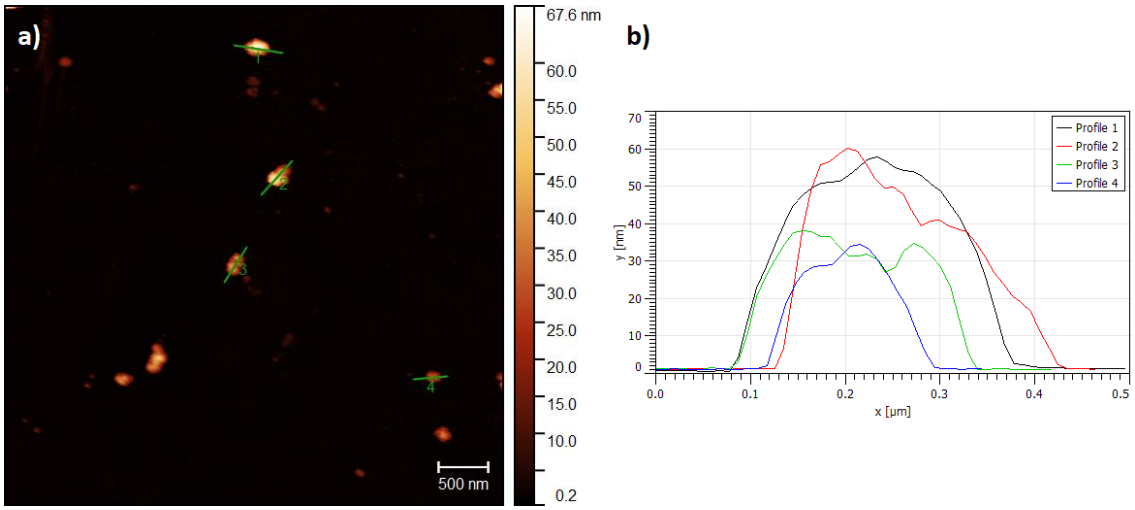

Figure 3.1.12: a) AFM image of **ND1**. **b)** The section analysis profile of the lines on AFM image.

3.1.3 Amidation of Nanodiamonds

Pristine Nanodiamonds and **ND1** were functionalized via amide bond generation between the amino group of the organic compound and carboxyl group on the surface of nanodiamonds, using typical protocols of carboxylic acid activation. Surface bound amino groups are useful to couple larger functional moieties on nanodiamonds.

3.1.3.1 Amidation of Nanodiamonds with N-Boc-PEG-Amine (P1) and N-Pht-PEG-Amine (P3) and Production of ND-NH_2

Amidation reactions with **P1** and **P3** were performed on nanodiamonds with differently activated carboxyl groups. The activation reactions of pristine ND and **ND1** with $SOCl_2$ at 70 °C for 24 hours yielded the chlorinated products **ND2** and **ND1.1** respectively. Subsequently, the amidation reaction was performed with **P1** at 100 °C, **ND2.1** and **ND1.2** (the latter deriving from **ND1**). When **ND1.1** were allowed to react with **P3** they lead to **ND1.4**. Moreover to understand if there is any difference in the degree of functionalization using the thionyl chloride approach or other activation agents as EDC, the reaction was repeated also with EDC•HCl, DMAP and HOBt (using **P1** as amine) obtaining **ND1.6** and **ND1.8** from pristine ND and **ND1** with **P1**, respectively (Figure 3.1.13).

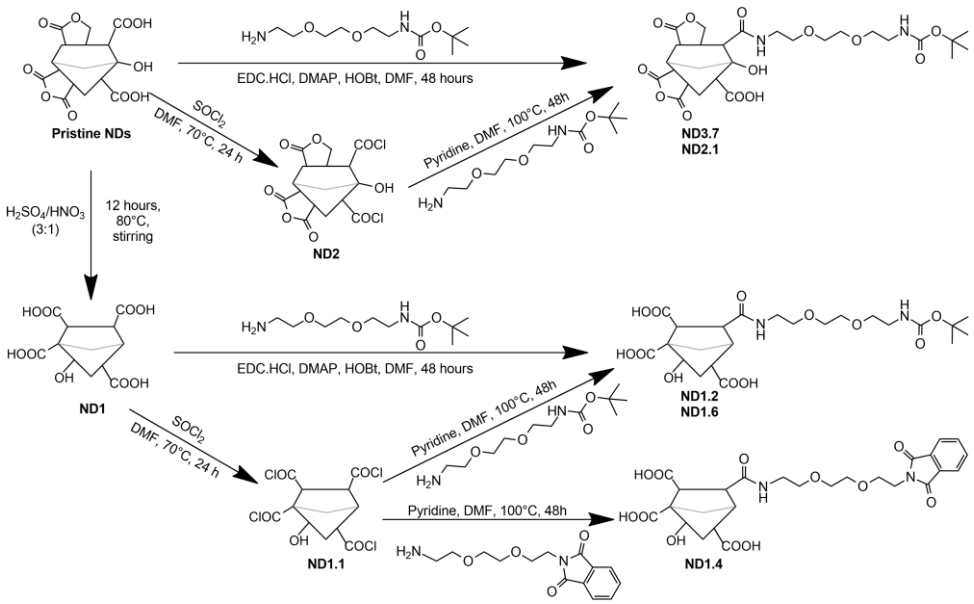

Figure 3.1.13: Flow chart of amidation reactions between nanodiamonds and **P1** and **P3**.

TGA was performed to calculate the degrees of functionalizations, as difference between the values corresponding to the weight loss at 450 °C of the considered compound to respect to the starting material. The degree of functionalization of the products yielded from the reactions with **P1** were measured by TGA and calculated as 235 µmol/g, 40 µmol/g, 152 µmol/g and 21 µmol/g, for **ND1.2**, **ND1.6**, **ND2.1** and **ND3.7**, respectively (Figure 3.1.14, d). For **ND1.4** which is **P3** functionalized oxidized ND, degree of functionalization was calculated 72 µmol/g (Figure 3.1.14, d) and from this it seems that the reactions in presence of Boc protected amine were more efficient. The degrees of functionalizations of the reactions with $SOCl_2$ as the activator of the carboxyl groups were higher than the reactions with HOBt, EDC•HCl and DMAP.

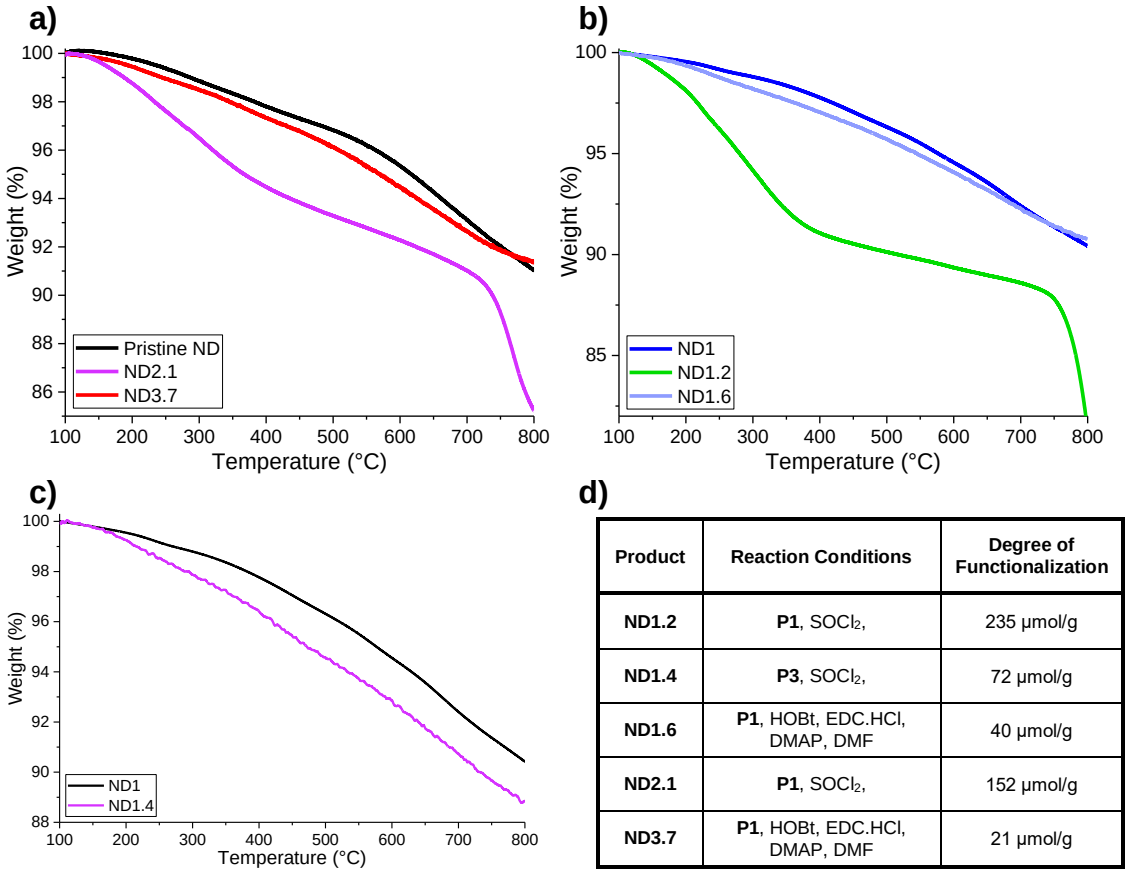

Product	Reaction Conditions	Degree of Functionalization
ND1.2	**P1**, $SOCl_2$,	235 µmol/g
ND1.4	**P3**, $SOCl_2$,	72 µmol/g
ND1.6	**P1**, HOBt, EDC.HCl, DMAP, DMF	40 µmol/g
ND2.1	**P1**, $SOCl_2$,	152 µmol/g
ND3.7	**P1**, HOBt, EDC.HCl, DMAP, DMF	21 µmol/g

Figure 3.1.14: TGA graphics of **a) ND2.1** and **ND3.7**, **b) ND1.2** and **ND1.6** and **c) ND1.4**, with comparison to the starting materials, and **d)** calculated degrees of functionalization.

FT-IR was performed in order to confirm the functionalization of nanodiamonds. Amide bond generation can be confirmed for the both products **ND2.1** and **ND1.2** by the presence of the amide bond peaks. Around 3500 cm^{-1}, NH stretching is clearly visible for **ND1.2,** while it is less evident for **ND2.1**. This could be due to the difference of the degree of functionalization. C=O stretching band of amide bond at 1620 cm^{-1} can not be distinguished as pristine NDs and **ND1** already contains C=O stretching band while C-N stretching band is found at 1260 cm^{-1} for both **ND1.2** and **ND2.1** products and it is very intense (Figure 3.1.15).

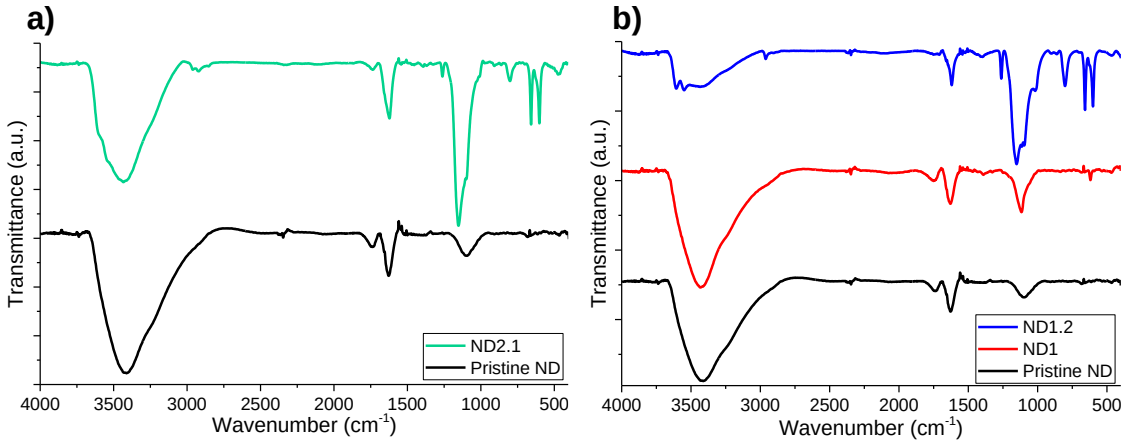

Figure 3.1.15: FT-IR spectra of **a) ND2.1** (green) and **b) ND1.2** (blue), with comparison to the starting materials. (Spectral acquisition mode: Transmission)

Raman spectroscopy was performed to confirm the persistence of diamond core and surface of the products, as expected (Figure 3.1.16).

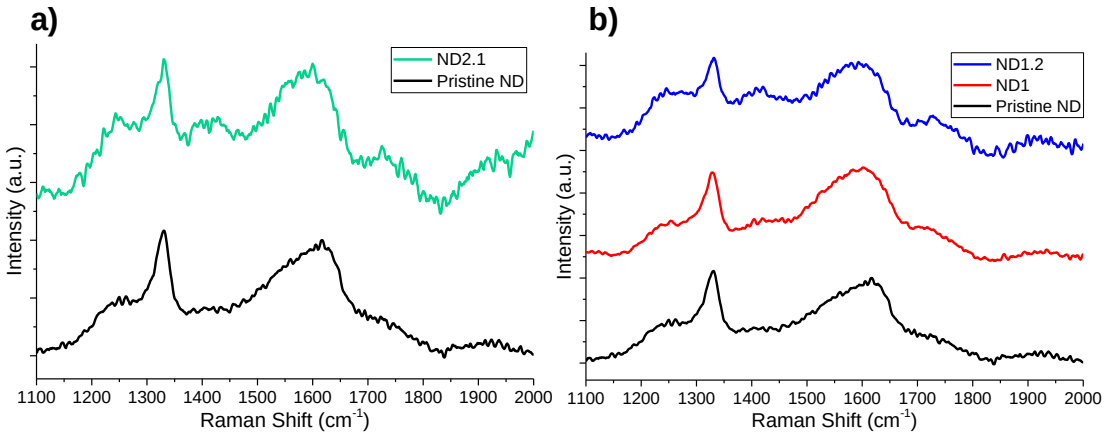

Figure 3.1.16: Raman spectra of **a) ND2.1** (green) and **b) ND1.2** (blue) with comparison to the starting materials.

Deprotection of the Protected Groups

The protecting groups present on the chains introduced by amidation were removed in order to expose the terminal amino groups to allow further functionalizations and also to increase the solubility in polar solvents. Boc deprotection of **ND1.2**, **ND1.6**, **ND2.1** and **ND3.7** was performed in acidic conditions by using HCl in 1,4-dioxane (4M) while the phthalimide group deprotection of **ND1.4**, yielding **ND1.5** (Figure 3.1.17), was performed by hydrazine. Thus, ND-NH_2 was synthesized with different methodologies.

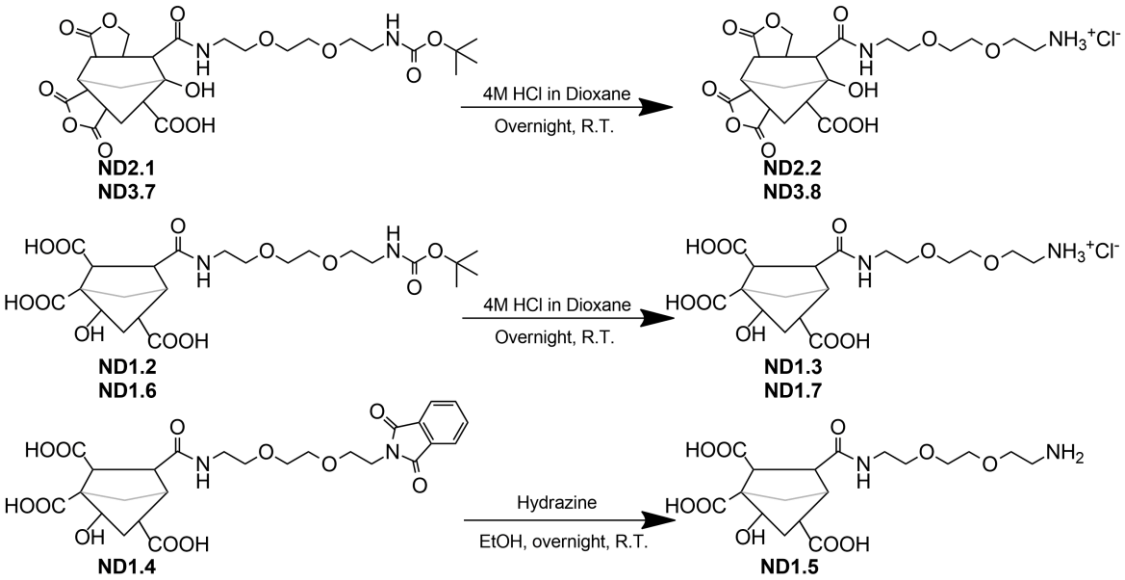

Figure 3.1.17: Deprotection reactions of Boc and Pht groups and synthesis of ND-NH_2.

Water dispersibility test show that the NDs with amino terminal groups (NDs-NH_2) gained affinity for polar solvents. As it is visible from Figure 3.1.18 (a), 48 hour after sonication **ND1.3** was still dispersed in water while oxidized and pristine nanodiamonds precipitate rapidly in 5 minutes (Figure 3.1.18, b) and they totally aggregate on the bottom of the vial 48 hour after sonication (Figure 3.1.18, c).

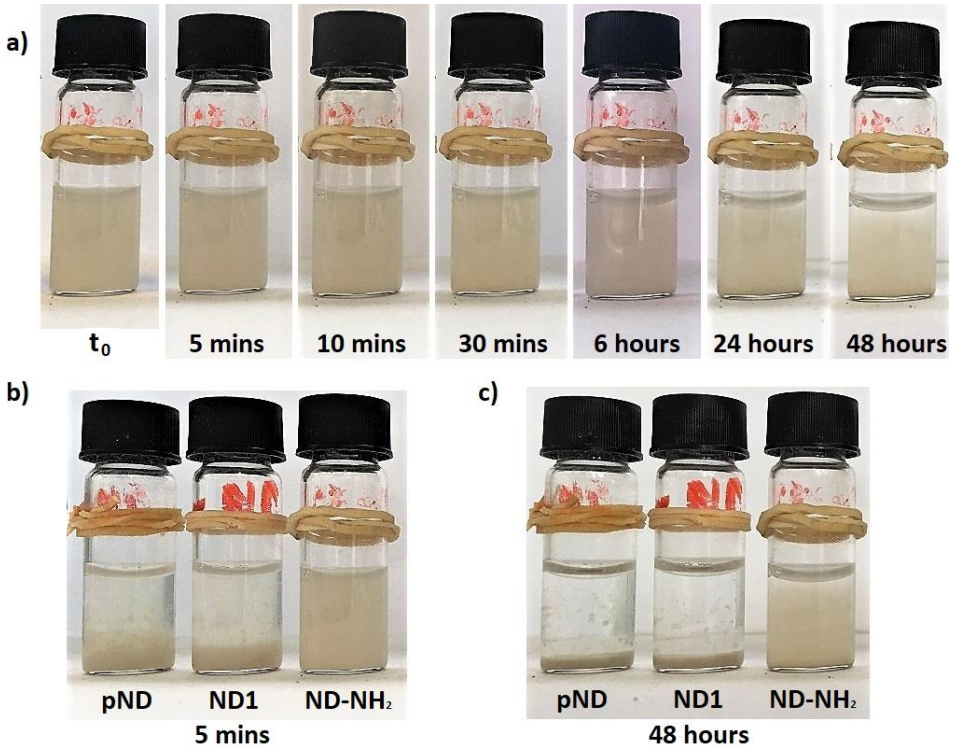

Figure 3.1.18: a) Water dispersibility test of ND-NH_2. Precipitation comparison of pristine nanodiamonds (pND), oxidized nanodiamonds (**ND1**) and ND-NH_2 (**ND1.3**) in **b)** 5 minutes and **c)** 48 hours. Time represents the interval between sonication and analyses.

TEM images were collected using the same concentration of NDs in water (1 mg/ml) to prepare the grids. As qualitative data, ND-NH_2 was found more dispersed than the starting NDs and, as expected, the particle size was retained (Figure 3.1.19).

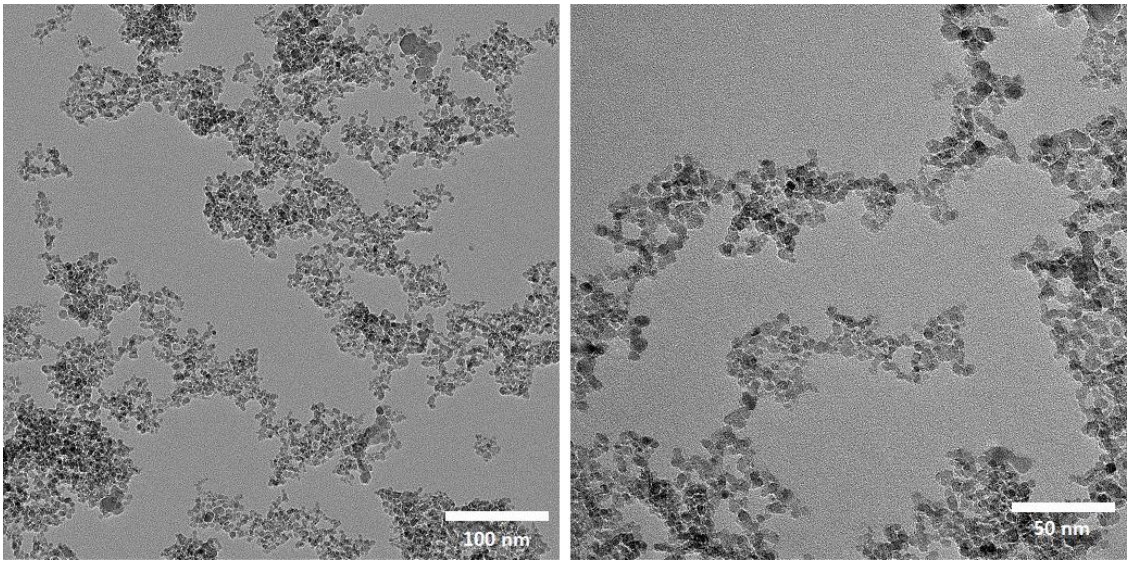

Figure 3.1.19: TEM images of ND-NH_2 (**ND1.3**).

AFM and EFM measurement were performed to investigate the aggregation behavior after the functionalization of nanodiamonds. AFM images show that the aggregates of ND-NH_2 on the silicon surface were of smaller dimension with respect to the pristine nanodiamonds and also much more dispersed (Figure 3.1.20).

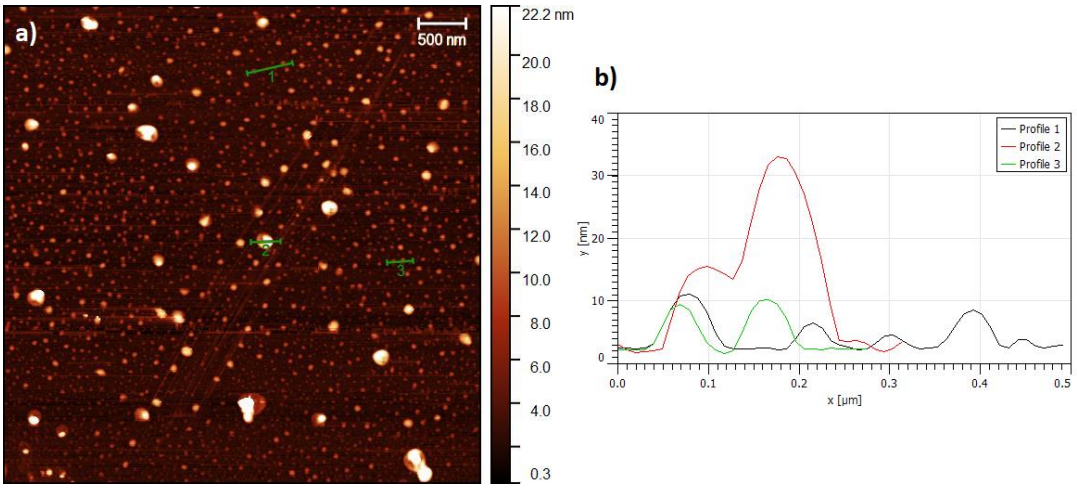

Figure 3.1.20: a) AFM image of ND-NH_2 (**ND1.3**) and **b)** the section analysis profile of the lines on AFM image.

FT-IR spectra of ND-NH_2 shows that C-N stretching band shifts from 1220 cm^{-1} to 1210 cm^{-1} for both products (Figure 3.1.21).

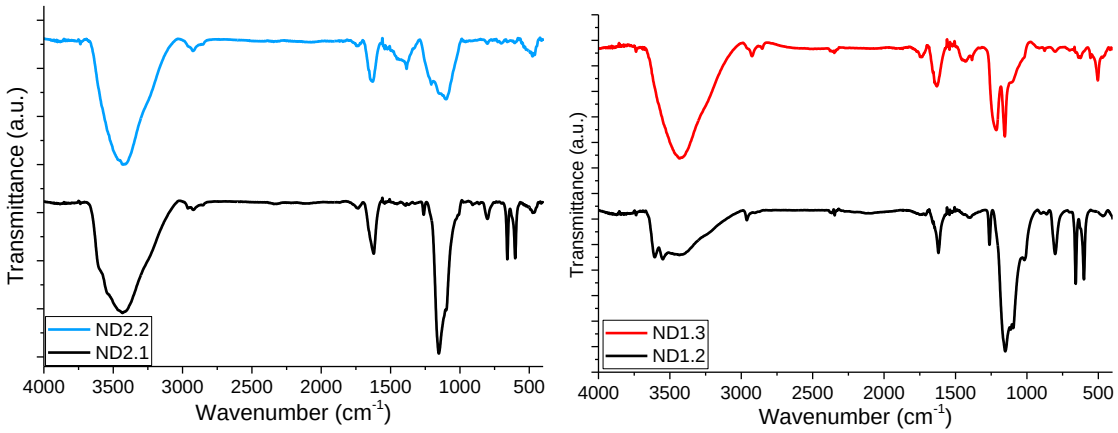

Figure 3.1.21: FT-IR spectra of ND-NH_2 from pristine ND (left) and from oxidized ND (**ND1**) (right). (Spectral acquisition mode: Transmission)

The biological activities of functionalized and characterized ND-NH_2 were investigated in Section 3.5 Evaluations of Carbon Nanostructures for Various Applications.

3.1.3.2 Coupling of ND-NH_2 (ND1.5) with Ru TrisBiPy (P8), FITC (P9) and Ferrocene acid (P10)

As mentioned in the Introduction, nanodiamonds can be studied and employed in many fields when functionalized, especially if the solubility drawback is overcome by introduction of amine groups. Moreover these amino terminal groups can be used as convenient binding point for other molecules in order to produce modified nanodiamonds presenting also the properties of the linked molecules. For this purpose, ND-NH_2 (**ND1.5**) was functionalized with RuTrisBiPy (**P8**), FITC (**P9**) and Ferrocene acid (**P10**), resulting in **ND1.5.1**, **ND1.5.2** and **ND1.5.3**, respectively.

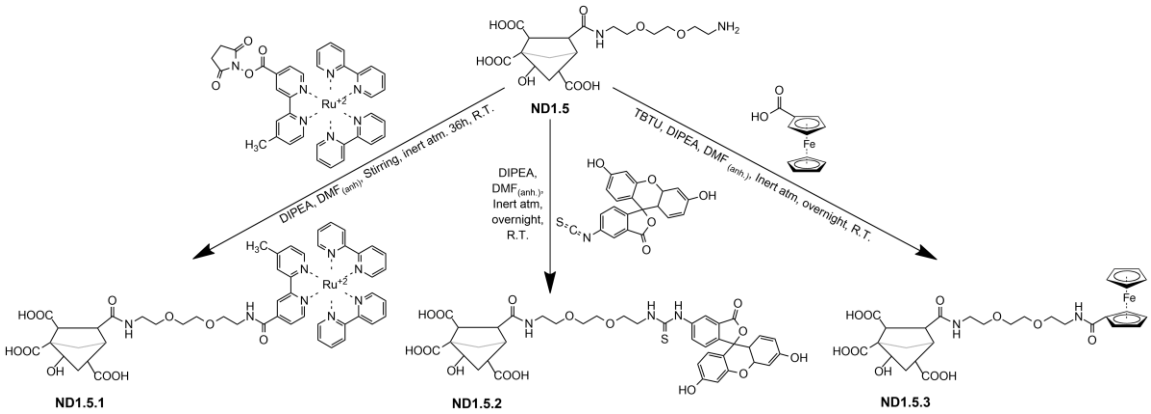

Figure 3.1.22: Coupling reactions between ND-NH_2 and **P8**, **P9** and **P10**

P8 and **P9** are fluorophores often used in combination with nanoparticles.[11-12] and in this work they were linked to NDs to improve their optical properties with the aim to introduce luminescence activity to the nanosystems for bioimaging applications. **P10** is an organometallic compound with excellent electron donor properties. Thus, electrochemical properties of nanodiamonds can be enhanced by the functionalization with this molecule. Additionally, **P10** functionalized nanodiamonds can be used in medical applications. In fact ferroquine, which is a ferrocene based derivative reported in literature as the most promising in biological application up to now, shows antimalarial activity and some other derivatives were investigated for their antitumoral activities.[13-15]

The compounds were characterized by TGA to calculate the loading degree of compounds **P8**, **P9** and **P10** on the nanodiamonds surface, resulting in 69

µmol/g, 123 µmol/g and 98 µmol/g for **ND1.5.1**, **ND1.5.2** and **ND1.5.3**, respectively (Figure 3.1.23).

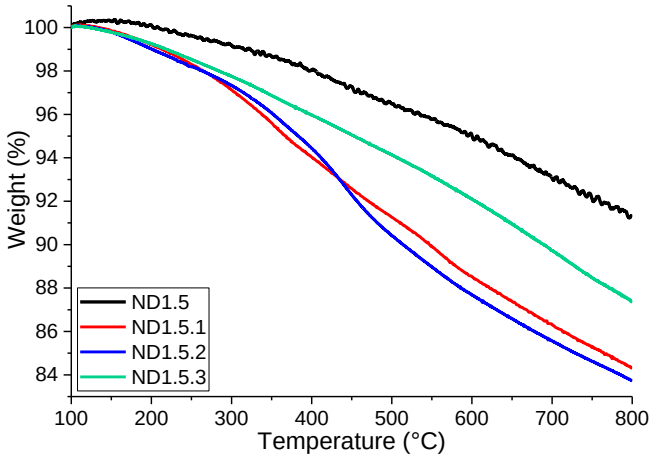

Figure 3.1.23: TGA graphics of **P8**, **P9** and **P10** coupled ND-NH_2 (**ND1.5**).

UV-visible and Fluorescence spectroscopy measurements were performed on **ND1.5.1** and **ND1.5.2**. Absorption and emission features of the coupled compounds were present in the spectra of functionalized nanodiamonds. For **ND1.5.1**, there following feature were clearly visible: the absorption peak at 285 nm, which corresponds to ligand centered π* ← π transition, and a broad Metal-to-Ligand Charge Transfer transition absorption peak around 450 nm (Figure 3.1.24, a). An emission peak was observed at around 610 nm, where **P8** emits. UV-vis spectra of **ND1.5.2** shows a peak around 495 nm which is characteristic absorbance peak for fluorescein isothiocyanate molecule (Figure 3.1.24, b). The highest emission of **ND1.5.2** was observed around 520 nm which confirmed the addition of fluorescence properties of **P9** to the non-fluorescent nanodiamonds. As fluorescence yield of ferrocene was reported zero in the literature[16], optical measurements were not performed on **ND1.5.3**.

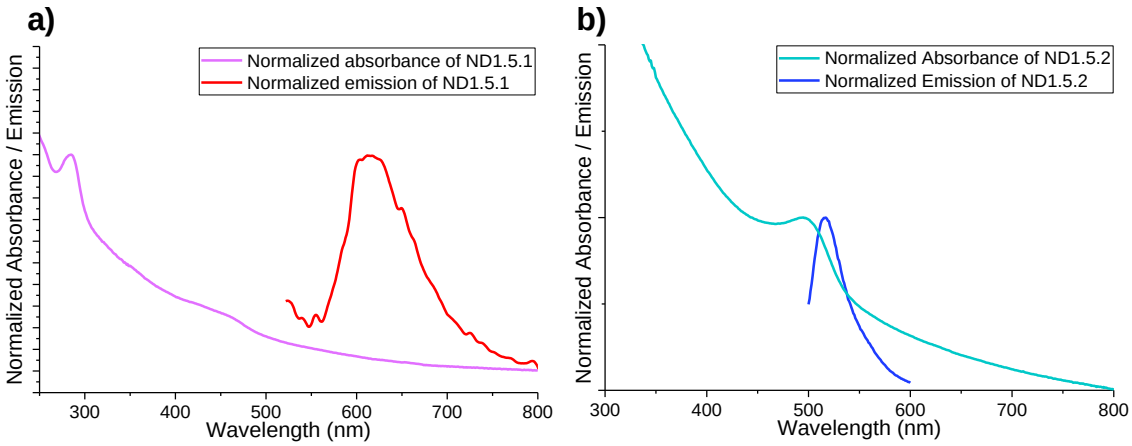

Figure 3.1.24: Normalized absorption and emission spectra of **P8** functionalized nanodiamond (**ND1.5.1**) and **P9** functionalized nanodiamond (**ND1.5.2**).

Further characterizations of **ND1.5.1** and **ND1.5.3** are ongoing in collaboration with the Department of Chemistry of the University of Bologna while cellular uptake assay of **ND1.5.2** was discussed in Section 3.5 Evaluations of Carbon Nanostructures for Various Applications.

3.1.3.3 Functionalization of Nanodiamonds with sugar and ionic liquid derivatives

Another approach to increase the water dispersibility of NDs has been the conjugation of NDs with sugar and ionic liquid derivatives. Moreover the chosen molecules can exert some biological properties. For these purposes, nanodiamonds were functionalized with Rhamnose-Amine (**P9**), Ionic Liquid-Amine (**P10**), Rhamnose-Ionic Liquid-Amine (**P11**), Hexyl α-L-rhamnopyranoside **(P12)**, Bulky sugar molecule (**P13**) and 3-Aminopropanenitrile (Figure 3.1.25). The reactions were performed following the normal procedure (in the presence of coupling reagents) but some blank reactions without activation methodologies were also performed to investigate the possible secondary interactions that could take place.

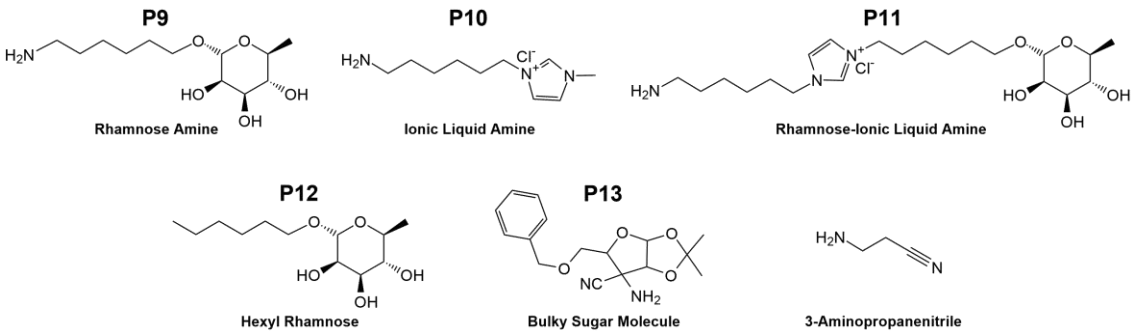

Figure 3.1.25: Molecular structure of Rhamnose Amine (**P9**), Ionic Liquid Amine (**P10**), Rhamnose-Ionic Liquid Amine (**P11**), Hexyl α-L-rhamnopyranoside **(P12)**, Bulky sugar molecule (**P13**) and 3-Aminopropanenitrile.

P9, **P10**, **P11**, **P12** and **P13** compounds were kindly provided by the research group of Prof. Nguyen Van Nhien and Prof. A. Ahad Hadad from the Université de Picardie Jules Verne.

Evaluation of the reactions with **P9** and **P12**

ND3.1a-b were synthesized from pristine nanodiamonds and rhamnose-amine (**P9**) using, in the case of **ND3.1a**, HOBt, EDC•HCl and DMAP while **ND3.1b** was performed in absence of the coupling reagents, as blank. The starting materials for **ND4.1a-e** products were oxidized nanodiamonds (**ND1**) and rhamnose-amine

(**P9**). The conditions of reactions were optimized in order to obtain better degree of functionalization. ND4.1a was prepared with HOBt, EDC•HCl and DMAP while **ND4.1b** was produced in absence of the coupling reagents. **ND4.1c** was obtained with the coupling agents, and with a double amount of **P9** with respect to **ND4.1b**. The reaction of **ND4.1d** was performed in Tris-HCl buffer (pH 7-8) in presence of NHS and EDC•HCl. **ND4.1e** was prepared with HBTU and TEA. **ND3.5** and **ND4.5** derived from pristine nanodiamonds and **ND1** respectively, in the absence of coupling reagents in order to investigate the interactions with **P12**, which is the alkylic analogous of **P9** (Figure 3.1.26).

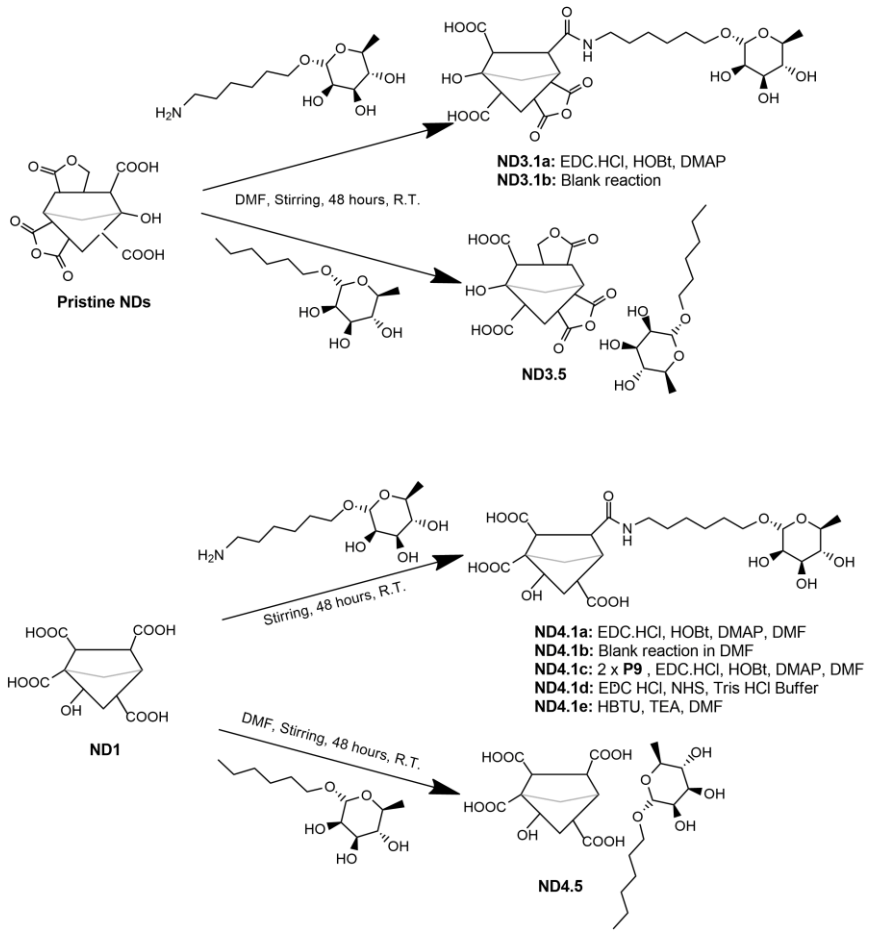

Figure 3.1.26: Reactions of pristine NDs and **ND1** with **P9** and **P12.** Synthesis of **ND3.1a-b**, **ND3.5**, **ND4.1a-e** and **ND4.5.**

TGA measurements were performed on **ND3.1a,b** and **ND4.1a-e** (Figure 3.1.27). The degrees of functionalization of the reactions with nanodiamonds and **P9** were compared. The **ND3.1a** resulted in relatively low degree of functionalization (49 µmol/g). The reaction performed without coupling reagents with pristine

nanodiamonds (**ND3.1b**) produced an interesting high degree of functionalization (220 µmol/g). Vice versa, the reaction with oxidized NDs with coupling reagents (**ND4.1a**) produced the highest degree of functionalization (246 µmol/g), while for **ND4.1b** (in absence of coupling reagents) the reaction resulted with relatively low degree of functionalization (5 µmol/g). As mentioned, **ND4.1c** was obtained by using double amount of **P9** and resulted in a degree of functionalization of 83 µmol/g. **ND4.1d** yielded 103 µmol/g of degree of functionalization. **ND4.1e** reaction which was performed with different coupling reagents was resulted with relatively low degree of functionalization (75 µmol/g). The degree of functionalization of blank reactions with **P12** (**ND3.5** and **ND4.5**) were interestingly higher than expected (Figure 3.1.27).

These results suggest that pristine detonation nanodiamonds naturally have enough appropriate functional groups such as epoxide rings that may allow the reactions with free amino groups,[17] and there is the need of a further investigation to confirm this hypothesis.

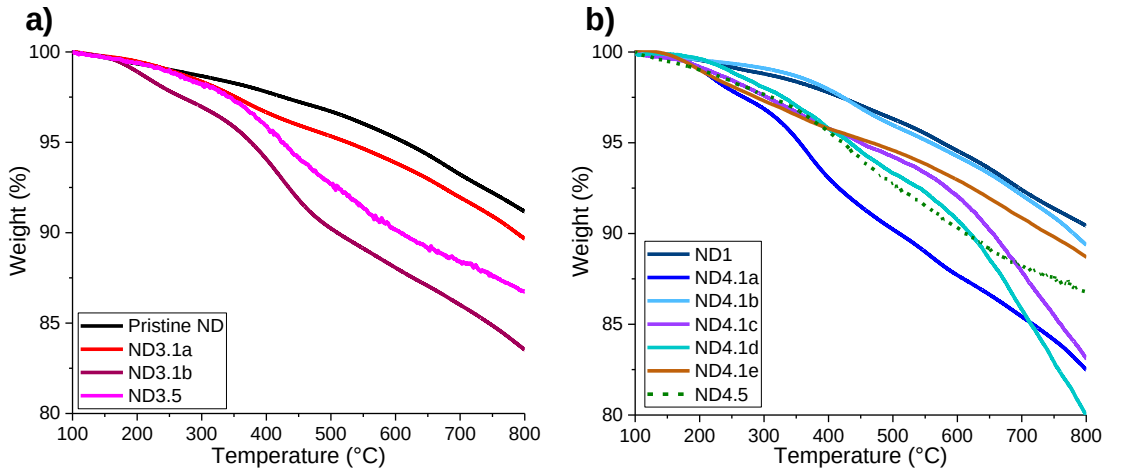

Product	Reaction Conditions	Degree of Functionalization
ND3.1a	HOBt, EDC.HCl, DMAP, DMF	49 µmol/g
ND3.1b	Only DMF	220 µmol/g
ND3.5	Only DMF	125 µmol/g

Product	Reaction Conditions	Degree of Functionalization
ND4.1a	HOBt, EDC.HCl, DMAP, DMF	246 µmol/g
ND4.1b	Only DMF	5 µmol/g
ND4.1c	HOBt, EDC.HCl, DMAP, DMF, 2x **P9**	83 µmol/g
ND4.1d	NHS, EDC.HCl, Tris-HCl buffer	103 µmol/g
ND4.1e	HBTU, TEA	75 µmol/g
ND4.5	Only DMF	114 µmol/g

Figure 3.1.27: TGA graphics and the calculated degree of functionalizations of the functionalized nanodiamonds yielded from the reaction between pristine nanodiamonds (**a**) or oxidized nanodiamonds (**b**) and **P9** and **P12**.

FT-IR spectra show that the **ND3.1b**, **ND4.1a** and **ND4.1d** have increased CH_2 symmetric and asymmetric stretching peaks between 2850 – 2930 cm^{-1}, which is related to **P9** structure. For the reactions with relatively high degree of functionalizations **(ND3.1b** and **ND4.1a)** and **ND4.1d**, a sharpened peak at 1055 cm^{-1} corresponding to the C-O stretching band, which is the most characteristic peak of **P9**, is present. While **ND4.1a** shows an obvious increase on intensity at 1660 cm^{-1}, a small increase of intensity was seen for **ND4.1d**. Amide I peak around 1660 cm^{-1} is a strong band characteristic of all amides that originates from C=O stretch vibrations. For **ND3.1a**, **ND4.1a** and **ND4.1d**, amide II band, a mixture of the C-N stretch and the N-H bend vibrations, is positioned at 1575 cm^{-1} and seems like a small shoulder. The results support the possibility of epoxide opening reaction for pristine nanodiamonds instead of amidation and further characterizations are required to confirm. The spectra of **ND3.5** and **ND4.5** were not significantly different than the spectra of their starting materials (pristine and oxidized nanodiamonds, respectively).

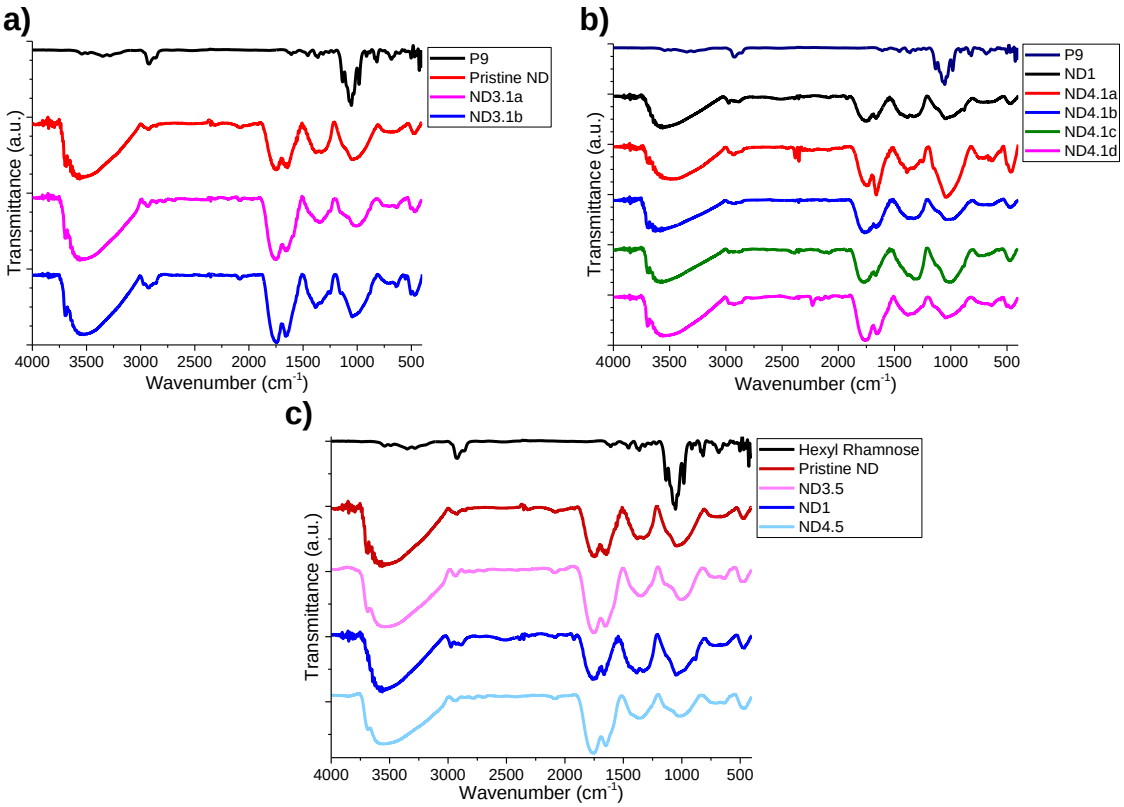

Figure 3.1.28: FT-IR spectra of **a) ND3.1a,b**, **b) ND4.1a-d**, and **c) ND3.5** and **ND4.5**. (Spectral acquisition mode: DRIFTS)

TEM images of the nanodiamonds before and after reaction suggest the overall integrity of the individual nanodiamonds was retained and functionalized nanodiamonds were well-dispersed on TEM grid (Figure 3.1.29).

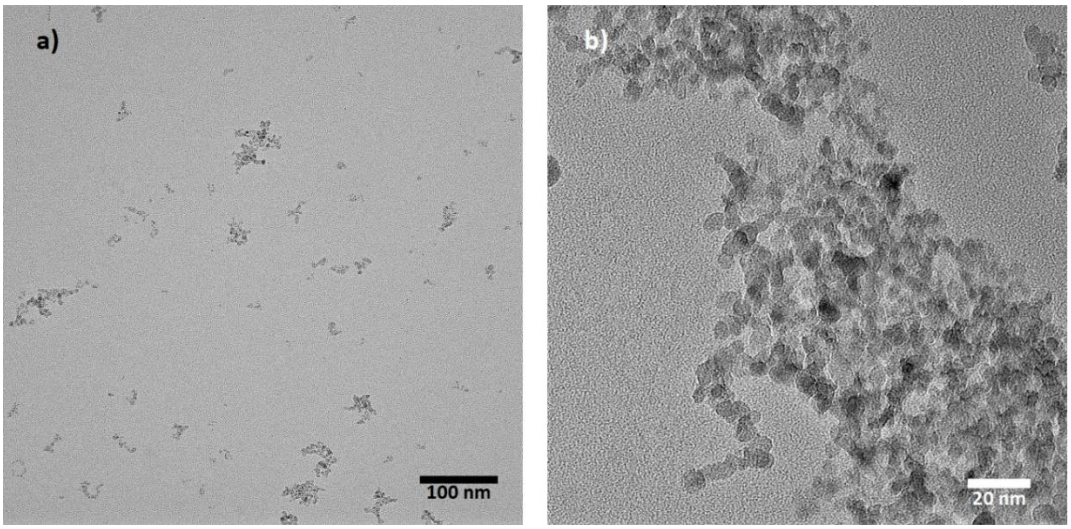

Figure 3.1.29: TEM images of **ND4.1a**

Besides in AFM images, the clusters of nanodiamonds were seen small and well-dispersed (Figure 3.1.30).

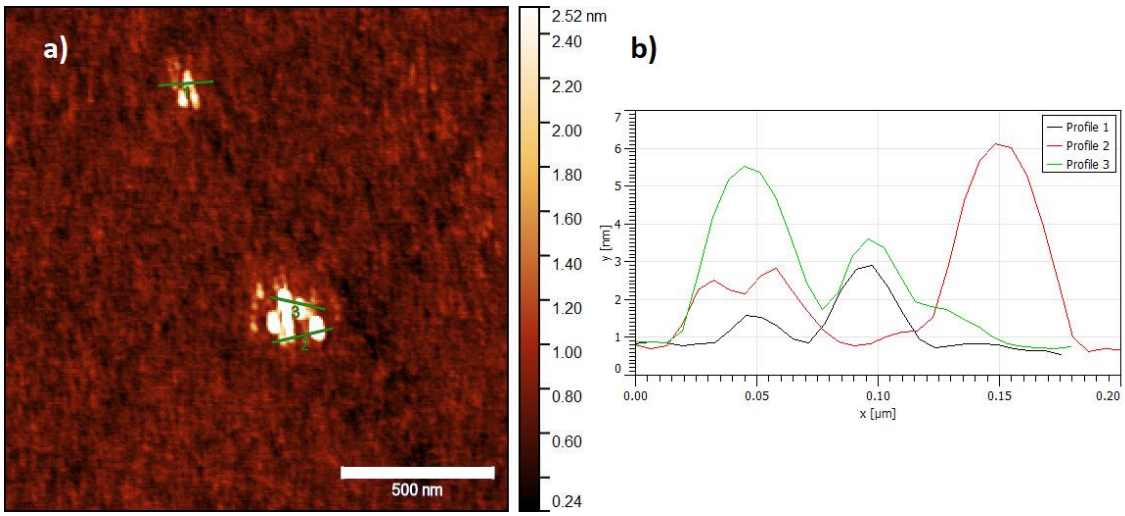

Figure 3.1.30: a) AFM image of **ND4.1a** and **b)** the section analysis profile of the lines on AFM image.

Dispersibility test for **ND4.1a** was performed with 1 mg nanodiamond in 1 mL of water. It was shown that functionalization with the sugar molecule (**P9**) significantly improved the solubility of Nanodiamonds in water (Figure 3.1.31).

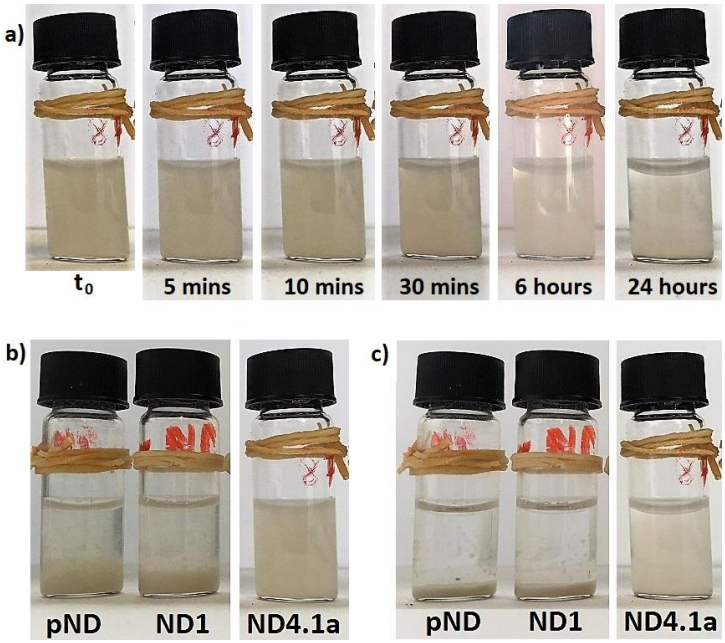

Figure 3.1.31: a) Water solubility test of rhamnose functionalized nanodiamonds (**ND4.1a**). Precipitation comparison of pristine nanodiamonds (pND), oxidized nanodiamonds (**ND1**) and **ND4.1a** in **b)** 5 minutes and **c)** 24 hours. Time represents the time after sonication.

Evaluation of the reactions with **P10**

ND3.2a,b samples were synthesized from pristine nanodiamonds and ionic liquid-amine (**P10**). **ND3.2a** was prepared with HOBt, EDC•HCl and DMAP while the reaction of **ND3.2b** was performed in absence of the coupling reagents while **ND4.2a,b** products yielded from the reactions between oxidized nanodiamonds (**ND1**) and ionic liquid-amine (**P10**) with (**ND4.2a**) or without (**ND4.2b**) coupling reagents.

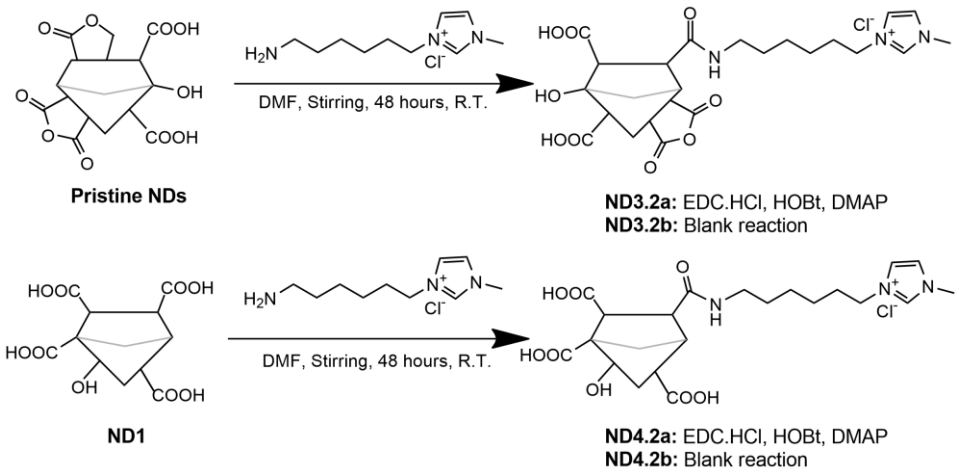

Figure 3.1.32: Reactions of pristine NDs and **ND1** with **P10.** Synthesis of **ND3.2a-b** and **ND4.2a-b.**

TGA characterizations of **ND3.2a,b** and **ND4.2a,b** were performed and the degrees of functionalization were compared (Figure 3.1.33). The **ND3.2a** resulted in low degree of functionalization (34 µmol/g), vice versa the blank reaction (**ND3.2b**) produced an interesting degree of functionalization (219 µmol/g). The reaction with oxidized NDs produced the highest degree of functionalization (446 µmol/g) with coupling reagents (**ND4.2a**), while for **ND4.2b** the reaction resulted with the degree of functionalization of 137 µmol/g.

The TGA results of the reactions with **P10** were similar to the ones obtained with **P9** with good functionalization of the oxidized nanodiamonds with amidation (**ND4.2.a**) and of pristine NDs with alternative reactions (**ND3.2b**). yielded higher degree of functionalization comparing to the one in presence of coupling reagents (**ND3.2a**), and also in case the results suggest that the reaction with pristine nanodiamonds occurs through epoxide opening instead of amidation and it needs to be further investigated.

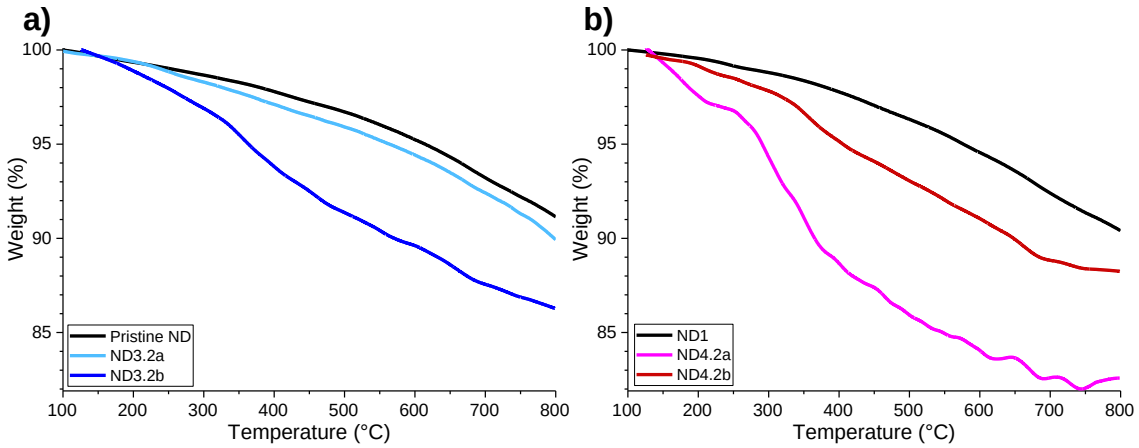

Product	Reaction Conditions	Degree of Functionalization
ND3.2a	HOBt, EDC.HCl, DMAP, DMF	34 µmol/g
ND3.2b	Only DMF	219 µmol/g

Product	Reaction Conditions	Degree of Functionalization
ND4.2a	HOBt, EDC.HCl, DMAP, DMF	446 µmol/g
ND4.2b	Only DMF	137 µmol/g

Figure 3.1.33: TGA graphics and the calculated degree of functionalizations of the functionalized nanodiamonds yielded from the reaction between pristine nanodiamonds (**a**) or oxidized nanodiamonds (**b**) and **P10**.

FT-IR spectra show that the **ND3.2b**, **ND4.2a** and **ND4.2b** have increased CH_2 symmetric and asymmetric stretching peaks between 2850 – 2930 cm^{-1}, which are related to the **P10** molecule. In **ND3.2b**, **ND4.2a** and **ND4.2b**, the peak at

1665 cm^{-1} sharpens and it can be related to C=N and C=C stretching of imidazolium ring,[18] and to amide I peak which originates from C=O stretch vibrations. The peak which can be related to C-N stretching of the secondary amine appears at 1250 cm^{-1} in the IR spectra of the reactions in the absence of coupling reactions (**ND3.2b** and **ND4.2b**). A small peak related to intramolecular vibrational modes of the skeletal vibration of the imidazolium ring was seen at around 620 cm^{-1} in the spectra of **ND3.2b** and **ND4.2a**.

The FT-IR results show that the peaks related to **P10** are visible in the spectra of functionalized products except **ND3.2a**, suggesting that the amount of carboxyl groups on the surface of pristine nanodiamonds is much lower than the epoxy groups.

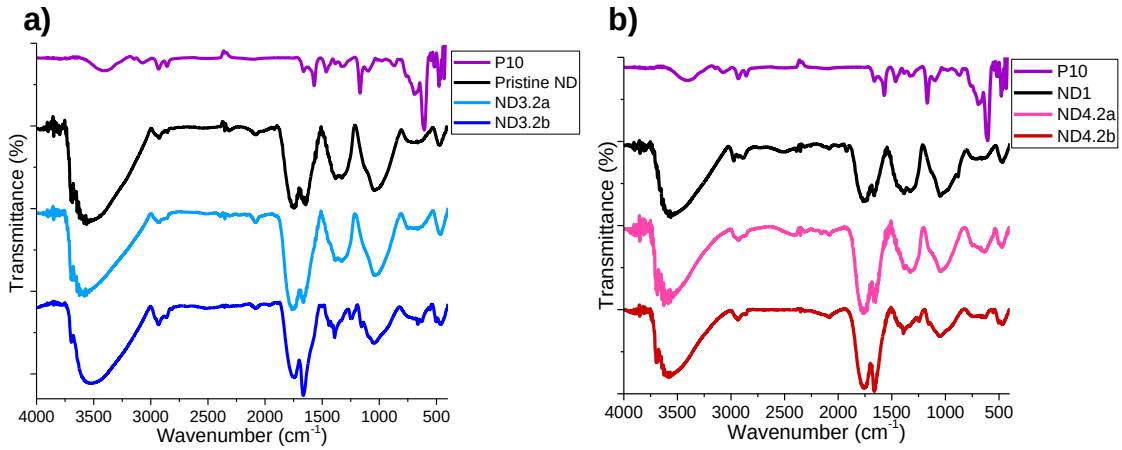

Figure 3.1.34: FT-IR spectra of **a) ND3.2a,b** and **b) ND4.2a,b**. (Spectral acquisition mode: DRIFTS)

TEM images of **ND4.2a** (the highest degree of functionalization) show that the overall integrity of the individual nanodiamonds after the functionalization was retained, as expected, and that **ND4.2a** aggregate more homogeneously than ND-NH_2 and **ND4.1a**.

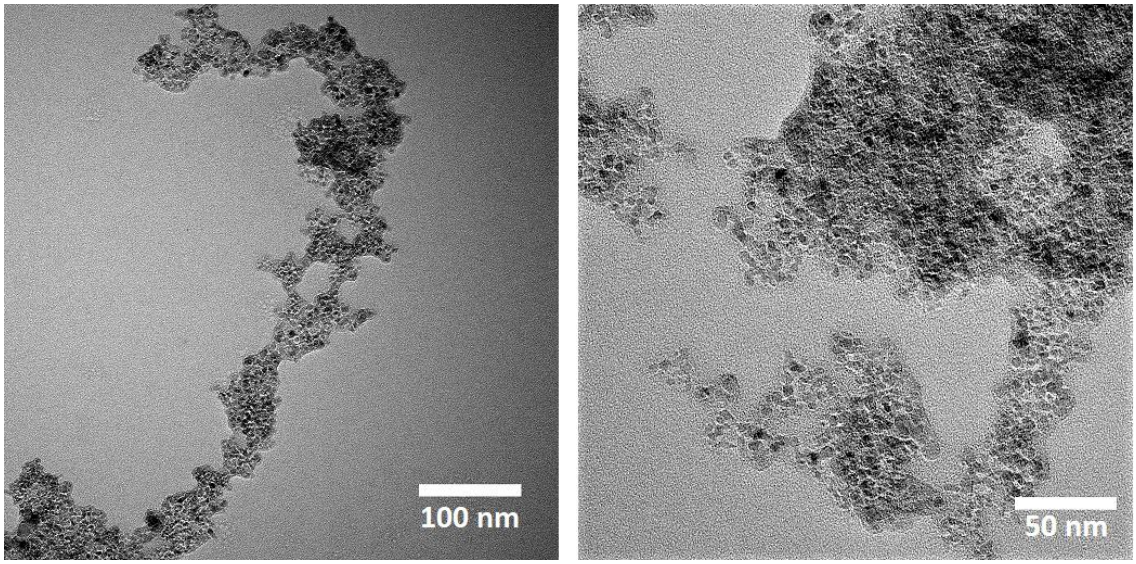

Figure 3.1.35: TEM images of **ND4.2a**

AFM images of **ND4.2a** show big aggregates on the silicon surface comparing to other functionalized nanodiamonds and confirms the connections between the aggregates as seeing in the TEM images.

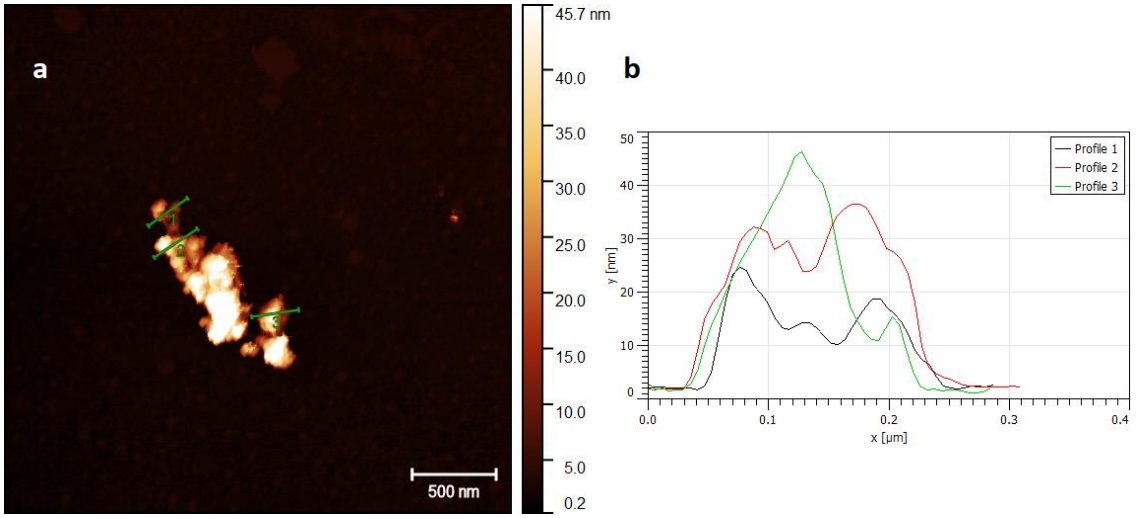

Figure 3.1.36: a) AFM image of **ND4.2a** and **b)** the section analysis profile of the lines on AFM image.

Water dispersibility test was performed on **ND4.2a** and the time of precipitation was quite increased: the pristine and oxidized nanodiamonds precipitate rapidly, while functionalized nanodiamonds **ND4.2a** were still water dispersed 24 hour after sonication (Figure 3.1.37).

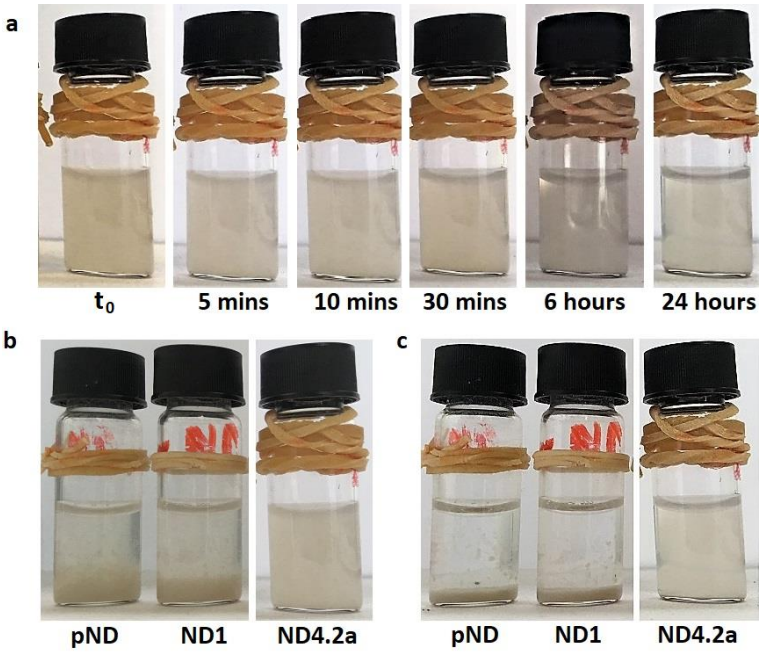

Figure 3.1.37: a) Water solubility test of Ionic Liquid functionalized nanodiamonds (**ND4.2a**). Precipitation comparison of pristine nanodiamonds (pND), oxidized nanodiamonds (**ND1**) and **ND4.2a** in **b)** 5 minutes and **c)** 24 hours. Time represents the time after sonication.

Evaluation of the reactions with both **P9** and **P10**

Simultaneous reactions with **P9** and **P10** were performed. **ND3.4** and **ND4.4** were synthesized by the simultaneous amidation reaction of **P9** and **P10** with pristine NDs and **ND1** following the scheme reported in Figure 3.1.38.

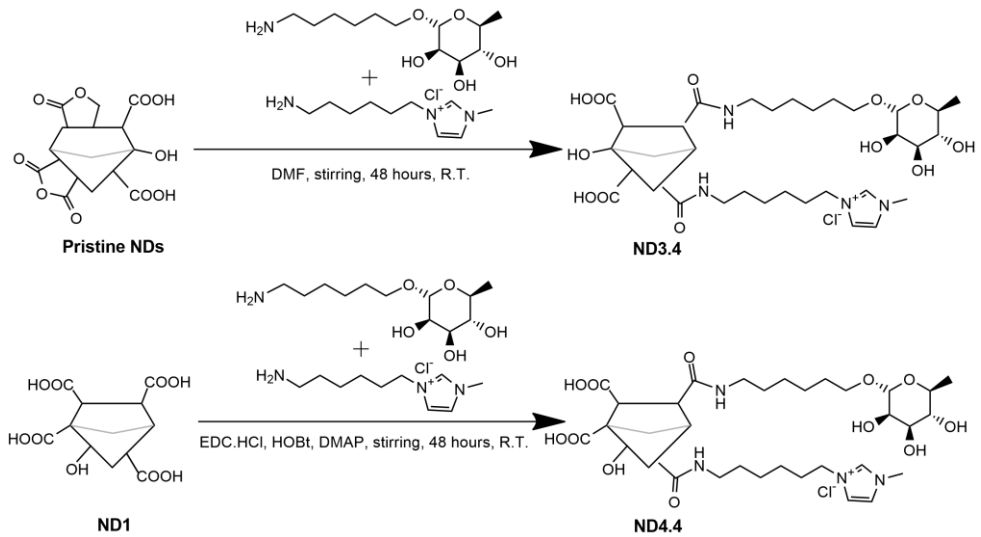

Figure 3.1.38: Reactions of pristine NDs and **ND1** with mixture of **P9** and **P10.** Synthesis of **ND3.4** and **ND4.4.**

TGA results are similar to the results of other ND products. It is shown that the reaction between pristine NDs and primary amine containing organic compounds (**ND3.4**) yielded with high degree of mean functionalization (115 µmol/g). The reaction with oxidized NDs in the presence of coupling reagents (**ND4.4**) yielded with slightly higher degree of functionalization (157 µmol/g) than **ND3.4**.

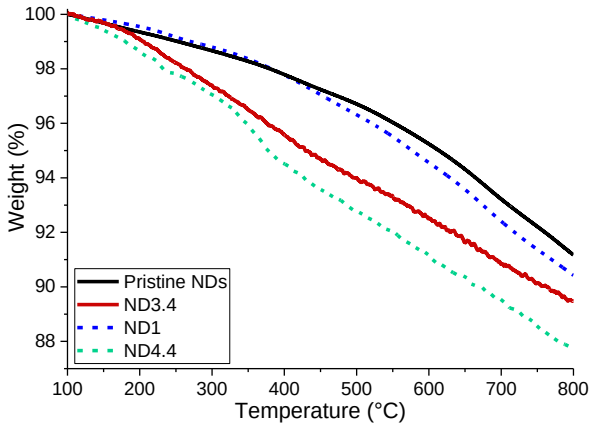

Product	Reaction Conditions	Degree of Functionalization*
ND3.4	Only DMF	115 µmol/g
ND4.4	HOBt, EDC.HCl, DMAP, DMF	157 µmol/g

Figure 3.1.39: TGA graphics and the calculated degree of functionalizations of the functionalized nanodiamonds yielded from the reaction between pristine nanodiamonds (**ND3.4**, solid red line) or oxidized nanodiamonds (**ND4.4**, green dash line) and both **P9** and **P10**. ⋆: The degrees of functionalization were calculated by accepting the reaction occurs between NDs, and the mixture of **P9** and **P10** in ratio of 1:1.

Evaluation of the reactions with **P11**

ND3.3a,b samples were synthesized from pristine nanodiamonds and rhamnose-ionic liquid-amine (**P11**). **ND3.3a** was prepared in the presence of HOBt, EDC•HCl and DMAP while the reaction of **ND3.3b** was performed in absence of the coupling reagents. **ND4.3a,b** products yielded from the reactions between oxidized nanodiamonds (**ND1**) and **P11**. Again **ND4.3a** was prepared in the presence of HOBt, EDC•HCl and DMAP while **ND4.3b** was produced without the coupling (Figure 3.1.40).

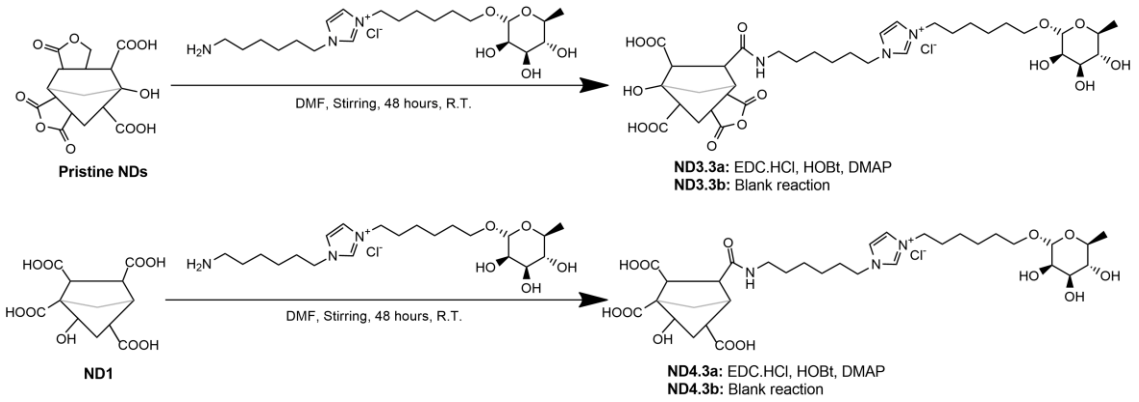

Figure 3.1.40: Reactions of pristine NDs and **ND1** with **P11.** Synthesis of **ND3.3a-b** and **ND4.3a-b.**

TGA data of the reactions with **P11** shows the similar results with other nanodiamonds reactions. The reaction of oxidized nanodiamonds (**ND1**) with **P11** in the presence of coupling reagents (**ND4.3a**) yielded with the highest degree of functionalization (184 µmol/g). The degrees of functionalization ordered from highest to lowest are as follows: **ND4.3a** (184 µmol/g), **ND4.3b** (91 µmol/g), **ND3.3b** (73 µmol/g) and **ND3.3a** (72 µmol/g). The results confirming that after the acid treatment, the surface of NDs becomes more active for amidation reactions.

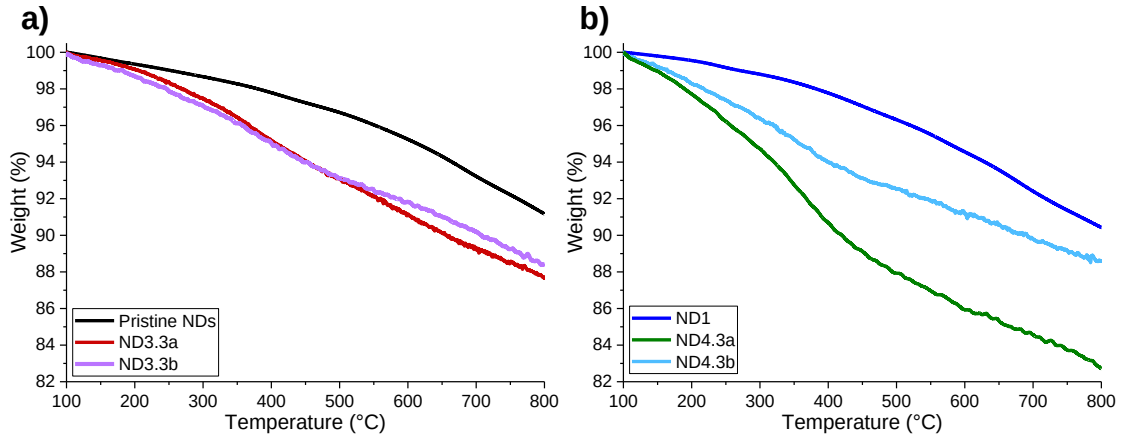

Product	Reaction Conditions	Degree of Functionalization
ND3.3a	HOBt, EDC.HCl, DMAP, DMF	72 µmol/g
ND3.3b	Only DMF	73 µmol/g

Product	Reaction Conditions	Degree of Functionalization
ND4.3a	HOBt, EDC.HCl, DMAP, DMF	184 µmol/g
ND4.3b	Only DMF	91 µmol/g

Figure 3.1.41: TGA graphics and the calculated degree of functionalizations of the functionalized nanodiamonds yielded from the reaction between pristine nanodiamonds (**a**) or oxidized nanodiamonds (**b**) and **P11**.

FT-IR spectra of **ND3.3a,b** present C-H stretch bands between 2860 cm^{-1} and 2695 cm^{-1}, and small shoulder of a possible mixture of the C-N stretch and the N-H bend vibrations at 1590 cm^{-1}. In the spectrum of **ND4.3a,** small shoulder of the mixture of the C-N stretch and the N-H bend vibrations at 1560cm^{-1} and a peak which can be related to C-N stretching of the secondary amine appears at 1250 cm^{-1}. The FT-IR spectrum of **ND4.3b** is not significantly different than the spectrum of **ND1**.

The water dispersibility of the latter compounds is under investigation.

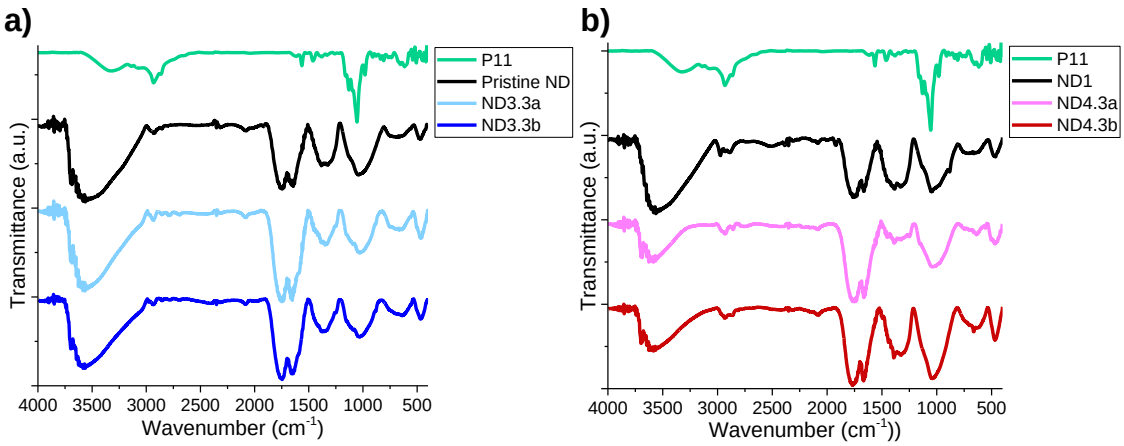

Figure 3.1.42: FT-IR spectra of **a) ND3.3a,b** and **b) ND4.3a,b**. (Spectral acquisition mode: DRIFTS)

Evaluation of the reaction with **P13**

In order to further investigate the reactivity of the NDs surface a bulky sugar molecule bearing a hindered amine group (derivative **P13**) was used to functionalize **ND1** in the presence of HOBt, EDC•HCl and DMAP.

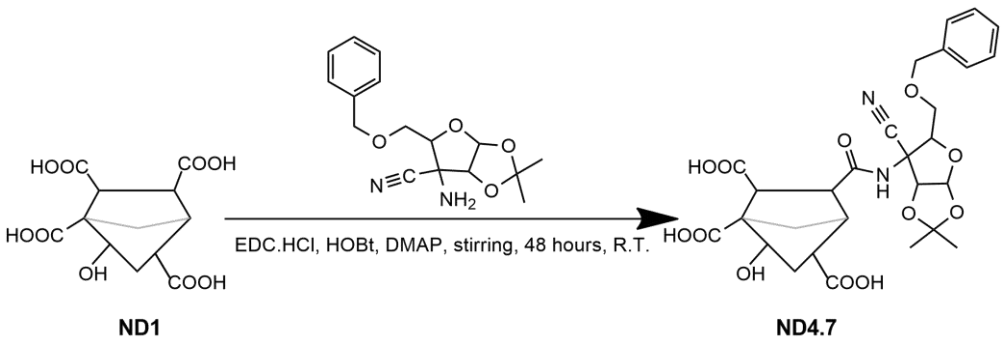

ND1 **ND4.7**

Figure 3.1.43: Reactions of pristine NDs and **ND1** with **P13.** Synthesis of **ND4.7.**

The degree of functionalization of **ND4.7** was 125 µmol/g. So even though the amino group of **P13** seems like "hard to reach" due to the bulky structure, the degree of functionalization of **ND4.7** was not significantly different from the equivalent reactions with other molecules in which the reactive portion was more easily available.

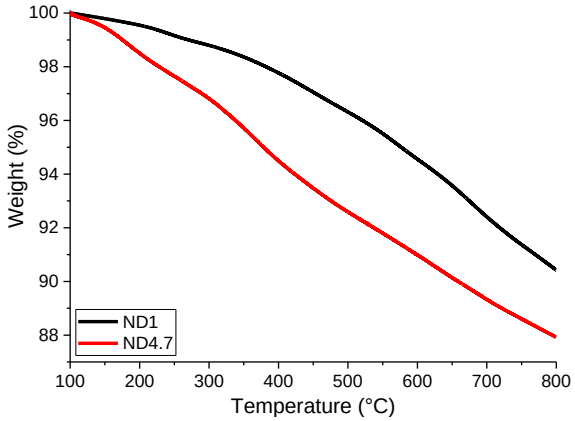

Figure 3.1.44: TGA graphics and the calculated degree of functionalizations of **ND4.7** deriving from the reaction between oxidized nanodiamonds (**ND1**) and **P13**.

Despite the good degree of functionalization, FT-IR spectrum was slightly different from the spectrum of **ND1** (starting material). In the IR spectrum of **ND4.7**, C≡N stretching peak at 2253 cm^{-1} appears different from **ND1**.

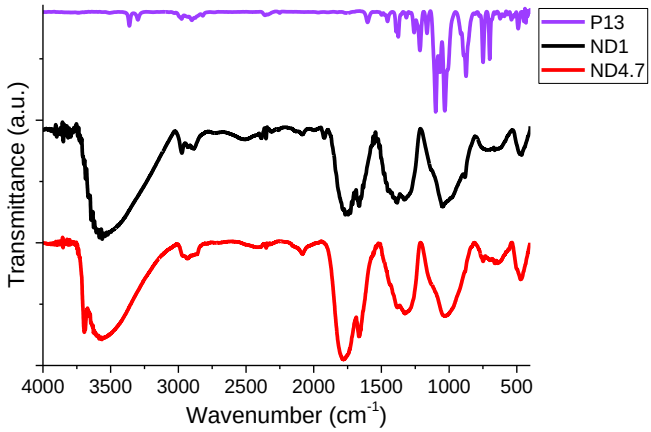

Figure 3.1.45: FT-IR spectra of **P13**, **ND1** and **ND4.7**. (Spectral acquisition mode: DRIFTS)

Evaluation of the reactions with 3-aminopropanenitrile

As anticipate in Figure 3.1.25, also the 3-aminopronenitrile was used to functionalize NDs, to take advantage of the nitrile chemistry. This functional group would enable different further functionalization reactions. **ND3.6a,b**

samples were synthesized from pristine nanodiamonds with (**ND3.6a**) and without coupling reagents (**ND3.6b**) and from oxidized nanodiamonds **ND1** (Figure 3.1.46). **ND4.6a** was prepared in the presence of HOBt, EDC•HCl and DMAP while **ND4.6b** was produced without the coupling reagents.

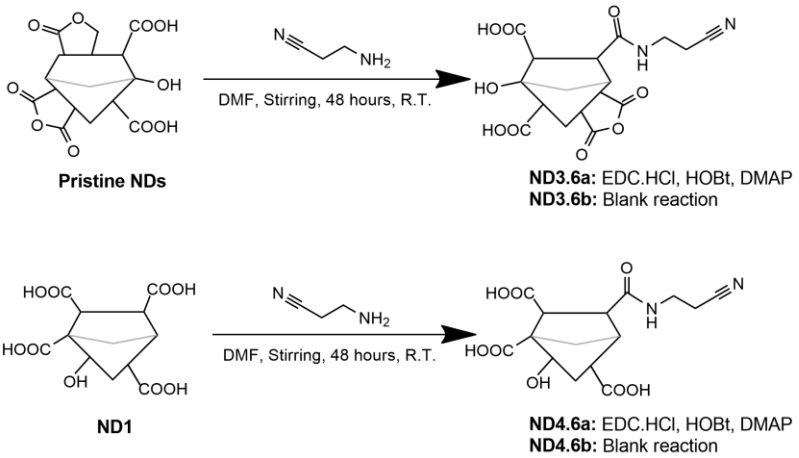

Figure 3.1.46: Reactions of pristine NDs and **ND1** with 3-aminopronenitrile**.** Synthesis of **ND3.6a-b** and **ND4.6a-b.**

TGA was performed and degrees of functionalization were calculated. The degrees of functionalization ordered from highest to lowest are as follows: **ND3.6b** (897 µmol/g), **ND3.6a** (702 µmol/g), **ND4.6a** (473 µmol/g) and **ND4.6b** (447 µmol/g). The degrees of functionalization of the reactions with 3-aminopropanenitrile were the highest in comparison with the functionalized products in this project. The reason may be due to the structural properties of 3-aminopropanenitrile as it is a short and small molecule. The high degree of functionalization can be explained with low steric effect of the 3-aminopropanenitrile comparing to other organic molecules used for functionalization reactions.

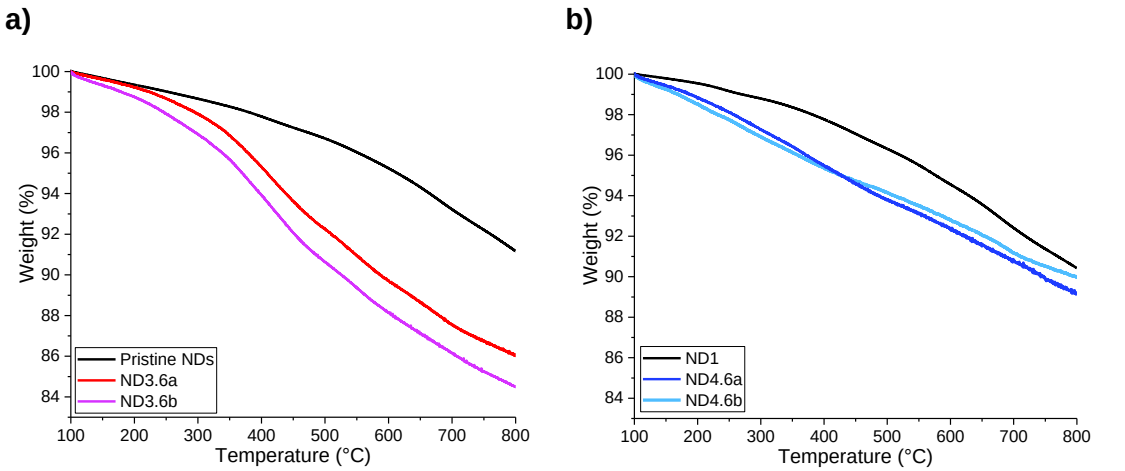

Product	Reaction Conditions	Degree of Functionalization
ND3.6a	HOBt, EDC.HCl, DMAP, DMF	702 μmol/g
ND3.6b	Only DMF	897 μmol/g

Product	Reaction Conditions	Degree of Functionalization
ND4.6a	HOBt, EDC.HCl, DMAP, DMF	473 μmol/g
ND4.6b	Only DMF	447 μmol/g

Figure 3.1.47: TGA graphics and the calculated degree of functionalizations of the functionalized nanodiamonds yielded from the reaction between pristine nanodiamonds (**a**) or oxidized nanodiamonds (**b**) and 3-aminopropanenitrile.

The spectra of **ND3.6a** contains a sharpened peak C-O stretching band at 1055 cm^{-1}. A peak which can be related to C-N stretch appears at 1250 cm^{-1} in the IR spectra of the reactions **ND3.6a** and **ND3.6b**. Different from the starting material (**ND1**), FT-IR spectrum of **ND4.6a** contains a band at 752 cm^{-1} which is related to N-H wagging absorbance. FT-IR spectra of **ND4.6a and ND4.6b** contain Amide II peak of secondary amide at 1585 cm^{-1}. A small peak of nitrile C≡N stretch at 2253 cm^{-1} appears in the spectra of **ND3.6a,b** and **ND4.6a,b**.

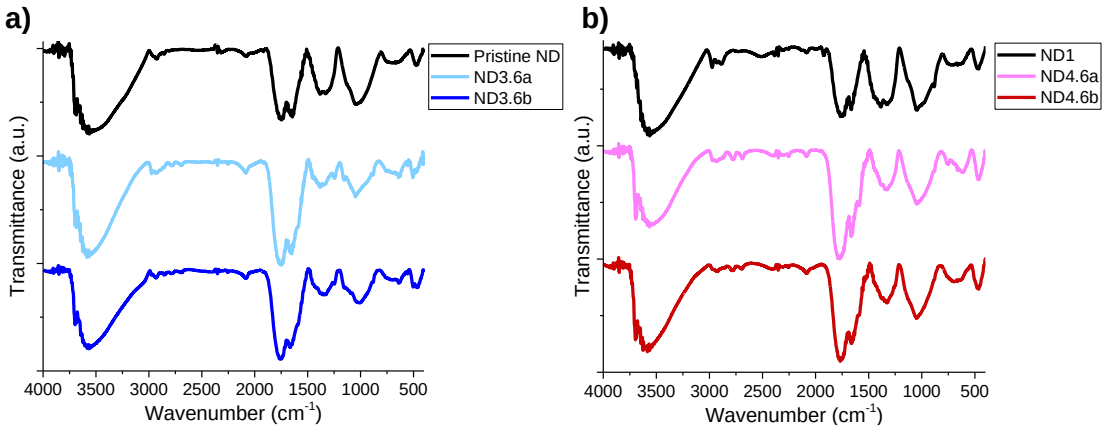

Figure 3.1.48: FT-IR spectra of **a) ND3.6a,b** and **b) ND4.6a,b**. (Spectral acquisition mode: DRIFTS)

NDs were functionalized with different methodologies in order to improve their properties and interesting results were found. The initial functionalization reactions were modified in order to find the best conditions to yield relatively high degree of functionalization. The results suggest that pristine detonation NDs can be functionalized in the absence of coupling reagents possibly through epoxide opening reaction. The mechanism of the reaction must be further investigated. The relatively best degree of functionalization was obtained from the reactions of oxidized ND (**ND1**) in the presence HOBt, EDC•HCl and DMAP comparing to those in other reaction conditions. Due to the strong acid treatment, the surface of NDs loses the different groups, gains more –COOH groups and becomes more reactive for amidation reactions. The functionalization of NDs was confirmed with different essential characterization methodologies. The biological behavior of all the NDs derivatives presented in this section are currently under investigation or will be studied in the next future.

3.2 Production, Functionalization and Characterization of Graphene Quantum Dots

Graphene Quantum Dots were produced from graphite and functionalized with **P5**, **P7**, **P9**, **P10** and **P11**. Functionalization studies were performed in order to add different biological properties such as increased biocompatibility and antimicrobial activity to the GQDs. Characterization studies were conducted with TGA, TEM imaging, AFM imaging, UV-vis, Fluorescence, and FT-IR spectroscopies.

3.2.1 Production and Characterization of Graphene Quantum Dots

Graphene Quantum Dots (**GQD1-3**) were produced through the oxidation and exfoliation of graphite powder. The process has two steps: oxidation and exfoliation of graphite into graphene oxide (GO), and oxidation and cutting GO into Graphene Quantum Dots. First step is a modified Hummers method (Figure 3.2.1).[19]

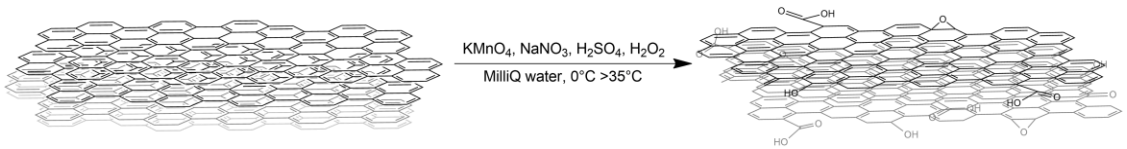

Figure 3.2.1: Oxidation and exfoliation of graphite into GO.

The second step includes an acid treatment with sonication at high temperature and different treatment durations were explored (24 hours for **GQD1**, 30 hours for **GQD2** and 36 hours for **GQD3,** Figure 3.2.2).

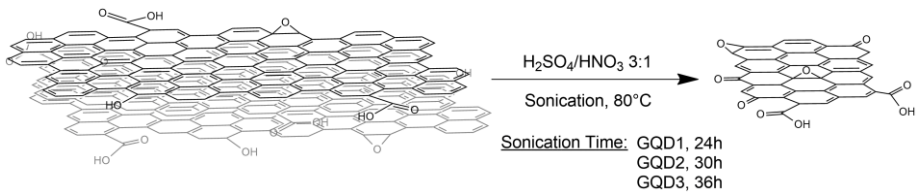

Figure 3.2.2: Oxidation, exfoliation and cutting GO in Graphene Quantum Dots.

TEM imaging was performed by the research group of Dr. Belén Ballesteros at Institut Català de Nanociència i Nanotecnologia (ICN2). The average diameter of Graphene Quantum Dots was 4 nm, mainly ranging between 2.3 and 5.7 nm (Figure 3.2.3).

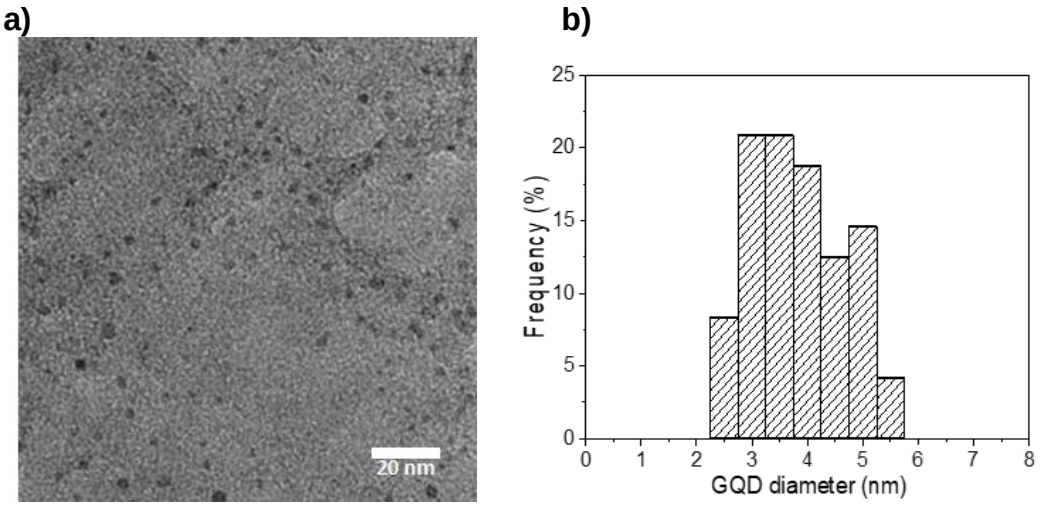

Figure 3.2.3 TEM image of GQDs (**GQD1**) and their size distribution.

AFM measurements were performed in order to confirm the exfoliation of the graphite layers (Figure 3.2.4). Median height value was measured as 0.6 nm and median radius was calculated 4.9 nm. The thickness of GQDs match with the single layer graphene thickness, in agreement with TEM measurements.

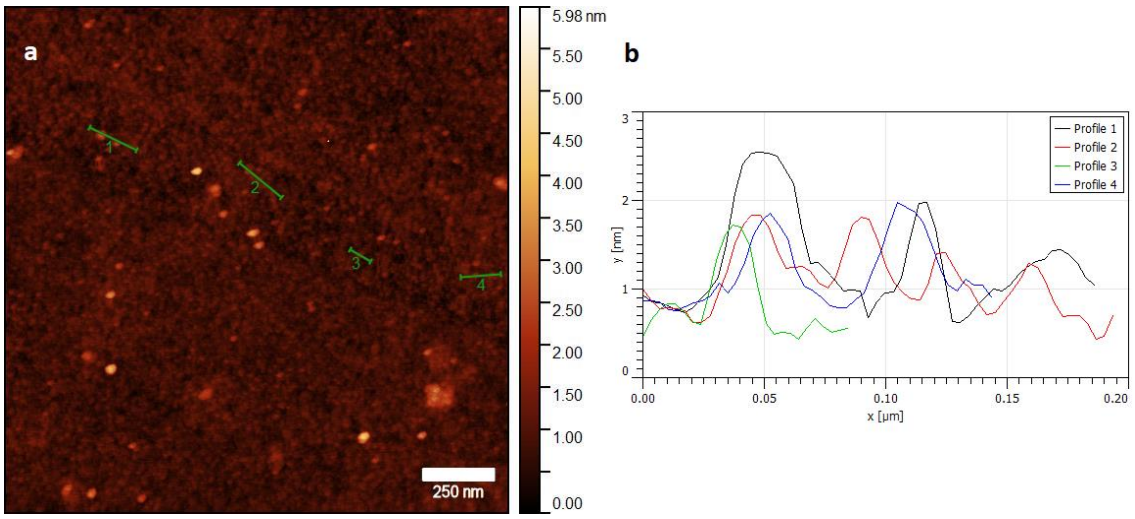

Figure 3.2.4: a) AFM image of **GQD2** and **b)** the section analysis profile of the lines on AFM image.

DLS measurements (Figure 3.2.5) were also performed and hydrodynamic diameter of GQDs was 26 nm. Hydrodynamic size is bigger than the size measured by TEM as DLS reports the diameter of a sphere which has the same translational diffusion coefficient as the GQDs. Another reason for big particle size distribution can be due to some aggregation because of the π–π stacking of

GQDs during the long lasting measurement periods in the relatively high concentration of sample solution.

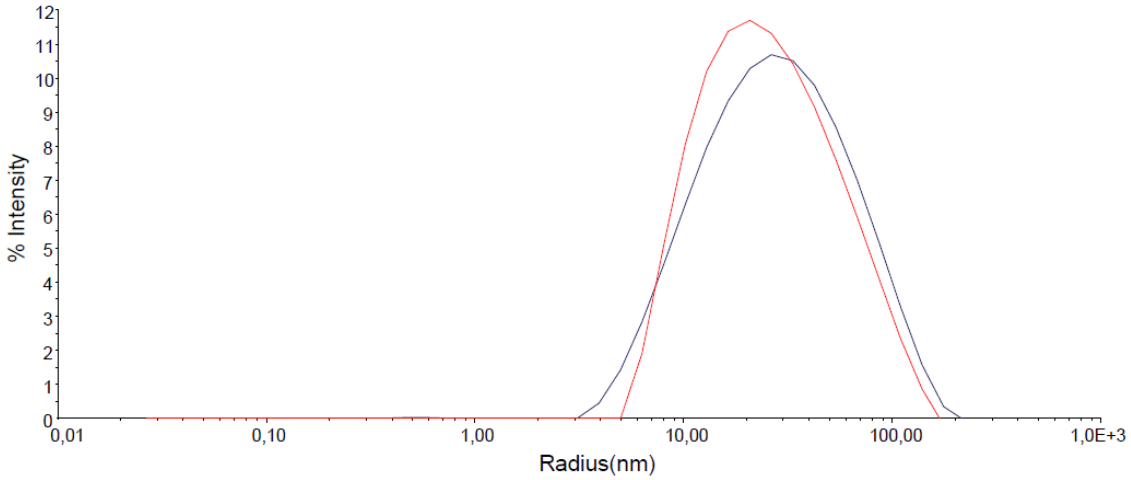

Figure 3.2.5: DLS measurements of **GQD2**.

FT-IR spectroscopy was performed on graphite, intermediate product **GO** and **GQD** (Figure 3.2.6). No specific band could have been detected in FT-IR spectrum of graphite while, after the reaction with the modified Hummers methodology, the spectrum of graphene oxide includes a wide OH stretch band around 3600 cm^{-1}, the vibrational absorption band of C=O stretching in carboxylic and/or carbonyl moiety at 1729 cm^{-1}, O–H bending at 1628 cm^{-1}, C-OH stretching band at 1390 cm^{-1} and C-O stretching band at 1056 cm^{-1}. The FT-IR spectrum of Graphene Quantum Dots contains the same absorption bands of graphene oxide with higher and sharper intensities and an extra band, which is related to C–O stretching vibration at 1235 cm^{-1}. The results of FT-IR spectroscopy show that oxygen containing groups were introduced through the two step reactions.

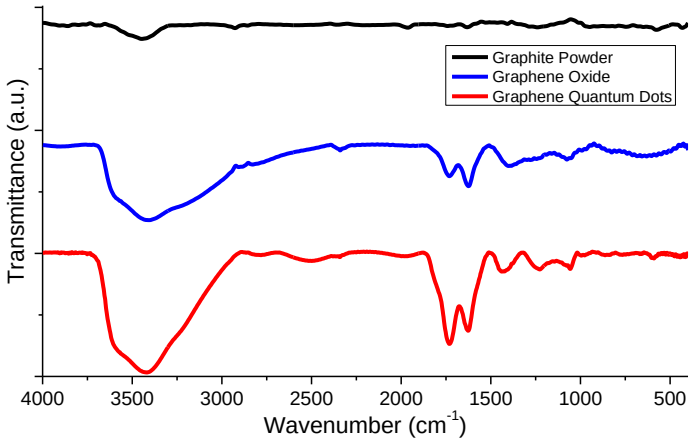

Figure 3.2.6: FT-IR spectra comparison of the products through the reactions (graphite → GO → GQD). (Spectral acquisition mode: Transmission)

Raman spectra of **GQD1-3**, graphene oxide and bulk graphite were measured using 532 nm laser. Raman spectrum of starting material graphite contains 2D band and a sharp G band and relatively lower intensity of D band. 2D band of graphite consists 2 components $2D_1$ and $2D_2$.[20-21] In Figure 3.2.6, 2D band components of starting material are present at 2680 cm^{-1} and 2720 cm^{-1} as a shouldered peak. The Raman spectrum of **GO** is characterized by a G band around 1593 cm^{-1}, which corresponds to the sp^2 carbon atoms, and a D band at 1353 cm^{-1}, which corresponds to the breathing mode of the disorder, which may arise from certain defects such as vacancies, grain boundaries and amorphous carbon species.[22] 2D band of **GO** was seen as very broaden peak of low intensity. In the case of Graphene Quantum Dots the 2D band almost disappears while the ratio of D/G bands increase as the acid treatment time increases.

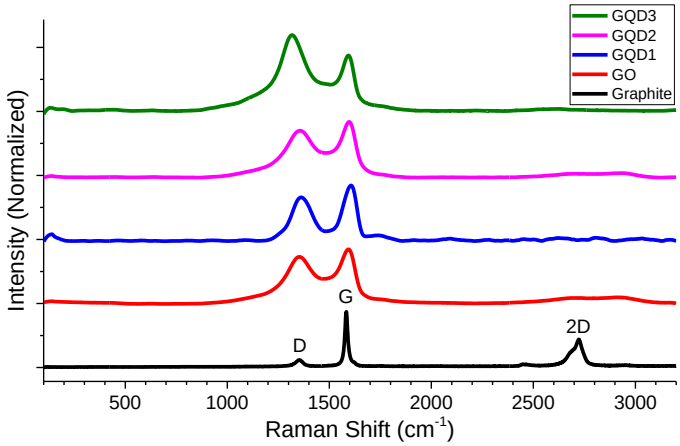

Figure 3.2.7: Comparison of the Raman spectra of bulk graphite, graphene oxide and graphene quantum dots (**GQD1-3**) measured at 532 nm.

TGA results show that the graphite retains its stability at high temperatures as it does not contain functional groups (Figure 3.2.8). Graphene oxide show great weight loss due to the addition of oxygen containing functional groups through the synthesis and weight loss of **GQD2** suggests the addition of more oxygen containing functional groups through the synthesis from Graphene Oxide.

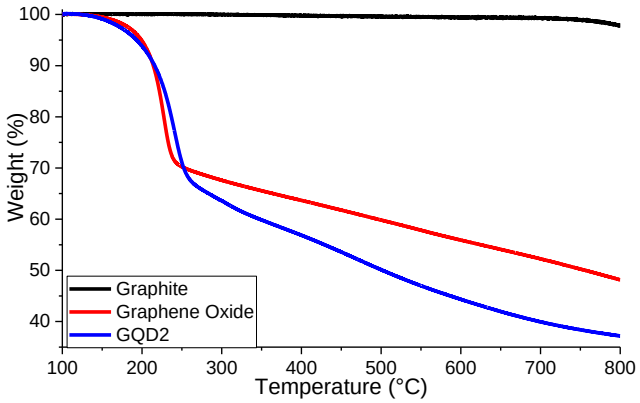

Figure 3.2.8: TGA graphics of Graphite, Graphene Oxide and Graphene Quantum Dots (**GQD2**)

UV-vis spectrum shows the highest absorbance at 223 nm which is due to π→π* transition of C=C bond. Fluorescence spectra show the highest intensity of emission at 550 nm when GQDs are excited at 340 nm. When the excitation wavelength was increased, the maximum fluorescence emission wavelength red shifted (Figure 3.2.9).

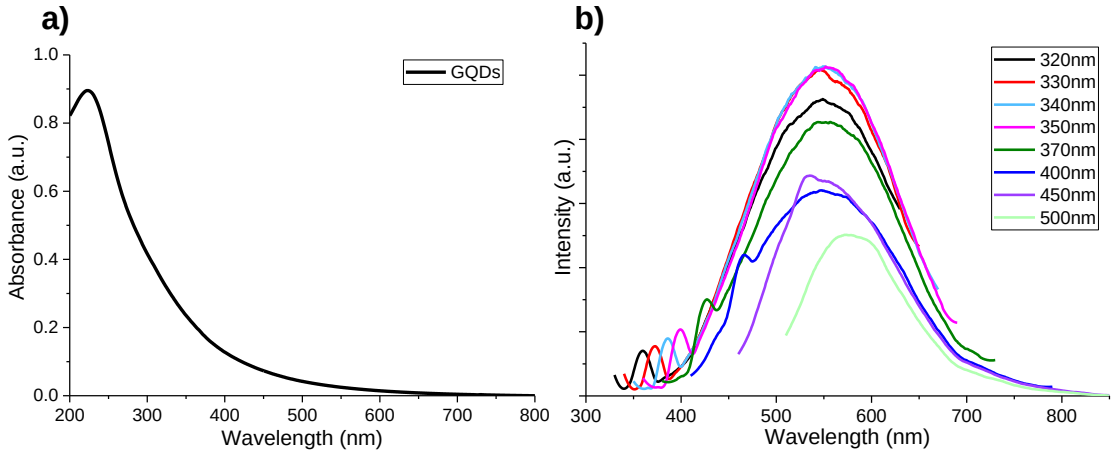

Figure 3.2.9: a) UV-vis spectrum of Graphene Quantum Dots **b)** Fluorescence spectroscopy of GQDs measured with different excitation wavelengths

3.2.2 Cycloaddition of N-Boc-PEG-Amino Acid (P5) and N-Pht-PEG-Amino Acid (P7)

Cycloaddition reactions were performed with protected group containing organic compounds.[23] By the deprotection of the Boc and Pht groups attached on GQDs, it is possible to increase the solubility and to exploit the exposed reactive group to further functionalization with different molecules. The reactions with **P5** and **P7** were performed on **GQD2** in water under reflux and yielded **GQD2.1** and **GQD2.2**, respectively (Figure 3.2.10). The so obtained products were characterized by FT-IR spectroscopy.

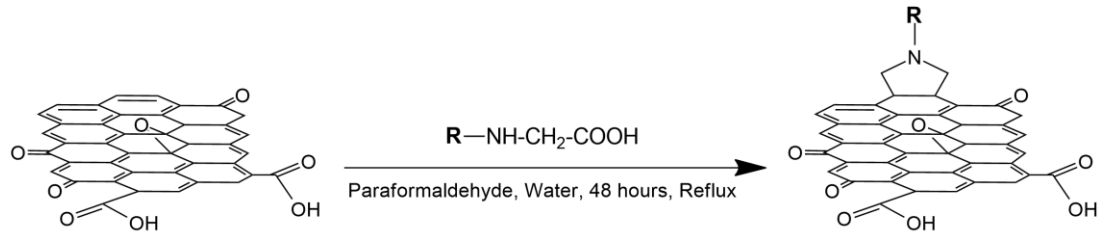

Product Name	R—NH-CH_2-COOH
GQD2.1	P5
GQD2.2	P7

Figure 3.2.10: Reaction chart of **GQD2.1** and **GQD2.2** synthesis.

The mechanism of the reaction can be described as in Figure 3.2.11. Azomethine ylides are one of the most reactive and versatile classes of 1,3-dipole.

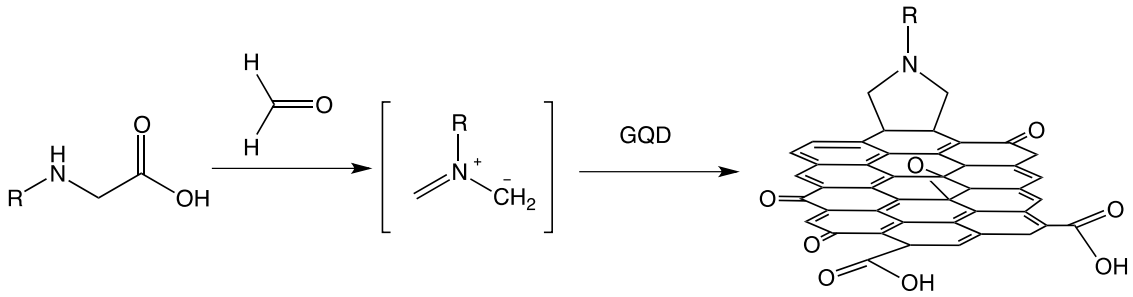

Figure 3.2.11: Mechanism of 1,3 cycloaddition reaction.

The FT-IR spectra of **GQD2**, **GQD2.1** and **GQD2.2** contain a wide OH stretch band around 3600 cm^{-1}, the vibrational absorption band of C=O and –COOH at

around 1710 cm^{-1}, C=C stretch band at around 1580 – 1600 cm^{-1}, C-OH stretching band at 1390 cm^{-1}, C–O stretching vibration at 1235 cm^{-1} and C-O stretching band around 1056 cm^{-1}. For both spectra of **GQD2.1** and **GQD2.2** different from **GQD2**, C-H stretching bands are present at 2920 cm^{-1} and 2847 cm^{-1}. The spectrum of **GQD2.1** includes a sharp peak at 1385 cm^{-1}, possibly related to the C-N stretching band and peaks at 795 cm^{-1} and 720 cm^{-1}, related to the out-of-plane vibrations of phthalimide group of **P5**. The spectrum of **GQD2.2** includes a broad peak at 1385 cm^{-1}, possibly related to the C-N stretching band and 1355 cm^{-1} related to CH_3 bending peak of Boc group of **P7**. The results of FT-IR spectroscopy show that **P5** and **P7** molecules were successfully introduced to graphene quantum dots through the cycloaddition reactions.

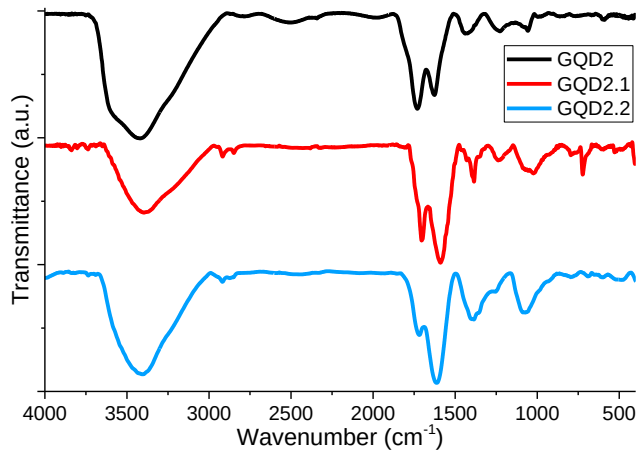

Figure 3.2.12: Comparative FT-IR spectra of **GQD2**, **GQD2.1** and **GQD2.2**.

3.2.3 Amidation of Graphene Quantum Dots with Rhamnose-Amine (P9), Ionic Liquid-Amine (P10) and Rhamnose-Ionic Liquid-Amine (P11)

Analogously to NDs, Graphene Quantum Dots were functionalized with **P9**, **P10** and **P11** in the presence the coupling reagents (EDC•HCl, NHS) and yielded **GQD2.3**, **GQD2.4** and **GQD2.5**, respectively. Blank reactions were performed using analogous procedure without coupling reagents and yielded **GQD2.3b**, **GQD2.4b** and **GQD2.5b**, respectively (Figure 3.2.13).

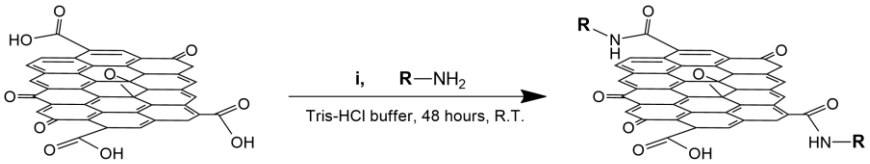

Product Name	i	R—NH_2
GQD2.3	EDC.HCl, NHS	P9
GQD2.3b		P9
GQD2.4	EDC.HCl, NHS	P10
GQD2.4b		P10
GQD2.5	EDC.HCl, NHS	P11
GQD2.5b		P11

Figure 3.2.13: Reaction chart of **GQD2.3-5** and **GQD2.3-5b** synthesis.

GQD2.3-5 and **GQD2.3-5b** reactions were characterized by FT-IR and UV spectroscopy and TGA.

TGA analyses (Figure 3.2.14) show that the degree of functionalization of **GQD2.3** is 210 µmol/g and the weight loss of the product of the blank reaction (**GQD2.3b**) is similar to the starting material (**GQD2**). The degree of functionalization of **GQD2.4** is found 155 µmol/g and the product of the analogue blank reaction (**GQD2.4b**) yielded with very low degree of functionalization (15 µmol/g). These results suggest that the GQDs surface is really reach in carboxylic

groups and in this case the presence of other groups ready to directly react with amines, as epoxides, seems to be definitely negligible.

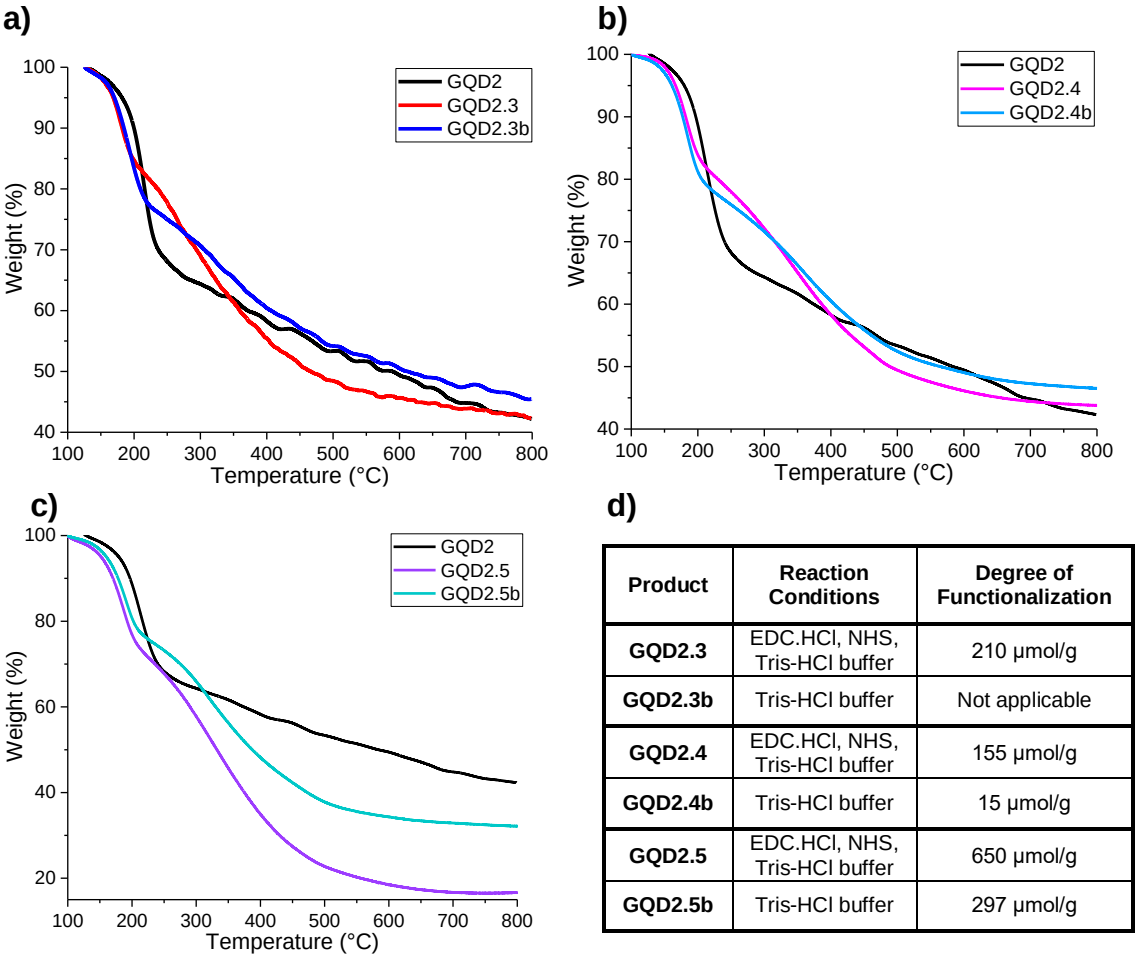

Product	Reaction Conditions	Degree of Functionalization
GQD2.3	EDC.HCl, NHS, Tris-HCl buffer	210 μmol/g
GQD2.3b	Tris-HCl buffer	Not applicable
GQD2.4	EDC.HCl, NHS, Tris-HCl buffer	155 μmol/g
GQD2.4b	Tris-HCl buffer	15 μmol/g
GQD2.5	EDC.HCl, NHS, Tris-HCl buffer	650 μmol/g
GQD2.5b	Tris-HCl buffer	297 μmol/g

Figure 3.2.14: TGA graphics of **a) GQD2.3** and **GQD2.3b**, **b) GQD2.4** and **GQD2.4b**, **c)** and **GQD2.5** and **GQD2.5b. d)** Calculated degrees of functionalization of functionalized GQDs.

The degrees of functionalization of **GQD2.5** and **GQD2.5b** were relatively high (650 μmol/g and 297 μmol/g, respectively). This is an unexpected result and should be investigated further, considering that the characteristics of the bond molecule are the combination of P9 and P10, which do not supramolecularly interact with GQDs.

Normalized UV-Vis spectroscopy spectra show that **P9** molecule has a sharp peak around 200 nm that is present as shoulder in **GQD2.3** spectrum. This shows as well similar characteristic absorbance of **GQD2**. There is no significant difference between the spectra of **GQD2** and **GQD2.3b**, coherently with the TGA results.

FT-IR spectra of **GQD2.3** and **GQD2.3b** (Figure 3.2.15) shows characteristics similar to the starting material **GQD2**. The spectrum of **GQD2.3** include a peak at 2980 cm^{-1} related to –C-H stretching and a sharpened peak of C-O stretching band at 1055 cm^{-1}, which are the most characteristic peaks of **P9**.

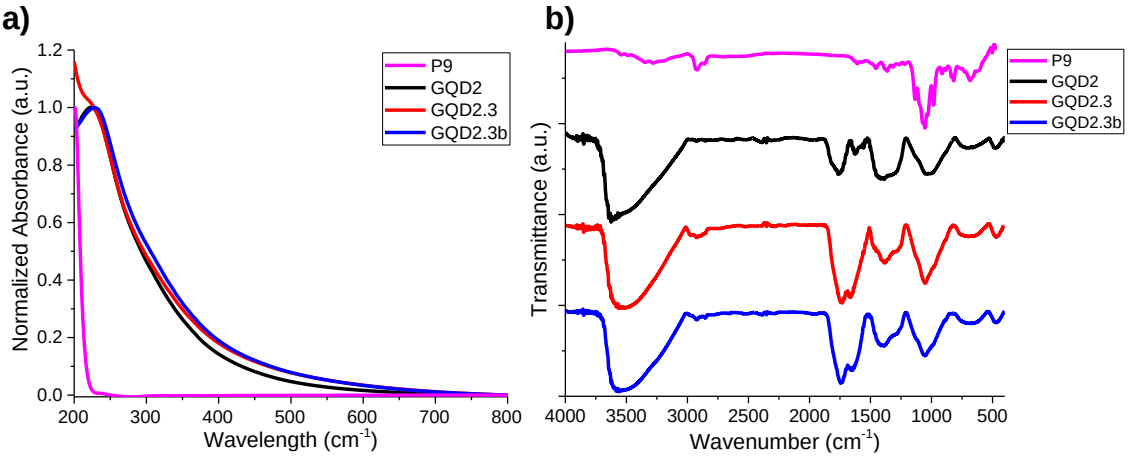

Figure 3.2.15: a) UV-Vis spectra and **b)** FT-IR spectra of **P9**, **GQD2**, **GQD2.3** and **GQD2.3b**. (Spectral acquisition mode: DRIFTS)

GQDs were produced from graphite through a mixed procedure of acid treatment and sonication with a new methodology. Properties of produced GQDs were confirmed with various characterization studies. Preliminary biological evaluations were performed and reported in Section 3.5.2.

The characterization results of functionalized GQDs show that the functionalization in the presence of EDC.HCl and NHS provide good degree of functionalization. The lower degrees of functionalization of blank analogue reactions point that GQDs can be functionalized through the amide bond generation in the suggested conditions. GQDs with different functional groups would provide improved nanosystems for a broad range of applications

3.3 Production, Functionalization and Characterization of Carbon Dots

3.3.1 Production and Characterization of Carbon Dots

Carbon Dots were produced through the pyrolysis of renewable biological resources, and more precisely **CD1**, **CD2** and **CD4** were synthesized from the chitin exoskeleton of an insect while **CD3** was synthesized from the chitin shell of shrimp (Figure 3.3.1). The chitin sources are produced by our collaborators in the Laboratory of Glycochemistry, Antimicrobials and Agroresources, Université de Picardie Jules Verne.

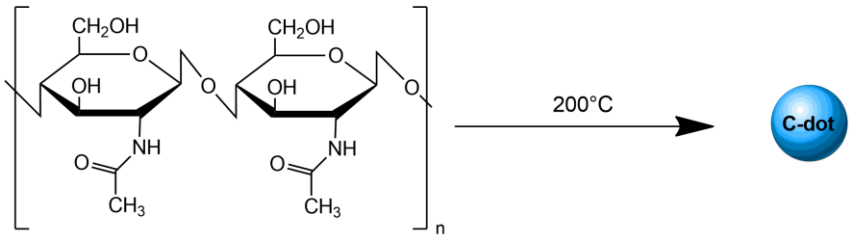

Product	Starting Material	Reaction Conditions
CD1	Exoskeleton of Insect	in EtOH, 24 hours
CD2	Exoskeleton of Insect	in EtOH, 30 hours
CD3	Chitin Shell of Shrimp	in EtOH, 24 hours
CD4	Exoskeleton of Insect	in the absence of solvent, 24 hours

Figure 3.3.1: Reaction chart of the synthesis of **CD1-4**

TGA was performed in order to investigate the thermal stability of as-produced carbon dots. **CD1** and **CD4** were not thermally stable at high temperatures and lose 85% and 99% of their weight at 600 °C, respectively (Figure 3.3.2). The decomposition rate of **CD4** dramatically increases after 300 °C. These results indicate that carbon dots are not thermally stable even in nitrogen atmosphere and functionalization would be hard to be detected and quantified by TGA.

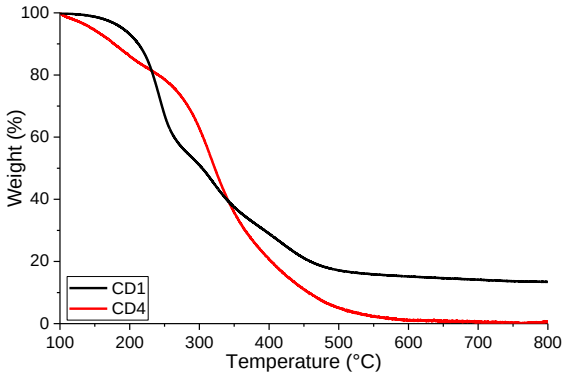

Figure 3.3.2: TGA graphic of Carbon Dot (**CD1**), performed under N_2 flow.

The UV spectra of produced carbon dots were similar to each other. It is evident from Figure 3.3.3-a that as-produced carbon dots show a prominent peak around 280 nm. This is due to the n→π* transition related to OH, NH_2, and carboxyl groups on the surfaces of the CDs.

In Figure 3.3.3-b, fluorescence spectra are reported and it is possible to appreciate that the maximum photoluminescence emission occurs around 430 nm, when carbon dots are excited at 250 nm. When the excitation wavelength was increased, the photoluminescence peak blue-shifted.

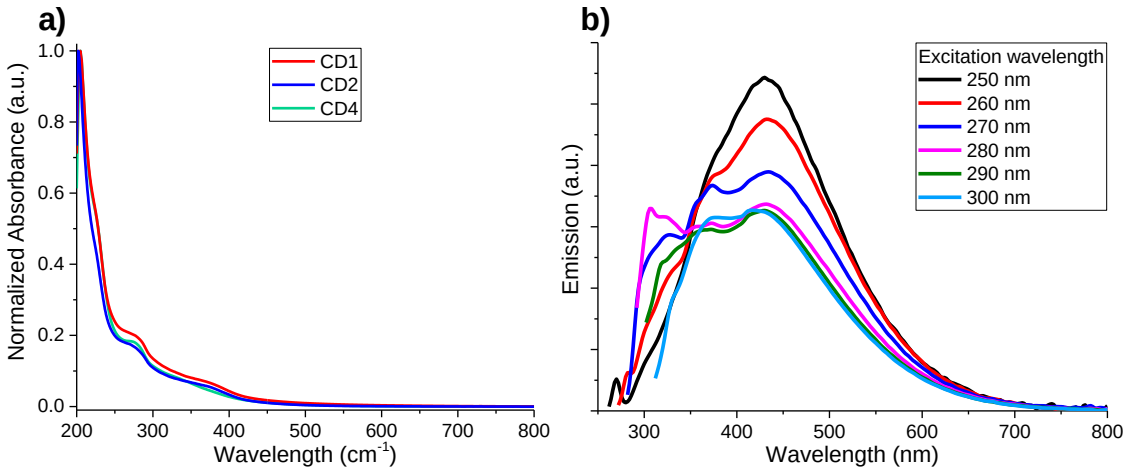

Figure 3.3.3: a) UV-Vis spectra of **CD1**, **CD2** and **CD4**, and **b)** Fluorescence spectra of **CD1** with different excitation wavelengths

The FT-IR spectra of the starting material and as-produced carbon dots (**CD1**, **CD2** and **CD4**) contain in common these bands: -OH stretching band at 3300 cm^{-1}, -C-H stretching bands at 2924 cm^{-1} and 2850 cm^{-1}, C=O stretching bands around 1730 cm^{-1} and 1517 cm^{-1}, C=C stretching band at 1665 cm^{-1}, C-H bending vibrations around 1440 cm^{-1}, C-N stretching band around 1370 cm^{-1} and C-O-C

stretching band at 1205 cm^{-1} and 1040 cm^{-1}. The FT-IR spectrum of **CD4** presents less intense oxygen related peaks as the production was performed in the absence of ethanol.

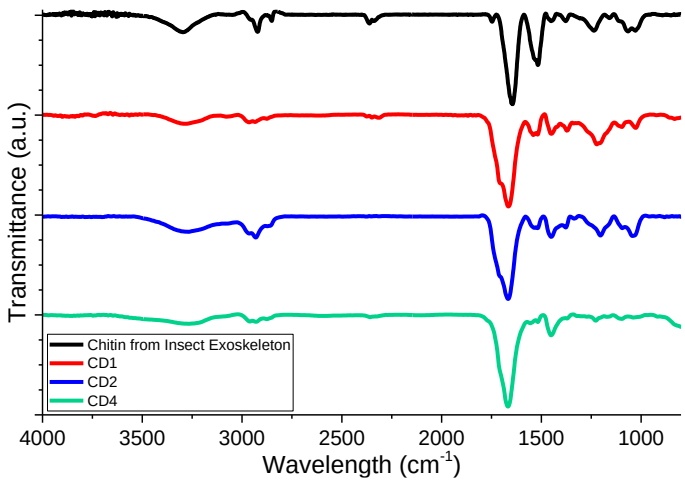

Figure 3.3.4: FT-IR spectra of starting material chitin from insect exoskeleton, **CD1**, **CD2** and **CD4**. (Spectral acquisition mode: ATR)

Characterization studies of **CD3** are ongoing. Other possible characterization methodologies are being evaluated.

A first attempt to functionalization of CDs was performed with **P9** and their characterization studies are still ongoing, but from the results so far obtained it is understandable that the preparation of CDs without solvent leads to more unstable materials without conferring special features so at the moment the best preparation procedure results to be the one with ethanol.

The characterization results suggest that CDs can be produced from natural renewable resources. This methodology provides cheap and easy production of CDs as the starting material, chitin, resources are derived from insect and shrimp which are reproducible and abundantly available in the nature. As-produced CDs are strongly fluorescent and require more characterization studies in order to define the material better.

3.4 Functionalization and Characterization of Multi-walled Carbon Nanotubes

3.4.1 Functionalization and Characterization of Nanocyl 7000 (NC7000) MWCNTs

3.4.1.1 Oxidation of Nanocyl 7000 MWCNTs

Pristine NC7000 MWCNTs were oxidized in order to increase the water dispersibility and create a proper surface for functionalizations through amide bond generation. As it was mentioned in the Introduction chapter, pristine MWCNTs can be described as rolled up graphene sheets and may contain small amount of defects on their surface. Acid treatment would introduce the carboxylic groups on the surface of MWCNTs and create an active surface for amidation reactions. For this purpose, pristine NC7000 MWCNTs were oxidized through the acid treatment with H_2SO_4 and HNO_3 mixture (3:1) in 10 hours.

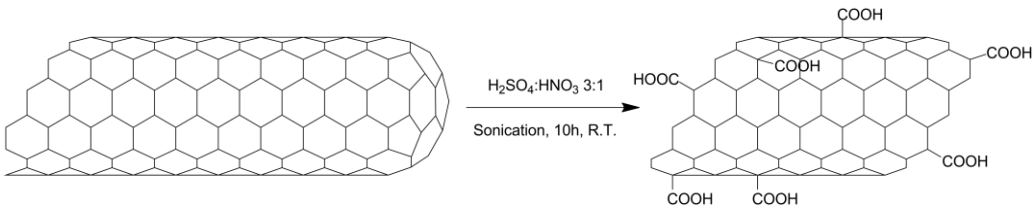

Figure 3.4.1: Preparation of **CNT1** through the oxidation of pristine Nanocyl 7000 MWCNTs.

TEM images were performed in order to study the effect of oxidation reaction. It was confirmed that the pristine MWCNTs have 9.5 nm of diameter and 1.5 µm of average length (Figure 3.4.2a) as reported in its technical data sheet.[24] After the oxidation reaction the diameter of **CNT1** was retained as expected (without unzipping of the material) and the average length was reduced to about 200 nm. MWCNTs shorter than 500 nm was aimed to be obtained by the acid treatment as Jain *et al.* reported them as less cytotoxic and more biocompatible.[25]

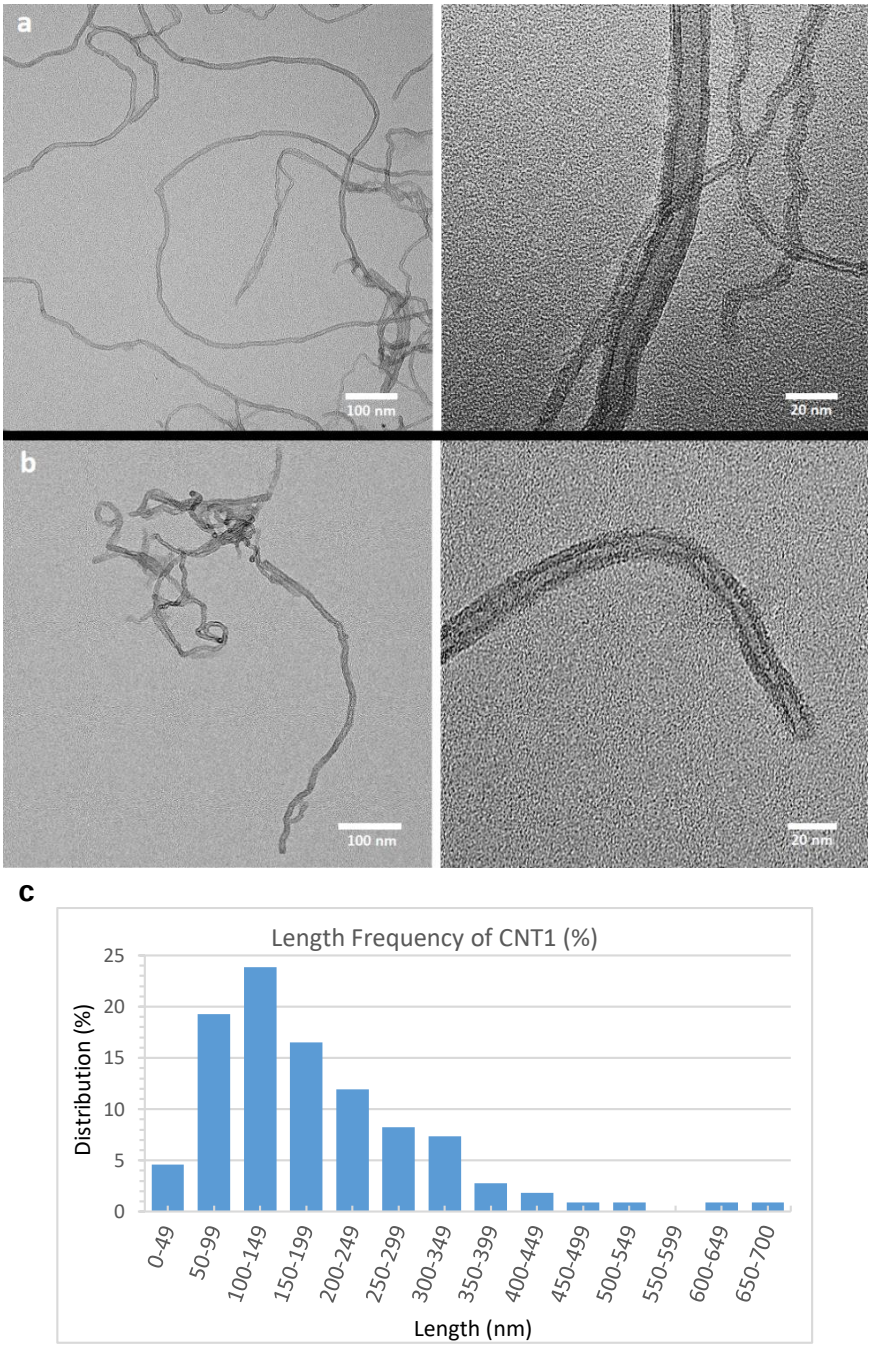

Figure 3.4.2: TEM images of **a)** pristine Nanocyl 7000 MWCNTs and **b) CNT1** and **c**) length distribution of **CNT1**.

Raman spectroscopy analyses were performed with a 532 nm laser and the obtained spectra of the starting material and the product were normalized in order to study the effect of oxidation. The most important bands seen in Figure 3.4.3 are the D band around 1350 cm^{-1}, G band at 1580 cm^{-1}, the second harmonic D' shoulder in G around 1610 cm^{-1}, 2D band at 2675 cm^{-1} and D+D' band around 2920 cm^{-1}. As it was shown in Figure 3.4.3b, intensity of D band increases and

intensity of 2D band decreases after the oxidation reaction. This result suggests that the disorder groups on the surface of MWCNTs increase and some defects were possibly introduced to the walls of MWCNTs.

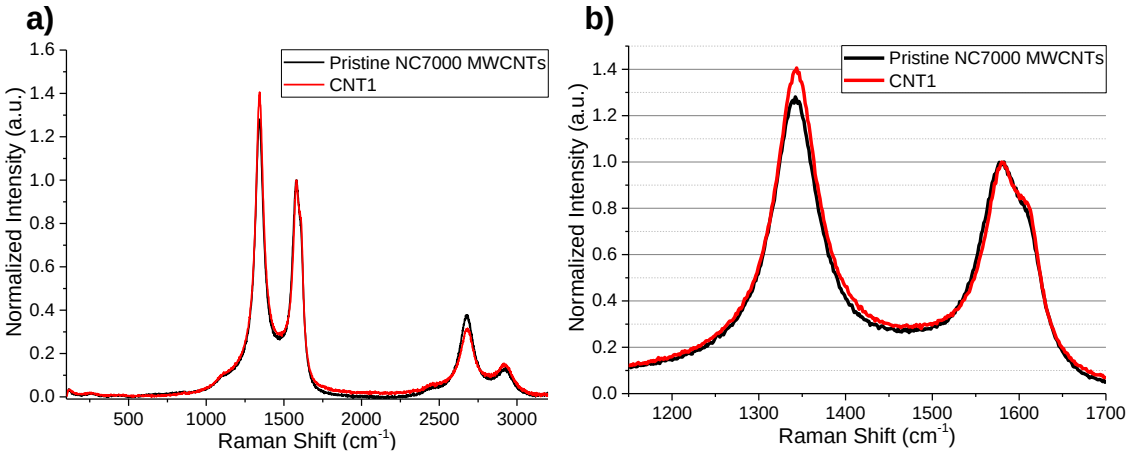

Figure 3.4.3: Comparative Raman spectra of pristine Nanocyl 7000 MWCNTs and **CNT1** between **a)** 100 – 3200 cm^{-1} Raman shift and **b)** 1100 – 1700 cm^{-1} Raman shift.

TGA was performed under N_2 atmosphere in order to confirm the addition of oxygen containing functional groups after the oxidation reaction. While pristine MWCNTs were thermally stable even at high temperatures, **CNT1** lost 14.6% of its weight at 450 °C.

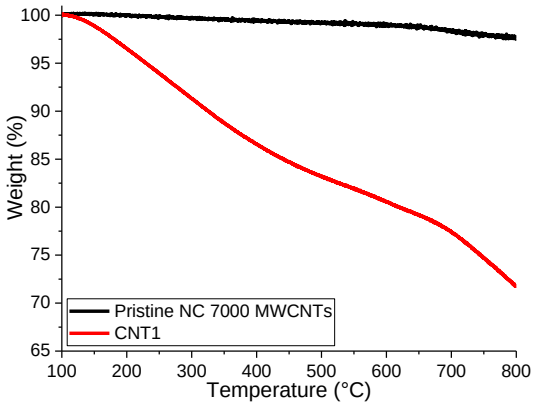

Figure 3.4.4: Comparative TGA graphics of pristine NC7000 MWCNTs and **CNT1**.

Water dispersibility test was performed by the sonication of 1 mg of nanotubes in 1 mL water. Before acid treatment, pristine NC7000 MWCNTs were not well-dispersible in water. Right after the sonication, big aggregates of MWCNTs were already visible while **CNT1** sample was well-dispersed and the dispersion was stable for 3 months.

3.4.1.2 Functionalization of CNT1 with P1 and Deprotection of Boc group

Oxidized MWCNTs were functionalized with **P1** molecule in order to introduce free amino groups on the surface of **CNT1** through the amide bond generation by the coupling with **P1** molecule and following deprotection of Boc group.

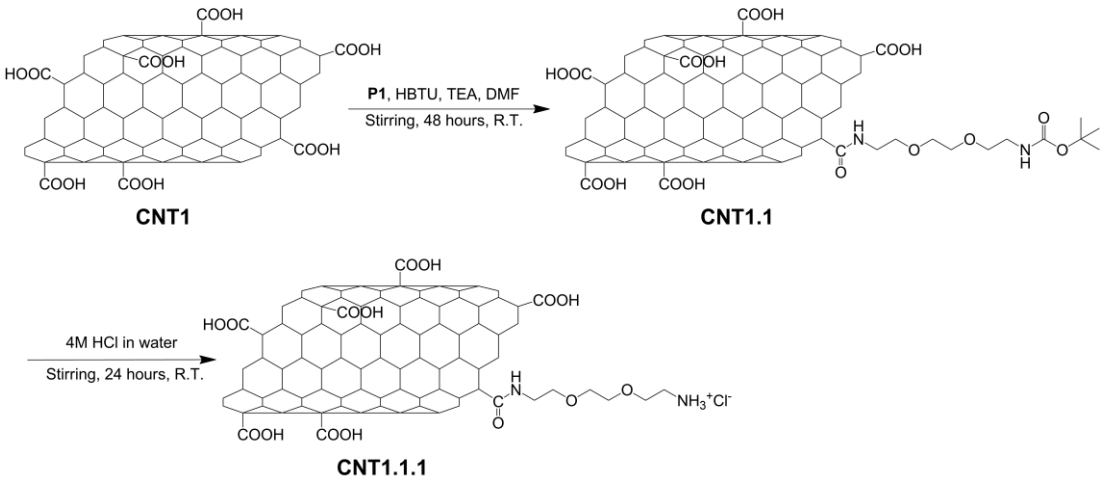

Figure 3.4.6: Synthesis of **CNT1.1** through the amidation of **P1** and synthesis of **CNT1.1.1** through the deprotection of Boc group.

The **P1** loading on **CNT1.1** was calculated by TGA. The degree of functionalization was 166 µmol/g, confirming a rather efficient coupling of **P1** on **CNT1**.

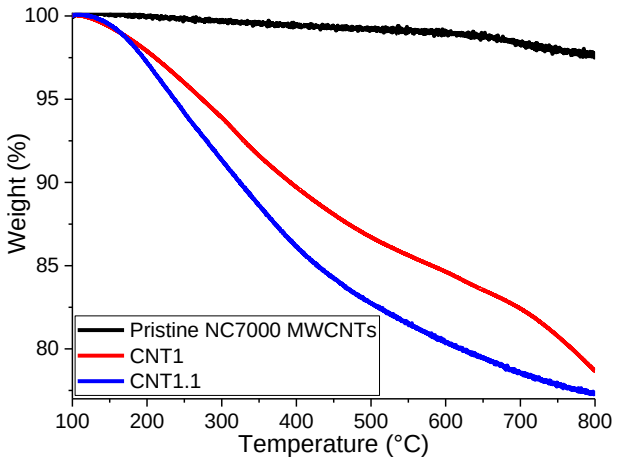

Figure 3.4.7: Comparative TGA graphics of **CNT1** and **CNT1.1**.

3.4.2 Functionalization and Characterization of NanoAmor 1237YJS (NA 1237YJS) MWCNTs

3.4.2.1 Functionalization of Pristine NA 1237YJS MWCNTs with 4-Aminobenzoic acid

As mentioned in the Introduction there is a variety of CNTs differing for length, number of walls, diameter and so on. In this work we explore the functionalization of few of them: the already cited Nanocyl 7000 and NA 1237YJS MWCNTs. The main difference among the two is their diameter, about 23-30 nm for the NanoAmor with respect to 10 nm of the NC7000.

As first functionalization methodology, the so-called Tour reaction was herein used for the modification of NA 1237YJS MWCNTs with 4-Aminobenzoic acid. In the first step of the reaction, the reductive dissociation of the diazonium salt of 4-aminobenzoic acid with loss of N_2 takes place, and the formation of an aryl radical occurs. This radical can react with C=C bonds and the carbon hybridization from sp^2 becomes sp^3.[26]

Functionalization of pristine NA 1237YJS MWCNTs with 4-Aminobenzoic acid was performed with isopentyl nitrite in DMF at 80°C. The reaction was performed for 2 hours yielding **CNT2a** and 4 hours **(CNT2b**).

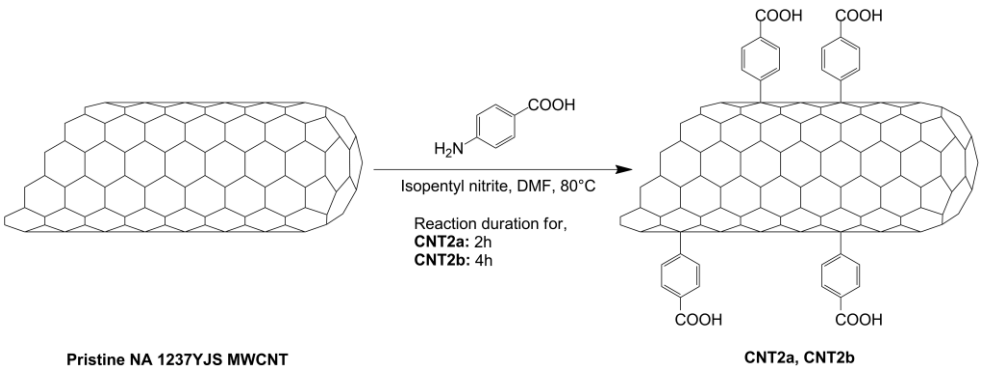

Figure 3.4.8: Synthesis of **CNT2a** and **CNT2b** through the arylation reaction of Pristine MWCNTs with 4-Aminobenzoic acid.

Raman spectroscopy was performed in order to investigate the effect of functionalization. For both pristine MWCNTs and **CNT2**, Raman spectra present D band at 1350 cm^{-1} and G band at 1588 cm^{-1}. After the functionalization with 4-Aminobenzoic acid, an increase of intensity was detected on D band in

normalized Raman spectra. This result suggests the increase of surface groups through the functionalization reaction.

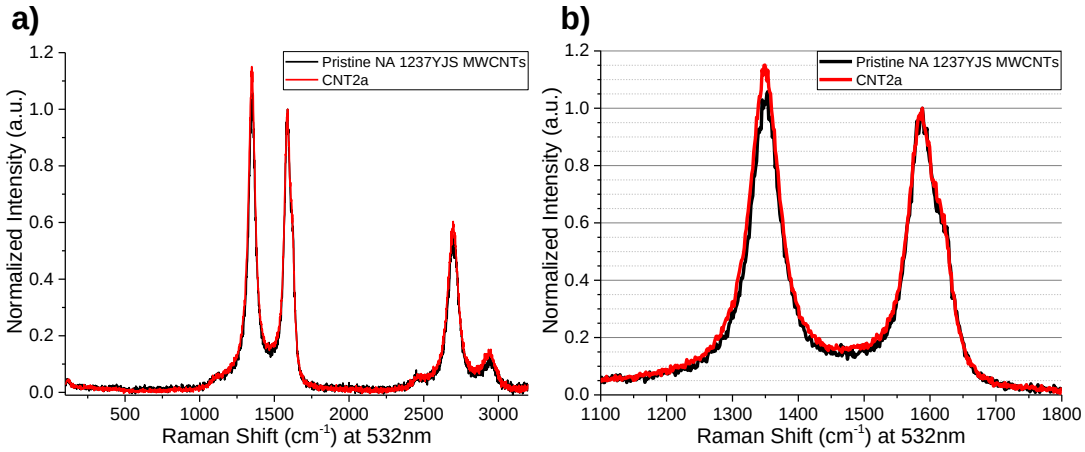

Figure 3.4.9: Raman spectra of Pristine NanoAmor 1237YJS MWCNTs and **CNT2a** between **a)** 100 and 3200 cm^{-1} Raman shift, and **b)** 1100 and 1800 cm^{-1} Raman shift.

TGA was performed to **CNT2a** and **CNT2b** in order to calculate the degree of functionalization and show the effect of reaction time on this. The degrees of functionalization of the reactions were calculated 270 µmol/g and 326 µmol/g for **CNT2a** and **CNT2b**, respectively. This shows that the molecule load on MWCNTs increases with the reaction time, but other studies previously performed in the laboratory highlight that there is no benefit in prolonging the reaction more than 4 hours.

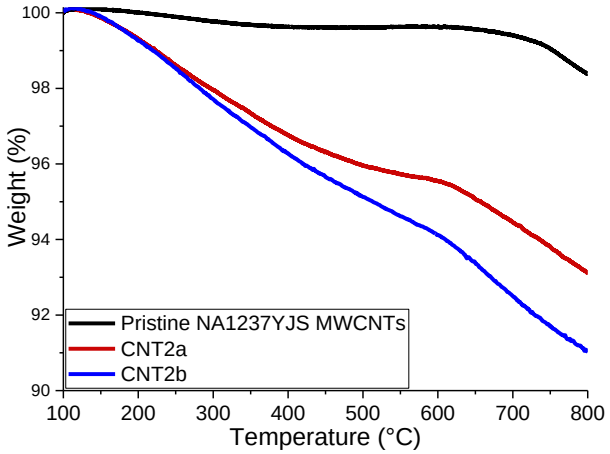

Figure 3.4.10: Comparative TGA graphics of pristine NanoAmor 1237YJS MWCNTs, **CNT2a** and **CNT2b**.

3.4.2.2 Functionalization of CNT2a with P3 and Deprotection of Pht group

CNT2a was functionalized with **P3** in the presence of HBTU and DIPEA in DMF at room temperature in 48 hours. It was an amidation reaction between amino group of **P3** and carboxyl group of **CNT2a**.

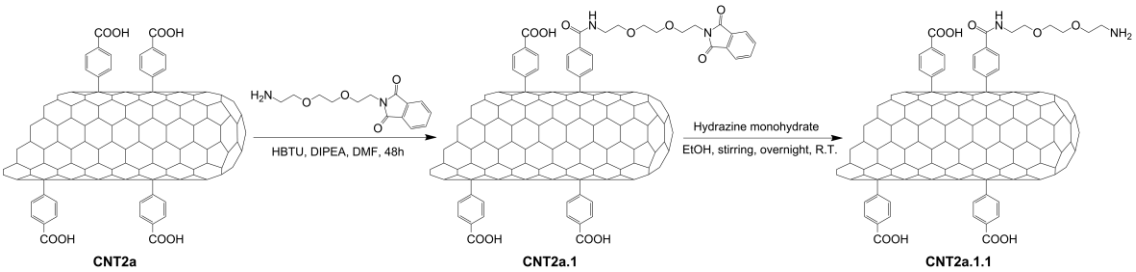

Figure 3.4.11: Synthesis of **CNT2a.1** and **CNT2a.1.1** through amidation of **P3** and deprotection of Pht group.

Raman spectroscopy was performed with 532 nm laser. The spectrum of **CNT2a.1** presents D band at 1350 cm^{-1} and G band at 1588 cm^{-1} same as **CNT2a** and pristine MWCNTs. As expected the intensity of D band did not significantly change with respect to **CNT2a**.

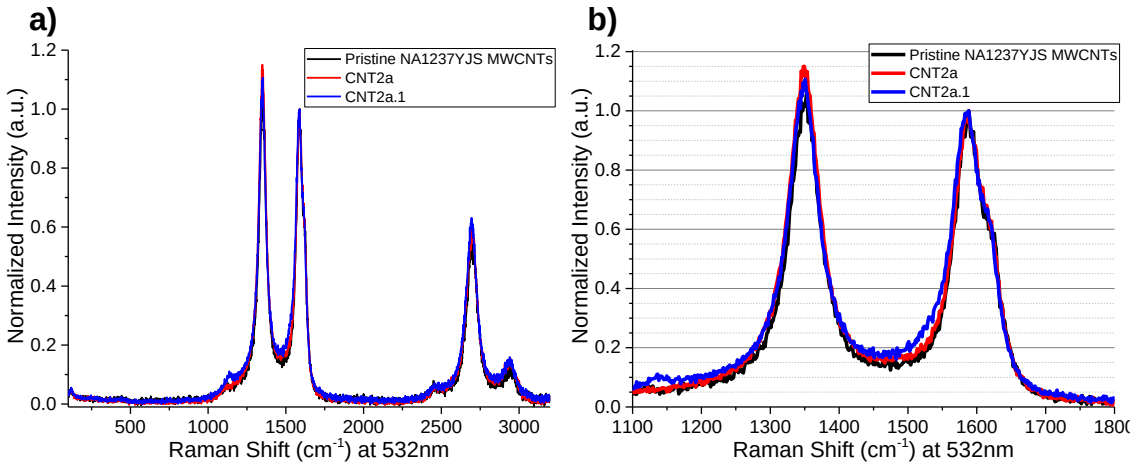

Figure 3.4.12: Raman spectra of pristine NanoAmor 1237YJS, **CNT2a** and **CNT2a.1** between **a)** 100 and 3200 cm^{-1} Raman shift, and **b)** 1100 and 1800 cm^{-1} Raman shift.

The degrees of functionalization were calculated 270 µmol/g, 60 µmol/g and 40 µmol/g for **CNT2a**, **CNT2a.1** and **CNT2a.1.1**, respectively. Amidation reaction with **P3** molecule occurred 1:4.5 ratio of carboxyl groups which were present on the surface of **CNT2a**. Resulting product **CNT2a.1** contains Pht group and the

deprotection ratio of Pht group was calculated 2:3 by the change of weight loss between **CNT2a.1.1** and **CNT2a.1**.

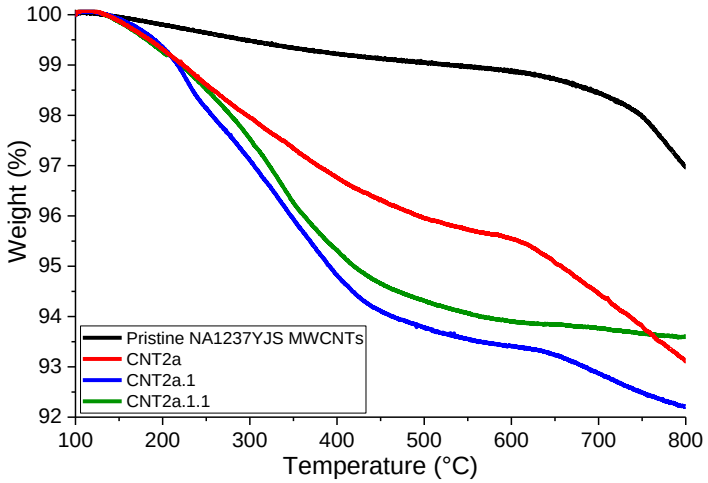

Figure 3.4.13: Comparative TGA graphics of Pristine NanoAmor 1237YJS, **CNT2a**, **CNT2a.1** and **CNT2a.1.1**.

Kaiser Test (Ninhydrin test) was performed in order to confirm the TGA results of **CNT2a.1.1** as the test is quantitatively sensitive to primary amine groups. The primary amine groups were calculated 36 µmol/g. The results of TGA and Kaiser Test were not significantly different.

The resulting product **CNT2a.1.1** will be evaluated by biological assays to study the biocompatibility.

3.4.2.3 Functionalization of CNT2a and CNT2b with both P1 and P3 and Deprotection of Pht and Boc Groups

MWCNTs functionalized with 4-Aminobenzoic acid **CNT2a** and **CNT2b** were double functionalized with **P1** and **P3**. The purpose of the functionalization with different protected groups containing molecules was to allow further functionalizations with two different molecules.[27] Thus, it allows to develop new drug carrier systems as it is possible to couple a targeting agent and a drug molecule on MWCNTs. Moreover the study allowed to explore how to tune the functionalization degree of the tubes.

The coupling reaction of **P1** and **P3** was performed with **CNT2a**, and **CNT2b** in DMF in the presence of DIPEA and HBTU in 48 hours at room temperature and yielded **CNT2a.2** and **CNT2b.a**, respectively.

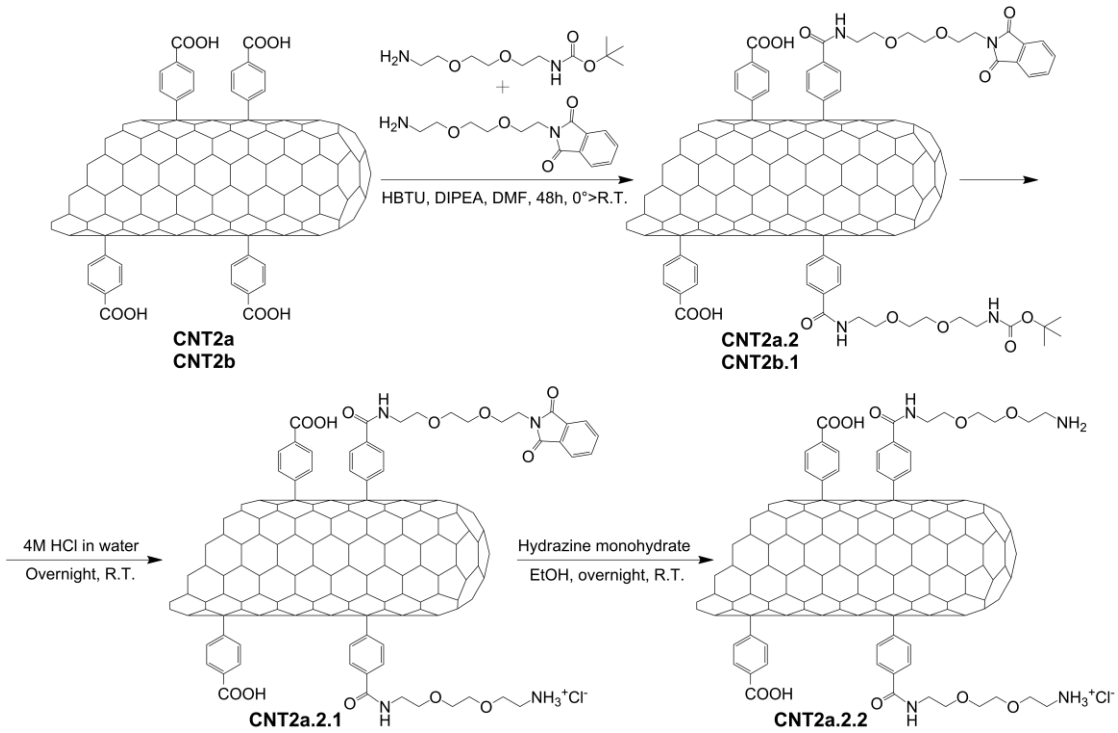

Figure 3.4.14: Synthesis of **CNT2a.2**, **CNT2b.1**, **CNT2a.2.1** and **CNT2a.2.2**.

TGA results show that the degree of functionalization of **CNT2b.1** product was higher (148 µmol/g) than **CNT2a.2** (88 µmol/g, assuming that the coupling of the **P1** and **P3** occurs 1:1 ratio). These results suggest that the amidation reaction occurred with 1:3 and 1:2.2 ratio of carboxyl groups which were present on the surface of **CNT2a** and **CNT2b**, respectively.

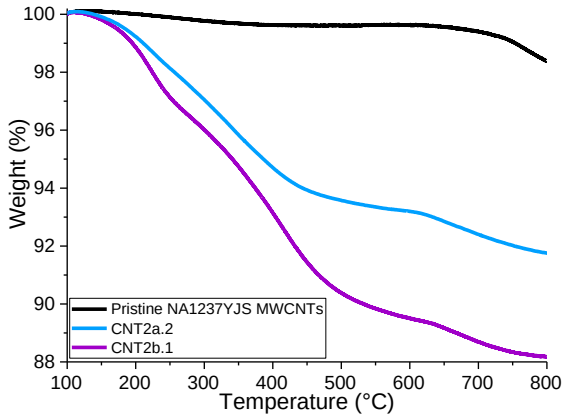

Figure 3.4.15: Comparative TGA graphics of Pristine NA1237YJS MWCNTs, **CNT2a.2** and **CNT2b.1**.

Kaiser Test was performed on deprotected compounds **CNT2a.2.1** and **CNT2a.2.2**, and primary amine groups were calculated 22 µmol/g and 38 µmol/g, respectively. Biological evaluations will be performed on the final products before and after deprotection.

3.4.2.4 Oxidation of NanoAmor 1237YJS MWCNTs

Pristine NanoAmor 1237YJS MWCNTs were also oxidized as in the case of pristine NC 7000 MWCNTs, in order to increase the water dispersibility and introduce oxygen containing surface groups for further functionalizations. By increasing the defects on the surface of MWCNTs through the oxidation, higher degree of functionalization can be obtained from the functionalization reactions. For this purpose, acid treatment was performed to introduce the carboxylic groups on the surface of MWCNTs through the acid treatment with H_2SO_4 and HNO_3 mixture (3:1) in 10 hours.

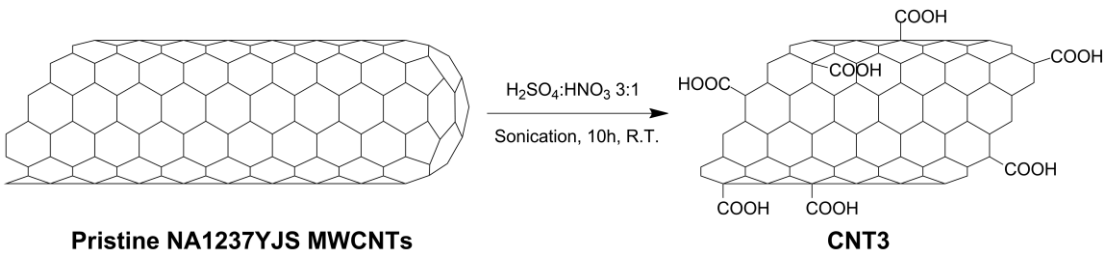

Figure 3.4.16: Oxidation reaction of NanoAmor 1237YJS MWCNTs.

TEM imaging was performed on pristine NanoAmor 1237YJS MWCNTs and **CNT3**. Outer and inner dimensions of pristine MWCNTs were confirmed with the product specifications 20 - 30 nm and 5 - 10 nm, respectively. The lengths of pristine nanotubes were distributed between 0.5 - 2 µm. The diameters of **CNT3** were not significantly different from the pristine MWCNTs and the oxidized MWCNTs preserved their multi-walled tubular structure while the average length of **CNT3** resulted about 200 nm. The size of oxidized MWCNTs were reduced to the desired size range which was reported by Jain *et al.* as less cytotoxic and more biocompatible.[25]

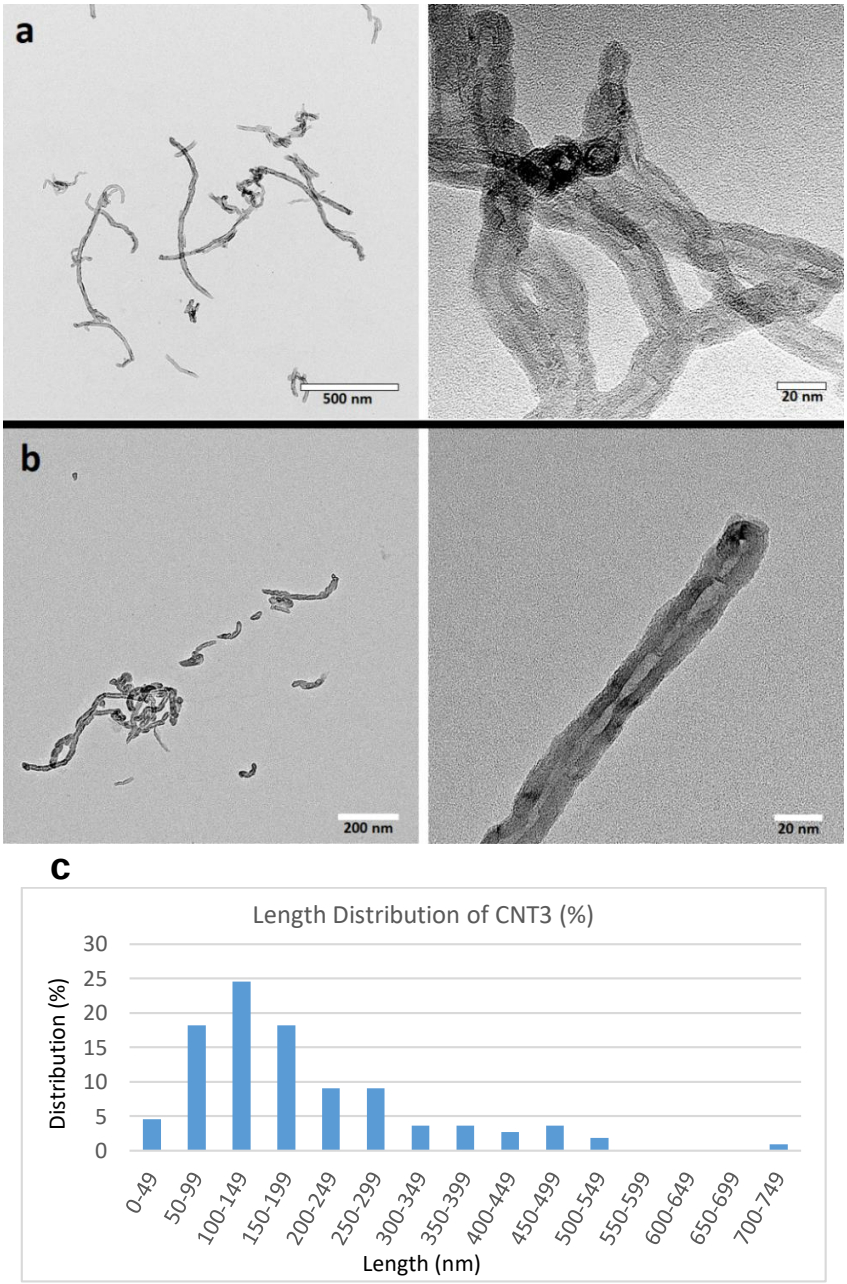

Figure 3.4.17: TEM images of **a)** pristine NanoAmor 1237YJS MWCNTs **b) CNT3** and **c**) length distribution of **CNT3**.

Raman spectra of **CNT3** and pristine MWCNTs were compared. The normalized spectra in Figure 3.4.18-b show that the intensity of D and D' band of **CNT3** was higher than the one of pristine MWCNTs. The intensity of 2D band decreases after the oxidation as the outer layers of **CNT3** are damaged by the treatment.

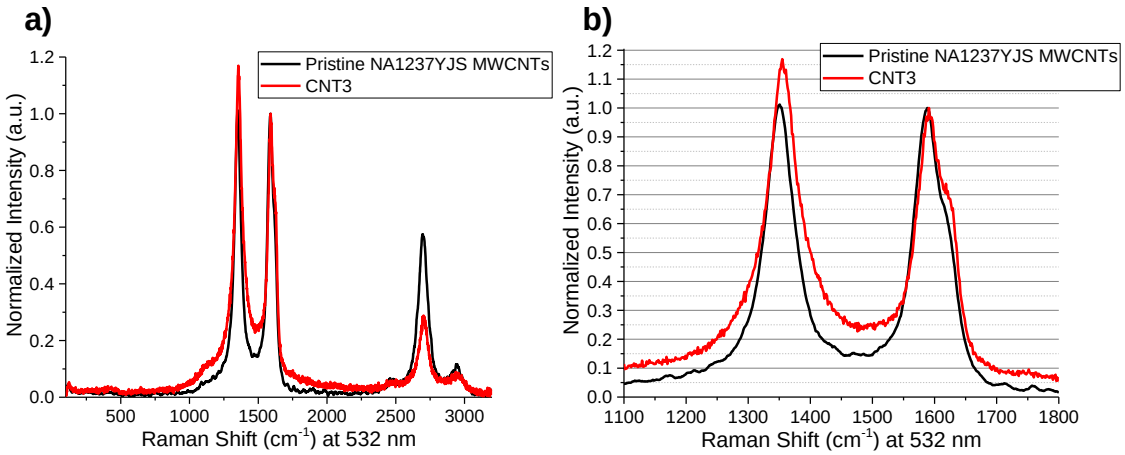

Figure 3.4.18: Raman spectra of pristine NanoAmor 1237YJS and **CNT3** between **a)** 100 and 3200 cm^{-1} Raman shift, and **b)** 1100 and 1800 cm^{-1} Raman shift.

Dispersibility of pristine NA1237YJS MWCNTs was tested and the dispersion was stable for 24 hours while the dispersion of **CNT3** was stable for 3 months with a concentration of 1 mg/mL in water.

3.4.2.5 Functionalization of CNT3 with P9, P10 and P11

Oxidized NA1237YJS MWCNTs (**CNT3**) were functionalized with **P9**, **P10**, **P11** and **P9**+**P10**. The functionalization reactions with **P9** were performed with two different conditions and the one giving the better results in terms of functionalization (HOBt, EDC•HCl and DMAP) was used for the other compounds.

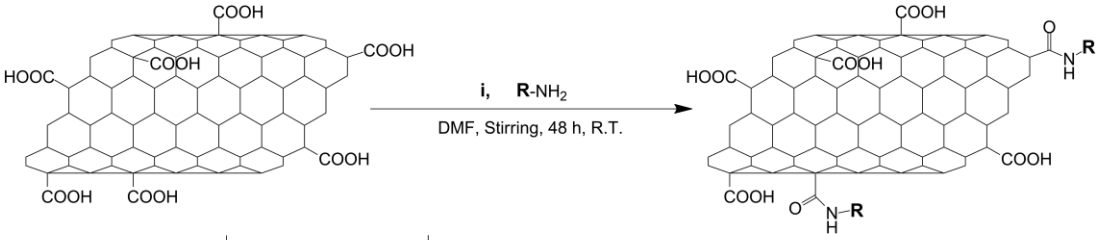

Product Name	i	R—NH_2
CNT3.1a	HBTU, TEA	P9
CNT3.1b	HOBt, EDC.HCl, DMAP	P9
CNT3.2	HOBt, EDC.HCl, DMAP	P10
CNT3.3	HOBt, EDC.HCl, DMAP	P11
CNT3.4	HOBt, EDC.HCl, DMAP	P9 + P10

Figure 3.4.19: Reaction conditions of **CNT3.1-4** products.

TGA was performed and the results of pristine MWCNTs, **CNT3**, **CNT3.1a**, **CNT3.1b** and **CNT3.2** were compared.

As mentioned the reaction performed with HBTU and TEA has very low degree of functionalization (10 µmol/g for **CNT3.1a**). CNT3.1b which was synthesized in the presence of **P9**, HOBt, EDC•HCl and DMAP has relatively higher degree of functionalization (80 µmol/g). Accordingly, **CNT3.2** was synthesized in the presence of **P10**, HOBt, EDC•HCl and DMAP and yielded with 102 µmol/g of degree of functionalization. For **CNT3.3**, the degree of functionalization was calculated 59 µmol/g, while for **CNT3.4** was calculated 66 µmol/g by assuming 1:1 coupling ratio of **P9** and **P10** molecules on **CNT3**.

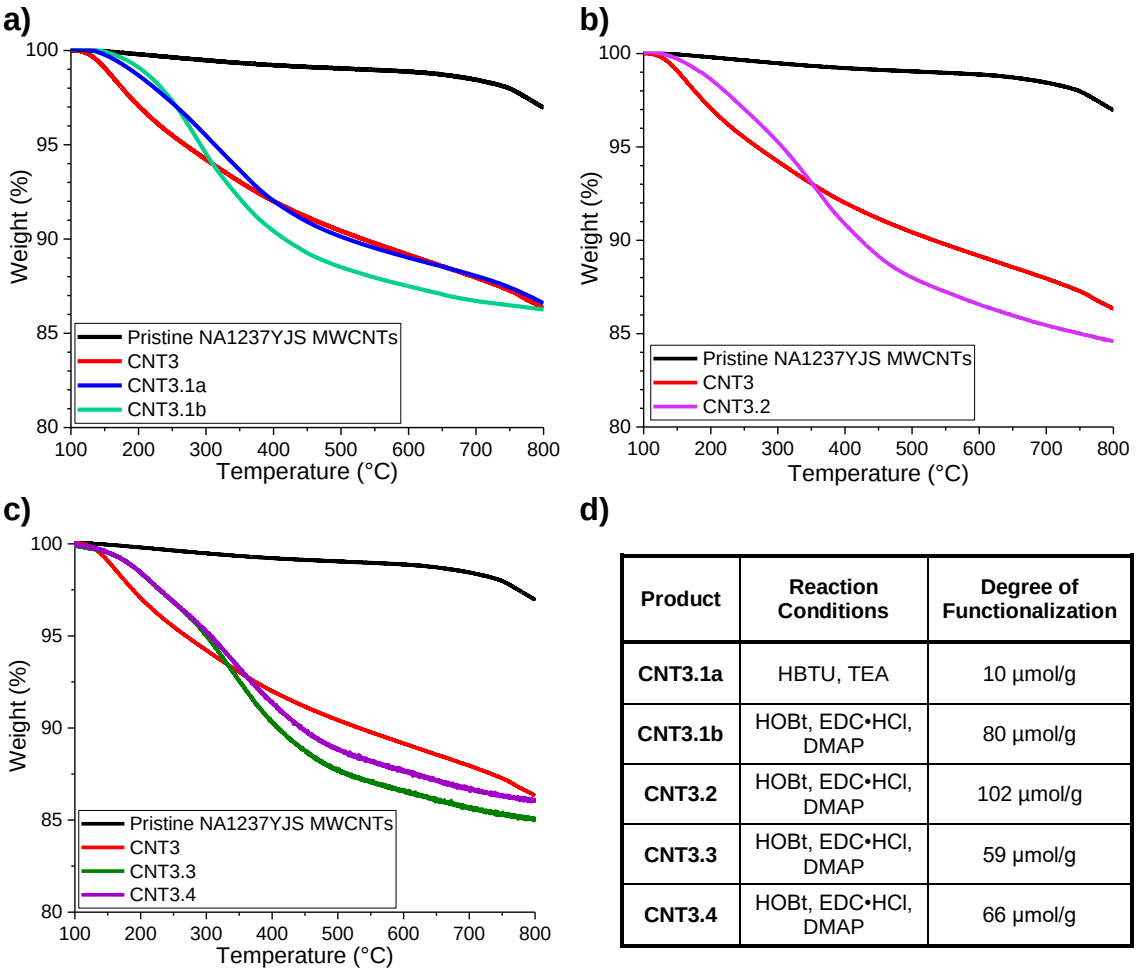

d)

Product	Reaction Conditions	Degree of Functionalization
CNT3.1a	HBTU, TEA	10 µmol/g
CNT3.1b	HOBt, EDC•HCl, DMAP	80 µmol/g
CNT3.2	HOBt, EDC•HCl, DMAP	102 µmol/g
CNT3.3	HOBt, EDC•HCl, DMAP	59 µmol/g
CNT3.4	HOBt, EDC•HCl, DMAP	66 µmol/g

Figure 3.4.20: Comparative TGA graphics of **a) P9** functionalized **CNT3** (**CNT3.1a** and **CNT3.1b**), **b) P10** functionalized **CNT3** (**CNT3.2**) **c) P11** functionalized and **P9**+**P10** functionalized **CNT3** (**CNT3.3** and **CNT3.4**, respectively) and **d)** calculated degrees of functionalization.

Functionalizations of MWCNTs were performed with different approaches in order to find best conditions to obtain high degree of functionalization. Pristine MWCNTs were functionalized through the arylation reaction with 4-aminobenzoic acid for different reaction time in order to create a functional coat on the surface of MWCNTs. This functionalization provide a further functionalizable surface with different properties since –COOH terminal functional groups were introduced. Another functionalization approach was perform with the acid treatment. Pristine MWCNTs were shortened by the oxidation reaction to the desired length for biomedical applications. –COOH groups introduced by the oxidation were utilized for the amidation reactions of organic compounds with different properties for biological applications.

3.5 Evaluations of Carbon Nanostructures for Various Applications

As it was deeply discussed in Chapter 1, it is fundamental to functionalize MWCNTs and NDs for their biomedical applications while GQDs and CDs can be used without functionalizations in bioimaging or photodynamic therapy. Carbon nanostructures require essential functional groups especially in order to have better biocompatibility and be delivered to the targeted tissues. For non-biomedical applications, carbon nanostructures can be used in their pristine form or can be functionalized in order to add new properties.

Different carbon nanostructures have been functionalized with various appendages and, in particular in the case of sugar and ILs, the units were introduced to NDs, GQDs and CNTs. The so obtained derivatives will be biologically evaluated, for example, for their antibacterial activity.

It will be possible to compare not only the importance of the variation of the introduced decoration on the same carbon nanostructure, but also, analyzing the results obtained by the different nanostructures presenting the same decoration, to understand which are the most important features due to the used carbon nanoforms.

In the following paragraphs some initial evaluations of NDs and GQDs are reported.

3.5.1 Biological Evaluations of Amino and FITC (P9) Functionalized Nanodiamonds

Biological evaluations of FITC functionalized NDs were performed by the group of Dr. Delogu at University of Sassari. All the biological data on NDs herein reported have been performed on the samples prepared in the frame of this work and of a previous PhD thesis work performed by Valentina Armuzza.

Cellular Uptake of Nanodiamonds

Cellular uptake of NDs was analyzed in human peripheral blood mononuclear cells (PBMCs). PBMCs were incubated in a 24-well plate (25×10^4 cells/well) with 5, 25, 50 and 100 μg/mL amounts of **ND1.5.2** for 24-hour incubation time.

The samples were imaged by a confocal microscopy (Leica TCS SP5 confocal microscope) and fluorescence signal of FITC was acquired using the 488 Argon blue laser line.

Fluorescein conjugated nanodiamonds (**ND1.5.2**) were investigated into T cells, B cells, NK cells and monocytes after 24-hour incubation time. The fluorescence imaging was performed with PBMCs incubated with 50 µg/mL intermediate concentration as it was decided. Human PBMCs were stained for Propidium iodide (PI) fluorescent signal to identify cell morphology and for PI/**ND1.5.2** signal to detect nanodiamonds internalization under fluorescence microscopy (Figure 3.5.1, b-c).

According to the fluorescence signal, NDs were mostly internalized by monocytes comparing to T and B lymphocytes, and natural killer (NK) cells. As monocytes are the only phagocytic cells among the PBMCs, they are able to internalize big molecules such as nanomaterials. It was reported that also CNTs are mostly internalized by monocytes.[28] The uptake results of CNTs and NDs performed with PBMCs comply with each other.

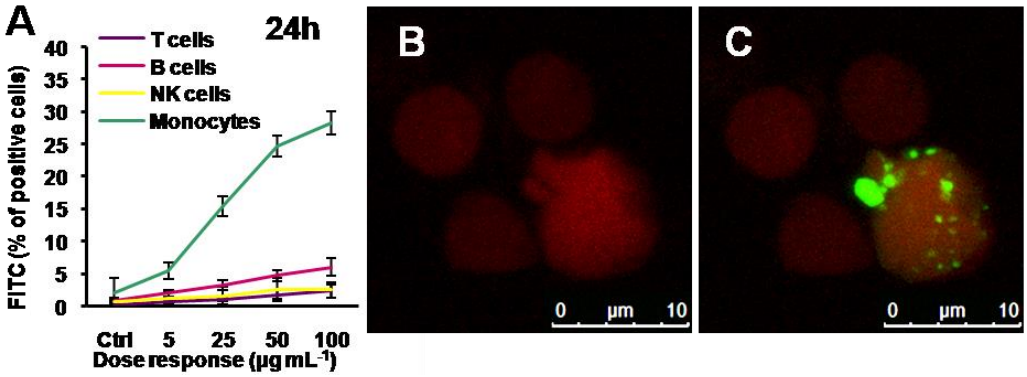

Figure 3.5.1: Uptake of FITC functionalized nanodiamonds (**ND1.5.2**) by human peripheral blood mononuclear cell (PBMC). **a)** Internalization of increasing doses of **ND1.5.2**, **b)** Images of PBMCs stained for PI fluorescent signal to identify cell morphology and **c)** for PI/**ND1.5.2** signal to detect nanodiamonds internalization.

Ex vivo viability assay on immune cells

Cell viability was evaluated on human PBMCs by flow cytometry using 7-AAD (7-amino-actinomycin D) stain, a fluorescent compound with strong affinity for DNA. 7-AAD cannot enter the cells with functional membrane but late apoptotic and

necrotic cells with compromised membranes allow 7-AAD into the nucleus. PBMCs (25 × 10^4 cells/well) were incubated for 6/12/24 hours with 5, 25, 50, and 100 µg/mL doses of oxidized NDs (**ND1**) and ND-NH_2 (**ND1.3**). Ethanol was used as a positive control group.

Viability data of lymphocytes (T, B and NK cells) were similar to controls at all doses and time points (6 h, 12 h and 24 h). Significant mortality was detected for monocytes at high concentration of NDs. High mortality of monocytes is possibly due to the high toxicity effect of **ND1** after 24-hour incubation. There is a significant mortality rate difference between two differently functionalized NDs. **ND1.3** shown lower mortality rate at the dose of 100 µg/mL than **ND1**.

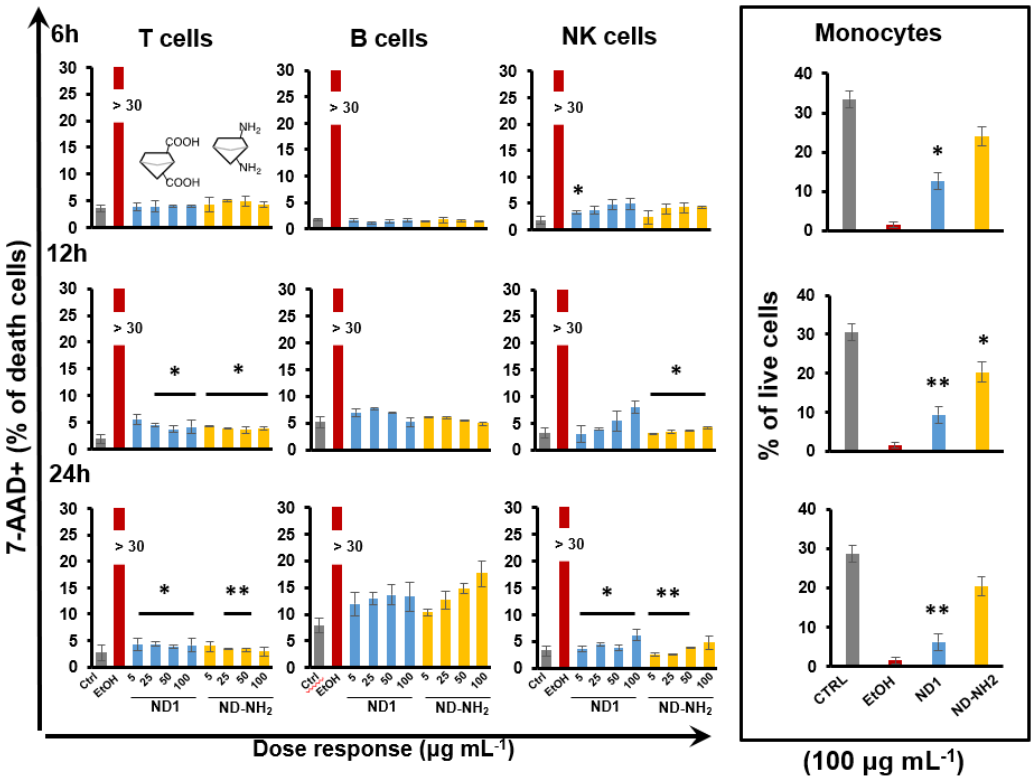

Figure 3.5.2: Cell viability test performed with 7-AAD (as DNA dye), **ND1** (blue) and **ND1.3** (yellow) on PBMCs. The graphics were shown the percentage of 7-AAD positive cells after 6-hour, 12-hour and 24-hour incubation time. (*, $p < 0.05$), (**, $p < 0.01$).

Other experiments to determine the possible alteration of the gene expression due to the cell exposure to **ND1** and **ND-NH_2** are currently undergoing c/o the University of Sassari and Sidra Medical and Research Center of Doha.

3.5.2 Preliminary Biological Evaluations of GQDs

Some preliminarily biological experiments have been performed on GQDs and the parent material (GO) were performed by Prof. G. Messa group at the Ospedale Ca' Granda (Milan).

LDH cytotoxicity assays performed on podocytes and EOMA (Murine hemangioendothelioma) cells showed a dosed-dependent cytotoxicity of GQDs and GO at all time points. For podocytes the LD_{50} of GO resulted 20 µg/mL while GQDs showed a lesser toxicity (LD50 resulted to be 30 µg/mL) and EOMA gave the same trend: 50 µg/mL for GO and 20 µg/mL for GQDs. These results highlighted how GQDs showed a lower toxicity in both type of cells compared to its precursor.

a)

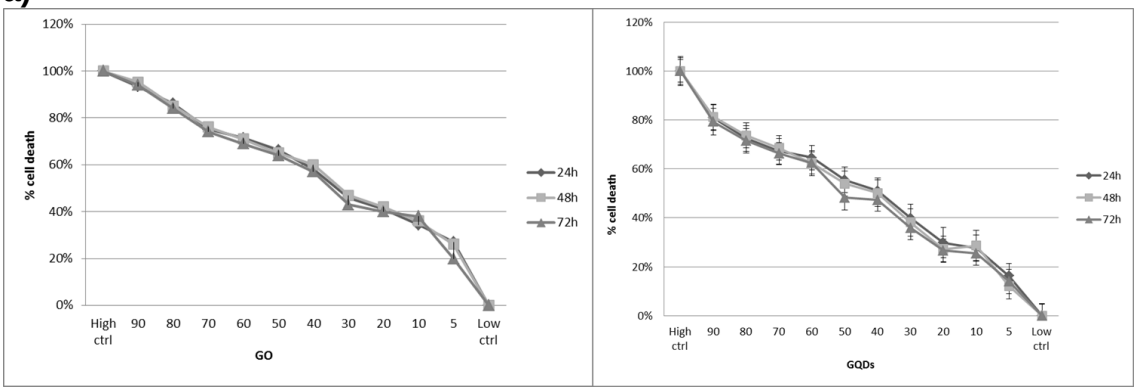

b)

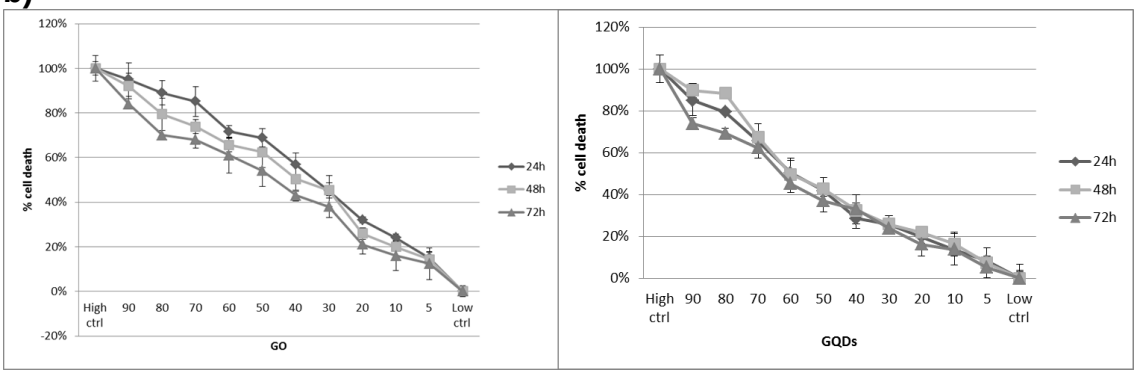

Figure 3.5.3: LDH Cytotoxicity assay performed on **a)** podocytes and on **b)** EOMA at the three time points, 24h, 48h and 72h using **GQDs** and **GO**.

It can be suggested that the production of GQDs through cutting, exfoliation and oxidation of GO is important for biomedical applications and provides relatively more biocompatible material comparing to its precursor.

The different physical and chemical properties of nanomaterials lead to their different interaction with biomolecules and cells.[27] It is therefore important to understand the preferential route of cellular uptake and degradation to better understand the interaction of the compound with its cellular target.

LysoTracker® Green DND-26 assay was performed on podocytes at 24, 48 and 72 h after treatment with 30 µg/mL of **GQDs**. After only 24 h no localization of the compound with lysosome was detected. Data were then confirmed by immunofluorescence. After 48 h there was the evidence of colocalization, which resulted to be maximum at 72 h. It denotes a slow cellular uptake of the compound by podocytes but highlights the preferential process of cellular uptake is endocytosis.

It is worth to notice that, unlike the colocalization or uptake studies performed with other carbon nanostructures, in the case of **GQDs** it was not necessary their conjugation with a fluorescent tag, being themselves fluorescent.

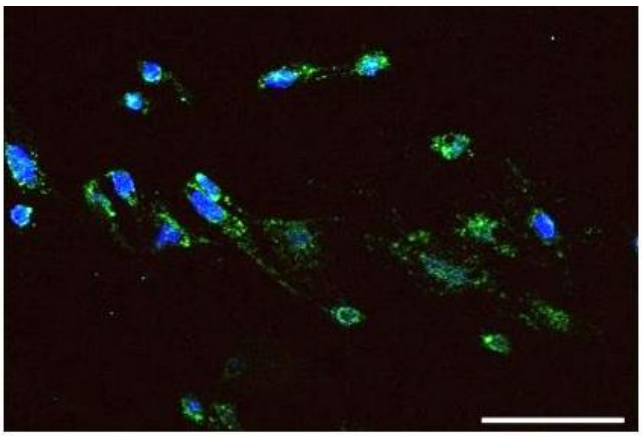

Figure 3.5.4: Confocal images of Lysotracker assay on podocytes at 24 h. Scale bar 40X.

3.5.3 Performance Evaluation of Flexible Electrochromic Devices with Carbon Nanostructures

The applications of nanotech products in electronics grow rapidly and carbon nanostructures have promising properties related to this field, so the performance in Flexible Electrochromic Devices in presence of carbon nanostructures has been evaluated.

Electrochromic materials are capable of displaying reversible optical absorbance changes upon electrically induced oxidation and reduction. Electrochromic devices have many advantages such as response to a small electrical voltage, low power consumption, pronounced optical contrast and reversibility. Their technology development is still in progress, because there are some disadvantages of the available materials to overcome such as short lifetime, degradation of the materials and long response time.

Carbon nanotubes were already evaluated in electrochromic devices and it was reported that electrochromic performance in many aspects is enhanced thanks to CNTs.[29] Hwang *et al.* reported that applications of GQDs in electrochromic devices can increase their cyclability and eliminate the electrolyte which may cause efficiency and/or degradation problems.[30] A blending methodology for electrochromic devices has been developed in Universidade NOVA de Lisboa in collaboration with the research group of Prof. Bonifazi (Cardiff University). By using this methodology, it is possible to spray coat the PET-ITO surface with carbon nanostructure/polymer mixture without leaving irregular stains and this methodology is patent pending. As carbon nanotubes and graphene quantum dots have increased the performance of electrochromic devices in different aspects, graphene quantum dots and amino functionalized nanodiamonds have been evaluated in electrochromic devices in order to study their effects on the device performances. The chosen GQDs were the **GQD2**, while the NDs were **ND3.8** and **ND1.7** presenting the amine terminating PEG chain and deriving from the amidation of pND and oxidized **ND1** respectively.

Preparation and characterization studies of electrochromic devices were carried out in collaboration with Prof. Parola and Prof. Laia (Universidade NOVA de

Lisboa). Thiophene-based electrochromic polymer (Figure 3.5.5) was synthesized by our collaborators at Universidade NOVA de Lisboa as described by Dyer *et al*.[30]

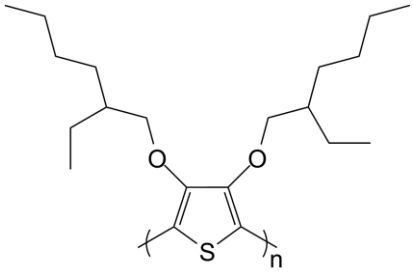

Figure 3.5.5: Structure of Thiophene based electrochromic polymer

The color of the polymer is orange when reduced and bleached blue when oxidized (Figure 3.5.6, a). As mentioned the blending of the electrochromic polymer and carbon nanostructure has been previously explored by Universidade NOVA de Lisboa in collaboration with Cardiff University. UV curable electrolyte Li^+ based denominated Ynv.El.® property of Ynvisible® with the patent nº 20140361211 was applied between the electrodes.

Preparation of Flexible Electrochromic Device

The carbon nanostructures and the electrochromic polymer were blended and spray-coated on PET/ITO substrate. Electrolyte was applied on the surface coated with the blend, and electrochromic device was assembled. As final step of the preparation, the electrochromic device was UV-cured as a necessary process due to the electrolyte. The same methodology was used to prepare a control device with electrochromic polymer in the absence of carbon nanostructures. Inner square of ECD represents the active electrode which the spectroelectrochemical measurements were performed and outer square is printed in order to maintain the charge balance of the active electrode. (Figure 3.5.6, b-c)

Characterization of as-prepared Flexible Electrochromic Device

In the first experiment, Graphene Quantum Dots (**GQD2**) and electrochromic polymer were blended in ratio of 1:10 and electrochromic device (**ED-GQD2-**

1:10) was prepared as described. The performances of this device were compared with the control one.

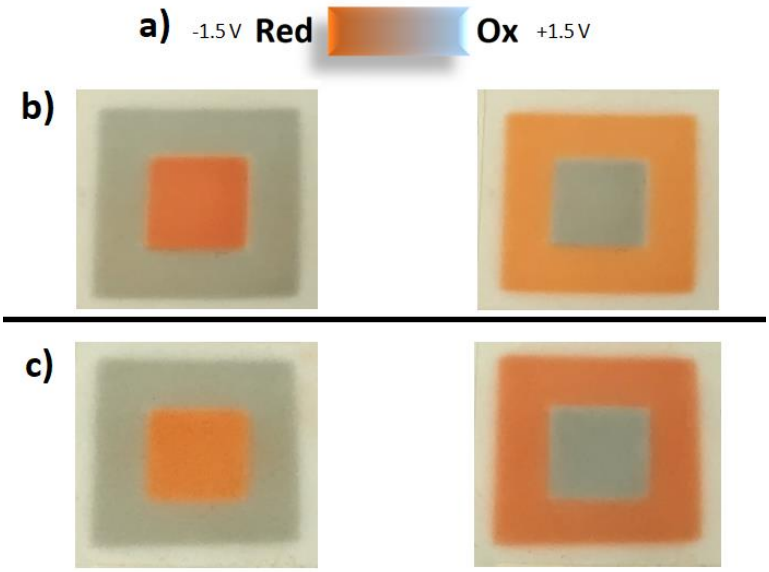

Figure 3.5.6: a) Illustration of color change between the reduced and oxidized state of thiophene-based electrochromic polymer. Reduced and oxidized state of **b)** only electrochromic polymer containing electrochromic device and **c)** the blend in ratio of 1:10 **GQD2:thiophene** polymer containing electrochromic device.

The **ED-GQD2-1:10** and the control device were characterized with Spectroelectrochemical techniques. Absorption spectra of both with different applied voltages were not significantly different. Absorbance change at 465 nm excitation was 0.48 and 0.51 for the control device, and **ED-GQD2-1:10**, respectively. Switching times in oxidation and reduction states of the ECD were calculated with the time for 90% change in transmittance of the device between oxidized and reduced states. Switching times to reach oxidized state were calculated as 3.7 and 4 seconds for the control device, and **ED-GQD2-1:10**, respectively. Switching times to reach reduced state were calculated as 5.2 and 5.8 seconds for the control device, and **ED-GQD2-1:10**, respectively.

Coloration efficiency is the power efficiency of the electrochromic devices and can be calculated through the division of the change in optical density by the amount of charge density injected. Oxidation Coloration Efficiencies were calculated 157 and 159 $C^{-1}.cm^2$ for the control device, and **ED-GQD2-1:10**, respectively. Reduction Coloration Efficiencies were calculated 208 and 185 $C^{-1}.cm^2$ for the control device and **ED-GQD2-1:10**, respectively (Figure 3.5.7).

These results show that the GQDs doping does not have significant effect on contrast change, switching time and coloration efficiency. As it was mentioned in the literature, it is expected to improve the stability and cyclability of the electrochromic devices.[30] The cyclability studies are ongoing in collaboration with Universidade NOVA de Lisboa.

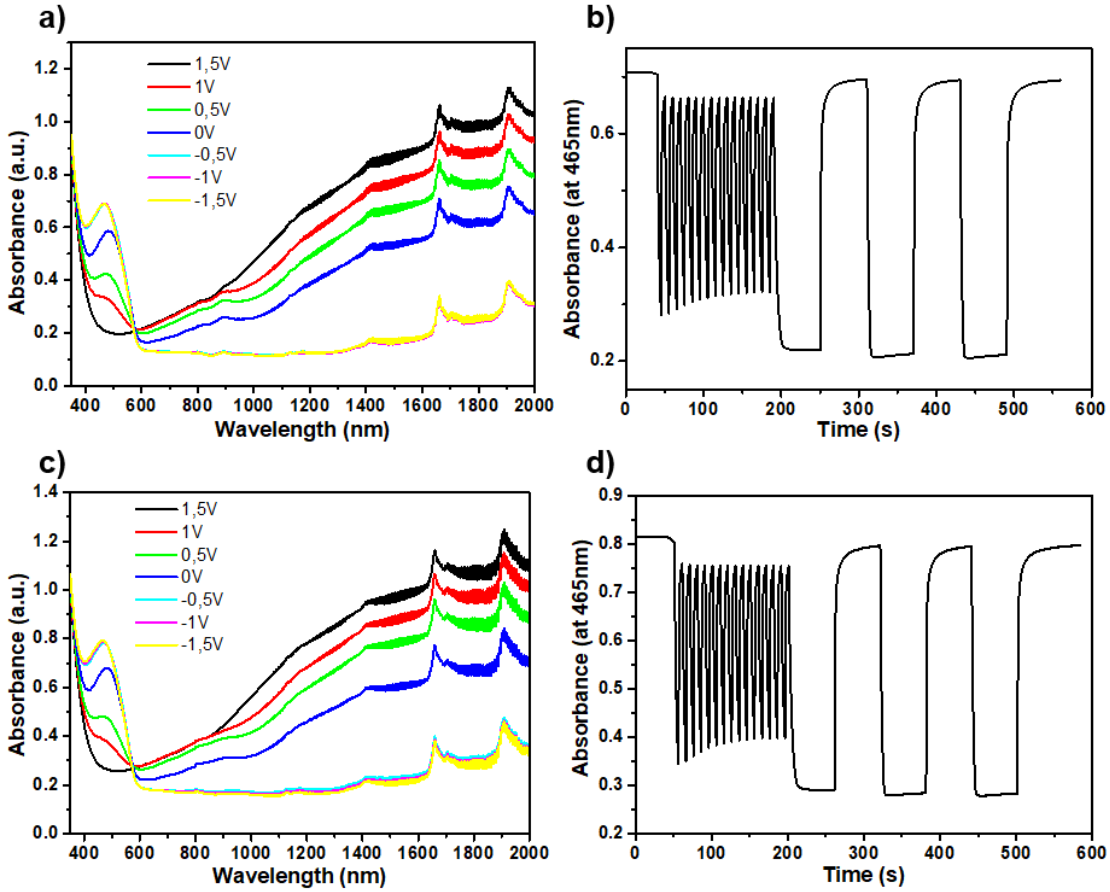

e)

Device	ΔAbs	ST_{Ox} (s)	ST_{Red} (s)	CE_{Ox} ($C^{-1}.cm^2$)	CE_{Red} ($C^{-1}.cm^2$)
Polymer	0.48	3.7	5.2	157	208
ED-GQD2-1:10	0.51	4	5.8	159	185

Figure 3.5.7: Optical measurements of prepared electrochromic devices. Absorption spectra of the ECD prepared with **a)** only polymer and **c) ED-GQD2-1:10** with different applied voltages. Electrochemical cycling between −1.5 and +1.5 V of the ECD **b)** only polymer and **d) ED-GQD2-1:10** followed by optical transmittance at 465 nm. **e)** Calculated absorbance change, switching time and coloring efficiency for oxidized and reduced states.

Further studies were performed increasing the concentration of the carbon nanostructures. In the second experiment, the blends for electrochromic devices were prepared with **GQD2**, **ND3.8** and **ND1.7** in ratio of 1:4 (w/w, carbon nanostructure:polymer) and named **ED-GQD2-1:4** or **Device b**, **ED-ND3.8-1:4** or **Device c** and **ND1.7-1:4** or **Device d**, respectively. The reference devise (**Device a**) was prepared, one more time, only with the electrochromic polymer (Figure 3.5.8).

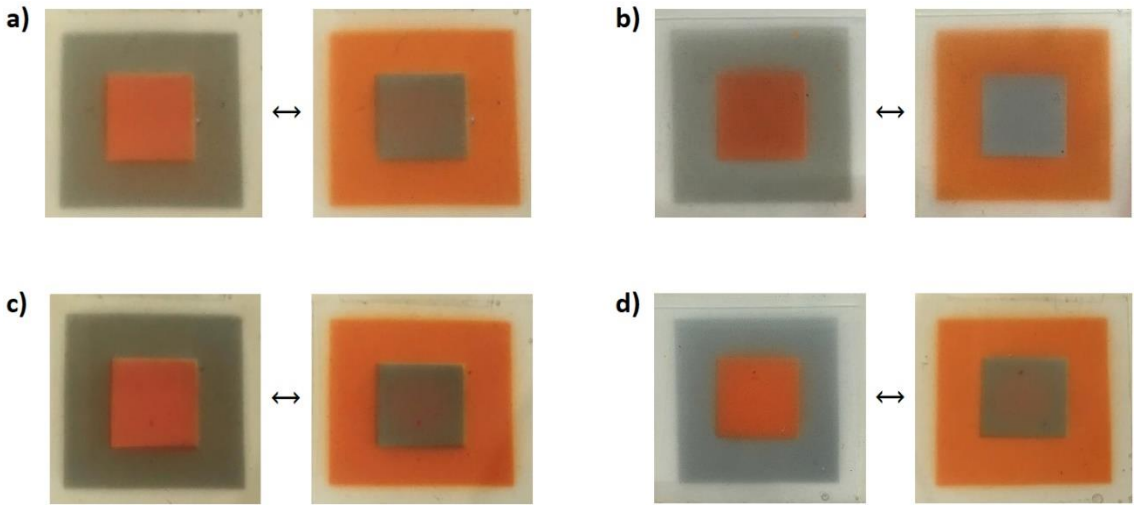

Figure 3.5.8: Reduced and oxidized states of **a) Device a**, **b) Device b**, c) **Device c**, and d) **Device d**.

These devices were preliminarily characterized by Spectroelectrochemical techniques. The absorption spectra were recorded at different applied voltages and the absorbance changes at 460 nm were evaluated. For **Device a**, **Device c** and **Device d** no significant differences were found, while in the case of **Device b** the calculated value is 0.46, significantly different than **Device a**. Moreover the absorbance spectrum of **Device b** differs in the oxidized state from **Device a** and this result suggest that **Device b** becomes more bleached than the control and it is an improvement for the system (Figure 3.5.9).

Device b switching times were slower but not significantly different than **Device a**. For **Device c**, the switching time to oxidized state was shortened but the switching time to reduced state was not changed. In the case of **Device d**, the switching time to oxidized state was relatively slower and the switching time to

reduced state was significantly faster and further experiments should be performed in order to understand the possible mechanisms.

Coloration efficiencies of the devices were not significantly different than the control.

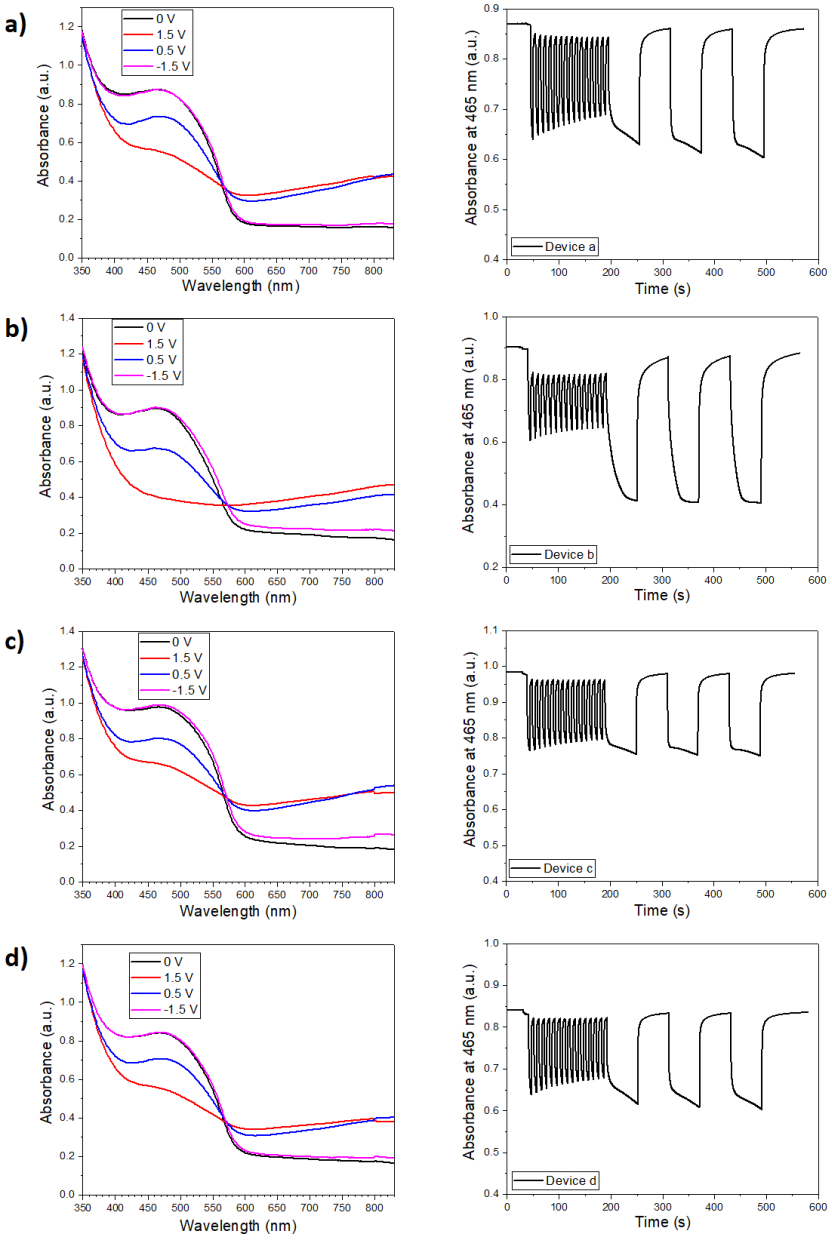

e)

Device	Content	ΔAbs	ST_{Ox} (s)	ST_{Red} (s)	CE_{Ox} ($C^{-1}.cm^2$)	CE_{Red} ($C^{-1}.cm^2$)
a	**Polymer**	0.25	15.2	10.9	129.09	98.96
b	**Polymer + GQD2**	0.46	19.2	14.8	120.72	122.28
c	**Polymer + ND3.8**	0.23	7.6	10.7	133.37	81.16
d	**Polymer + ND1.7**	0.22	30.9	5.5	94.85	125.64

Figure 3.5.9: Optical measurements of prepared electrochromic devices. Absorption spectra and Continuous monitoring of the change in percent transmittance at λ_{max}=460 nm during switching between −1.5 and +1.5 V of the ECDs prepared with **a)** only polymer and **b) GQD2**:polymer (1:4), **c) ND3.8**:polymer (1:4), and **d) ND1.7:**polymer (1:4). **e)** Calculated absorbance change, switching time and coloring efficiency for oxidized and reduced states.

Bibliography

1. G. Pastorin, W. Wu, S. Wieckowski, J.-P. Briand, K. Kostarelos, M. Prato, A. Bianco; *Chemical Communications* **2006,** (11), 1182-1184.
2. M.-Y. Mistou, I. C. Sutcliffe, N. M. van Sorge; *FEMS Microbiology Reviews* **2016,** *40* (4), 464-479.
3. J. Sloothaak, D. I. Odoni, V. A. P. Martins dos Santos, P. J. Schaap, J. A. Tamayo-Ramos; *PLOS Genetics* **2016,** *12* (12), e1006468.
4. A. F. M. Cláudio, M. C. Neves, K. Shimizu, J. N. Canongia Lopes, M. G. Freire, J. A. P. Coutinho; *Green chemistry : an international journal and green chemistry resource : GC* **2015,** *17* (7), 3948-3963.
5. L. Carson, P. K. W. Chau, M. J. Earle, M. A. Gilea, B. F. Gilmore, S. P. Gorman, M. T. McCann, K. R. Seddon; *Green Chemistry* **2009,** *11* (4), 492-497.
6. A. R. Dias, J. Costa-Rodrigues, M. H. Fernandes, R. Ferraz, C. Prudêncio; *ChemMedChem* **2017,** *12* (1), 11-18.
7. V. N. Mochalin, O. Shenderova, D. Ho, Y. Gogotsi; *Nature Nanotechnology* **2011,** *7* (1), 11-23.
8. S. Osswald, G. Yushin, V. Mochalin, S. O. Kucheyev, Y. Gogotsi; *Journal of the American Chemical Society* **2006,** *128* (35), 11635-11642.
9. T. Ando, M. Ishii, M. Kamo, Y. Sato; *Journal of the Chemical Society, Faraday Transactions* **1993,** *89* (11), 1783-1789.
10. T. Jiang, K. Xu; *Carbon* **1995,** *33* (12), 1663-1671.
11. E. L. Sciuto, M. F. Santangelo, G. Villaggio, F. Sinatra, C. Bongiorno, G. Nicotra, S. Libertino; *Sensing and Bio-Sensing Research* **2015,** *6*, 67-71.
12. S. Santra, D. Dutta, B. M. Moudgil; *Food and Bioproducts Processing* **2005,** *83* (2), 136-140.
13. C. Ornelas; *New Journal of Chemistry* **2011,** *35* (10), 1973-1985.
14. C. Biot, G. Glorian, L. A. Maciejewski, J. S. Brocard, O. Domarle, G. Blampain, P. Millet, A. J. Georges, H. Abessolo, D. Dive, J. Lebibi; *Journal of Medicinal Chemistry* **1997,** *40* (23), 3715-3718.
15. V. J. Fiorina, R. J. Dubois, S. Brynes; *Journal of Medicinal Chemistry* **1978,** *21* (4), 393-5.
16. R. E. Bozak; *Photochemistry in the Metallocenes in Advances in Photochemistry (eds. N. Pitts, G. S. Hammond ,W. A. Noyes)*. 1971; Vol. 8, p 227-244.
17. I. A. Vacchi, C. Spinato, J. Raya, A. Bianco, C. Ménard-Moyon; *Nanoscale* **2016,** *8* (28), 13714-13721.
18. D. Elhamifar, B. Karimi, A. Moradi, J. Rastegar; *ChemPlusChem* **2014,** *79* (8), 1147-1152.
19. W. S. Hummers, R. E. Offeman; *Journal of the American Chemical Society* **1958,** *80* (6), 1339-1339.
20. R. J. Nemanich, S. A. Solin; *Physical Review B* **1979,** *20* (2), 392-401.
21. A. C. Ferrari; *Solid State Communications* **2007,** *143* (1), 47-57.
22. F. Tuinstra, J. L. Koenig; *The Journal of Chemical Physics* **1970,** *53* (3), 1126-1130.
23. V. Georgakilas, K. Kordatos, M. Prato, D. M. Guldi, M. Holzinger, A. Hirsch; *Journal of the American Chemical Society* **2002,** *124* (5), 760-761.
24. www.nanocyl.com/product/nc7000/. (accessed 11-11-2018).
25. S. Jain, V. S. Thakare, M. Das, C. Godugu, A. K. Jain, R. Mathur, K. Chuttani, A. K. Mishra; *Chemical Research in Toxicology* **2011,** *24* (11), 2028-2039.
26. M. S. Strano, C. A. Dyke, M. L. Usrey, P. W. Barone, M. J. Allen, H. Shan, C. Kittrell, R. H. Hauge, J. M. Tour, R. E. Smalley; *Science* **2003,** *301* (5639), 1519-1522.

27. G. Pastorin, W. Wu, S. Wieckowski, J. P. Briand, K. Kostarelos, M. Prato, A. Bianco; *Chem Commun (Camb)* **2006,** (11), 1182-4.
28. L. G. Delogu, E. Venturelli, R. Manetti, G. A. Pinna, C. Carru, R. Madeddu, L. Murgia, F. Sgarrella, H. Dumortier, A. Bianco; *Nanomedicine* **2012,** *7* (2), 231-243.
29. S. Liu, L. Xu, F. Li, W. Guo, Y. Xing, Z. Sun; *Electrochimica Acta* **2011,** *56* (24), 8156-8162.
30. E. Hwang, S. Seo, S. Bak, H. Lee, M. Min, H. Lee; *Advanced Materials* **2014,** *26* (30), 5129-5136.

4 Experimental Part

4.1 Materials

Reagents and solvents were purchased from *Sigma Aldrich, VWR, Acros Organics, Thermo Scientific and Fluorochem*. Deuterated solvents were purchased from *Sigma Aldrich*. Ultrapure water was produced from a *Millipore Milli-Q*® filtration system.

Multi-walled carbon nanotubes were purchased from *Nanostructured & Amorphous Materials* (stock number: Nanoamor 1237YJS) and *Nanocyl* (Nanocyl 7000).

Detonation Nanodiamonds were purchased from *Adámas Nanotechnologies*.

Graphite powder was purchased from *Sigma Aldrich*.

Polytetrafluoroethylene (PTFE) filtration systems for the washing procedure of carbon nanomaterials were from *Merck Millipore*.

Dialysis sacks for the cleaning process of GQDs and CDs are purchased from *Sigma Aldrich* (molecular weight cut off: 12-14 KDa).

A **functionalized Ru(II)TrisBipy** molecule **(P8)** Bis(2,2′-bipyridine)-4′-methyl-4-carboxybipyridine-ruthenium N-succinimidyl ester-bis(hexafluorophosphate) was provided by our collaborators from Dipartimento di Chimica «Giacomo Ciamician», Università degli Studi di Bologna.

Rhamnose Amine (P9) ((2R,3R,4R,5R,6S)-2-((6-aminohexyl)oxy)-6-methyltetrahydro-2H-pyran-3,4,5-triol), **Ionic Liquid Amine (P10)** (3-(6-aminohexyl)-1-methyl-1H-imidazol-3-ium chloride), **Rhamnose-Ionic Liquid Amine (P11)** (1-(6-aminohexyl)-3-(6-(((2R,3R,4R,5R,6S)-3,4,5-trihydroxy-6-methyltetrahydro-2H-pyran-2-yl)oxy)hexyl)-1H-imidazol-3-ium chloride), **Hexyl α-L-rhamnopyranoside (P12)** and a **Bulky Sugar** molecule **(P13)** 6-amino-5-((benzyloxy)methyl)-2,2-dimethyltetrahydrofuro[2,3-d][1,3]dioxole-6-carbonitrile were synthesized by our collaborators from Laboratory of Glycochemistry,

Antimicrobials and Agroresources, Université de Picardie Jules Verne (Amiens, France). These molecules were mentioned with their aliases in this thesis.

Chitin from Insect and **Chitin from Shrimp** are provided as well by our collaborators from Université de Picardie Jules Verne.

4.2 Instruments and Characterization Methods

4.2.1 Nuclear Magnetic Resonance (NMR)

^{1}H-NMR spectrometry was performed using *Varian 270 MHz* or *Varian 400 MHz*. Chemical shifts are reported in ppm using the solvent residual signal as an internal reference ($CDCl_3$: δ_H = 7.26 ppm). The resonance multiplicity was described as s (singlet), bs (broad singlet), d (doublet), t (triplet), m (multiplet).

4.2.2 Thermogravimetric Analysis (TGA)

TGA analysis were run on the *TGA Q500 (TA Instruments)* under N_2 gas flux, unless otherwise specified. The process was started with an isotherm at 100 °C for 20 minutes and followed by a heating ramp of 10 °C per minute to 830 °C. Gas flow rate was 10 mL/min for balance and 90 mL/min for sample. Each TGA characterization was done at least twice using about 1 mg of sample each time. Reported percentages of the weight loss are average of at least two measurements. The weight loss at 450°C was used for the calculations of degree of functionalization as the organic compounds used to functionalize carbon nanostructures are removed below 450°C.

$$Degree\ of\ Functionalization\ (\mu mol/g) = \frac{Weight\ loss\ (\%) \cdot 10^4}{Molecular\ weight\ of\ the\ functional\ group}$$

4.2.3 Transmission Electron Microscopy

TEM analyses were performed using a *TEM Philips EM208* with an accelerating voltage of 100 kV. For the sample grid preparation, 1 mg of the sample was dispersed in 40 mL of MilliQ water or DMF and 1-2 drop of the suspension was deposited on a TEM grid (200 or 300 mesh), Holey, Lacey and Film Carbon Grids.

4.2.4 Atomic Force Microscopy and Electrostatic Force Microscopy

AFM and EFM measurements were performed in Tapping-Mode (TM-AFM), in air at room temperature. Two different instruments were used to acquire AFM images. *Multimode Scanning Probe Microscope (Veeco)* was operated by *Nanoscope IIIa controller* software for only AFM measurements and *R80-AFM (APE Research)* hardware was operated by *SW649 SPM Control System*

software for both AFM and EFM measurements. The n-type semiconductive silicon tips from *MikroMasch* were used for the measurements. Data analysis of the AFM and EFM images was carried out using *Gwyddion 2.50* software.
AFM cantilever: HQ:NSC15/AL_BS (µmasch)
EFM cantilever: HQ:DPE-XSC11-D (µmasch)

4.2.5 Infrared Spectroscopy

Infrared Spectroscopy was performed using 3 different techniques which are transmission FTIR, attenuated total reflection (ATR), and diffuse reflectance infrared Fourier transform (DRIFT).
Transmission FTIR spectra were recorded on a *Perkin Elmer System 2000 FTIR*. Pellets of the samples were prepared by mixing 0.5 mg of the product with dry KBr.
ATR FTIR spectra were obtained by using a *Shimadzu IRaffinity-1S FTIR* with a *Shimadzu MIRacle 10* germanium prism at the laboratories of Université de Picardie Jules Verne (UPJV, France).
DRIFT was performed with *Thermo Scientific Nicolet iS10 FT-IR Spectrometer* with *Smart Collector DRIFT apparatus* in laboratories of UPJV (France).

4.2.6 RAMAN Spectroscopy

Raman spectroscopy was performed on *Renishaw inVia Raman microscope*, equipped with lasers at 532 nm, 633 nm or 785 nm. Solid samples were deposited on a microscope slide.

4.2.7 Ultraviolet–Visible Spectroscopy

UV-vis spectra were recorded using a *Varian Cary 5000* spectrophotometer with quartz and/or disposable cuvettes.

4.2.8 Kaiser Test (Ninhydrin Test)

Kaiser test[1] kit was purchased from *Sigma Aldrich*. The kit contains phenol in ethanol (80%), KCN in H_2O/pyridine and Ninhydrin in ethanol (6%). The test was performed to determine the degree of primary amine groups on the synthesized products. The procedure begins with dispersing 0.5 mg of product in 75 µL of phenol solution and 100 µL KCN solution. The mixture is sonicated for 5 minutes

in an ultrasonic bath. 75 µL of ninhydrin solution are added to the well-dispersed mixture, and it is heated at 120 °C for 10 minutes. The mixture is cooled and diluted with ethanol in water (60%) to a final volume of 3 mL. It is centrifugated at 3000 rpm (996 G-force) for 10 min and the supernatant is taken to measure the absorption at 570 nm, using as blank a solution obtained in the same way but without CNTs. The amine loading in the CNTs samples was calculated by using the absorbance value at 570 nm. At least two separate measurements were performed to have an average value.

$$\frac{\mu mol}{g} = \frac{\left[Abs_{Sample} - Abs_{Blank}\right] \cdot dilution\ (mL) \cdot 10^6}{\varepsilon \cdot Sample\ weight\ (mg)}$$

(molar extinction coefficient, ε= 15000 M^{-1} cm^{-1}).

4.2.9 Fluorescence Spectroscopy

Fluorescence Spectra were recorded on a Cary Eclipse Fluorescence Spectrophotometer with quartz cuvettes (10 mm pathlength).

4.2.10 Dynamic Light Scattering (DLS)

DLS measurements were performed *Wyatt DynaPro NanoStar* Dynamic Light Scattering instrument. Samples were prepared as a dispersion with a concentration of 0.02 mg/mL in water by sonicating 30 minutes. For the measurements, 1 cm disposable cuvettes were used.

4.2.11 Thin Layer Chromatography (TLC)

TLC assessments were performed on *Merck* pre-coated aluminum plates with silica gel 60 F_{254}.

4.2.12 Column Chromatography

Purifications with column chromatography were carried out with silicagel (*Merck Kieselgel* 60 - 200 mesh ASTM).

4.3 Chemical Procedures

4.3.1 Organic Reactions

4.3.1.1 Synthesis of Product 1 (P1)

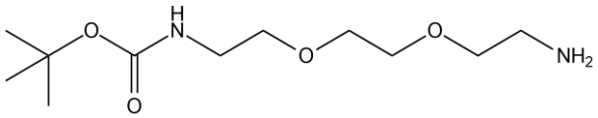

A solution of di-*tert*-butyl dicarbonate (9.8 g, 0.045 mol) in THF (150 mL) was added dropwise to a solution of 2,2'-(ethylenedioxy)bis(ethylamine) (50.0 g, 0.34 mol) in THF (150 mL) in 2 hours at 0 °C. The mixture was stirred overnight at room temperature. The solvent was removed under vacuum obtaining a white slurry. The concentrated compound was dissolved in water (200 mL) and filtered through celite to remove the non-water-soluble double protected by-product. The aqueous layer was washed by diethyl ether (50 mL) to remove di-*tert*-butyl dicarbonate. Then, the aqueous layer was extracted by DCM (200 mL x 3) and backwashed with water (50 mL x 2) to remove the other by-products. The organic layer was dried with $NaSO_4$, filtered and concentrated under vacuum. **Product 1** was obtained as yellowish viscous oil (Yield: 73%, 8.25 g, 0.033 mol). ^{1}H NMR ($CDCl_3$, 270 MHz): 1.44 (s, 9H), 2.88 (t, J = 4.9 Hz, 2H) 3.31 (q, J = 4.6 Hz, 2H), 3.52-3.60 (m, 8H), 5.19 (bs, 1H). The characterization is in agreement with literature.[2]

4.3.1.2 Synthesis of Product 2 (P2)

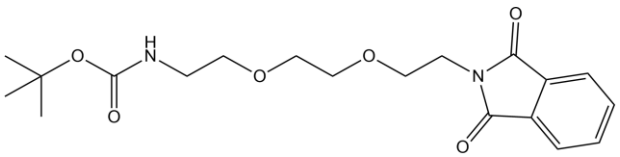

P1 (7 g, 0.028 mol) and phthalic anhydride (4.18 g, 0.028 mol) were dissolved in toluene (125 mL) and stirred under reflux at 120 °C overnight. The solvent was removed under vacuum. The product was purified by flash chromatography using toluene/AcOEt (7:3) as eluent. **P2** was obtained as colorless viscous oil (Yield: 93%, 10 g, 0.026 mol). ^{1}H NMR ($CDCl_3$, 270 MHz): 1.43 (s, 9H), 3.24 (t, J = 5 Hz, 2H), 3.46 (m, 2H), 3.55 (m, 2H), 3.61 (m, 2H), 3.74-3.91 (m, 4H), 5.00 (bs, 1H), 7.73 (m, 2H), 7.83 (m, 2H). The characterization is in agreement with literature.[2]

4.3.1.3 Synthesis of Product 3 (P3)

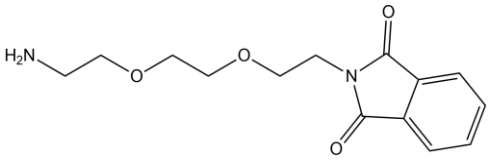

P2 (7.6 g, 0.020 mol) was dissolved in DCM (10 mL) and the solution was placed in ice bath (0 °C). TFA (20 mL) was added dropwise to the solution while stirring. The temperature of the solution was increased to room temperature for 24 h. Then the solvent was removed under vacuum. The concentrated product was dissolved in DCM (20 mL) and triturated in diethyl ether (100 mL). The solvents are removed by filtration. The white crystal **P3** was dried under vacuum. (Yield: 85%, 6.7 g, 0.017 mol). ^{1}H-NMR (270 MHz, $CDCl_3$): 3.27 (m, 2H), 3.61 (m, 4H), 3.75 (m, 4H), 3.90 (m, 2H), 7.74 (m, 2H), 7.86 (m, 2H), 8.03 (s, 2H). The characterization is in the agreement with literature.[2]

4.3.1.4 Synthesis of Product 4 (P4)

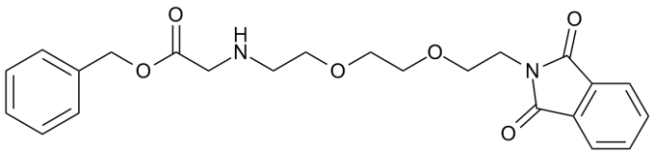

A solution of benzyl bromoacetate (3.87 g, 0.017 mol) in THF (150 mL) was added dropwise to a solution of **P3** (8.25 g, 0.021 mol) and TEA (4.3 g, 0.042 mol) in THF (200 mL) in an ice bath (0 °C). The ice bath removed after 3 hours and the mixture was stirred overnight. The solvent was removed under vacuum. The product was dissolved in ethyl acetate/isopropyl alcohol (9:1) mixture (100 mL). White crystals were filtered on celite. For the purification, column chromatography was performed to the filtrate (AcOEt/iPrOH, 9:1). **P4** was obtained as white powder. (Yield: 49%, 3.55 g, 0.008 mol). ^{1}H NMR ($CDCl_3$, 270 MHz): 2.04 (br, 1H), 3.17 (m, 14H), 5.20 (s, 2H), 7.70 (m, 2H), 7.82 (m, 2H). The characterization is in the agreement with literature.[2]

4.3.1.5 Synthesis of Product 5 (P5)

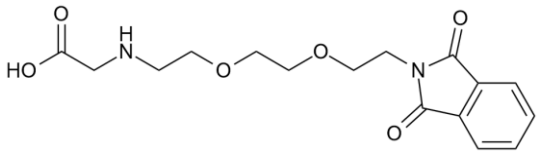

P4 (3.45 g, 0.008 mol) was dissolved in EtOH (100 mL). Argon/vacuum cycles were performed to the solution several times in order to remove oxygen. 10 wt. % loading Palladium on carbon (Pd/C) (50 mg) was added to the solution. The solution was purged with hydrogen gas several times and the solution was stirred overnight under H_2 atmosphere. Palladium was removed by filtering through celite. EtOH was removed under vacuum. **P5** was obtained as white powder. (Yield: 95%, 3.10 g, 0.008 mol) ^{1}H NMR ($CDCl_3$, 270 MHz): 3.26 (bs, 1H), 3.30-3.96 (m, 14 H), 7.70 (m, 2 H), 7.81 (m, 2H), 8.85 (bs, 1H). The characterization is in the agreement with literature.[2]

4.3.1.6 Synthesis of Product 6 (P6)

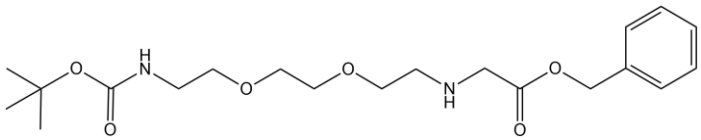

A solution of benzyl bromoacetate (3.97 g, 0.017) in THF (125 mL) was added dropwise to a solution of **P1** (4.3 g, 0.017 mol) and TEA (2.1 g, 0.021 mol) in THF (125 mL) in an ice bath (0 °C). The ice bath was removed after 3 hours and the mixture was stirred overnight. The solvent was removed under vacuum. The product was dissolved in ethyl acetate/isopropyl alcohol (9:1) mixture (100 mL). White crystals were filtered by using celite. For the purification, column chromatography was performed to the filtrate (AcOEt/iPrOH, 9:1). **P6** was obtained as an oily liquid. (Yield: 68%, 4,58 g, 0.012 mol) ^{1}H NMR ($CDCl_3$, 270 MHz) 1.44 (s, 9H), 2.95 (m, 2H), 3.30 (m, 2H) 3.45-3.70 (m, 10H), 5.19 (s, 2H), 5.21 (bs, 1H), 7.36 (s, 5H). The characterization is in the agreement with literature.[2]

4.3.1.7 Synthesis of Product 7 (P7)

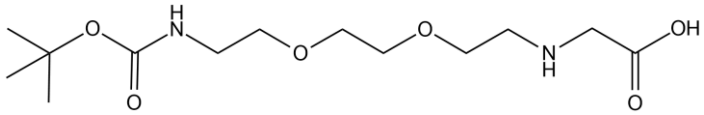

P6 (4.35 g, 0.011 mol) was dissolved in MeOH (50 mL). Argon/vacuum cycles were performed to the solution several times in order to remove oxygen. 10 wt. % loading Palladium on carbon (Pd/C) (50 mg) was added to the solution. The solution was purged with hydrogen gas several times. The solution was stirred overnight under H_2 atmosphere. Palladium was removed by filtering through celite. MeOH was removed under vacuum. **P7** was obtained as white powder. (Yield: 99% 3.35 g, 0.011 mol) ^{1}H NMR ($CDCl_3$, 270 MHz): 1.43 (s, 9H), 3.20-3.40 (m, 4H), 3.54 (m, 2H), 3.60-3.75 (m, 6H), 3.92 (m, 2H), 5.34 (bs, 1H). The characterization is in the agreement with literature.[2]

4.3.2 Reactions of Detonation Nanodiamonds (4-5 nm)

4.3.2.1 Preparation of ND1 (Oxidation of NDs)

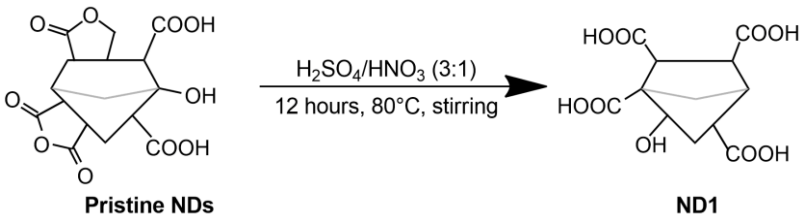

Pristine NDs **ND1**

1 g of pristine NDs was dispersed in 300 mL of H_2SO_4/HNO_3 (3:1) mixture and sonicated for a few minutes. The mixture was heated to 80 °C and stirred for 24 hours. Subsequently, the NDs were filtered and washed with water for a few times. Once reached the neutral pH, the NDs were washed with DMF, MeOH and Et_2O. Then, the filtrate was dried under vacuum (955 mg).

4.3.2.2 Preparation of ND1.1 (Chlorination of ND1)

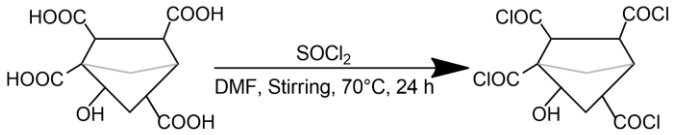

ND1 **ND1.1**

50 mg of **ND1** were refluxed with 85 mL of $SOCl_2$ in 2 mL anhydrous DMF at 70 °C in 24 hours in an inert atmosphere. The reaction mixture was dried under vacuum. Subsequently, without any gas contamination, the coupling reaction was performed.

4.3.2.3 Preparation of ND1.2 (Boc-Peg-Amine Coupling on ND1.1)

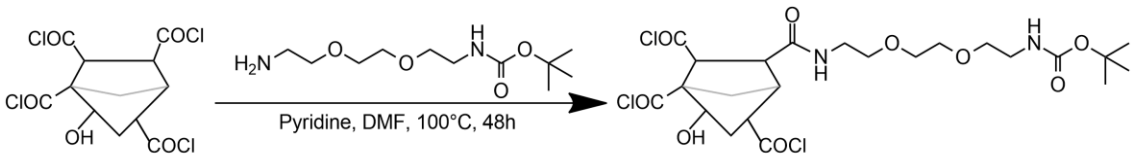

ND1.1 **ND1.2**

50 mg of **ND1.1** were dispersed in 1.5 mL of anhydrous pyridine and 50 mL of anhydrous DMF in an inert atmosphere. 1 g of **P1** was added to the dispersion. The mixture was refluxed at 100 °C for 48 hours. The product was filtered and washed with DMF, water, MeOH and EtO_2, respectively. **ND1.2** was dried under vacuum (58 mg).

4.3.2.4 Preparation of ND1.3 (Boc Deprotection of ND1.2)

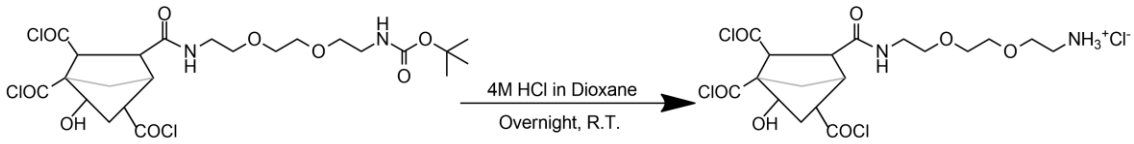

ND1.2 **ND1.3**

10 mg of **ND1.2** were dispersed in 10 mL of 4M HCl in dioxane. The reaction mixture was stirred overnight at room temperature. The product was filtered and washed with water, DMF, water, MeOH and EtO_2, respectively. **ND1.3** was dried under vacuum (8.5 mg).

4.3.2.5 Preparation of ND1.4 (Pht-Peg-Amine Coupling on ND1.1)

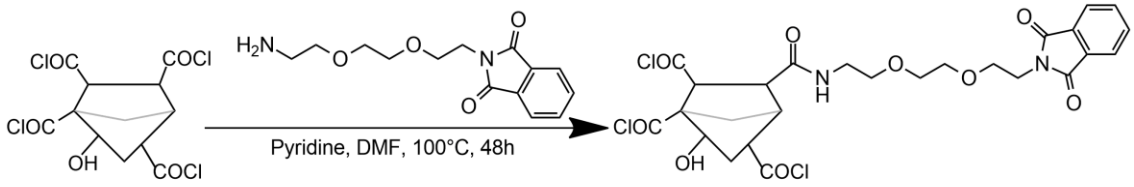

ND1.1 **ND1.4**

100 mg of **ND1.1** were dispersed in 3 mL of anhydrous pyridine and 100 mL of anhydrous DMF in an inert atmosphere. 3.14 g of **P3** (0.008 mol) were added to the dispersion. The mixture was refluxed at 100 °C for 48 hours. The resulting product **(ND1.4)** was filtered and washed with DMF, water, MeOH and EtO_2, and dried under vacuum (93 mg).

4.3.2.6 Preparation of ND1.5 (Pht Deprotection of ND1.4)

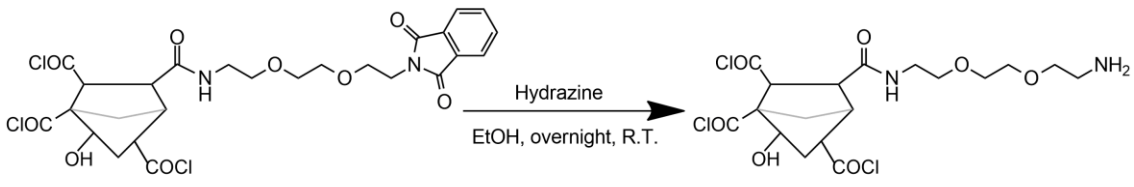

ND1.4 **ND1.5**

85 mg of **ND1.4** was dispersed in EtOH (85 mL). Hydrazine monohydrate (1.5 mL) was added dropwise to the solution. The solution was stirred overnight at room temperature. The product **(ND1.5)** was filtered and washed with EtOH, DMF, water, MeOH and EtO_2 and dried under vacuum (74 mg).

4.3.2.7 Preparation of ND1.5.1 (Ru TrisBiPy Coupling on ND1.5)

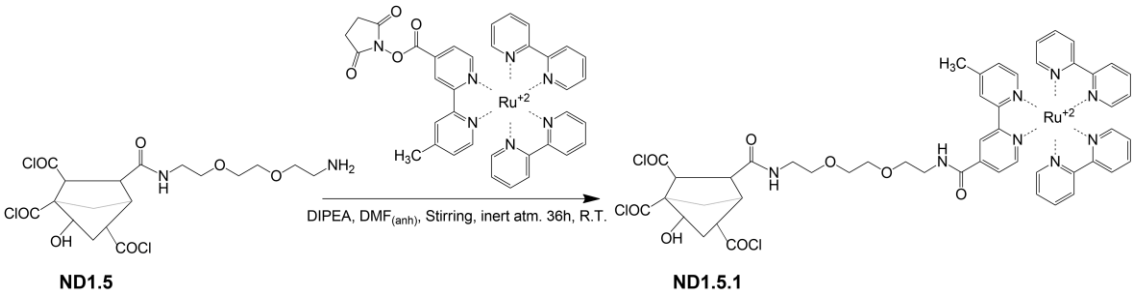

ND1.5 ND1.5.1

10 mg of **ND1.5** were dispersed in anhydrous DMF (10 mL) in an inert atmosphere. DIPEA (15 mg, 0.020 mL, 0.120 mmol) and **P8** (4 mg, 0.004 mmol) were added to the mixture. The reaction was performed with stirring in 36 hours under an inert atmosphere of argon at room temperature. The product **ND1.5.1** was filtered and washed with DMF, water, MeOH and EtO_2, and dried under vacuum (10 mg).

4.3.2.8 Preparation of ND1.5.2 (FITC Coupling on ND1.5)

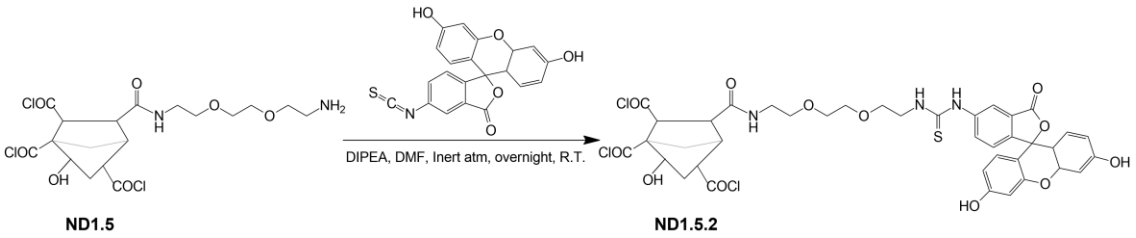

ND1.5 ND1.5.2

10 mg of **ND1.5** were dispersed in anhydrous DMF (2.5 mL) in an inert atmosphere. Fluorescein isothiocyanate, isomer I (22 mg, 0.065 mmol) and DIPEA (20 mg, 0.027 mL, 0,150 mmol) were added to the reaction. The solution was stirred overnight under an inert atmosphere at room temperature. The resulting product **(ND1.5.2)** was filtered and washed with DMF, water, MeOH and EtO_2, and dried under vacuum (9 mg).

4.3.2.9 Preparation of ND1.5.3 (Ferrocene carboxylic acid Coupling on ND1.5)

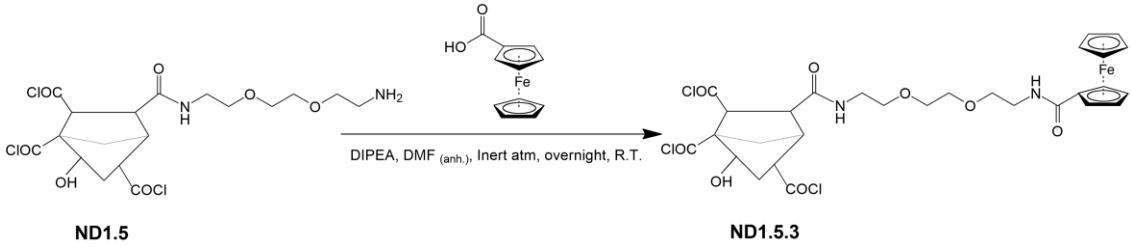

20 mg of **ND1.5** were dispersed in anhydrous DMF (20 mL) in inert atmosphere. Ferrocene carboxylic acid (2.6 mg, 0.011 mmol), DIPEA (4.2 mg, 0.006 mL, 0,033 mmol) and TBTU (7 mg, 0.022 mmol) were added to the dispersion, and it was placed in an ice bath (0 °C) and stirred for 1 hour under nitrogen. Subsequently, the solution was removed from the ice bath and stirred overnight under inert atmosphere at room temperature. The resulting product **(ND1.5.3)** was filtered and washed with DMF, water, MeOH and EtO_2, and dried under vacuum (18.8 mg).

4.3.2.10 Preparation of ND1.6 (Boc-Peg-Amine Coupling on ND1)

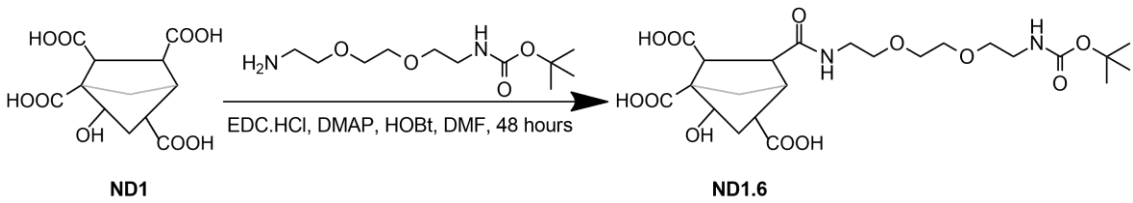

200 mg of **ND1** was dispersed in DMF (180 mL) sonicating for 15 minutes. EDC•HCl (1600 mg, 8.33 mmol) was added to the solution and the mixture was stirred for 30 mins. HOBt (638 mg, 4.17 mmol) and DMAP (204 mg, 1.67 mmol) were added to the reaction mixture. Thereafter, **P1** (414 mg, 1.67 mmol) was dissolved in DMF (20 mL) and added to the reaction mixture. The mixture was stirred for 48 hours at room temperature. The product **(ND1.6)** was filtered and washed with DMF, water, MeOH and EtO_2, and dried under vacuum (185 mg).

4.3.2.11 Preparation of ND1.7 (Boc Deprotection of ND1.6)

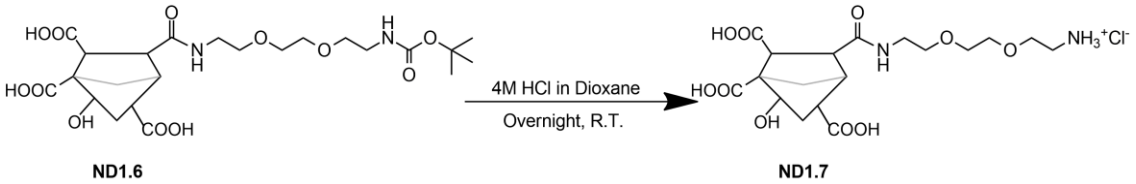

ND1.6 ND1.7

130 mg of **ND1.6** were dispersed in 130 mL of 4M HCl in dioxane. The reaction mixture was stirred overnight at room temperature. The final product **(ND1.7)** was filtered and washed with water, DMF, water, MeOH and EtO_2, and dried under vacuum (126 mg).

4.3.2.12 Preparation of ND2 (Chlorination of Pristine NDs)

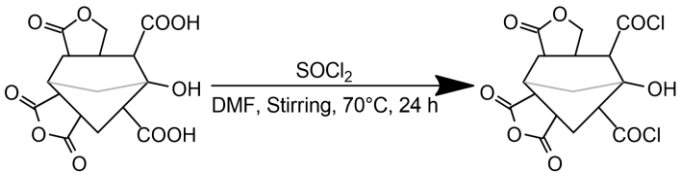

Pristine NDs ND2

50 mg of pristine detonation NDs were refluxed with 85 mL of $SOCl_2$ in 2 mL anhydrous DMF at 70°C in 24 hours in an inert atmosphere. The reaction mixture was dried under vacuum. Right after the chlorination, without any gas contamination, the coupling reaction was performed.

4.3.2.13 Preparation of ND2.1 (Boc-Peg-Amine Coupling on ND2)

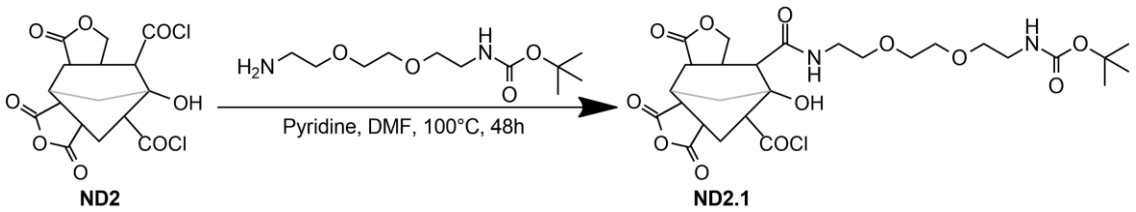

ND2 ND2.1

50 mg of **ND2** were dispersed in 1.5 mL of anhydrous pyridine and 50 mL of anhydrous DMF in an inert atmosphere. 1 g of **P1** (0.004 mol) was added to the dispersion. The mixture was refluxed at 100 °C for 48 hours. The product **(ND2.1)** was filtered and washed with DMF, water, MeOH and EtO_2, respectively. The final product was dried under vacuum (60 mg).

4.3.2.14 Preparation of ND2.2 (Boc Deprotection of ND2.1)

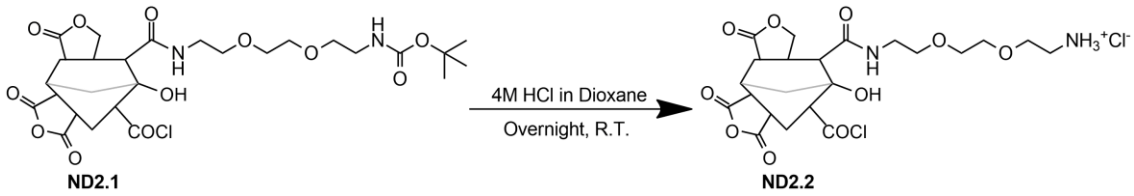

10 mg of **ND2.1** were dispersed in 10 mL of 4M HCl in dioxane. The reaction mixture was stirred overnight at room temperature. The final product **(ND2.2)** was filtered and washed with water, DMF, water, MeOH and EtO_2, and dried under vacuum (6.5 mg).

4.3.2.15 Preparation of ND3.1a and ND3.1b (Rhamnose-Amine Coupling on Pristine NDs)

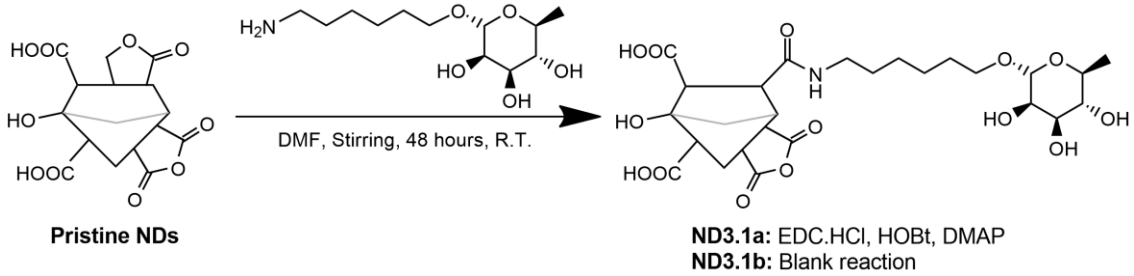

20 mg of pristine ND were well-dispersed in DMF (20 mL). EDC•HCl (160 mg, 0.835 mmol) were added to the dispersion and the mixture was stirred for 30 mins then HOBt (64 mg, 0.418 mmol) and DMAP (20 mg, 0.163 mmol) were added. Later, **P9** (44 mg, 0.167 mmol) was dissolved in DMF (2 mL) and added to the reaction mixture. The mixture was stirred for 48 hours at room temperature. The product **(ND3.1a)** was filtered and washed with DMF, water, MeOH and EtO_2, and dried under vacuum (17.9 mg).

A blank reaction was performed using an analogous procedure for the preparation of **ND3.1b** without adding EDC•HCl, HOBt and DMAP (16.7 mg).

4.3.2.16 Preparation of ND3.2a and ND3.2b (Ionic Liquid Amine Coupling on Pristine NDs)

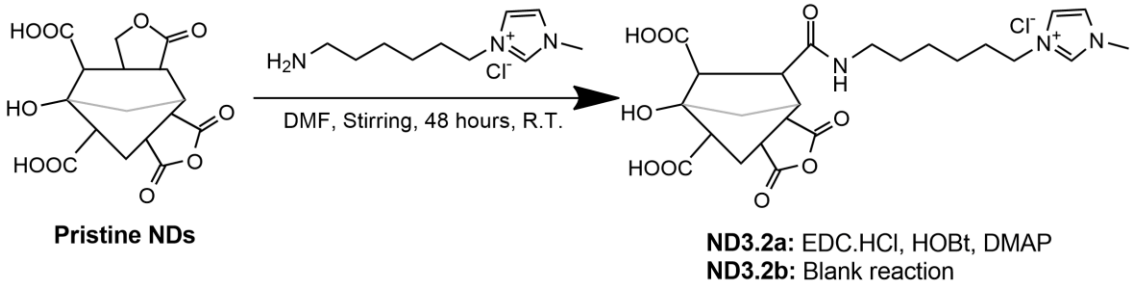

10 mg of pristine ND were dispersed in DMF (10 mL) by sonication for 15 minutes. EDC•HCl (80 mg, 0.417 mmol) was added to the solution and the mixture was stirred for 30 mins. HOBt (32 mg, 0.209 mmol) and DMAP (10 mg, 0.082 mmol) were added to the reaction mixture. Subsequently, **P10** (18 mg, 0.083 mmol) was dissolved in DMF (2 mL) and added to the reaction mixture. The mixture was stirred for 48 hours at room temperature. The product **(ND3.2a)** was filtered and washed with DMF, water, MeOH and EtO_2, and dried under vacuum (9.2 mg).

A blank reaction was performed using an analogous procedure for the preparation of **ND3.2b** without adding EDC•HCl, HOBt and DMAP (9.1 mg).

4.3.2.17 Preparation of ND3.3a and ND3.3b (Rhamnose-Ionic Liquid Coupling on Pristine NDs)

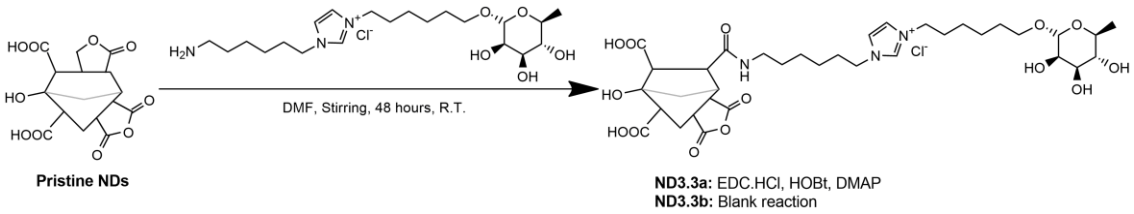

10 mg of pristine ND were sonicated in DMF (10 mL) for 15 minutes. EDC•HCl (80 mg, 0.417 mmol) was added to the solution and the mixture was stirred for 30 mins. HOBt (32 mg, 0.209 mmol) and DMAP (10 mg, 0.082 mmol) were added to the reaction mixture. Subsequently, **P11** (37 mg, 0.083 mmol) was dissolved in DMF (2 mL) and added to the reaction mixture. The mixture was stirred for 48 hours at room temperature. The product **(ND3.3a)** was filtered and washed with DMF, water, MeOH and EtO_2, and dried under vacuum (8.5 mg).

A blank reaction was performed using an analogous procedure for the preparation of **ND3.3b** without adding EDC•HCl, HOBt and DMAP (9 mg).

4.3.2.18 Preparation of ND3.4 (Rhamnose-Amine and Ionic Liquid Amine Coupling on Pristine NDs)

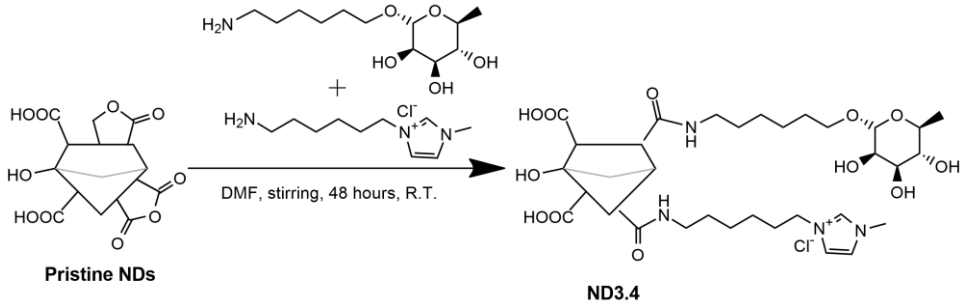

15 mg of pristine ND were dispersed in DMF (15 mL) sonicating for 15 minutes. The mixture was stirred for 30 mins. **P9** (16.5 mg, 0.063 mmol) and **P10** (13.7 mg, 0.063 mmol) were dissolved in DMF (2 mL) and added to the solution. The mixture was stirred for 48 hours at room temperature. The product **(ND3.4)** was filtered and washed with DMF, water, MeOH and EtO_2, and dried under vacuum (13.3 mg).

4.3.2.19 Preparation of ND3.5 (Hexyl α-L-rhamnopyranoside blank reaction)

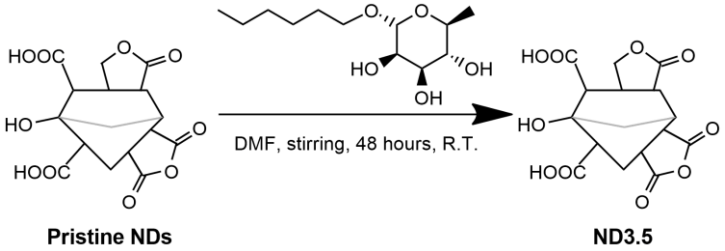

10 mg of pristine ND were dispersed in DMF (10 mL) sonicating for 15 minutes. The mixture was stirred for 30 mins. **P12** (20.6 mg, 0.083 mmol) was dissolved in DMF (2 mL) and added to the solution. The mixture was stirred for 48 hours at room temperature. The product **(ND3.5)** was filtered and washed with DMF, water, MeOH and EtO_2, and dried under vacuum (8.1 mg).

4.3.2.20 Preparation of ND3.6a and ND3.6b (3-Aminopropanenitrile Coupling on pristine NDs)

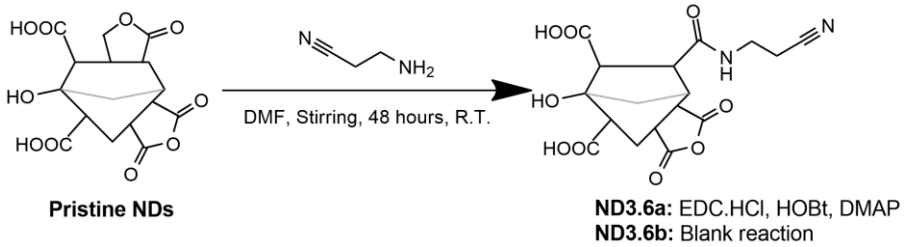

15 mg of pristine ND were dispersed in DMF (15 mL) sonicating for 15 minutes. EDC•HCl (120 mg, 0.625 mmol) was added to the solution and the mixture was stirred for 30 mins. HOBt (48 mg, 0.312 mmol) and DMAP (15.5 mg, 0.125 mmol) were added to the reaction mixture. 3-Aminopropanenitrile (8.8 mg, 0.125 mmol) was added to the reaction mixture. The mixture was stirred for 48 hours at room temperature. The product **(ND3.6a)** was filtered and washed with DMF, water, MeOH and EtO_2, and dried under vacuum (12 mg).

A blank reaction was performed using an analogous procedure for the preparation of **ND3.6b** without adding EDC•HCl, HOBt and DMAP (12.7 mg).

4.3.2.21 Preparation of ND3.7 (Boc-Peg-Amine Coupling on Pristine NDs)

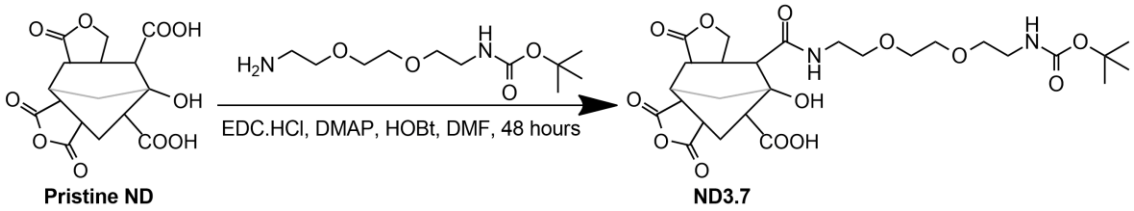

200 mg of pristine ND was dispersed in DMF (180 mL) by sonication for 15 minutes. EDC•HCl (1600 mg, 8.33 mmol) was added to the solution and the mixture was stirred for 30 mins. HOBt (638 mg, 4.17 mmol) and DMAP (204 mg, 1.67 mmol) were added to the reaction mixture. Subsequently, **P1** (414 mg, 1.67 mmol) was dissolved in DMF (20 mL) and added to the reaction mixture. The mixture was stirred for 48 hours at room temperature. The product **(ND3.7)** was filtered and washed with DMF, water, MeOH and EtO_2, and dried under vacuum (196 mg).

4.3.2.22 Preparation of ND3.8 (Boc Deprotection of ND3.7)

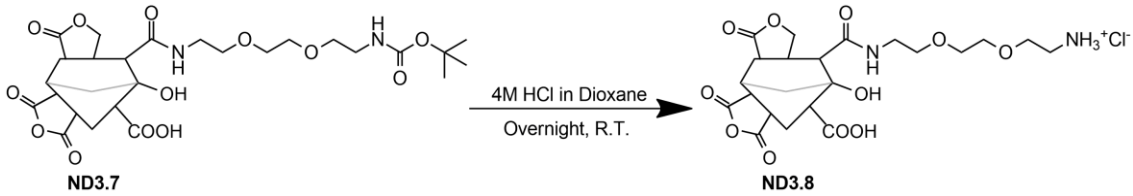

130 mg of **ND3.7** were dispersed in 130 mL of 4M HCl in dioxane. The reaction mixture was stirred overnight at room temperature. The final product **(ND3.8)** was filtered and washed with water, DMF, water, MeOH and EtO_2, and dried under vacuum (128 mg).

4.3.2.23 Preparation of ND4.1a-e (Rhamnose-Amine Coupling on ND1)

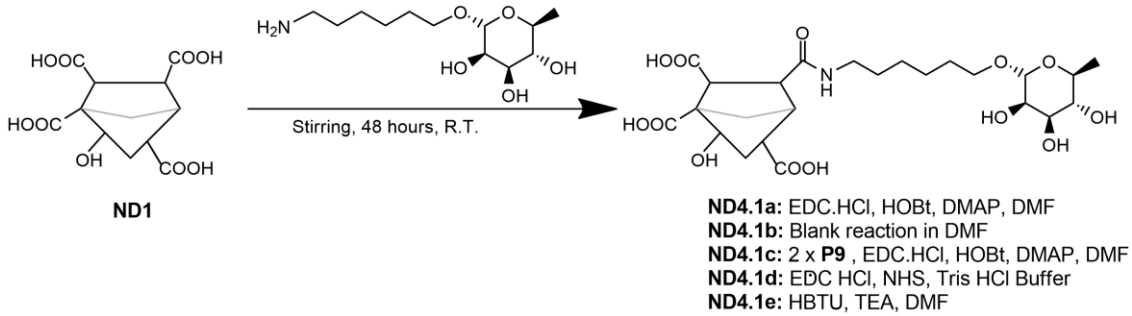

ND4.1a: 10 mg of **ND1** were well-dispersed in DMF (10 mL). EDC•HCl (80 mg, 0.417 mmol) was added and the suspension was stirred for 30 mins. HOBt (32 mg, 0.209 mmol) and DMAP (10 mg, 0.082 mmol) were added to the reaction mixture. Subsequently, **P9** (22 mg, 0.084 mmol) was dissolved in DMF (2 mL) and added to the reaction mixture. The mixture was stirred for 48 hours at room temperature. The product **(ND4.1a)** was filtered and washed with DMF, water, MeOH and EtO_2, and dried under vacuum (8.5 mg).

ND4.1b: a blank reaction was performed using an analogous procedure for the preparation of **ND4.1b** without adding EDC•HCl, HOBt and DMAP (7.8 mg).

ND4.1c: For the preparation of **ND4.1c**, the same procedure used to prepare **ND4.1a** was repeated but with a double amount of **P9** (44 mg, 0.168 mmol) in order to study the effect of its concentration (8.2 mg).

ND4.1d: 15 mg of **ND1** were dispersed in 15 mL of Tris-HCl buffer (pH 7-8) by sonication for 1 hour. EDC•HCl (120 mg, 0.625 mmol) and NHS (36 mg, 0.313

mmol) were added to the reaction mixture. The mixture was placed in an ice bath and stirred for 2 hours. **P9** (33 mg, 0.125 mmol) was added to the mixture and stirred for 48 hours at room temperature. The product **(ND4.1d)** was filtered and washed with water, DMF, water, MeOH and EtO_2, and dried under vacuum (13.8 mg).

ND4.1e: 10 mg of **ND1** were dispersed in DMF (10 mL) by sonication for 15 minutes. **P9** (10 mg, 0.043 mmol), TEA (51 mg, 0.07 mL, 0.503 mmol) and HBTU (100 mg, 0.256 mmol) were added to the reaction. The mixture was stirred for 48 hours at room temperature. The resulting product **(ND4.1e)** was filtered and washed with DMF, water, MeOH and EtO_2, and dried under vacuum (8 mg).

4.3.2.24 Preparation of ND4.2a and ND4.2b (Ionic Liquid Amine Coupling on ND1)

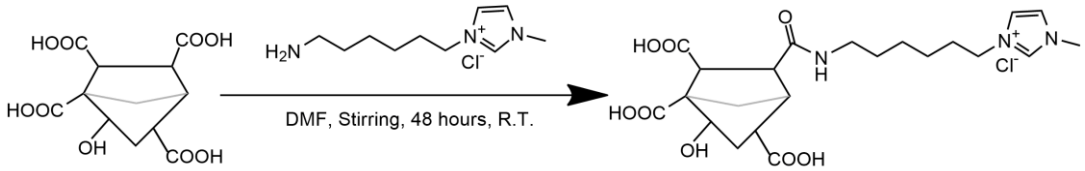

15 mg of ND1 was dispersed in DMF (15 mL) by sonication for 15 minutes. EDC•HCl (120 mg, 0.625 mmol) was added to the solution and the mixture was stirred for 30 mins. HOBt (48 mg, 0.312 mmol) and DMAP (15.5 mg, 0.125 mmol) were added to the reaction mixture. Subsequently, **P10** (27 mg, 0.125 mmol) was dissolved in DMF (2 mL) and added to the reaction mixture. The mixture was stirred for 48 hours at room temperature. The product **(ND4.2a)** was filtered and washed with DMF, water, MeOH and EtO_2, and dried under vacuum (9.2 mg).

A blank reaction was performed using an analogous procedure for the preparation of **ND4.2b** without adding EDC•HCl, HOBt and DMAP (8.7 mg).

4.3.2.25 Preparation of ND4.3a and ND4.3b (Rhamnose-Ionic Liquid Amine Coupling on ND1)

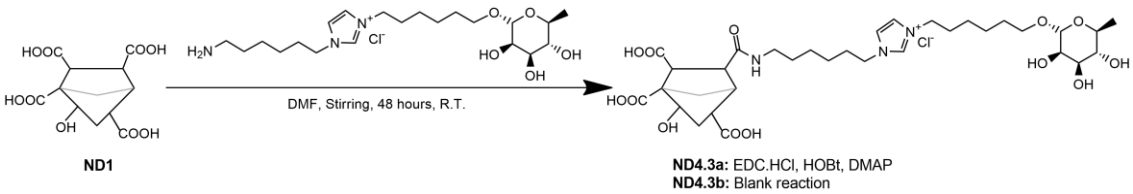

10 mg of **ND1** were sonicated in DMF (10 mL) for 15 minutes. EDC•HCl (80 mg, 0.417 mmol) was added to the suspension and the mixture was stirred for 30 mins. HOBt (32 mg, 0.209 mmol) and DMAP (10 mg, 0.082 mmol) were added to the reaction mixture. Subsequently, **P11** (37 mg, 0.083 mmol) was dissolved in DMF (2 mL) and added to the reaction mixture. The mixture was stirred for 48 hours at room temperature. The product **(ND4.3a)** was filtered and washed with DMF, water, MeOH and EtO_2, and dried under vacuum (8.2 mg).

A blank reaction was performed using an analogous procedure for the preparation of **ND4.3b** without adding EDC•HCl, HOBt and DMAP (8.4 mg).

4.3.2.26 Preparation of ND4.4 (Rhamnose-Amine and Ionic Liquid Amine Coupling on ND1)

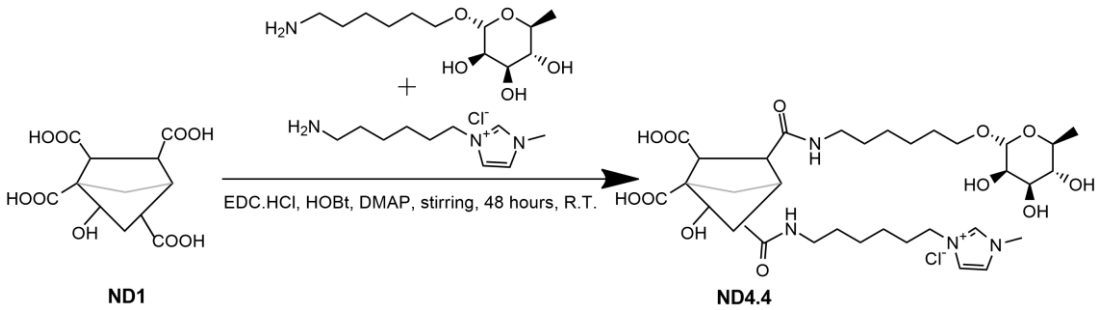

15 mg of **ND1** were sonicated in DMF (15 mL) for 15 minutes. EDC•HCl (120 mg, 0.625 mmol) was added to the solution and the mixture was stirred for 30 mins. HOBt (48 mg, 0.312 mmol) and DMAP (15.5 mg, 0.125 mmol) were added to the reaction mixture. Subsequently, **P9** (16.5 mg, 0.063 mmol) and **P10** (13.7 mg, 0.063 mmol) were dissolved in DMF (4 mL) and the solution was added to the reaction mixture. The mixture was stirred for 48 hours at room temperature. The product **(ND4.4)** was filtered and washed with DMF, water, MeOH and EtO_2, and dried under vacuum (14.2 mg).

4.3.2.27 Preparation of ND4.5 (Hexyl α-L-rhamnopyranoside blank reaction)

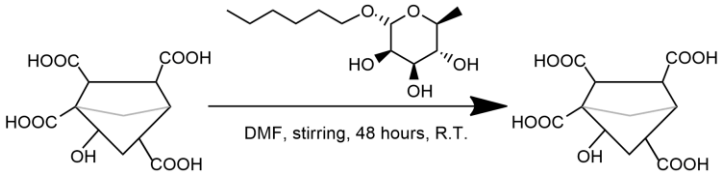

ND1 **ND4.5**

10 mg of **ND1** were dispersed in DMF (10 mL) by sonication for 15 minutes. The mixture was stirred for 30 mins. **P12** (20.6 mg, 0.083 mmol) was dissolved in DMF (2 mL) and added to the suspension. The mixture was stirred for 48 hours at room temperature. The product **(ND4.5)** was filtered and washed with DMF, water, MeOH and EtO_2, and dried under vacuum (7.1 mg).

4.3.2.28 Preparation of ND4.6a and ND4.6b (3-Aminopropanenitrile Coupling on ND1)

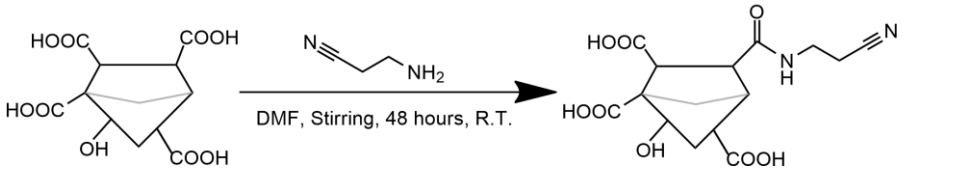

ND1

ND4.6a: EDC.HCl, HOBt, DMAP
ND4.6b: Blank reaction

15 mg of **ND1** were dispersed in DMF (15 mL) by sonication for 15 minutes. EDC•HCl (120 mg, 0.625 mmol) was added to the suspension and the mixture was stirred for 30 mins. HOBt (48 mg, 0.312 mmol) and DMAP (15.5 mg, 0.125 mmol) were added to the reaction mixture. 3-Aminopropanenitrile (8.8 mg, 0.125 mmol) was added to the reaction mixture. The mixture was stirred for 48 hours at room temperature. The product **(ND4.6a)** was filtered and washed with DMF, water, MeOH and EtO_2 and dried under vacuum (12.7 mg).

A blank reaction was performed using an analogous procedure for the preparation of **ND4.6b** without adding EDC•HCl, HOBt and DMAP (13.2 mg).

4.3.2.29 Preparation of ND4.7 (CN-Sugar Amine Coupling on ND1)

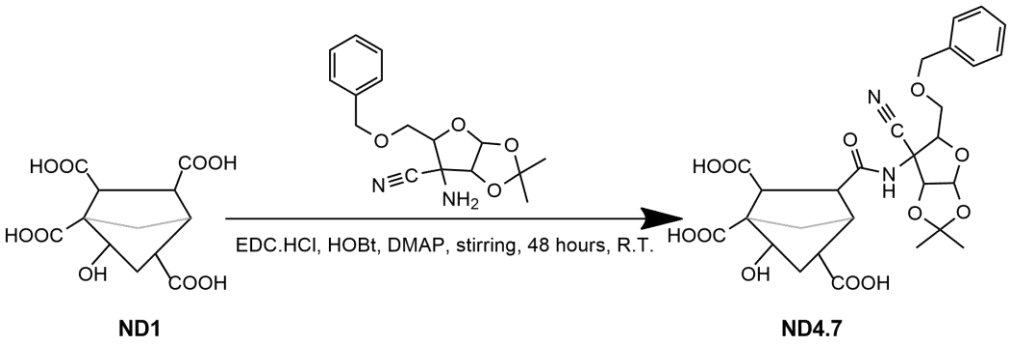

10 mg of **ND1** were well-dispersed in DMF (10 mL) with a sonicator. EDC•HCl (80 mg, 0.417 mmol) was added to the solution and the solution was stirred for 30 mins. HOBt (32 mg, 0.209 mmol) and DMAP (10 mg, 0.082 mmol) were added to the reaction mixture. Subsequently, **P13** (25.5 mg, 0.084 mmol) was added to the reaction mixture. The mixture was stirred for 48 hours at room temperature. The product **(ND4.7)** was filtered and washed with DMF, water, MeOH and EtO_2, and dried under vacuum (9.2 mg).

4.3.3 Reactions of Graphene Quantum Dots

4.3.3.1 Preparation of GO1 and GO2 (Oxidation and Exfoliation of Graphite)

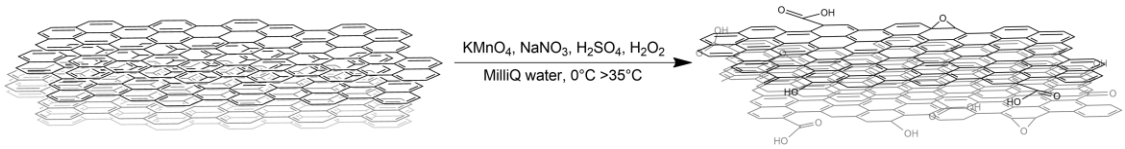

Oxidation of Graphite

This process is a modified Hummers method.[3] 3 g of graphite powder, 1.5 g of $NaNO_3$ (0.018 mol) and 70 mL of H_2SO_4 (1.31 mol) were placed in a round bottom flask and stirred for 30 minutes in an ice bath at 0 °C. Subsequently, 9 g of $KMnO_4$ were added to the mixture and stirred for 5 minutes at 0 °C. The ice bath was removed and the mixture was stirred at 35 °C for 30 minutes. 138 mL of MilliQ water was slowly added to the mixture. The mixture was heated to 100 °C and stirred for 15 minutes. 420 mL of MilliQ water and 3 mL of H_2O_2 (0.03 mol) were added to the mixture and stirred at room temperature for 1 hour. The mixture was left to decant. Dark yellow/orange colored supernatant was removed. 500 mL of MilliQ water was added to the mixture and it was stirred for 15 minutes and left to decant overnight. The supernatant was removed and this washing process was repeated for 5 more times. At the end of the washing process, black colored dense mixture was loaded into the dialysis sacks to remove the acid residue. The dialysis sacks were placed in MilliQ water and the dialysis water was changed until reaching pH 5.

Exfoliation of Graphite Oxide (Production of Graphene Oxide)

After the dialysis process, the mixture was centrifuged at 4000 rpm (1771 G-force) for 30 minutes and the supernatant was removed. This process was repeated for 3 times. Subsequently, the precipitate was divided equally into 12 centrifuge tubes and each tube was filled with MilliQ water to a final volume of 45 mL, sonicated for 15 minutes and subsequently centrifuged at 4000 rpm (1771 G-force) for 20 minutes. The dark brown/black colored supernatant was

collected. This sonication-centrifugation-collection process was repeated for 8 times. The volume of the collected supernatant was reduced under vacuum and subsequently the resulting product, graphene oxide (**GO1**) was lyophilized.

The remaining centrifugate of graphite oxide was sonicated for 15 minutes and centrifugated at 3000 rpm (996 G-force) for 20 minutes. The supernatant was collected. This sonication-centrifugation-collection process was repeated for 4 times. The collected product (**GO2**) was lyophilized. (**GO1**: 2.42 g, **GO2**: 185 mg, Yield: 87%)

4.3.3.2 Preparation of GQD1, GQD2 and GQD3 (Oxidation and Exfoliation of GO1)

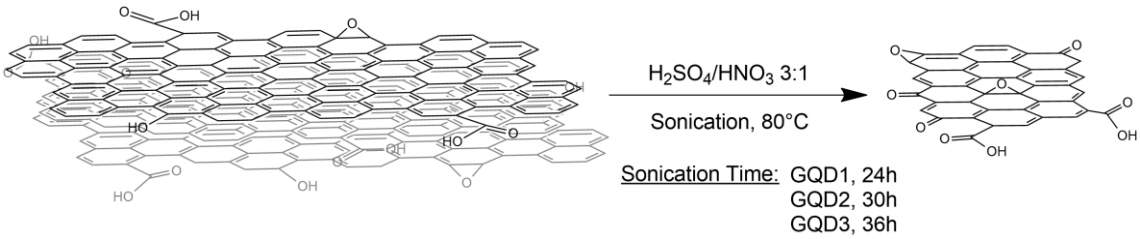

GO1 (80 mg) was equally divided in 8 glass vials. To each vial, sulfonitric acid (H_2SO_4:HNO_3 3:1) (2.5 mL) was added. The vials were well closed with a screw cap and sealed with parafilm and adhesive tape. The closure of the caps is a critical step to keep acid vapor inside the vials. The well-sealed vials were placed in a sonic bath for 24 hours (3 x 8 hours) at 80 °C. Every two hours, the vials positions were changed. During the process, the ruined, colored or leaky caps were replaced by new ones. At the end of the sonication, the vials were left to cool down to room temperature, then they were slowly and carefully filled with MilliQ water. After 30 minutes the orange colored solutions were transferred into the dialysis sacks (12000 Da, flat width 35 mm). Subsequently, the filled sacks were dialyzed with MilliQ water until the pH of the dialysis solution reaches pH 5-6. The solution (**GQD1**) was transferred from the dialysis sacks into a glass container, stored at 4 °C protected from light.

To calculate the production yield, 20 mL of **GQD1** were lyophilized and the recovered product was weighted (total 63 mg).

This procedure was repeated changing the time of sonication for different batches, in order to evaluate how this parameter could influence to the GQD characteristics. So, while for **GQD1** the sonication was applied for 24 h, in the case of **GQD2** it was prolonged to 30 h (61 mg, Yield: 76.3%) and for **GQD3** to 36 h (58 mg).

4.3.3.3 Preparation of GQD2.1 and GQD2.2 (Cycloaddition of P5 and P7 on GQD2)

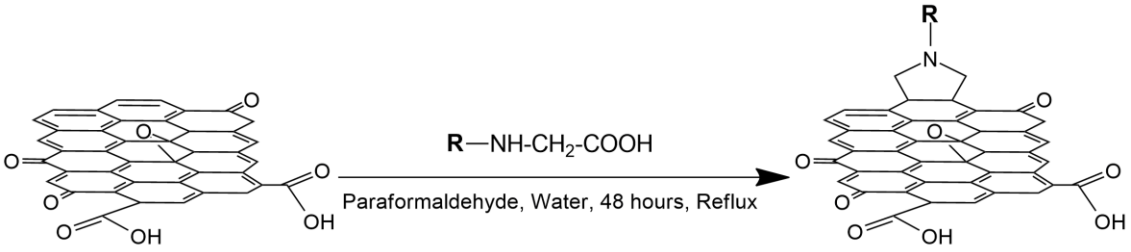

Product Name	R—NH-CH_2-COOH
GQD2.1	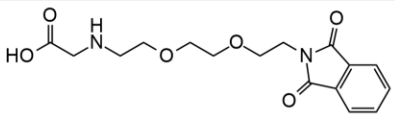
GQD2.2	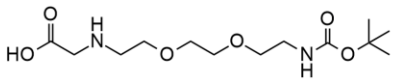

GQD2 (10 mg) was dissolved in MilliQ water (10 mL) by sonication. The so obtained solution was heated to reflux. **P5** (total amount 100 mg, 0.294 mmol) and paraformaldehyde (total amount 60 mg, 2 mmol) were added to the solution in 4 times, every 2 hours during the reaction. After the last addition, the reaction was cooled down and stirred overnight at room temperature. The solution was transferred into dialysis sacks. The dialysis sacks were placed in MilliQ water. The dialysis solution was replaced 5 times with fresh MilliQ water every 8 hours. The solution **(GQD2.1)** was lyophilized (9.3 mg).

The same procedure was performed using **P7** instead of **P5** for the production of **GQD2.2** (9.6 mg).

4.3.3.4 Preparation of GQD2.3, GQD2.3b, GQD2.4, GQD2.4b, GQD2.5 and GQD2.5b (Coupling of P9, P10 and P11 on GQD2)

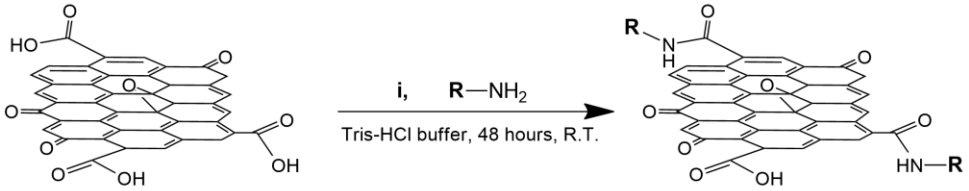

Product Name	i	R—NH_2
GQD2.3	EDC.HCl, NHS	P9
GQD2.3b		P9
GQD2.4	EDC.HCl, NHS	P10
GQD2.4b		P10
GQD2.5	EDC.HCl, NHS	P11
GQD2.5b		P11

GQD2 (10 mg) was sonicated with 10 mL of Tris-HCl buffer (pH 7-8) for 30 minutes. EDC•HCl (80 mg, 0.417 mmol) and NHS (24 mg, 0.208 mmol) were added to the reaction mixture. The mixture was placed in an ice bath and stirred for 2 hours. **P9** (22 mg, 0.084 mmol) was added to the mixture and stirred for 48 hours at room temperature. The solution was transferred into the dialysis sacks and dialyzed for 2 days with MilliQ water. The dialysis solution was changed 5 times in 2 days. The resulting solution **(GQD2.3)** was lyophilized (9.2 mg).

The same process was repeated with **P10** and **P11** instead of **P9** for the production of **GQD2.4** (8.9 mg) and **GQD2.5** (9.2 mg), respectively.

Blank reactions were performed using an analogous procedure without adding EDC•HCl and NHS for the preparation of **GQD2.3b** (9 mg), **GQD2.4b** (8.9 mg) and **GQD2.5b** (9.2 mg).

4.3.4 Reactions of Carbon Dots

4.3.4.1 Production of Carbon Dots (CD1, CD2, CD3 and CD4)

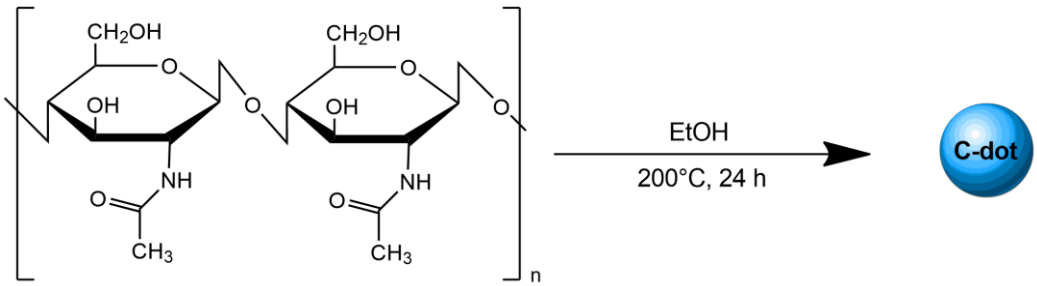

Chitin from Insect (200 mg) was cut into very small pieces in order to increase the exposed surface. The chitin was placed in Teflon container with EtOH (10 mL) and high-pressure vessel reactor was closed well. The reactor was placed in a preheated oven at 200 °C and left for 24 hours. The reactor was taken out from the oven and left to cool down. The reaction mixture was transferred into a beaker and sonicated for 2 minutes. When the big pieces precipitate again, the supernatant was transferred into the plastic centrifuge tubes and centrifuged at 3000 rpm (996 G-force) for 20 minutes. The yellow colored supernatant was taken and conserved in a fridge **(CD1)**. For the calculation of the yield, 2 mL of solution were dried under reduced pressure and the obtained product was weighted (total 55.2 mg).

CD2 was analogously produced applying 30 hours of heating instead of 24 hours (57.8 mg).

The same procedure of **CD1** was repeated with **Chitin from Shrimp** instead of the **Chitin from Insect** for the production of **CD3** (28.8 mg).

CD4 was produced following the methodology described for **CD1**, but without the addition of EtOH (40 mg).

4.3.4.2 Preparation of CD1.1, CD1.1b, CD4.1 and CD4.1b (Functionalizations of Carbon Dots with Rhamnose Amine)

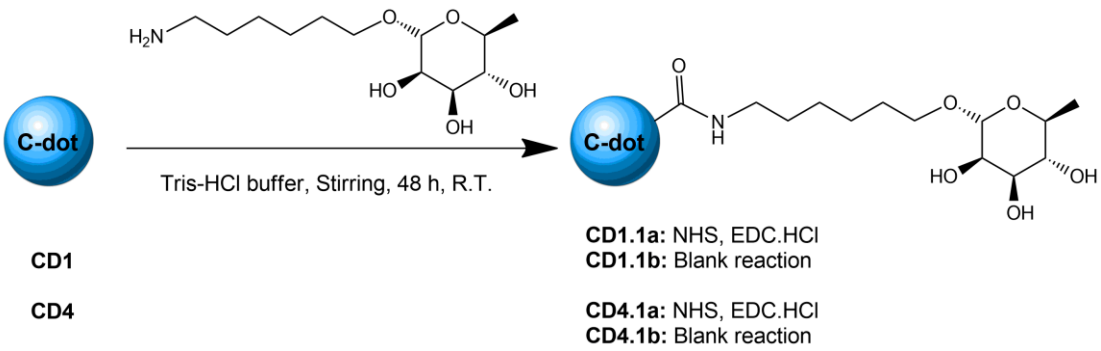

CD1 (10 mg) was sonicated with 10 mL of Tris-HCl buffer (pH 7-8) for 30 minutes. EDC•HCl (80 mg, 0.417 mmol) and NHS (24 mg, 0.208 mmol) were added to the reaction mixture. The mixture was stirred for 2 hours. **P9** (22 mg, 0.084 mmol) was added to the mixture and stirred for 48 hours at room temperature. The resulting solution was transferred into the dialysis sacks and dialyzed in MilliQ water for 2 days. Dialysis solution was changed 5 times totally. The resulting reagent free solution **(CD1.1)** was lyophilized (2.3 mg).

The same procedure was applied on **CD4** for the production of **CD4.1** (3.5 mg).

Blank reactions were performed using an analogous procedure without adding EDC•HCl and NHS for the preparation of **CD1.1b** (3.1 mg) and **CD4.1b** (2.1 mg), respectively.

4.3.5 Reactions of Multi-Walled Carbon Nanotubes (MWCNTs)

4.3.5.1 Nanocyl 7000 (NC 7000) MWCNTs

4.3.5.1.1 Preparation of CNT1 (Oxidation of Pristine NC 7000 MWCNTs)

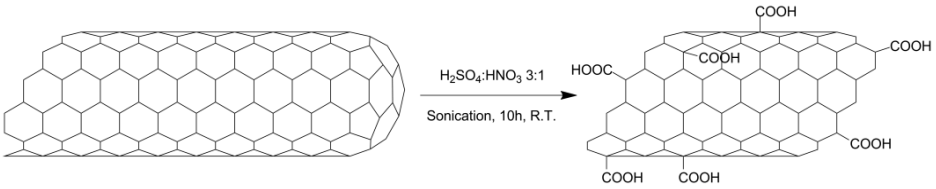

Pristine NC 7000 MWCNTs (500 mg) were dispersed in Sulfonitric Acid (H_2SO_4:HNO_3 3:1) (125 mL). The mixture was sonicated for 10 hours at room temperature. During the sonication, the water of the sonic bath was changed as the temperature increased. The mixture was slowly and carefully neutralized with NaOH in an ice bath. The resulting product **(CNT1)** was filtered and washed with water, MeOH and EtO_2, and dried under vacuum (455 mg).

4.3.5.1.2 Preparation of CNT1.1 (Coupling of P1 on CNT1)

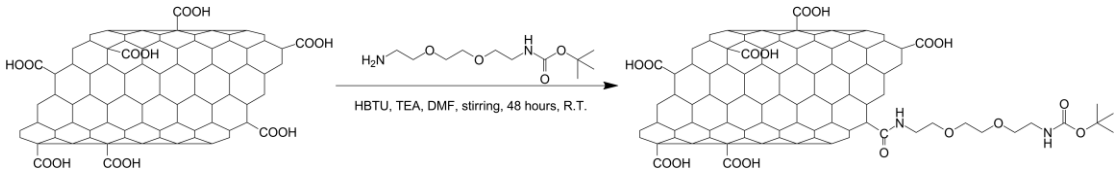

CNT1 (200 mg) was dispersed in DMF (200 mL) by sonication. **P1** (496 mg, 0.2 mmol) and TEA (1.1 g, 1.4 mL, 10 mmol) were added to the mixture and well dissolved. Subsequently, HBTU (1.9 g, 5 mmol) was added to the reaction. The reaction mixture was stirred for 48 hours at room temperature. The product **(CNT1.1)** was filtered and washed with DMF, MeOH and EtO_2, and dried under vacuum (196 mg).

4.3.5.1.3 Preparation of CNT1.1.1 (Deprotection of Boc on CNT1.1)

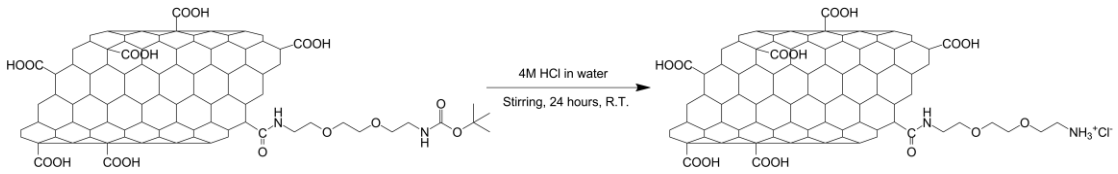

CNT1.1 (38 mg) was sonicated in 4M HCl in water (60 mL) for 15 minutes. The well-dispersed reaction mixture was stirred for 24 hours at room temperature.

The product **(CNT1.1.1)** was filtered and washed with water, MeOH and EtO_2, and dried under vacuum (35 mg).

4.3.5.1.4 Preparation of CNT1.1.2 (Deprotection of Boc and Methylation of CNT1.1)

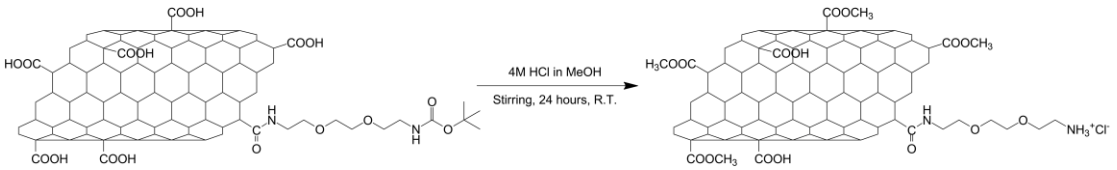

CNT1.1 (76 mg) was dispersed in 4M HCl in MeOH (105 mL) with a sonicator. The reaction mixture was stirred for 24 hours at room temperature. The product **(CNT1.1.2)** was filtered and washed with water, MeOH and EtO_2 and dried under vacuum (71 mg).

4.3.5.2 NanoAmor 1237YJS (NA 1237YJS) MWCNTs

4.3.5.2.1 Preparation of CNT2a and CNT2b (Tour reaction on Pristine NA 1237YJS MWCNTs)

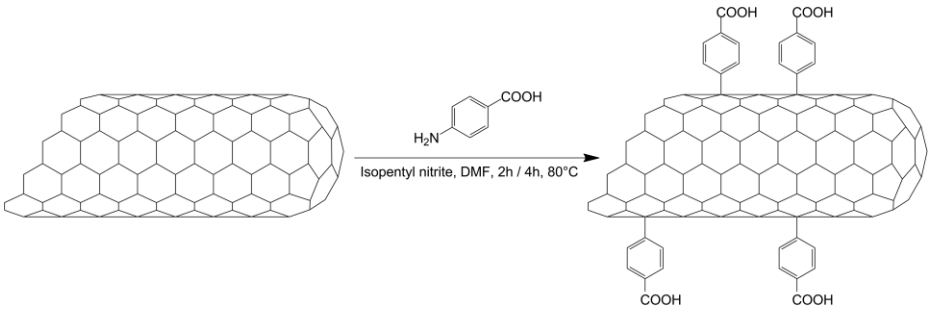

Pristine NA 1237YJS MWCNTs (100 mg) were dispersed in DMF (100 mL) by sonication. 4-Aminobenzoic acid (1.37 g, 10 mmol) was added to the mixture and well-dispersed. Isopentyl nitrite (3.5 g, 4 mL, 30 mmol) was added to the reaction slowly. The reaction was stirred at 80 °C for 2 hours. The resulting product **(CNT2a)** was filtered and washed with DMF, water, MeOH and EtO_2 and dried under vacuum (82 mg).

For the preparation of **CNT2b**, the same procedure was used but increasing the reaction time to 4 hours instead of 2. (97 mg).

4.3.5.2.2 Preparation of CNT2a.1 (Coupling of P3 on CNT2a)

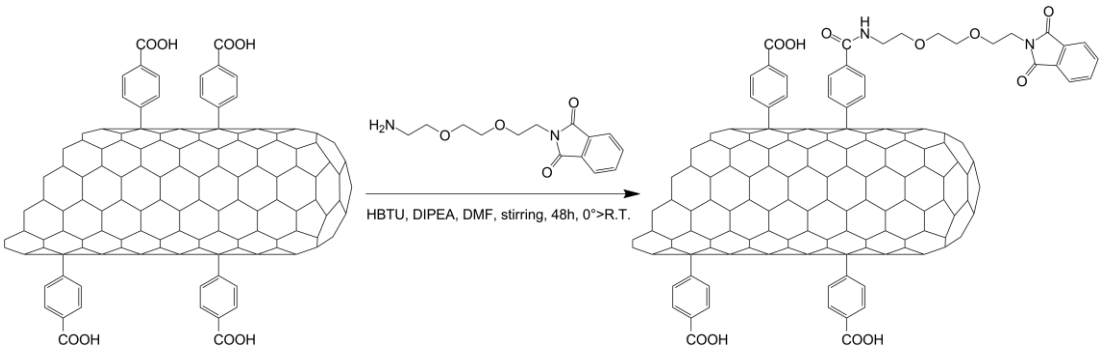

CNT2a (40 mg) was sonicated in DMF (40 mL) for 10 minutes and the mixture was cooled down to 0 °C in an ice bath. DIPEA (11.13 g, 86 mmol, 15 mL) and HBTU (3.77 g, 10 mmol) were added to the reaction mixture and stirred for 30 minutes at 0 °C. **P3** (650 mg, 1.67 mmol) was added to the mixture and stirred for 30 minutes at 0 °C. The reaction mixture was removed from the ice bath and stirred for 48 hours at room temperature. The product **(CNT2a.1)** was filtered and washed with DMF, water, MeOH and EtO_2 and dried under vacuum (35 mg).

4.3.5.2.3 Preparation of CNT2a.1.1 (Deprotection of Pht on CNT2a.1)

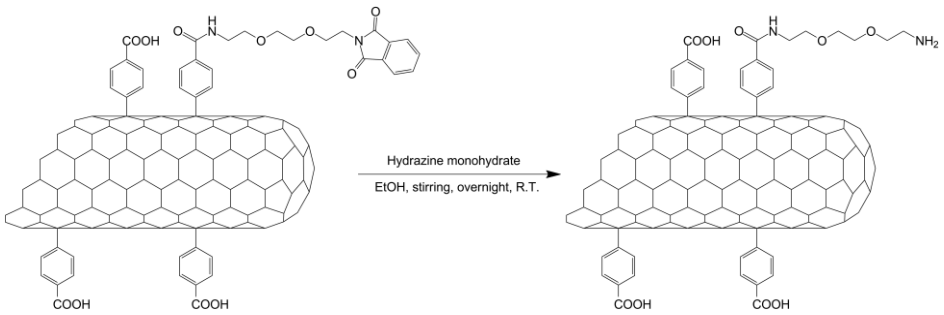

CNT2a.1 (30 mg) was dispersed in EtOH (30mL). Hydrazine monohydrate (413 mg, 8.25 mmol, 400 µL) was added to the well-dispersed mixture. The reaction mixture was stirred overnight at room temperature. The final product **(CNT2a.1.1)** was filtered and washed with water, MeOH and EtO_2, and dried under vacuum (27 mg).

4.3.5.2.4 Preparation of CNT2a.2 and CNT2b.1 (Coupling of P1 and P3 on CNT2a and CNT2b)

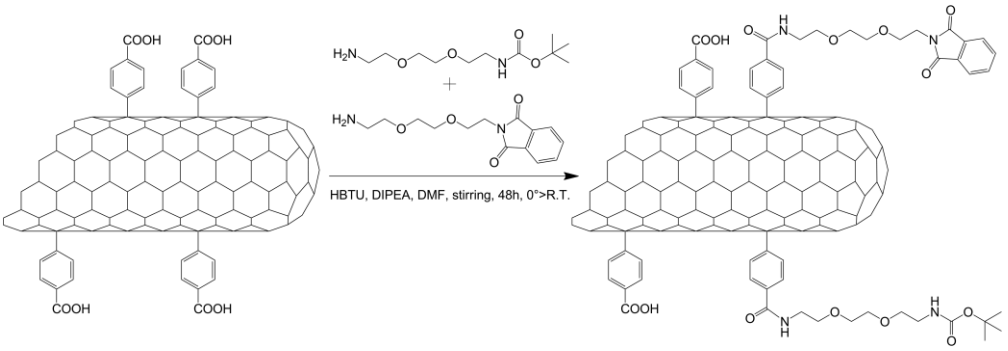

CNT2a (30 mg) was dispersed in DMF (30 mL) with a sonicator and the mixture was cooled down to 0 °C in an ice bath. DIPEA (8.4 g, 65 mmol, 11.30 mL) and HBTU (2.85 g, 7.5 mmol) were added to the reaction mixture and stirred for 30 minutes at 0 °C. **P1** (310 mg, 1.25 mmol) and **P3** (488 mg, 1.25 mmol) was added to the mixture and stirred for 30 minutes at 0 °C. The reaction mixture was removed from the ice bath and stirred for 48 hours at room temperature. The product **(CNT2a.2)** was filtered and washed with DMF, water, MeOH and EtO_2, and dried under vacuum (25 mg).

CNT2b.1 (26.5 mg) was produced with the same process starting from **CNT2b** instead of **CNT2a**.

4.3.5.2.5 Preparation of CNT2a.2.1 (Deprotection of Boc on CNT2a.2)

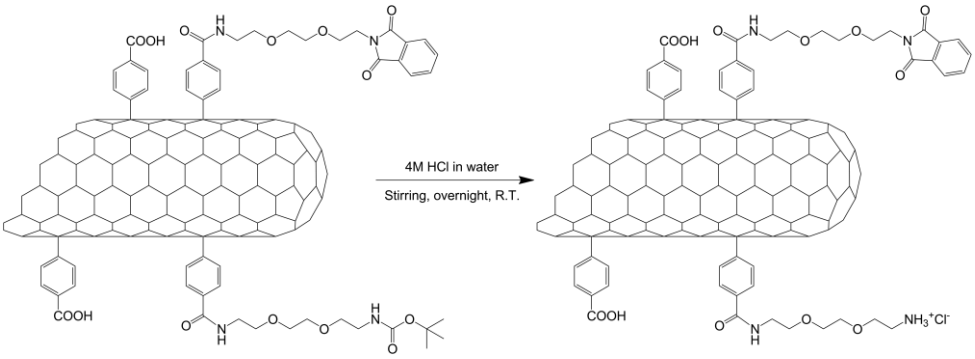

CNT2a.2 (20 mg) was dispersed in 4M HCl in water (30 mL) by sonication. The reaction was stirred overnight at room temperature. The final product **(CNT2a.2.1)** was filtered and washed with water, MeOH and EtO_2, and dried under vacuum (14 mg).

4.3.5.2.6 Preparation of CNT2a.2.2 (Deprotection of Pht on CNT2a.2.1)

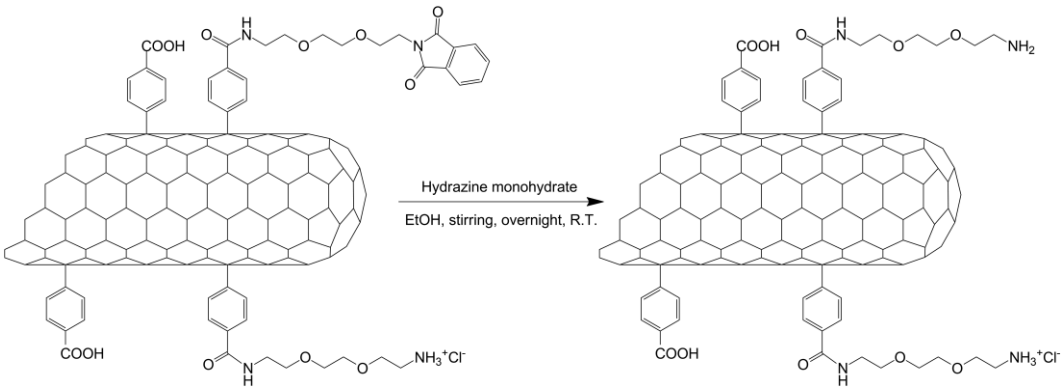

CNT2a.2.1 (4 mg) was dispersed in EtOH (4 mL) by sonication. Hydrazine monohydrate (57 mg, 1.13 mmol, 55 µL) was added to the mixture. The reaction was stirred overnight at room temperature. The final product **(CNT2a.2.2)** was filtered and washed with water, MeOH and EtO_2, and dried under vacuum (4 mg).

4.3.5.2.7 Preparation of CNT3 (Oxidation of Pristine NA 1237YJS MWCNTs)

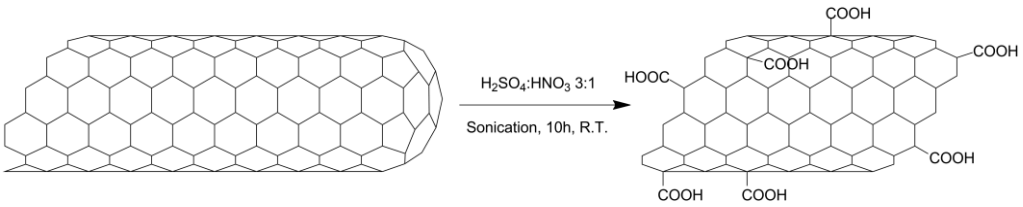

Pristine NA 1237YJS MWCNTs (400 mg) were dispersed in Sulfonitric Acid (H_2SO_4:HNO_3 3:1) (350 mL). The mixture was sonicated for 10 hours at room temperature. During the sonication, the water of the sonic bath was changed as the temperature increased. The mixture was slowly and carefully neutralized with NaOH in an ice bath. The resulting product **(CNT3)** was filtered and washed with water, MeOH and EtO_2, and dried under vacuum (355 mg).

4.3.5.2.8 Preparation of CNT3.1-4 (Coupling of P9, P10 and P11 on CNT3)

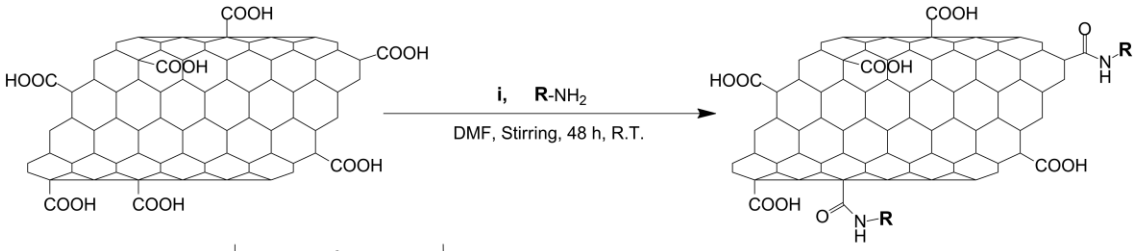

Product Name	i	R—NH_2
CNT3.1a	HBTU, TEA	P9
CNT3.1b	HOBt, EDC.HCl, DMAP	P9
CNT3.2	HOBt, EDC.HCl, DMAP	P10
CNT3.3	HOBt, EDC.HCl, DMAP	P11
CNT3.4	HOBt, EDC.HCl, DMAP	P9 + P10

CNT3.1a: CNT3 (10 mg) was dispersed in DMF (10 mL) by sonication. **P9** (13 mg, 0.050 mmol), TEA (50 mg, 0.5 mmol, 69 µL) and HBTU (94 mg, 0.25 mmol) were added to the reaction mixture, respectively. The mixture was stirred for 48 hours at room temperature. The product **(CNT3.1a)** was filtered and washed with DMF, water, MeOH and EtO_2, respectively and dried under vacuum (10 mg).

CNT3.1b: CNT3 (50 mg) was sonicated in DMF (50 mL) for 15 minutes. EDC•HCl (400 mg, 2.086 mmol) was added to the reaction. The mixture was stirred for 2 hours at room temperature. HOBt (160 mg, 1.043 mmol) and DMAP (51 mg, 0.417 mmol) were added to the reaction mixture. Subsequently, **P9** (110 mg, 0.417 mmol) was dissolved in DMF (5 mL) and added to the reaction mixture. The mixture was stirred for 48 hours at room temperature. The product **(CNT3.1b)** was filtered and washed with DMF, water, MeOH and EtO_2, and dried under vacuum (48 mg).

CNT3.2 and CNT3.3: The same procedure was repeated for the production of **CNT3.2** (47.5 mg) and **CNT3.3** (49 mg) with **P10** (90 mg, 0.417 mmol) and **P11** (188 mg, 0.417 mmol) instead of **P9**, respectively.

CNT3.4: For the coupling of Rhamnose Amine and Ionic Liquid Amine at the same time, the same steps were performed with both **P9** (55 mg, 0.208 mmol) and **P10** (45 mg, 0.208 mmol) instead of **P9** alone (110 mg, 0.417 mmol) (45 mg).

Bibliography

1. E. Kaiser, R. L. Colescott, C. D. Bossinger, P. I. Cook; *Anal Biochem* **1970,** *34* (2), 595-8.
2. G. Pastorin, W. Wu, S. Wieckowski, J. P. Briand, K. Kostarelos, M. Prato, A. Bianco; *Chem Commun (Camb)* **2006,** (11), 1182-4.
3. W. S. Hummers Jr, R. E. Offeman; *Journal of the American Chemical Society* **1958,** *80* (6), 1339-1339.

5 Conclusions

Carbon nanostructures used in this project were NDs, GQDs, CDs and MWCNTs. To improve their properties, big variety of functionalizations were performed. Functionalizations were mainly performed with **P1**, **P3**, **P9**, **P10**, **P11** and FITC molecules. Carbon nanostructures were characterized by thermogravimetric analysis (TGA), transmission electron microscopy (TEM), atomic force microscopy (AFM), electrostatic force microscopy (EFM), dynamic light scattering (DLS), Raman, infrared (IR) and UV-visible spectroscopies.

NDs were functionalized with different molecules in order to increase their solubility and introduce useful properties for possible applications. The surface of pristine detonation nanodiamonds contain different functional groups. In order to create homogeneous surface with increased the amount of carboxylic groups, the surface of NDs were oxidized through an acid treatment. Dispersibility and aggregate size of NDs was not changed significantly after oxidation with sulfuric and nitric acid mixture. Subsequently, functionalizations of NDs with tert-butyl(2-(2-(2-aminoethoxy)ethoxy)ethyl)carbamate (**P1**) and 2-(2-(2-(2-aminoethoxy) ethoxy)ethyl)isoindoline-1,3-dione (**P3**) were performed on pristine and oxidized NDs in the presence of different coupling reagents. It was seen that pristine nanodiamonds have been functionalized with good values, however the degree of functionalization of oxidized nanodiamonds derived products yielded relatively higher degree of functionalization. Pht and Boc groups were deprotected in order to have amino terminal chain which lets further functionalizations and is demonstrated to increase water dispersibility of NDs, significantly. NDs with amino terminal functional groups are functionalized with FITC, ferrocenecarboxylic acid, and Ru TrisBiPy (**P8**).

Biological evaluations with FITC conjugated NDs and NDs with amino terminal functional groups were performed in peripheral blood mononuclear cells (PBMCs) in order to investigate biocompatibility of NDs. With the bioassays, it is demonstrated that detonation nanodiamonds were mostly internalized by monocytes among the other PBMCs: T and B lymphocytes, and natural killer

(NK) cells. It is shown that there is a significant difference between mortality rate of two differently functionalized NDs. NDs with amino terminal functional groups cause lower mortality rate at the dose of 100 μg mL^{-1} than oxidized NDs. It can be suggested that pristine NDs require surface functionalizations in order to be used in biomedical applications.

ECD technology is still in early stages and requires some improvements. Preliminary spectroelectrochemical tests were performed with ND and electrochromic polymer blend containing electrochromic devices (ECDs) in order to improve the performance. It was seen that NDs tune the switching time of ECDs without having an effect on absorbance difference between the oxidized and reduced states.

In different series of reactions, NDs were functionalized with rhamnose (**P9**), two different imidazolium containing ionic liquids (**P10** and **P11**), 6-amino-5-((benzyloxy)methyl)-2,2-dimethyltetrahydrofuro[2,3-d][1,3]dioxole-6-carbonitrile (**P13**) and 3-aminopropionitrile through amide bond generation. The functionalization reactions with the mentioned molecules were usually performed in 4 different conditions: pristine NDs in the presence of coupling reagents, pristine NDs in the absence of coupling reagents, oxidized NDs in the presence of coupling reagents and oxidized NDs in the absence of coupling reagents. The high degree of functionalization were mostly obtained from the reactions of oxidized NDs in the presence of coupling reagents and pristine NDs in the absence of coupling reagents. This result may suggest that surface of pristine NDs can let covalent or non-covalent functionalizations. Covalent reactions may occur via epoxide ring opening as the surface of pristine nanodiamonds contain various types of oxygen containing groups. Same reaction conditions were used with **P12** which is a **P9** derivative without amino group. On TGA graph, it was seen that the molecule is loaded on NDs and it requires further characterization studies to define the mechanism.

Graphene quantum dots are attractive and interesting member of carbon nanostructures due to the superior properties such as zero-dimensional structure, fluorescence, semiconductivity, biocompatibility and water-solubility.

GQDs were produced with the methodology developed by the research group. The methodology was modified in order to improve reproducibility and increase the oxygen containing groups on the surface of GQDs. GQDs were functionalized with rhamnose (**P9**) and two different imidazolium containing ionic liquids (**P10** and **P11**) through amide bond generation, and with 2-((2-(2-(2-(1,3-dioxoisoindolin-2-yl)ethoxy)ethoxy) ethyl)amino)acetic acid (**P5**) and 2,2-dimethyl-4-oxo-3,8,11-trioxa-5,14-diazahexadecan-16-oic acid (**P7**) through cycloaddition reaction. The reactions with rhamnose and two different imidazolium containing ionic liquids were performed in the presence and in the absence of coupling reagents. The reactions in the presence of coupling reagents yielded with significantly higher degree of functionalization. The reactions with **P11** both in the presence and in absence of coupling reagents were resulted with high degree of functionalizations. This result may be due to the non-covalent interactions between the GQD and the molecule. Further characterizations should be performed. Preliminary characterizations of cycloaddition reactions of **P5** and **P7** with GQDs suggest that the molecules were loaded on GQDs. Further characterization studies are needed.

LDH cytotoxicity assays of GQDs were performed on podocytes and EOMA (Murine hemangioendothelioma) cells and showed a dosed-dependent cytotoxicity of GQDs and GO. The results demonstrated that GQDs show lower toxicity in both type of cells compared to its precursor (GO). For biomedical applications, GQDs would be a better choice than GO.

GQDs were blended with a thiophene-based electrochromic polymer for the spectroelectrochemical characterizations. No significant change was detected for the ratio of 1:10 (GQD:electrochromic polymer). The blending ratio was modified to 1:4 and a significant change of absorbance difference between oxidized and reduced state was observed. Further characterizations are needed in order to understand the concentration dependence and mechanism of the absorbance change. However, the obtained results show GQDs are promising blending materials for electrochromic devices. The performance improvements of ECDs containing GQDs would accelerate the development new ECDs.

Carbon dots are attracting attention of researchers due to their excellent optical properties and good biocompatibility. Thus, development of the production methodologies are important. CDs were produced from chitin derived from two different natural resources which are cheap and renewable: insect exoskeleton and shell of shrimp. The development of methodology is still in progress and further characterizations are needed. Characterizations performed so far demonstrated that as-produced CDs are highly fluorescent. Production of Carbon Dots from renewable resources are low-cost and important for their future eco-friendly applications.

Multi-walled carbon nanotubes (MWCNTs) are focus of interest for the development of novel nanocomposites, nanoelectronics, and drug nanocarriers due to their attractive electronic, optical, mechanical and chemical properties. MWCNTs were functionalized with **P1** and **P3** in order to prevent aggregation and allow further reactions. Functionalization reactions were modified in order to increase the degree of functionalization. Functionalizations with **P9**, **P10** and **P11** were performed in order to increase the solubility of MWCNTs and add the biological properties of the molecules. The characterization results suggest that the reactions resulted in good degree of functionalization with the suggested coupling reagents. The functionalizations were confirmed with different characterization methodologies. Biological evaluations should be performed in order to investigate the effects of functionalized MWCNTs.

In this project, carbon nanostructures were functionalized, characterized and evaluated for their possible applications. The promising results demonstrated that GQDs and NDs can be used in the process of ECD technology development however further investigations are required with different electrochromic compounds. MWCNTs and NDs were functionalized with various organic compounds and their biological evaluation will provide interesting and comparative data for their future applications. The biological activity of different carbon nanostructures functionalized with same/similar approach and same organic molecules will be confronted.